THE UNIVERSITY
of EDINBURGH

Regulation of fission yeast cell polarity by stress-response pathways

Delyan Mutavchiev

Thesis presented for the degree of Doctor of Philosophy

Institute of Cell Biology

The University of Edinburgh

January 2017

Declaration

I hereby declare that this thesis was composed by me and the research presented is my own original work. Where other individuals have made contributions, this has been clearly stated within the text. This work has not been submitted for any other degree or professional qualification.

24.04.2017

Acknowledgements

First and foremost, I would like to thank my supervisor Prof. Ken Sawin for the opportunity to do my PhD in his lab. Ken's guidance, patience, and, above all, passion for science helped me immensely throughout my PhD and were instrumental in my development as a scientist. Thank you, Ken, for showing me the ropes, for all our discussions, and for every insightful idea or advice. Thank you, for staying positive and optimistic in difficult times and always encouraging me to think differently and keep trying.

I would also like to thank all the past and current members of the Sawin lab: Dr. Eric Lynch, Dr. Weronika Borek, Dr. Sanju Ashraf, Dr. Xun Bao, Dr. Su ling Leong, Dr. Harish Thakur, Dr. Ye Dee Tay, Hayley Johnson, and Ana Rodriguez. Thank you, for always being helpful, positive, fun, and very patient with me in the lab. Furthermore, I would like to thank Dr. Marcin Leda for our scientific discussions and help with experiments. Additionally, I would like to thank my second supervisor Prof. Andrew Goryachev for helpful discussions and advice during my PhD. I am also very grateful to Dr. Eric Schirmer for his mentoring and help which started during my Master's degree and continued throughout my PhD. I would like to thank Dr. David Kelly for his great help and patience when dealing with my microscopy problems. Furthermore, I would like to thank Dr. Christos Spanos for his contribution and advice with my mass spectrometry experiments and data analysis. I would also like to extend my gratitude towards the many researchers who have shared knowledge, insight, or reagents and have thus contributed greatly to the advancement of my PhD work.

I thank the Wellcome Trust, as well as the team behind the WTCCB Wellcome Trust PhD programme for giving me the opportunity and financial support to pursue a PhD degree and for the chance to travel and communicate my findings on an international level.

I am also very thankful to all my friends who shared the PhD experience with me in Edinburgh and have been caring, supportive, and always up for doing something fun outside the lab. Special thanks go to my former flatmate Dr. Sophie Kneeshaw who has always been a great friend and has stuck around through both happy and difficult times.

I would like to especially thank my partner and soon-to-be doctor, Lisa Iurchenko. Thank you so much for your endless care and support, especially during the writing of this thesis.

Finally, I would like to thank my family for their support over these years. Скъпи мамо и татко, благодаря ви, за всичко, което сте направили и продължавате да правите за мен с всеки жест, дума, и действие. Вашата помощ и постоянна подкрепа са най-ценните подаръци, които някога съм получавал и без които тази теза вероятно нямаше да е реалност. Скъпи баби и дядовци, благодаря ви, че ми пододохте ръка да тръгна по този вълнуващ и предизвикателен път и че винаги сте били до мен- тялом и духом. Скъпи роднини, благодаря ви за всички позитивни и окуражаващи пожелания, които ми изпращахте по време на моето учение. Обичам ви.

Abstract

Cell polarisation is a key biological process crucial for the functioning of essentially all cells. Regulation of cell polarity is achieved through various processes determined by both internal and external factors. An example of the latter is that cell polarity can be disrupted or lost as a consequence of a variety of external stresses. When facing such stresses, cells adapt to unfavourable conditions by activating a range of molecular signalling pathways, collectively termed 'stress response'. Despite the connections between external stress and cell polarity, whether stress-response signalling regulates cell polarisation and what the molecular basis for such regulation remains an open question. The fission yeast *Schizosaccharomyces pombe* presents an excellent biological platform to study the complexity of cell polarity regulation on a systematic level. This study is aimed at understanding the functional relationship between stress-response signalling and maintenance of cell polarity in this model organism.

The findings presented in this thesis set the basis for establishing a functional link between the activation of the *S.pombe* stress-response pathway and the activity of the master regulator of cell polarity- the Rho GTPase Cdc42. Here, I describe experiments that identify an active involvement of the stress-response mitogen-activated kinase (MAPK) Sty1 in the dispersal of active Cdc42 from the sites of growth. This new role for Sty1 occurs independently from its involvement in transcription regulation and other previously identified signalling pathways involving Sty1. Furthermore, I also find that Sty1's involvement in Cdc42 regulation has direct implications for fission yeast physiology as it is essential for the maintenance of cellular quiescence upon nitrogen starvation. This thesis also focuses on identifying the targets of Sty1 orchestrating the active Cdc42 disruption. Here, I describe a candidate-based approach, where I investigate the role of proteins from the Cdc42 regulatory network during Sty1 activation. Additionally, I present a global phospho-proteomics approach to identify novel targets of Sty1 and offer preliminary findings which might explain Sty1's involvement in Cdc42 regulation.

Lay Summary

The phenomenon of cell polarity refers to the spatial differences in shape, structure, and function of cells. The processes that regulate establishment and maintenance of cell polarity are implicated in various aspects of human physiology– development, immunity, and diseases such as cancer. To govern cell polarity, many cellular components work together forming dynamic regulatory networks. Such interactions allow fundamental cell functions such as polarised growth and directed transport of cellular material. Thus, understanding how cell polarity is regulated is a key question in biology, the answer to which could provide insights not only into the basic principles of cellular function but also to the understanding and treatment of various diseases.

Cell polarity can be affected by a variety of external stresses which cells face during their lifespans such as fluctuations in temperature, osmotic pressure, or oxidation. To adapt to adverse surroundings, cells induce a spectrum of reactions, collectively termed ‘stress response’. Intriguingly, upon facing such stresses, the cell’s polarisation is often adversely affected, suggesting that cell polarity regulation could be part of the stress response. Despite that, how stress response is connected to the regulation of polarity on a molecular level remains an open question. In this thesis, I explore this question by studying fission yeast - a unicellular organism that exhibits a distinct, highly polarised pattern of growth. The experiments described in this work, discover a novel link between fission yeast stress response and regulation of polarity. My main findings show that a key stress-response protein called Sty1 is actively involved in the regulation of the main cell polarity determinant – the protein Cdc42. Furthermore, I focus on the molecular details of this newly-found connection and its implications for fission yeast physiology.

Table of Contents

List of Figures

List of Tables

Abbreviations

3-BrB 4-Amino-1-tert-butyl-3-(3-bromobenzyl)pyrazolo[3,4-d]pyrimidine

ABC Ammonium bicarbonate

ACN Acetonitrile

AEBSF 4-(2-Aminoethyl) benzenesulfonyl fluoride

ATP Adenosine Triphosphate

bp Base pair

BSA Bovine serum albumin

CDC Cell Division Cycle

CRIB Cdc42/Rac Interactive Binding

CytA Cytochalasin A

Da Dalton

DMSO Dimethylsulfoxide

DNA Deoxyribonucleic Acid

dNTP Deoxyribonucleotide

DTT Dithiothreitol

EDTA Ethylenediaminetetraacetic acid

EMM Edinburgh Minimal Media

EtOH Ethanol

g gravity

GDP Guanosine diphosphate

GFP Green fluorescent protein

GTP Guanosine triphosphate

h Hour

HMT Homemade Taq

HPLC High-pressure liquid chromatography

IPTG Isopropylthio-β-D-galactosidase

L Litre

LatA Latrunculin A

LSB Laemmli Sample Buffer

MAPK Mitogen-Activated Protein Kinase

min Minute

MS Mass Spectrometry

MT Microtubule

OD Optical Density

O/N Overnight

ORF Open reading frame

PAGE Polyacrylamide Gel Electrophoresis

PBS Phosphate Buffered Saline

PCR Polymerase Chain Reaction

PEG Polyethylene glycol

PMSF Phenylmethanesulphonyl fluoride

RT Room temperature

rpm Revolutions per minute

SAPK Stress-Activated Protein Kinase

SDS Sodium dodecyl sulfate

SILAC Stable isotope labelling with amino acid in cell culture

SPA Synthetic Sporulation Agar

TBS Tris Buffered Saline

TEMED N,N,N',N'-Tetramethylethylenediamine

TFA Trifluoroacetic acid

WT Wild-type

YES Yeast Extract Supplemented

YFP Yellow Fluorescent Protein

Chapter 1

Introduction

1.1 Cell polarisation as a fundamental biological process

Cell polarity is defined as the ability of a cell to generate asymmetry in cell shape, protein distribution, and cell function along one or more defined geometrical axes. Cell polarisation is an essential and evolutionary conserved biological process that is ubiquitous in virtually all living systems – from single-cell organisms, such as bacteria and yeast, to multicellular organisms such as worms, flies, plants, and mammals (Thompson, 2013; Treuner-Lange & Søgaard-Andersen, 2014).

It is hypothesised that cell polarity is an ancient cellular property that initially evolved as a mechanism for the differential distribution of cellular material at cell division, a function still maintained in modern organisms (Macara & Mili, 2008). Polarised cell divisions are thought to have emerged to prevent loss of fitness associated with the inheritance of deleterious materials such as damaged DNA, oxidised proteins, or protein aggregates. Segregation of such materials into one 'older' daughter cell leads to the rejuvenation of the other 'younger' daughter cell allowing it to go through multiple future divisions and thus ensuring the survival of the whole population (Ackermann *et al*, 2007; Macara & Mili, 2008). Throughout evolution, cell polarisation has become critical for a wide variety of functions both on single-cell and multi-cellular level.

For example, the uniformly growing single-cell yeast *Saccharomyces cerevisiae* becomes highly polarised to undergo asymmetric cell division in a process called 'budding' (Slaughter *et al*, 2009). During budding, the symmetry of the mother cell is broken by the formation of a small bud on the plasma membrane where the polarisation machinery is concentrated to promote the growth of the new daughter cell (Figure 1.1, A). Asymmetric cell division is also crucial for the determination of cell fate in the dividing embryos of multi-cellular organisms. For example, at the single-cell stage of the embryo of the nematode *Caenorhabditis elegans*, polarity proteins define two distinct domains of the cell membrane along the anterior-posterior axis of the cell (Figure 1.1, B; Goldstein & Macara, 2007; Knoblich, 2008; Hoege & Hyman, 2013). These polarity domains mediate the partitioning of different membrane and cytoplasmic determinants of cellular fate to allow for their differential segregation during division. In this way, the daughter cells of a single mother can differentiate to fulfil different functions during development. Another example for cell polarity comes from epithelial tissues, where cells exhibit polarisation along their apical-basal axis

which is defined by the distinct protein compositions of the apical and basal plasma membranes of an epithelial sheet (Figure 1.1, C; Nelson, 2009; St Johnston & Ahringer, 2010). Epithelial sheets serve as selective barriers between the inside and outside environments of an organism. The distinct compositions of the apical and basal membranes allow the selective directional transport of molecules across the epithelial sheet. Such molecules could include nutrients, signalling molecules, or waste products. In addition, epithelial tissues also exhibit planar cell polarity (PCP) which aligns cells and cellular structures along a defined direction in the epithelial plane (McNeill, 2010; Devenport, 2014). For example, in the fruit fly *Drosophila melanogaster*, PCP defines the orientations of hairs on the wings (Figure 1.1, E) or the orientations of photoreceptor clusters in sections of the eye. In contrast to the apical-basal polarity in epithelial cells, migrating cells exhibit front-rear polarity which facilitates directed growth through the formation of cell protrusions and adhesions to the extracellular matrix at the leading edge of the cell (Figure 1.1, D; Nelson, 2009). Front-rear polarity in migrating cells plays a key role during morphogenesis, wound healing, and tissue renewal (Mayor & Etienne-Manneville, 2016).

Importantly, establishment and maintenance of cell polarity is linked to various aspects of human health and disease, including functioning of the immune system, growth and regeneration of neurons, and asymmetric division of stem cells (Giebel, 2008; Tahirovic & Bradke, 2009; Dustin *et al*, 2010; de la Torre-Ubieta & Bonni, 2011). Additionally, the loss of polarisation in epithelial cells is also considered one of the hallmarks of tumorigenesis and metastasis initiation (McCaffrey & Macara, 2011; Macara & McCaffrey, 2013).

Due to the widespread and potentially evolutionary ancient appearance of cell polarisation, there is a large diversity of molecular pathways that establish and maintain cell polarity. However, despite appearing seemingly unrelated, the basic mechanisms of cell polarisation follow a common paradigm involving several coupled chemical or mechanochemical events (Bois *et al*, 2011; Howard *et al*, 2011; Goehring & Grill, 2013). The first event is the local breaking of cellular symmetry, that is, the local disruption of the uniform distribution of a certain cellular component at either single-molecule or macromolecular level (Li & Bowerman, 2010). Symmetry breaking can be induced by a directed external or internal stimulus or

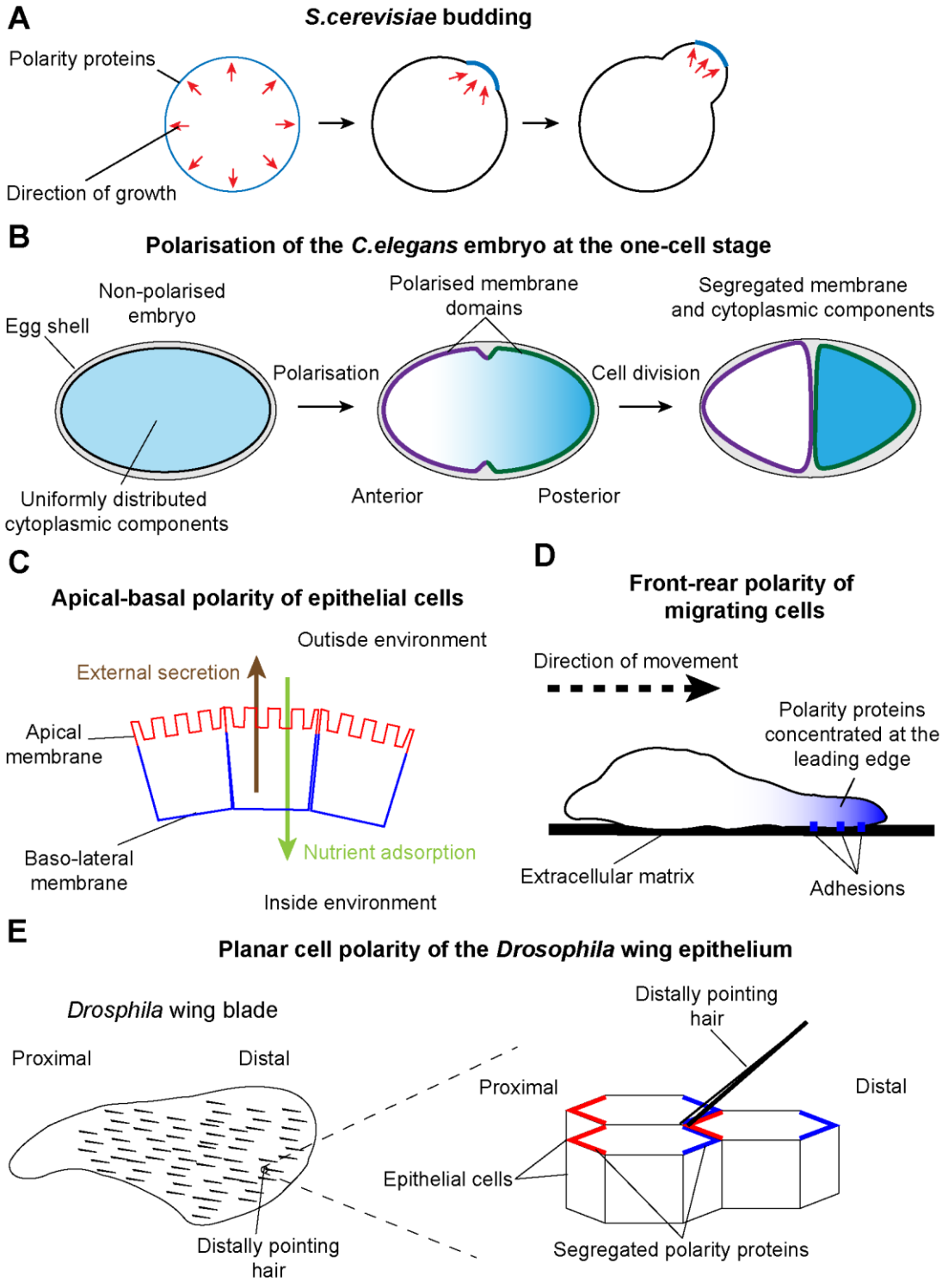

Figure 1.1. Examples of cell polarisation. Simplified schematic overview of various cell polarisation processes. (A) Cell polarisation during budding in *S.cerevisiae*. (B) Polarisation of the *C.elegans* embryo during the first division. Adapted from Hoege & Hyman, 2013. (C) Apical-basal polarity of epithelial cells. (D) Front-rear polarity of migrating cells. (E) Planar cell polarity of the epithilial cells on a *Drosophila* wing disc. Adapted from Devenport, 2014.
Objects are not drawn to scale.

occur as a result of stochastic fluctuation. Next, the symmetry breaking event needs to be coupled with local signal amplification and long-range inhibition, an idea originally conceived by Alan Turing (Turing, 1952). The local signal amplification typically constitutes a self-enhancing activation loop, which allows the initial signal generated from symmetry breaking to be propagated (Goehring & Grill, 2013). However, on its own, such a self-amplifying loop will convert more and more of the system to an 'activated' state and thus would not be sufficient to generate a steady, polarised pattern. Thus, the activation loop must be coupled to a long-range inhibition mechanism which can take various forms such as a rapidly-diffusing inhibitor of the signal amplification reaction or a depletion of one of the components of the signal amplification reaction (Bois *et al*, 2011). These three coupled events (symmetry breaking, local signal amplification, and long-range inhibition) constitute a basic conceptual framework for establishment and maintenance of cell polarisation which can be applied to a diverse range polarisation processes (Goehring & Grill, 2013).

Despite the discovery and characterisation of numerous molecular pathways involved in cell polarisation in a variety of organisms, understanding cell polarity on an integrated, systems level in any given organism remains a major challenge in cell biological research. This is especially true for multicellular organisms due to the inherent complexity of the cell polarisation pathways, often consisting of large numbers of molecular players many of which share redundant functions. Thus, one approach towards obtaining a systems-level understanding of cell polarity is the investigation of core polarisation pathways in simpler biological organisms that possess many of the evolutionally conserved cell polarity genes found in more complex organisms. One such organism is the single-cell fission yeast *Schizosaccharomyces pombe*, which has become a popular eukaryotic model for the investigation of diverse cellular processes due to its genetic tractability and fast growth.

1.2 Cell polarity in the model organism *S.pombe*

The cells of the fission yeast *S.pombe* have a distinct rod-shaped morphology defined by their rigid cell wall. *S. pombe* cells are non-motile and approximately 12 µm in length and 4 µm in width (Mitchison & Nurse, 1985). *S.pombe* cells grow through tip-extension from their geometrical cell ends followed by division by medial fission, resulting in two daughter cells of identical size. In response to harsh environmental

conditions, fission yeast cells form dormant spores enveloped by a protective outer spore wall (Arellano *et al*, 2000; García *et al*, 2006). Once more favourable growth conditions occur, spores germinate by exiting dormancy and initiating outgrowth.

In fission yeast, cell polarity is intimately coupled with directed cell growth (Martin & Arkowitz, 2014). *De-novo* establishment of polarity occurs during the process of spore germination, where intrinsically depolarised spores initiate polarised outgrowth. This happens through the symmetry-breaking formation of a polarity cap, followed by growth-tension-induced breaking of the outer spore wall and the formation of a polarized tube (Bonazzi *et al*, 2014). Once cells have established a growth polarity axis they proceed with their vegetative (mitotic) cell cycle, where they undergo several polarity transitions (Figure 1.2, A). Immediately after division, daughter cells first initiate growth on only one of their geometric ends. This is the so-called 'old end' which previously existed in the mother cell. Later in the cell cycle of the daughter cell, growth is also initiated at the 'new' end, which was formed by the septation of the mother cell. This transition from monopolar to bipolar tip-growth is termed 'New End Take Off' (NETO; Mitchison & Nurse, 1985; Martin & Chang, 2005). Prior to cell division, growth at the tips stops and the growth machinery is reorganised at the cell middle. This transition facilitates cytokinesis, as the growth machinery is involved in the formation of a cytokinetic ring and the deposition of cell material to form a septum (Hayles & Nurse, 2001; Martin & Arkowitz, 2014). In addition to polarity transitions during vegetative growth, fission yeast cells also re-organise their polarisation during sexual differentiation and mating, which are triggered by the depletion of nitrogen in the growth environment (Davey, 1998). In response to nitrogen starvation, cells arrest their growth and, after 2 divisions, depolarise their growth machinery until a suitable mating partner is found (see also Chapter 3, Section 3.2.8). To facilitate mating, the growth is then re-initiated towards the mating partner in a process referred as 'shmooing' (Figure 1.2 B; Davey, 1998; Bendezú & Martin, 2013).

Importantly, polarity transitions throughout the life of a fission yeast cell are tightly regulated by both internal and external factors. For example, NETO is synchronised with the transition between G1-S and G2 phases of the cell cycle, as cells arrested in G1 or S exhibit monopolar growth, while cells arrested in G2 exhibit

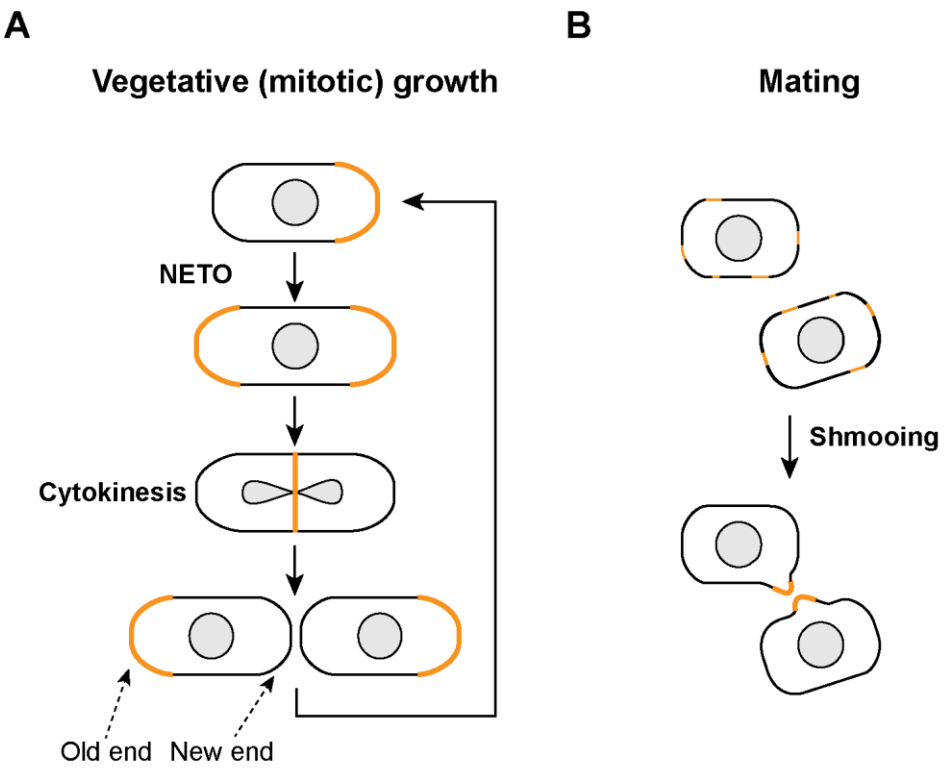

Figure 1.2. Cell polarity transitions in fission yeast. A schematic representation of the polarity transitions in fission yeast cells during the vegetative cell cycle (A) or during the initiation of mating (B) . In both schematics, the sites of polarised growth where the growth/polarity machinery is concentrated are marked in orange. The cells depicted in (B) start from a depolarised G0 state which induced by nitrogen starvation. Details on the transition from vegatative growth to G0 upon nitrogen starvation are further introduced in Chapter 3, Section 3.2.8.

bipolar growth (Mitchison & Nurse, 1985). The growth environment also affects NETO, as cells grown in nutrient-poor, minimal medium undergo NETO with delayed timing compared to cells grown in rich medium. Additionally, previous studies have identified many proteins whose function affects NETO, such as various kinases or cytoskeletal-binding proteins (Matsusaka *et al*, 1995; Verde *et al*, 1998; Bähler & Pringle, 1998; Glynn *et al*, 2001; Snaith & Sawin, 2003; Castagnetti *et al*, 2005). However, the exact sequence of events and the underlying molecular mechanisms that drive NETO remain open questions in fission yeast biology.

An additional example of a highly regulated polarity transition is the re-organisation and correct positioning of the growth machinery during cell division,

which depends on various signalling events, relating to the current size of the cell or the positioning of the cell nucleus (Tran *et al*, 2001; Wood & Nurse, 2015). Finally, during shmooing, initiation of growth towards the mating partner is dependent on the concentrations of external pheromone signals, as well as the functioning of internal signalling pathways that transduce such signals to direct cell polarisation (Bendezú & Martin, 2013; Merlini *et al*, 2016; Dudin *et al*, 2016).

The described dynamic transitions in cell polarisation, as well as the distinct cell morphologies associated with these transitions, make fission yeast cells an excellent model for the study of cell polarity and its regulation. Importantly, fission yeast polarisation relies on the same molecular entities as polarisation in multicellular eukaryotes: small GTPases; the microtubule and actin cytoskeletons; polarity landmarks; and specialised membrane lipids (Martin & Arkowitz, 2014). In the next two sections, I will focus on the roles of the small Rho GTPase Cdc42 and the microtubule cytoskeleton in fission yeast polarity regulation. An overview of the role of the actin cytoskeleton in fission yeast polarity will be introduced as a starting point at the beginning of Chapter 3.

1.3 The small Rho-GTPase Cdc42 - a key regulator of fission yeast cell polarity

1.3.1 Rho GTPases – universal regulators of polarity

To achieve polarisation, cells must regulate the concerted action of various polarity proteins in order to facilitate the previously mentioned fundamental processes of symmetry breaking, local signal amplification, and long-range inhibition. Such regulation is largely carried out by evolutionarily-conserved small GTPases from the Ras superfamily, which control signalling events within the cell by acting as molecular switches (Bourne *et al*, 1990; Wennerberg *et al*, 2005). Among the Ras-related small GTPases, the Rho (Ras homologous) family has the most prominent involvement in cell polarity regulation (Park & Bi, 2007; Iden & Collard, 2008). There are more than 20 members of the Rho family, including the well-characterized RhoA, Rac1, and Cdc42 GTPases (Etienne-Manneville & Hall, 2002). Like other regulatory GTPases, Rho GTPases utilise the simple chemical process of cycling between an ‘active’ (GTP-bound) and an ‘inactive’ (GDP-bound) state to control a variety of processes (Jaffe & Hall, 2005; Figure 1.3). Rho GTPases are normally associated with the plasma membrane by the post-translational addition of

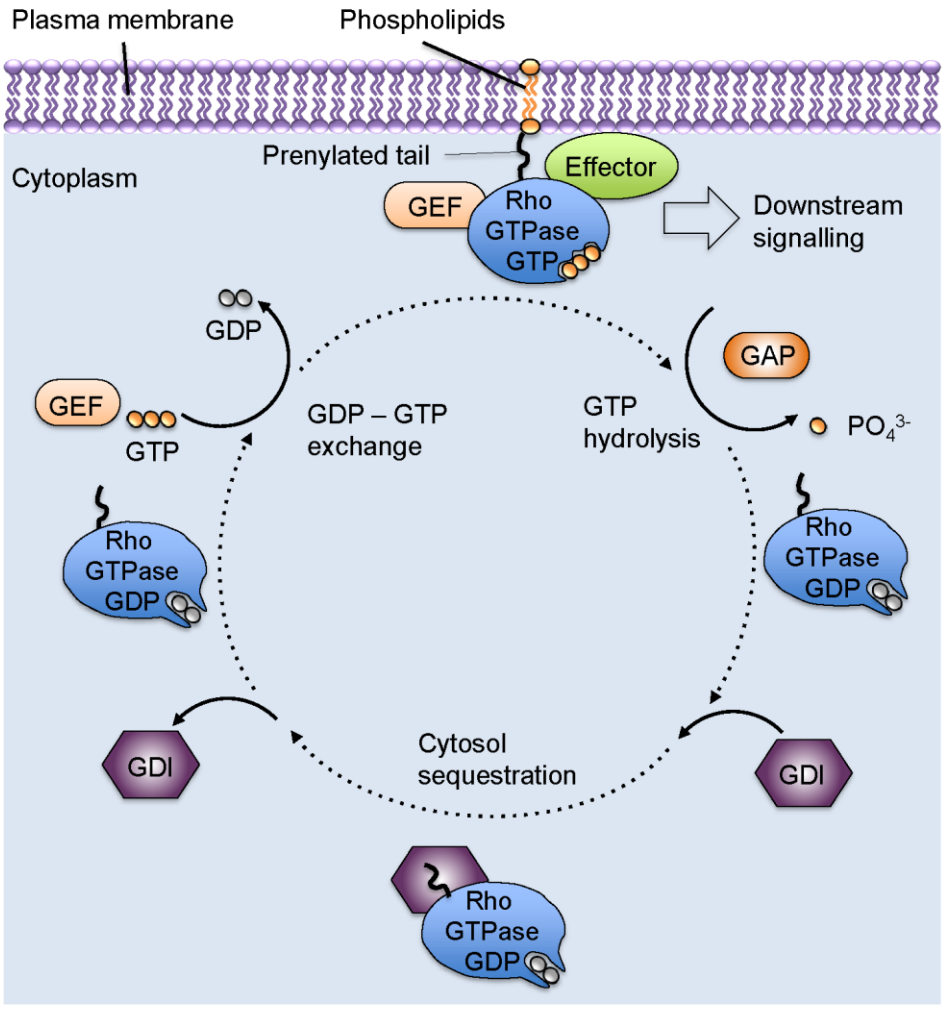

Figure 1.3. Function and regulation of Rho GTPases. A schematic representation of the regulation cycle of a typical member of the Rho family of GTPases. Rho GTPases exist in two states - GTP-bound 'active' state and a GDP-bound 'inactive' state. In their active state, Rho GTPases can interact and activate effector proteins that influence various downstream signalling events. Rho GTPases are activated by several types of proteins.The guanine nucleotide exchange factors (GEFs) serve as activators catalysing nucleotide exchange, while the GTPase activating proteins (GAPs) act as inhibitors by promoting GTP hydrolysis. Additionally, guanine nucleotide dissociation inhibitors (GDIs) can sequester inactive Rho GTPases to the cytosol by masking their prenylated tails, responsible for Rho GTPase plasma membrane binding. Figure adapted from Iden & Collard, 2008.

lipid-modifications in their C-terminal regions, allowing the interaction with phospholipids in the plasma membrane (Wennerberg & Der, 2004; Wennerberg *et al*, 2005). These lipid modifications consist of either farnesylation or geranylgeranylation (collectively termed prenylation) and occur on the cysteine residue of a 'CAAX' -motif (C - cysteine, A- aliphatic, X- any amino acid) found in all Rho GTPases.

The activity of Rho GTPases is controlled by several classes of proteins (Figure 1.3). Guanine nucleotide exchange factors (GEFs) serve as activators for Rho GTPases by catalysing the GDP to GTP nucleotide exchange (Schmidt & Hall, 2002). On the other hand, GTPase activating proteins (GAPs) inactivate Rho GTPases by promoting GTP hydrolysis to GDP – a process which has an intrinsically low rate in the absence of a GAP (Bernards, 2003). Another class of proteins involved in Rho regulation are the guanine nucleotide dissociation inhibitors (GDIs), which bind to GDP-bound Rho GTPases and prevent the dissociation from GDP and thus also prevent spontaneous Rho activation (DerMardirossian & Bokoch, 2005). Furthermore, GDIs can prevent the membrane association of Rho GTPases by binding and masking their lipid-modified tails and thus sequestering the Rho GTPases to the cytoplasm.

In their active state, Rho GTPases perform their regulatory functions by participating in conformation-specific interactions with various downstream effector proteins (Bishop & Hall, 2000). Rho GTPase effectors include proteins with diverse functions such as kinases, lipases, oxidases, as well as various scaffold proteins. While a relatively small number of Rho GTPase-effector interactions have been studied in structural detail, an overarching function of the Rho-effector binding is the activation of the effector through the relief of its autoinhibition (Jaffe & Hall, 2005). Additionally, Rho GTPases can recruit effectors to particular locations within the cell, thus spatially concentrating the effector's function or facilitating the effector's incorporation into larger molecular assemblies.

Because of the rich functional diversity of Rho GTPase effectors, Rho GTPases regulate many different cellular processes important for cellular organisation and polarity. Most commonly, they are known to be involved in the organisation of the cytoskeleton, where they affect actin and microtubule filament formation, positioning, and dynamics (Iden & Collard, 2008). Some examples of such functions are the formation of filopodia and lamellipodia promoted by Cdc42 and Rac1

activity during neuronal growth, or the Rac1-dependent microtubule stabilisation during axonal polarisation (Kozma *et al*, 1995; Watabe-Uchida *et al*, 2006). In addition, formation and regulation of actomyosin filaments that mediate contractile forces within the cell are dependent on the function of RhoA and its downstream effectors, such as ROCK kinase (Jaffe & Hall, 2005; Mayor & Etienne-Manneville, 2016). Another example of the functions of Rho GTPases is their involvement in cell-to-cell adhesion. For instance, during epithelial cell-cell pairing, downstream signalling indicating the accumulation of E-cadherin at sites of cell-cell contact is mediated through activation of Rac1 and Cdc42, which facilitate the maturation of the adhesions and the establishment of apical-basal polarity (Kim *et al*, 2000b; Nakagawa *et al*, 2001). Other Rho GTPase functions include control of proliferation through regulating cell-cycle transitions and facilitating cytokinesis, regulation of membrane-trafficking, and even aspects of cellular metabolism (Etienne-Manneville & Hall, 2002).

In mammals, there are approximately 20 Rho GTPases, 70 Rho GEFs, 60 Rho GAPs, and three Rho GDIs (Iden & Collard, 2008). Importantly, many of the mentioned functions of Rho GTPases can be mediated by more than one Rho GTPase through the same or distinct molecular pathways. As an additional layer of complexity, Rho GEFs and Rho GAPs can be either specific for a single Rho GTPase or have multiple Rho GTPase targets. Furthermore, Rho GEFs and GAPs often not only regulate Rho GTPase activity but also define downstream signalling by specifying particular Rho GTPase-effector interactions through direct binding and recruitment of effectors. Rho GEFs and GAPs expression can be constrained to a specific tissue or a particular stage of development which contributes to the diversity of functions that can be mediated by Rho GTPases (Iden & Collard, 2008).

In fission yeast, there are six Rho GTPases – Rho1 to Rho5 and Cdc42. Similar to their budding yeast homologs, both Rho1 and Cdc42 are essential for viability (Miller & Johnson, 1994; Arellano *et al*, 1996). Rho1 has been demonstrated to play an important role in the activation of the 1-3-β-D-glucan synthase enzyme which produces the 1-3-β-D-glucan polymer that is the main structural component of the yeast cell wall (Arellano *et al*, 1996; Nakano *et al*, 1997). In addition, there are indications that Rho1 might be involved in the formation of Arp2/3-mediated actin patches, as switching off Rho1 expression leads to the disappearance of actin structures at the fission yeast cell tips (Arellano *et al*, 1997). Studies on the functions of Rho2 to Rho5 are very limited. Rho2 function seems to be closer to Rho1 with some

involvement in cell wall synthesis and actin regulation (Nakano *et al*, 1997). Furthermore, Rho2 overexpression has been demonstrated to induce the accumulation of morphological defects and aberrant septation (Hirata *et al*, 1998). Rho3 and Rho4 are thought to be involved in polarised secretion through promoting exocyst complex function and are particularly important for cytokinesis and septum formation (Wang *et al*, 2003; Santos *et al*, 2003; Nakano *et al*, 2011). As the fission yeast Cdc42 Rho GTPase is the main subject of investigation in this thesis work, I will further focus the discussion in this section on Cdc42 function and regulation.

1.3.2 Cdc42 has central role in polarity regulation from yeast to mammals

The Rho family GTPase Cdc42 is among the best characterised universal regulators of cell polarity found in eukaryotes- from unicellular yeasts to multicellular flies, worms, and mammals (Etienne-Manneville, 2004). The Cdc42 gene bears the 'cell division cycle' name given to the cell cycle-related genes isolated from pioneering genetic screens in the budding yeast *S.cerevisiae* performed by Leland Hartwell in the 1970s (An overview by Reid *et al*, 2015). However, while *CDC42* was not among the original 35 *CDC* genes, its direct activator, the GEF *CDC24,* was. *CDC42* was first identified in a phenotypic screen in *S.cerevisiae* for additional mutants that exhibit defects similar to the original *CDC24* mutants (Adams *et al*, 1990). Strains carrying a temperature-sensitive *CDC42* mutation failed to form a bud at restrictive temperature and instead continued to grow in an isotropic, non-polarized manner.

Since its discovery, many advances have been made in elucidating Cdc42's role in budding yeast polarisation. At the site of bud emergence, active Cdc42 has been shown to directly promote the organisation of septins – a family of proteins which form hetero-oligomeric ring structures to act as a diffusion barrier separating the mother and daughter cells' cytoplasms (Caviston, 2003; Iwase *et al*, 2006; Okada *et al*, 2013). This is achieved through Cdc42's interaction with the Gic1 and Gic2 effector proteins, shown to participate in septin regulation (Brown *et al*, 1997; Iwase *et al*, 2006; Sadian *et al*, 2013). Interestingly, Cdc42's role in regulating septins appears to be conserved in mammalian cells, where two functional homologs of Gic1 and Gic2, Borg1 and Borg2, have been identified (Joberty *et al*, 2001; Sheffield *et al*, 2003).

Furthermore, Cdc42 has a well-established role in polarising the actin cytoskeleton during budding. This is achieved by several Cdc42-dependent

pathways. For example, Cdc42 recruits and activates the two p21-activated kinases (PAKs) Cla4 and Ste20, whose activity regulates the type I myosins Myo3 and Myo5 (Wut *et al*, 1996; Wu *et al*, 1997). Type I myosins, together with the Cdc42-recruited proteins Bee1 (ortholog of mammalian WASp) and Vrp1 facilitate the polarised polymerisation of Arp2/3 actin filaments at the bud-site (Lechler *et al*, 2001). Additionally, Cdc42 has been shown to recruit (but not activate) the formin Bni1, responsible for the directed nucleation of actin cables which serve as tracks for the delivery of secretory vesicles towards the sites of growth (Dong *et al*, 2003). Cdc42 also promotes directed exocytosis at the bud site by interacting with components of the exocyst complex such as Sec3, Sec4, and Exo70 (Adamo *et al*, 2001; Zhang *et al*, 2001; Wu *et al*, 2010). Finally, Cdc42's function is not only important for *S.cerevisiae* budding but also for its shmooing during mating. Cdc42 promotes the directed growth towards the mating partner based on a gradient of pheromone signals released by each mating partner (Etienne-Manneville, 2004; Martin & Arkowitz, 2014).

Many of the Cdc42 functions in cell polarisation discovered in the unicellular budding yeast also appear to be conserved in multicellular organisms such as worms, flies, and mammals (Etienne-Manneville, 2004). However, as multicellular organisms need far more complex coordination of cell polarity, there is a more diverse range of both Cdc42 regulators and downstream effectors. As mentioned in the previous section, some the functions of Cdc42 in multicellular organisms are shared with other Rho GTPases such as Rac1.

Similar to budding yeast, mammalian Cdc42 plays an important role in remodelling of the actin cytoskeleton through the activation of PAK kinases. Mammalian PAK1 kinase is important for the filamentous actin rearrangements in membrane ruffles and lamellipodia at the leading edges of migratory cells such as fibroblasts and leukocytes (Bokoch, 2003). Furthermore, active Cdc42 binds and activates WASP (Wiskott-Aldrich syndrome protein), which in turn recruits and activates the Arp2/3 complex to polymerise actin and form filopodia (Machesky & Insall, 1999; Kim *et al*, 2000a; Pollard & Borisy, 2003).

Cdc42 also has a well-established function in regulating the organisation of the microtubule cytoskeleton. For example, in the developing *C.elegans* embryo, asymmetric positioning of the mitotic spindle is dependent on the anterior-polarized PAR (partition defective) complex consisting of the scaffolds PAR-3 and PAR-6, and

the atypical protein kinase C- 3(aPKC-3; (Grill *et al*, 2001; Goldstein & Macara, 2007; Hoege & Hyman, 2013). Cdc42 binding to PAR-6 induces a conformational change in PAR-6 that leads to the activation aPKC-3 (Joberty *et al*, 2000; Garrard *et al*, 2003). Consistent with this function, loss of Cdc42 function using RNAi silencing leads to multiple polarity defects in the *C.elegans* embryo (Gotta *et al*, 2001). In mammals, a complex consisting of Cdc42, mammalian PAR-6, and the aPKC PKCζ regulates microtubule-driven centrosome repositioning in migrating astrocytes during wound-healing or in epithelial cells subjected to shear stress (Etienne-Manneville & Hall, 2001; Tzima *et al*, 2003). In mammalian migratory cells, Cdc42 has been found to regulate microtubule polarity by capturing microtubules at the plasma membrane through its interaction with the IQGAP1 protein (Fukata *et al*, 2002). IQGAP1 binds to the microtubule-plus-tip associated protein Clip-170, and disruption of either the Cdc42-IQGAP1 or IQGAP1-Clip-170 interactions lead to both defects in microtubule organisation and cell polarity (Fukata *et al*, 2002; Noritake *et al*, 2005).

The Cdc42-PAR-6-aPKC complex also has an important role in the determination of apical-basal polarity in *Drosophila* epithelia. It associates with the apical determinants Bazooka (PAR-3) and the Crumbs-Stardust complexes, where Cdc42-activated aPKC facilitates the specification of the apical membrane (Thompson, 2013). This is achieved by aPKC-mediated phosphorylation of the basolateral determinant Lethal giant larvae (Lgl) which excludes it from the apical membrane (Betschinger *et al*, 2005). Furthermore, aPKC also phosphorylates Crumbs and facilities its self-recruitment to the apical membrane, constituting a positive-feedback loop (Fletcher *et al*, 2012). Interestingly, the Cdc42-Par6-aPKC complex has analogous functions in mammalian epithelia, where its function is essential for initiation of epithelial polarisation by the formation of tight junctions (Etienne-Manneville, 2004).

While these examples of Cdc42 function in unicellular or multicellular context do not constitute a comprehensive list of all identified Cdc42 roles in eukaryotes, they exemplify the evolutionarily conserved central role of Cdc42 in controlling cell polarisation. Thus, it is not surprising that many cell polarisation processes in fission yeast are also dependent on Cdc42, its regulators, and effectors.

1.3.3 Function of Cdc42 in *S.pombe* – interactions with effectors and downstream consequences

The Cdc42 gene is essential for fission yeast viability, as *cdc42*Δ spores form small and round cells which are unable to grow substantially or to proceed through the cell cycle (Miller & Johnson, 1994). Cdc42 localises primarily to the plasma membrane but can be also detected on internal endomembranes, such as the nuclear envelope, Golgi, or secretory vesicles (Merla & Johnson, 2000; Bendezú *et al*, 2015). The active form of Cdc42 is localised to the sites of active growth at the cell tips during interphase and at the septum during division (Tatebe *et al*, 2008). During spore germination, clusters of active Cdc42 define a dynamic polar cap through which symmetry-breaking is achieved (Bonazzi *et al*, 2014).

At the cell membrane, Cdc42-GTP participates in several processes important for cell polarisation and growth (for a graphical overview of Cdc42 function and regulation in fission yeast interphase cells, see Figure 1.4; A and B). Probably the best characterised Cdc42 function in fission yeast is its binding and activation of the formin For3 (Feierbach & Chang, 2001). When active, For3 mediates the nucleation of actin cables from the cell tips, which in turn function as tracks for myosin-dependent transport of vesicles towards the cell tip. Like other related formins, For3 is regulated by autoinhibition, in which the N-terminal Dia inhibitory domain (DID) of For3 interacts with the C-terminal Dia autoregulatory domain (DAD), forcing a 'closed' For3 confirmation (Wallar & Alberts, 2003; Li & Higgs, 2005; Wallar *et al*, 2006). This closed conformation restricts the function of the For3 Formin-homology 1 (FH1) and FH2 domains, responsible for binding to actin monomers and stabilising actin filament intermediates to accelerate actin cable nucleation. Cdc42-GTP binding to the N-terminal DID domain of For3 has been proposed to localise For3 to the cell tips and relieve For3 autoinhibition, allowing For3 to adopt an 'open' conformation where the FH1-FH2 domains can perform their function (Martin *et al*, 2007). This is supported by the finding that expression of a For3 mutant in which autoinhibition is disrupted can rescue some of the morphological defects observed in temperature-sensitive *cdc42* mutants grown at restrictive temperatures (Martin *et al*, 2007). Furthermore, For3 localisation to the cell tips is also mediated by binding to actin- and formin-binding protein Bud6, which interacts with the C-terminal DAD domain of For3. Consistent with this idea, For3 is partially mislocalized in *bud6*Δ cells, and *bud6*Δ cells display some defects in actin cable organisation (Martin *et al*, 2007). Finally, For3 localisation to the cell tips, as well as its binding to Cdc42-GTP, appear to be promoted by the function of another Cdc42-effector, the essential Boi-family protein Pob1 (Toya *et al*,

1999; Rincón *et al*, 2009). Pob1 localises to cell tips by binding to Cdc42-GTP, where it participates both in recruiting For3 and relieving its autoinhibition. Pob1 mutants in which either binding to Cdc42-GTP or binding to For3 is disrupted show similar phenotypes of partial For3 mislocalization and defective actin cables (Rincón *et al*, 2009). However, while genetic studies have highlighted the roles of Cdc42-GTP, Bud6, and Pob1 in For3 recruitment and activation, it remains unclear how each of these proteins contributes to this process on a structural level, and what the defined sequence of events underlying For3 regulation is.

Similar to its function in budding yeast, Cdc42 activity has been suggested to stimulate directed exocytosis in fission yeast (Bendezú & Martin, 2011). As mentioned previously, direct interactions between Cdc42 and the Sec3, Sec4, and Exo70 components of the exocyst complex have been demonstrated in the budding yeast *Saccharomyces cerevisiae*, and homologous interactions are likely present in *S.pombe* (Adamo *et al*, 2001; Wu *et al*, 2010; Estravís *et al*, 2011; Bendezú *et al*, 2012; Kokkoris *et al*, 2014). Furthermore, Pob1 function has also been proposed to stimulate exocytosis, as *pob1-ts* mutants show similar defects in growth as mutants where For3 and another component of the exocyst complex, Sec8, have been simultaneously disrupted (Nakano *et al*, 2011).

S.pombe cells contain two PAK kinases, Shk1 and Shk2 (Ottilie *et al*, 1995; Yang *et al*, 1998). Out of the two, Shk1 is essential for viability, and *shk1*Δ mutants arrest as small round cells, similar to *cdc42*Δ mutants. This suggests that Shk1 has an essential role in mediating Cdc42 function in growth and polarity. Interestingly, expression of budding yeast Ste20 is sufficient to rescue the lethality of *shk1*Δ in *S.pombe*, suggesting that the two proteins have highly conserved functions. However, unlike Ste20 in budding yeast, there is little data on what the molecular targets of Shk1 are. One study has reported that the polarity landmark Tea1 (discussed later in the chapter) might be among the substrates of Shk1, as deletion of Tea1 can rescue some of the severe morphological defects caused by the loss of function of the conserved Shk1 inhibitor Skb15 (Kim *et al*, 2003). However, while Shk1 is able to phosphorylate Tea1 *in vitro*, the occurrence and significance of Shk1-driven Tea1 phosphorylation have not yet been demonstrated *in vivo*. Furthermore, Shk1 has also been implicated in phosphorylating the myosin II regulatory light chain Rlc1, regulating the coordination and rate of actomyosin contraction during cytokinesis (Loo & Balasubramanian, 2008). Deletion of the other *S.pombe* PAK kinase, Shk2, is not

lethal and relatively little is known about the physiological function of Shk2 (Yang *et al*, 1998; Sells *et al*, 1998). One report suggests a possible interaction between Shk2 and the Cell-Wall-Integrity pathway MAPKKK Mkh1 (Merla & Johnson, 2001). Intriguingly, the lethality of Shk2 overexpression is suppressed in *mkh1*Δ mutants, although the implications of this genetic interaction have not been further investigated.

1.3.4 Regulation of fission yeast Cdc42

The various processes orchestrated by Cdc42 make the spatial regulation of its activity central to organising fission yeast cell polarity. Locally, Cdc42's activation is carried out by two Cdc42 GEFs, Scd1 and Gef1 (Chang *et al*, 1994; Coll *et al*, 2003). While single deletion of either GEF results in viable cells, deletion of both GEFs is lethal, indicating that Scd1 and Gef1 are the only two essential activators of Cdc42 (Coll *et al*, 2003). Interestingly, deletion of Scd1 results in a different phenotype from deletion of Gef1. Scd1 deletion leads to round-shaped cells with no detectable Cdc42-GTP at the cell tips (Chang *et al*, 1994; Tatebe *et al*, 2008). In contrast, *gef1*Δ cells exhibit some defects in bipolar growth initiation and formation of the septum but no significant changes in cell shape (Coll *et al*, 2003). The different phenotypes observed upon single deletion of each of the GEFs suggest that while the functions of the two GEFs in activating Cdc42 overlap, there likely are aspects of Cdc42 regulation specific to each GEF. Both GEFs appear to share a similar localisation pattern: at cell tips during interphase, and at the site of septation during cytokinesis (also further discussed in Chapter 4; Coll *et al*, 2003; Kelly & Nurse, 2011; Das *et al*, 2015; Wei *et al*, 2016).

Scd1 localisation is mainly regulated by its binding to the scaffold protein Scd2 (Chang *et al*, 1994; Endo *et al*, 2003; Kelly & Nurse, 2011). Scd2 serves as a platform for bringing together several proteins, including Cdc42 and Shk1 (Chang *et al*, 1999; Endo *et al*, 2003; Wheatley & Rittinger, 2005). Scd2 is also a Cdc42 effector, as it specifically binds to GTP-bound Cdc42 (Endo *et al*, 2003). Since Cdc42-GTP recruitment of Scd2 also leads to the recruitment of the Cdc42 activator Scd1, these interactions constitute a positive feedback loop, essential for the establishment and maintenance of Cdc42-GTP at the cell tips. Consistent with this idea, in *scd2*Δ cells, Scd1 does not localise to the cell tips and cells show a round phenotype, similar to *scd1*Δ cells (Kelly & Nurse, 2011). Furthermore, the round shape of *scd2*Δ cells can be restored to normal by targeting Scd1 to the cell tips by expressing a Scd1 fusion

with the N-terminus of For3, which is sufficient for tethering to the cell tips. In addition to Scd2, Scd1 has been demonstrated to bind the Ras-like GTPase Ras1 (homolog of budding yeast Rsr1) which is also implicated in polarity regulation, as its deletion leads to morphological defects such as round shape (Fukui *et al*, 1986; Fukui & Yamamoto, 1988). However, since Ras1 associations with either Cdc42 or Scd2 have not been demonstrated, how Ras1-Scd1 binding contributes to Cdc42 regulation remains unclear.

Some aspects of Gef1 regulation have been attributed to the activity of the NDR kinase Orb6 (Verde *et al*, 1998). A recent study has demonstrated that Orb6 phosphorylation of Gef1 at Ser112 leads to Gef1's sequestration to the cytoplasm through the binding of the 14-3-3 protein Rad24 (Das *et al*, 2015). Thus, Gef1 binding to Rad24 prevents Gef1's association with Cdc42 at the plasma membrane. In agreement with this, Orb6 inhibition results in the formation of mislocalized patches of Cdc42 activity which coincide with Gef1 enrichment at the plasma membrane (further discussed in Chapter 4; Das *et al*, 2009). Furthermore, it has been suggested that Gef1 localisation might be regulated through binding of the polarity landmark protein Tea4 (Kokkoris *et al*, 2014). This is based on the observation that ectopically-targeted Tea4 at the cell sides is sufficient to recruit Gef1 and promote limited ectopic growth. Finally, during cytokinesis Gef1 localisation might be dependent on the BAR-domain-containing protein Hob3 (Coll *et al*, 2007). Hob3 is reported to bind both Cdc42 and Gef1 at the site of septation. Furthermore, *hob3*Δ cells show no detectable Cdc42 localisation at the septum during cytokinesis, as well as cytokinetic defects similar to *gef1*Δ cells. However, the

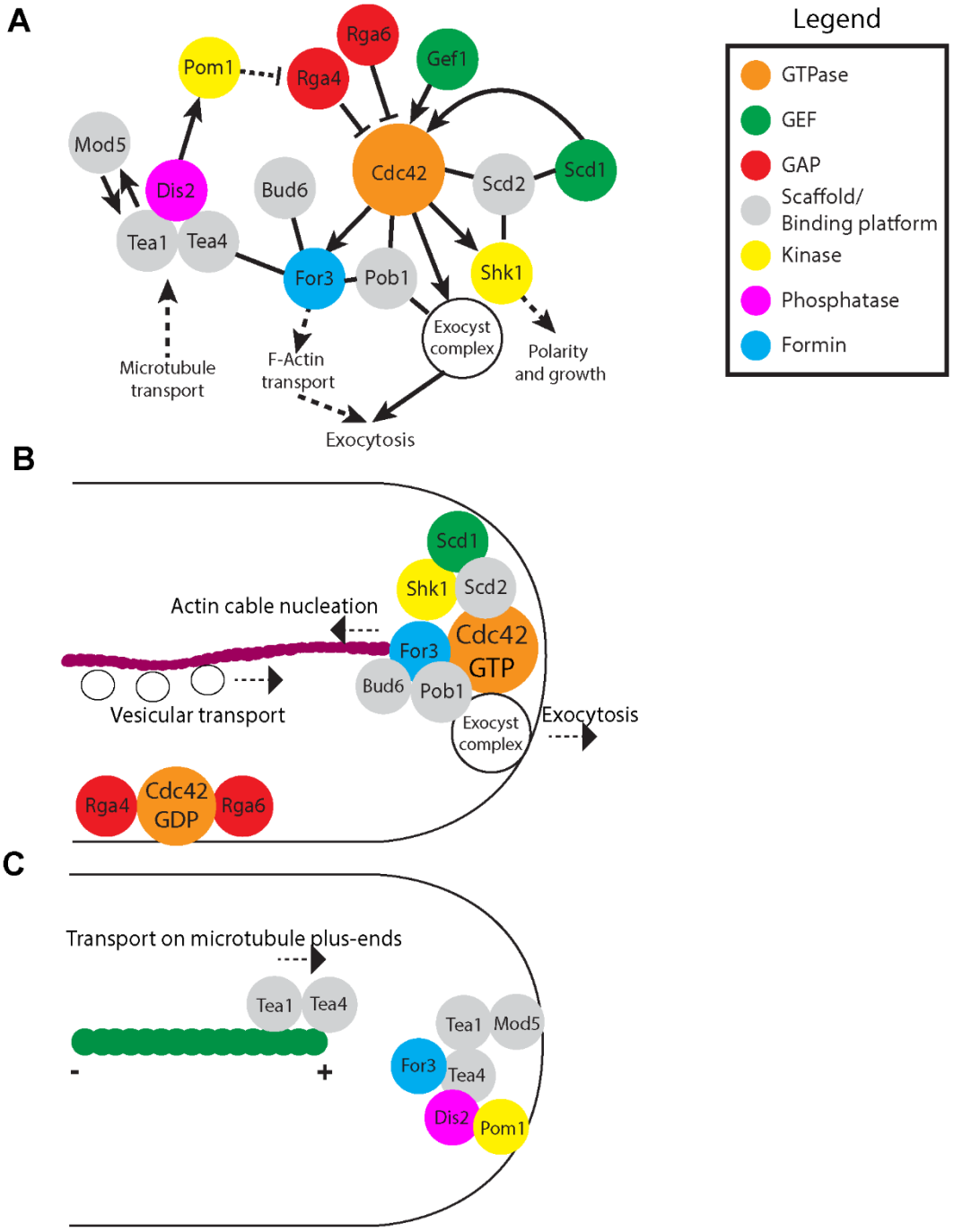

Figure 1.4. Overview of fission yeast polarity regulation by Cdc42 and the microtubule cytoskeleton. (A) Schematic representation of the network of established interactions regulating cell polarity in fission yeast, centered around Cdc42's role as a major driver of growth. Interactions legend: straight line - direct binding; arrowhead - activation/positive interaction; blunt-end arrowhead - inhibition/negative intearction; dashed line - indirect effect. (B) Overview of the spatial distribution of Cdc42's regulators and effectors at the cell tips and the cell sides during interphase vegetative growth. Directionality of downstream polarisation processes mediated by Cdc42 represented by dashed arrows. (C) Overview of the spatial distribution of microtubule-based polarity determinants.

exact molecular function of the Hob3-Cdc42-Gef1 complex and its role in determining Cdc42-GTP spatial distribution during cytokinesis remains an open question (Rincon *et al*, 2007).

While eight Rho GAPs have been identified in fission yeast, only Rga4, and recently Rga6, have been reported to specifically affect the activity of Cdc42 (Das *et al*, 2007; Tatebe *et al*, 2008; Kelly & Nurse, 2011; Revilla-Guarinos *et al*, 2016). Single deletion of either GAP results in cells with shorter length and broader width, while a double GAP deletion results in cells with round morphology. Both Rga4 and Rga6 localise to the plasma membrane and are excluded from the zones of active growth where Cdc42-GTP is localised. However, Rga4 and Rga6 do not appear to co-localise (Revilla-Guarinos *et al*, 2016). The exclusion of Rga4 from the area of active growth is controlled by the Pom1 kinase, which resides at the cell tips, where it is delivered via the microtubule network by the Tea1/Tea4 polarity complex, discussed later in this chapter (Tatebe *et al*, 2008; Hachet *et al*, 2011; Kokkoris *et al*, 2014).

Finally, the *S.pombe* genome also encodes for a predicted GDI, Rdi1, but this does not appear to play a significant role in Cdc42 dynamics (Wood *et al*, 2002; Bendezú *et al*, 2015).

In order to define and maintain spatially distinct areas of Cdc42 activity, the complex interactions between the Cdc42 activators and effectors (the Cdc42 module) are often organised in feedback loops (Martin, 2015). Positive feedback loops amplify the initial signal for Cdc42 activation and reinforce the stability of the Cdc42 module, while negative feedback loops decrease the sensitivity of the established Cdc42 module to the concentration of polarity factors, and thus provide buffering and robustness (Howell *et al*, 2012; Martin & Arkowitz, 2014). An example of a positive feedback loop is the described interaction between Cdc42-GTP, the scaffold Scd2, and the GEF Scd1. Experimental work, combined with mathematical modelling on the analogous loop in budding yeast (Cdc42, scaffold Bem1, and GEF Cdc24), has revealed that such self-enforcing amplification mechanism, limited by diffusion and substrate depletion (here termed as the Goryachev-Pokhilko model), is sufficient to explain the formation of spatially distinct active Cdc42 clusters without the requirement for pre-existing polarity ques (Butty *et al*, 2002; Goryachev & Pokhilko, 2008; Howell *et al*, 2009). The stabilization of a single cluster can be further achieved through global inhibition mediated by freely-diffusing cytoplasmic GAPs which

hydrolyse GTP to GDP and inhibit the population of Cdc42 that is away from the cluster. This is particularly relevant in relation to the problem of symmetry-breaking during spore germination as cytoskeleton-dependent feedback loops (discussed further below) are not required for polar cap formation and spore outgrowth (Bonazzi *et al*, 2014). Thus, while alternative models to the Goryachev-Pokhilko model are both theoretically possible and, in part, supported by experimental evidence, there is a broad consensus that the Cdc42 module can self-organise and establish polarity in a previously non-polarised stochastic system (Martin, 2015; Goryachev & Leda, 2017).

In addition, cytoskeleton-dependent feedback loops have been proposed to participate in Cdc42 regulation. A possible example of such a loop in fission yeast is the self-enhancing loop between microtubule-delivered Tea1 and its prenylated tether Mod5. Cell tip-localized Mod5 facilitates the anchoring of Tea1 and in turn, Tea1 spatially restricts and concentrates Mod5 at the cell tips (Snaith & Sawin, 2003; Bicho *et al*, 2010a). As Tea1 might be involved in Cdc42 regulation (discussed at length in next section), such a microtubule-dependent positive-feedback loop might also contribute to establishment and maintenance of the Cdc42 cluster. Actin-dependent feedback mechanisms have also been proposed, and I will discuss those at length in Chapter 3. Together with positive feedback loops, negative feedback loops for Cdc42 regulation have also been predicted. Their existence is evidenced by the observed dynamic oscillations in Cdc42-GTP levels between the two fission yeast tips, which can only be explained by some form of delayed negative feedback originating from the Cdc42 module (Das *et al*, 2012). However, the molecular mechanisms behind such negative feedback are yet to be discovered.

1.4 Other determinants of fission yeast cell polarisation – the microtubule cytoskeleton and the Tea1/Tea4 polarity landmarks

In addition to the function of Cdc42, cell polarity in fission yeast is also determined by the organisation and function of the microtubule cytoskeleton (for a graphical overview of microtubule-dependent polarity regulation in fission yeast interphase cells, see Figure 1.4; A and C). In interphase cells, microtubules are organised in 3 to 5 antiparallel bundles which are nucleated around the cell nucleus or from the nuclear periphery (Sawin & Tran, 2006). Microtubule bundles align along the long axis of the

cell and extend their plus-ends towards the cell tips. This organisation is achieved through the function of several microtubule-associated proteins which mediate microtubule filament nucleation, bundling, sliding, and stabilisation (Sawin & Tran, 2006). Furthermore, cell shape also contributes to the alignment of microtubule bundles, as fission yeast cells grown in a physically-constricted environment that induces cell bending exhibit microtubule organisation adapted to the bent shape (Terenna *et al*, 2008; Minc *et al*, 2009).

The importance of microtubules for cell morphogenesis has been demonstrated in various contexts in which the microtubule cytoskeleton has been depolymerised by the use of drug perturbations and/or specific protein mutations (Umesono *et al*, 1983; Sawin & Nurse, 1998; Sawin & Snaith, 2004). Cells lacking microtubules show clear defects in the positioning of their growth sites and often initiate growth at ectopic locations away from the cell tips. Further work has revealed that microtubules contribute to cell polarisation by facilitating the transport of polarity proteins towards the cell tips, where such proteins can both mark the sites of polarised growth and promote the function of the growth machinery (Martin & Arkowitz, 2014). Two key polarity proteins, transported to the cell tips on microtubule plus-ends are Tip elongation aberrant 1 (Tea1) and Tea4 (Verde *et al*, 1995; Mata & Nurse, 1997; Martin *et al*, 2005).

The Tea1 protein contains several kelch-repeats at its N-terminus, which mediate its binding to microtubule-plus ends (Martin *et al*, 2005). At its C-terminus, Tea1 largely consists of an alpha-helical coiled-coil which is important for plasma membrane binding (Snaith *et al*, 2005). It was originally isolated in a screen for mutants exhibiting altered morphology, as *tea1-* cells displayed curved or T-shaped morphology (Snell & Nurse, 1994). In *tea1*-deficient cells such morphological phenotypes arise from the cell's inability to accurately position the polarity machinery at the cell tips, resulting in initiation of ectopic growth and the formation of new growth axis (Verde *et al*, 1995; Mata & Nurse, 1997; Sawin & Snaith, 2004; Tatebe *et al*, 2005). Tea1 binding to microtubules is dependent on its interaction with the CLIP-170 fission yeast homolog Tip1, which in turn relies on the kinesin Tea2 and the EB1 fission yeast homolog Mal3 (Busch *et al*, 2004; Busch & Brunner, 2004; Bieling *et al*, 2007). As mentioned previously, once delivered to the cell tips, Tea1 is captured by the prenylated anchor protein Mod5, which increases the residence time of Tea1 at the cell tips and is essential for Tea1 tip localisation in the absence of microtubule

delivery (Snaith & Sawin, 2003). Consistent with this idea, Tea1 is still delivered to the tips on microtubules in *mod5*Δ cells but it fails to anchor properly at the plasma membrane and its levels at the tips are significantly reduced. Interestingly, in *tea1*Δ cells Mod5 localisation is homogenously spread along the cell membrane, indicating that Tea1 function also involves spatially concentrating Mod5 at the cell tips (Snaith & Sawin, 2003). Based on the different turnover rates of Tea1 and Mod5 at the tips, mathematical models have predicted that Mod5 does not simply have a stoichiometric anchor role in tethering Tea1 to the tip plasma membrane, rather it acts as a catalyst for incorporation of multiple Tea1 proteins into a stable and robust polarity network (Bicho *et al*, 2010a).

Tea4 (also known as Wsh3) is the binding partner of Tea1 and contains an SH3 domain and RVxF (Arginine-Valine-Any amino acid- Phenylalanine) motif both of which confer binding to the serine/threonine protein PP1 phosphatase Dis2 (Martin *et al*, 2005; Alvarez-Tabarés *et al*, 2007). Tea4's C-terminus shows direct binding to Tea1 *in vitro*, and Tea4 localisation to the cell tips is abolished in *tea1*Δ cells *in vivo*. However, Tea1 localisation to the cell tips is not affected in *tea4*Δ cells. Thus, likely due to its binding to Tea1, Tea4 is also dependent on microtubule-based transport and all the proteins mediating Tea1 delivery and anchorage to the cell tips including Tip1, Tea2, and Mod5 (Martin *et al*, 2005). Analogous to *tea1*Δ cells, *tea4*Δ cells show morphological defect such as curved or T-shape (Tatebe *et al*, 2008). Furthermore, both *tea1*Δ and *tea4*Δ mutants fail to undergo NETO and grow in a strictly monopolar fashion (Mata & Nurse, 1997; Martin *et al*, 2005). Taken together, all of this evidence suggests that Tea1 and Tea4 form a complex with a shared function in polarity regulation. This regulation is hypothesised to occur through controlling the Cdc42 polarity module; however, the details of how this is achieved are still not entirely clear.

For instance, the Tea1-Tea4 complex has been shown to recruit For3 to the cell tips through binding to Tea4. As For3 can bind Cdc42-GTP and also promote actin cable nucleation, a Tea1/Tea4 – For3 interaction has been proposed to link the function of the microtubule cytoskeleton, the Cdc42 module, and the actin cytoskeleton (Martin *et al*, 2005). However, it should be noted that while the Tea1/Tea4 – For3 interaction is required for initiation of NETO, Tea1/Tea4-independent localisation of For3 is also observed at the old ends of *tea1*Δ *or tea4*Δ cells (Martin *et al*, 2005). Furthermore, For3 is not essential for polarised growth or

bipolar growth *per se*, as some *for3*Δ cells exhibit strictly bipolar growth (but no NETO transition) after completing division (Feierbach & Chang, 2001).

The tea1-tea4 complex is thought to regulate Cdc42 activity by controlling the localisation of the GAP Rga4 (Tatebe *et al*, 2008). This is achieved through the recruitment of the dual-specificity tyrosine regulated kinase (DYRK) Pom1 by Tea4. This interaction brings together Pom1 and the protein phosphatase Dis2, which, as mentioned previously, also binds Tea4 (Hachet *et al*, 2011). Dis2 then dephosphorylates Pom1, thus allowing Pom1 to bind to the plasma membrane through a positively charged region in the middle of the protein. Since Pom1 phosphorylation prevents plasma membrane binding and Pom1 is able autophosphorylate itself, Pom1 membrane binding weakens the further Pom1 is from Dis2 (Hachet *et al*, 2011). This is proposed to create a Pom1 concentration gradient from the cell tips to the cell middle. As mentioned previously, Pom1 activity is proposed to exclude Rga4 from the plasma membrane, thus facilitating stronger Cdc42 activation at the tips. This is supported by the fact that in *pom1*Δ cells Rga4 is not spatially restricted to the cell sides but found on the non-growing ends and the cell sides (Tatebe *et al*, 2008). However, Rga4 is still excluded from the growing tips in *pom1*Δ cells, suggesting that there might be additional mechanisms of Rga4 regulation by Tea1-Tea4 complex or other polarity regulators. Finally, the molecular mechanisms of Pom1-driven Rga4 exclusion are currently unknown but likely involve phosphorylation, as Pom1 overexpression leads to more phosphorylated and less soluble Rga4 (Tatebe *et al*, 2008).

Tea4 was also proposed to interact with Gef1, as ectopically targeted Tea4 was able to recruit the GEF to the cell sides (Kokkoris *et al*, 2014). However, while this ectopic recruitment led to an increase of Cdc42-GTP at the cell sides, it was not sufficient to initiate substantial growth, suggesting that while Tea1-Tea4 landmark may contribute to polarisation, it is not sufficient to drive polarised growth on its own.

1.5 Extracellular stresses and cell polarity in fission yeast

Apart from internal cues such as the asymmetrical distribution of polarity proteins, organisation of the cytoskeleton, or the progression of the cell cycle, fission yeast cell polarity and growth are also affected by changes in the extracellular environment. Evidence for external regulation of cell polarity in fission yeast is largely phenomenological, originating from experiments subjecting cells to different direct

physical stresses, such as heat, gravity, and radiation, or to changes in their growth environment such as limiting nutrients, increasing medium osmolarity, or increasing concentration of oxidative agents.

For example, in response to heat stress caused by a temperature increase, cells undergo a period of depolarization which lasts approximately 30-45 min and is evidenced by the cessation of growth and dispersal of Cdc42-GTP, Scd1, and Gef1 from the cell tips. However, the molecular mechanisms orchestrating the dispersal, and its functional significance, remain unclear. One hypothesis is that redistribution of the polarity proteins and, consequently, the redistribution of the growth machinery might help cells to strengthen their cell walls and repair any damages in cell wall integrity arising from the heat stress (Levin, 2005).

Depolarization of the fission yeast actin cytoskeleton and transient cessation of growth has also been commonly observed in response to a variety of stresses such as high osmolarity, heat, and hypergravity (Rupes *et al*, 1999; Bao *et al*, 2001; Petersen & Hagan, 2005; Soto *et al*, 2007; Robertson & Hagan, 2008). It has been proposed that changes in actin organisation in response to stress are mediated by the Ca^{2+}/calmodulin-dependent (CaMMK)-like protein kinase Ssp1, which has been shown to localise to the cell tips following osmotic shock (Matsusaka *et al*, 1995; Rupes *et al*, 1999). However, Ssp1 function is probably not solely responsible for actin depolarization, as some actin depolarization is still observed with a delay after osmotic shock in *ssp1*Δ cells. Furthermore, how Ssp1 mediates actin organisation is still unknown.

Several stresses have also been shown to affect microtubule dynamics, which, as previously discussed, likely has direct implications for polarity as it affects Tea1/Tea4 positioning. For example, during osmotic shock, microtubules show a transient cessation of dynamic behaviour, remaining 'frozen' for about a minute, followed by fragmentation of the microtubule bundles (Robertson & Hagan, 2008). A recent study has also demonstrated that glucose starvation leads to a severe destabilisation of microtubules within 5 to 10 minutes following glucose limitation in the growth medium (Kelkar & Martin, 2015). The microtubule destabilisation is mediated by the kinase Pka1 which negatively regulates the microtubule stabiliser CLIP-170 associated protein (CLASP) Cls1 (also known as Peg1). The glucose starvation-induced microtubule collapse results in very short or no microtubule

bundles in the cell's cytoplasm and leads to Pom1 accumulation at the cell sides, through aberrant positioning of Tea4 (Kelkar & Martin, 2015). As Pom1 is also involved in a size-dependent checkpoint controlling the commitment to division, glucose-starvation-induced Pom1 localisation to the cell sides results in delayed entry into mitosis (Moseley *et al*, 2009; Deng & Moseley, 2013; Kelkar & Martin, 2015). Finally, fission yeast cell polarisation is also affected during nitrogen starvation, which is introduced at greater length in Chapter 3.

1.6 The Stress-Activated Protein Kinase pathway in fission yeast

While it is largely unknown how various extracellular stresses directly affect cell polarity, a good starting point would be to understand the signalling pathways that are activated in response to such stresses. Eukaryotic cells respond to unfavourable external conditions through the controlled activation of a spectrum of reactions, many of which are mediated by conserved, three-tier, mitogen-activated protein (MAP) kinase pathways. MAPK pathways are often downstream of a variety of cell receptors and sensors which can detect changes in the extracellular environment and signal downstream in the presence of stress. The stress signal is transduced and amplified by the activation of a three-tier relay via the sequential phosphorylation of a MAP kinase kinase kinase (MAPKKK), MAP kinase kinase (MAPKK), and MAP kinase (MAPK). Upon activation, the final MAPK participates in the further phosphorylation of a wide-range of downstream targets, which facilitate the adaptive response to the stress input. While the majority of the described targets are transcription factors, MAPK can also modify additional components such as other kinases and cytoskeleton-associated proteins, directly influencing their function (Widmann *et al*, 1999).

The main stress response pathway in fission yeast cells is the Stress-Activated Protein Kinase (SAPK) pathway. The SAPK pathway consists of the MAPKKKs Win1 and Wis4 (also known as Wak1), the MAPKK Wis1, and the MAPK Sty1 (also known as Spc1 or Phh1; homolog of mammalian p38 MAPK kinase; Millar *et al*, 1995; Shiozaki & Russell, 1996; Samejima *et al*, 1997; Cuadrado & Nebreda, 2010). The SAPK pathway is activated in response to a variety of stresses which include oxidative, osmotic, heat and cold stress, hypergravity, DNA damage, nutrient limitation, and exposure to heavy metals (Shiozaki *et al*, 1998; Nguyen *et al*, 2000;

Soto *et al*, 2002, 2007; Petersen & Nurse, 2007; Papadakis & Workman, 2014). Two more MAPK pathways have been identified in fission yeast: the Cell Integrity Pathway (CIP; Mkh1-Pek-Pmk1) also involved in stress response and the Pheromone Signalling Pathway (Byr2-Byr1-Spk1) involved in the response to nitrogen starvation and initiation of mating (Pérez & Cansado, 2010; Papadakis & Workman, 2014). While the CIP pathway is activated in response to some of the same stresses as the SAPK pathway, such as osmotic, heat, gravity, and oxidative stress, there is considerably less known about its function compared to the SAPK pathway. Between the SAPK and CIP pathways, the CIP pathway is considered to have a reinforcing but not critical role in stress response. This is the case since mutants deficient in the CIP pathway are generally less sensitive to stress compared to mutants deficient in the SAPK pathway, which lose viability when exposed to most stresses (Pérez & Cansado, 2010). Thus, I will mainly focus my introduction on the activation and function of the SAPK pathway (for a graphical overview see Figure 1.5).

While the Sty1 SAPK pathway was originally identified almost 20 years ago, very little is known about its upstream activation in response to the various previously mentioned stresses. Probably the best characterised pathway for SAPK activation is the response to oxidative stress from the addition of hydrogen peroxide (H_2O_2). The addition of H_2O_2 activates a phosphorelay module consisting of the two sensor histidine kinases Mak2 and Mak3, the histidine-phosphotransferase Mpr1, and the response regulator Mcs4 (Shiozaki *et al*, 1997; Nguyen *et al*, 2000; Morigasaki & Shiozaki, 2010; Morigasaki *et al*, 2013). Upon oxidative stress, Mak2 and Mak3 undergo autophosphorylation on a histidine residue in their C-terminal domains (Buck *et al*, 2001). The phosphorylation is then transferred on an aspartate residue first on Mpr1 and then on Mcs4 via a classic Histidine-Aspartate phosphate-transfer reaction, typical for two-component signalling systems identified in bacteria (Stock *et al*, 2000). Phosphorylated Mcs4 then activates the Win1 and Wis4 kinases to trigger the SAPK pathway (Nguyen *et al*, 2000; Buck *et al*, 2001). Intriguingly, Mcs4 has also been identified to form a stabilising complex with the Win1/Wis4 MAPKKKs, which is important for their ability to interact and activate the MAPKK Wis1 in response to stresses other than oxidation, such as hyperosmolarity (Morigasaki *et al*, 2013). In response to heat-stress, Sty1 activation is mostly independent of the function of the MAPKK and the MAPKKKs and occurs through negative regulation of the Pyp1 phosphatase (Shiozaki *et al*, 1998; Nguyen & Shiozaki, 1999). Pyp1 together with

Pyp2 are the two main phosphatases for Sty1 and are able to dephosphorylate Sty1 on residue Tyr173, which is important for its activation (Millar *et al*, 1995a). How heat stress inhibits Pyp1 function is currently not understood, although it has been reported that both Pyp1 and Pyp2 become insoluble when extracted from cells previously subjected to heat stress (Nguyen & Shiozaki, 1999). Thus, reduction in Pyp1 activity during heat stress leads to higher levels of Sty1 activity. Analogous Pyp1-dependent Sty1 regulation has been also proposed in the response to arsenite stress (Rodríguez-Gabriel & Russell, 2005). A similar mechanism of Sty1 activation has also been suggested in response to nutrient limitation, where the target of rapamycin (TOR) complex down-regulates Pyp2 levels upon shifting cells to a nutrient-poor medium (Petersen & Nurse, 2007). Currently, how SAPK pathway is activated in response to any of the other previously mentioned stresses remains unknown.

Unlike heat, arsenite, and nutrient stress, most other stresses appear to depend on the Wis4/Win1 activation of Wis1 (Pérez & Cansado, 2010). To achieve this, Wis4 and Win1 associate with Wis1 and phosphorylate it on two residues, Ser469 and Thr473, located on the C-terminus of Wis1 (Shiozaki *et al*, 1998). Upon activation, Wis1 associates with Sty1 and phosphorylates it on residues Thr171 and

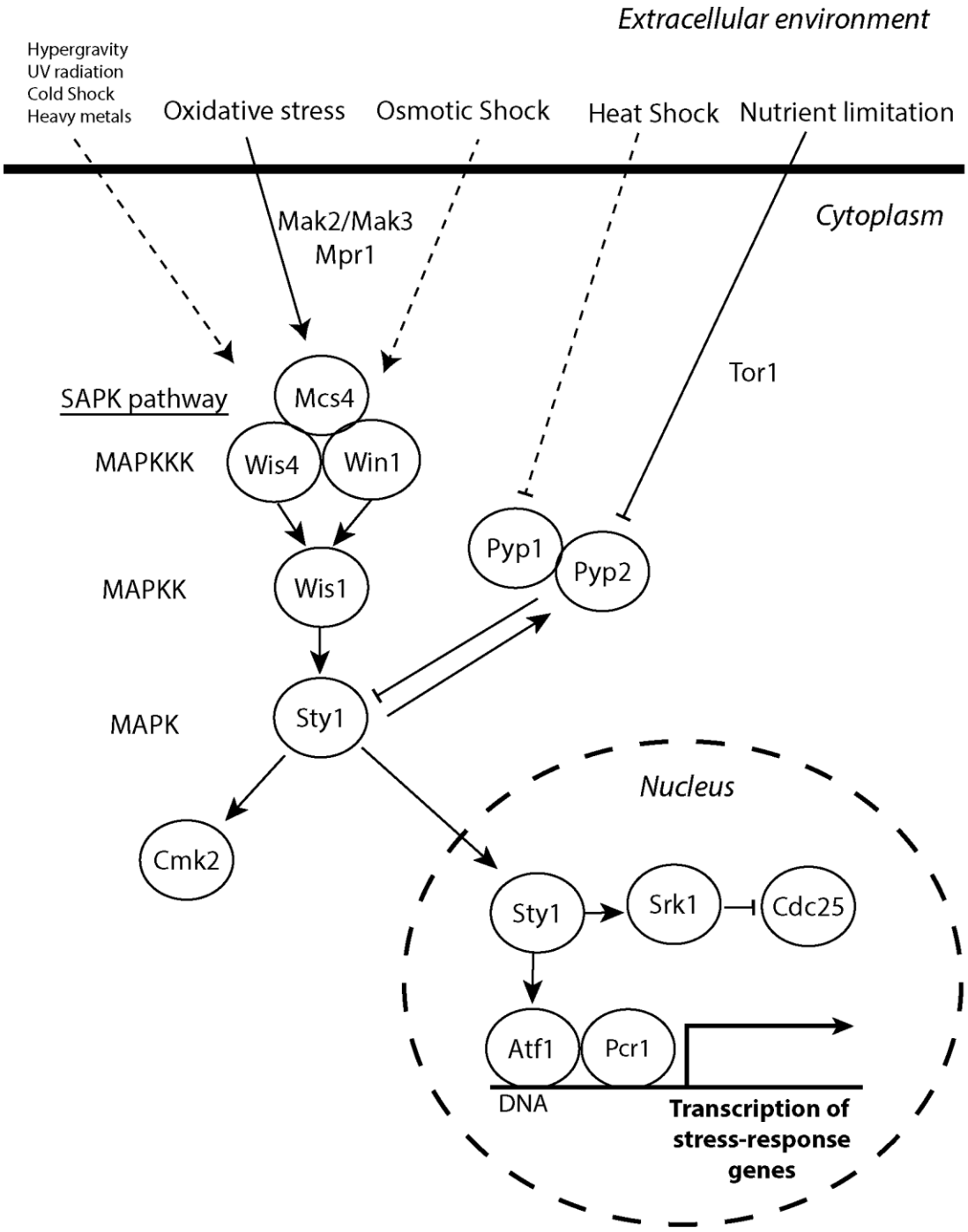

Figure 1.5. Overview of fission yeast stress-response mediated by the SAPK pathway. A schematic overview of the SAPK stress-response pathway. Interactions legend: arrowheads - activation/positive interaction; blunt-end arrowhead - inhibition/negative intearction; dashed line - indirect effect.

Tyr173 (Shiozaki & Russell, 1995; Millar *et al*, 1995a; Shiozaki *et al*, 1998). Most, but not all, of activated Sty1 migrates into the nucleus together with Wis1 in a process that is likely dependent on some form of active nuclear transport, as Wis1's 70 kDa size is too large for passive diffusion through the nuclear pores (Nguyen *et al*, 2002). Afterwards, Sty1 can be exported out of the nucleus independently from Wis1, by the exportin Crm1 (Gaits & Russell, 1999). Wis1 export from the nucleus is dependent on a nuclear export sequence (NES) on its N-terminus (Nguyen *et al*, 2002). Importantly, Wis1 localisation into the cytoplasm is essential for Sty1 activation and nuclear import, as both these processes are disrupted in cells expressing nucleus-restricted Wis1, where the NES was replaced by a nuclear localisation sequence (NLS; Nguyen *et al*, 2002). These findings suggest that Sty1 activation occurs strictly in the cytoplasm, where the MAPKKKs are also localised. Sty1 activation upon stress is transient, with varying kinetics and duration, depending on the nature and magnitude of the stress (Pérez & Cansado, 2010). An important factor in the Sty1 activation kinetics is the delayed negative feedback loop mediated by the Pyp1 and Pyp2 phosphatases (Degols *et al*, 1996; Wilkinson *et al*, 1996; Nunez *et al*, 2009; Kowalczyk *et al*, 2013). The negative feedback is possible because expression of Pyp1 and Pyp2 is stimulated by Sty1 activity. Furthermore, Pyp2 protein stability is enhanced by Sty1-dependent phosphorylation. Thus, higher expression/stabilisation of Pyp1 and Pyp2 eventually leads to the dephosphorylation and deactivation of Sty1.

Sty1's function subsequent to its activation is mostly associated with control of gene expression to facilitate recovery from stress (Chen *et al*, 2003). This is mainly achieved through the direct phosphorylation of the bZIP-domain containing transcription factor Atf1 (homolog of mammalian ATF2) in the nucleus (Takeda *et al*, 1995; Wilkinson *et al*, 1996). How Sty1-phopshorylation mechanistically promotes the function of Atf1 is still debated. Originally, Sty1-dependent Atf1 phosphorylation was considered necessary only for the functional activation of Atf1, as Atf1 was found to be constitutively associated with the regulatory elements of the genes it regulates (Wilkinson *et al*, 1996). Such elements include the CRE (cAMP response element) and CRE-like motifs found in the promoter regions of Atf1-regulated genes. However, other studies have suggested that Sty1-dependent Atf1 phosphorylation is necessary for the association of Atf1 with CRE motifs (Neely & Hoffman, 2000; Reiter *et al*, 2008). In addition, there is also evidence that Atf1 still has transcriptional activity even in the absence of Sty1 phosphorylation, as a phospho-null mutant of Atf1, where all

predicted Sty1 phosphorylation sites are mutated to alanine, is still transcriptionally active (Lawrence *et al*, 2007). Thus, it has been proposed that the primary role of Sty1-dependent Atf1 phosphorylation may rather be to stabilise the Atf1 protein, by preventing its degradation by the ubiquitin-proteasome system (Lawrence *et al*, 2009). This is consistent with the findings that Atf1 levels increase upon Sty1 activation, and Atf1 association with the ubiquitin-ligase Fbh1 is abolished in response to various stresses (Lawrence *et al*, 2009). Atf1 forms a heterodimer complex with another transcription factor Pcr1, which is not phosphorylated by Sty1 but is essential for Atf1's DNA association and activity (Sansó *et al*, 2008).

Apart from Atf1, only a few for other direct targets of Sty1 have been identified. Sty1 has been shown to phosphorylate the two MAPK-activated kinases Cmk2 and Srk1, although the full functional implications of both phosphorylation events are not entirely clear (Sánchez-Piris *et al*, 2002; Smith *et al*, 2002; López-Avilés *et al*, 2008). Cmk2 is a type II calcium/calmodulin-dependent Ser/Thr protein kinase whose function has been implicated in the adaptation to oxidative stress, as Cmk2 deficient cells show increase sensitivity to H_2O_2 exposure. In response to oxidative stress, it has been demonstrated that Sty1 phosphorylates Cmk2 on residue Thr411 *in vivo* (Sánchez-Piris *et al*, 2002). Srk1, whose name stands for Sty1-regulated kinase, is phosphorylated by Sty1 on residue Ser 463 in response to both osmotic and oxidative stress (Smith *et al*, 2002). Srk1 is reported to normally bind Sty1 in non-stress conditions (López-Avilés *et al*, 2008). Upon phosphorylation, Srk1 dissociates from Sty1 and phosphorylates and deactivates the mitotic regulator phosphatase Cdc25, which in turn delays the progression of the cell cycle by transiently arresting cells in the G2-M transition of the cell cycle (López-Avilés *et al*, 2005). Finally, Sty1 function has also been implicated in the phosphorylation of another mitotic regulator, the Polo-like kinase Plo1, although this process is likely mediated by Sty1 indirectly (Petersen & Hagan, 2005; Petersen & Nurse, 2007). I will further introduce Sty1-dependent Plo1 phosphorylation in Chapter 3.

Scope of this thesis

The study presented in this thesis is aimed at understanding the functional connections between stress response and cell polarity regulation in fission yeast. More specifically, I investigate in detail the potential role of the stress-response MAP kinase Sty1 in regulating the Cdc42 polarity module.

In Chapter 3, I first describe the early experiments that led to the discovery of Sty1-dependent Cdc42 regulation. The initial motivation in connecting stress signalling to cell polarity originated from a re-evaluation of the disruptive effects of the actin-depolymerising drug Latrunculin A (LatA) on the localisation and function of the Cdc42 module. Because LatA triggers not only actin depolymerisation but also the activation of the Sty1 MAPK pathway, I speculated that LatA-driven Sty1 activation, rather than actin depolymerisation, might be involved in the disruption of the Cdc42 module. Thus, I describe experiments that test this idea and show that indeed Sty1 MAPK signalling is required for disruption of the Cdc42 module in response to LatA. Later in the chapter, I further investigate in greater detail different aspects of Sty1-dependent Cdc42 regulation and show its importance for fission yeast physiology in processes such as entry and maintenance of nitrogen-starvation-induced quiescence.

In Chapter 4, I investigate possible mechanisms of Sty1-dependent Cdc42 regulation by looking at the behaviour of polarity factors implicated in Cdc42 regulation during Sty1 activation. I also describe experiments related to the role of the polarity landmark Tea1 in the recovery of polarised growth following Sty1-driven disruption of Cdc42 polarity.

In Chapter 5, I describe the methodology and preliminary findings of a global phospho-proteomics approach to identify novel targets of Sty1 which might explain its involvement in Cdc42 polarity regulation.

This thesis also contains two Appendix sections. In Appendix 1, I describe the construction and use of different novel CRIB reporters for Cdc42 activity. In Appendix 2, I explore how Latrunculin A activates stress-response signalling and offer preliminary findings aimed at elucidating this question.

Chapter 2

Materials and methods*

*Some of the methods described in this chapter have been published in:

Mutavchiev, D.R., Leda, M., Sawin, K.E, *Remodeling of the fission yeast Cdc42 cell polarity module via the Sty1 p38 stress-activated protein kinase pathway*. (Current Biology, 2016)

2.1 Growth and storage of fission yeast strains

Fission yeast were mainly grown in rich yeast extract medium (YE5S) or Edinburgh minimal medium (EMM2). Compositions and specific variations of the media are described below:

YE5S: 0.5% (w/v) Difco Yeast Extract, 3.0% (w/v) glucose, 250 mg/L each of adenine, histidine, leucine, lysine hydrochloride, and uracil.

EMM2: 14.7 mM potassium hydrogen phthalate, 15.5 mM Na_2HPO_4, 2% glucose, 1X salts (50X salt stock solution: 52.5 g/L $MgCl_2$•$6H_2O$, 0.735 mg/L $CaCl_2$•$2H_2O$, 50 g/L KCl, 2 g/L Na_2SO_4), 1X vitamins (1000X vitamin stock: 1 g/L pantothenic acid, 10 g/L nicotinic acid, 10 mg/L biotin), 1X minerals (10,000X mineral stock: 5 g/L boric acid, 4 g/L $MnSO_4$, 4 g/L $ZnSO_4.7H_2O$, 2 g/L $FeCl_2.6H_2O$, 0.4 g/L molybdic acid, 1 g/L KI, 0.4 g/L $CuSO_4.5H_2O$, 10 g/L citric acid), and 5 g/L NH_4Cl. Amino acid supplements (200 mg/L) and glucose (2%) are added as required.

PMG: As EMM2 but 3.75 g/L L-glutamic acid monosodium salt is used instead of NH_4Cl as a nitrogen source. If PMG was used for live-cell imaging, supplements and glucose were added after autoclaving.

Low-N EMM2: Identical to EMM2 but 0.5 g/L NH_4Cl was used instead of 5 g/L.

EMM2-N: As EMM2 but lacks NH_4Cl altogether.

EMM2-SILAC: As EMM2 with the following changes: NH_4Cl concentration is at 640 mg/L (12 mM final); only amino acid supplements are 80 mg/L Arginine and 60 mg/L Lysine for light medium and 80 mg/L Arginine-6 and 60 mg/L Lysine-8 for heavy medium.

2% Difco Bacto agar was added for growth on solid plates. G418 (Geneticin), Nourseothricin (Nat), Hygromycin B (all at 100 µg/mL), and Blasticidin-S (at 10 µg/mL) were added when required for selection.

When working with *SISA* strains (including mating), to prevent activation of Sty1, 3BrB-PP1 (4-Amino-1-tert-butyl-3-(3-bromobenzyl)pyrazolo[3,4-d]pyrimidine; A602985) was added to liquid media (5µM 3BrB-PP1 final concentration) and to solid media (5µM, or 30µM 3BrB-PP1 when waking strains, to prevent possible suppressor mutations). As Sty1 activation in *SISA* strain was found to have adverse effects on the cell's physiology and was ultimately lethal, 1 in a 100 *SISA* cells forced to grow in 3BrB-PP1-free media was found to develop suppressor mutations.

Cultures were grown at either 25°C or 30°C on plates and liquid. Liquid cultures were continuously stirred by either 160 rpm shaker or 50 rpm rotating-wheel. For storage, fission yeast cultures were placed in YE5S + 25% Glycerol and kept at -80°C.

2.2 Genetic crosses

Fission yeast mating was performed on SPA5S plates (2% Difco Bacto agar, 30 g/L glucose, 5 g/L KH2PO4, amino acid supplements and 1X vitamins (as for EMM)). Strains to be mated were placed in close proximity onto the plate, mixed with 10 µl of distilled water, and placed at 25°C or 28 °C for 2 days to form asci. Next, either tetrad dissection or random spore analysis was performed. Tetrad dissection was done using a MSM 400 apparatus (Singer Instruments). For random spore, a patch of asci was resuspended in 300 µL dH_2O and incubated in 9 µL Snail Helicase (Thermo Scientific) at 32°C for 3-4 hours. Next, the digested asci were sonicated with several 5s pulses with 39% amplitude to achieve better separation and plated on an appropriate medium. Grown spores (1-2 mm diameter) from either method were subsequently replica plated on selection media.

2.3 Fission yeast DNA extraction

A single fission yeast colony was patched on a suitable plate one day prior to the DNA extraction. When patch reached approximately 0.5 cm^2 in size, cells were collected with a 200 µL tip and suspended in 30 µL of 0.25% (w/v) SDS in 1X TE pH 8.0 in a 200 µl PCR tube. The suspended cells were then incubated at 100°C for 5 min in a PCR machine. Finally, the boiled cells were centrifuged in a Technico-Mini mini-centrifuge for 30 seconds at RT. The supernatant was then used as DNA extract for colony PCR (see Section 2.4)

2.4 PCR amplification of DNA and colony PCR

Polymerase chain reaction (PCR) amplification of DNA was performed using a variety of thermal cyclers including PTC-200 (MJ Research), Biometra Uno (Biometra), and T-gradient (Biometra). When PCR products were used for cloning, gene tagging, or sequencing, the reactions were performed using Phusion High-Fidelity DNA Polymerase (Thermo Scientific) or Q5 High-Fidelity DNA Polymerase (NEB). When performing colony PCR a combination of homemade Taq (HMT) and Pwo polymerase was used. The following general reaction and cycling conditions were used:

Phusion/Q5 High-Fidelity polymerase PCR

Component	Concentration	Temperature cycles
Phusion HF buffer/ Q5 Reaction buffer	1X	1. 98°C for 2 min
Template DNA (plasmid)	1 ng/µL	2. 98°C for 15 sec
dNTPs (dATP, dTTP, dGTP, dCTP)	200 µM each	3. 50-70°C for 20 sec
Forward primer	0.5 µM	4. 72°C for 4 min
Reverse primer	0.5 µM	5. Steps 2-4 for 35 cycles
Phusion/Q5 polymerase	0.02 U/µL	6. 72 °C for 5 min
ddH_2O to desired volume		7. 20°C hold

HMT/Pwo polymerase colony PCR

Component	Concentration	Temperature cycles
*Buffer IV	1X	1. 95°C for 2 min
Template DNA (DNA extract)	0.5-1 µL extract	2. 95°C for 15 sec
dNTPs (dATP, dTTP, dGTP, dCTP)	500 µM each	3. 50-70°C for 20 sec
Forward primer	0.2 µM	4. 72°C for 4 min
Reverse primer	0.2 µM	5. Steps 2-4 for 35 cycles
$MgCl_2$	3.5 mM	6. 72 °C for 5 min
Triton X-100	1% (w/v)	7. 20°C hold
HMT polymerase	0.2 U/µL	
Pwo polymerase	0.003 U/µL	
ddH_2O to desired volume		

*10X Buffer IV contains 750 mM Tris-HCl pH 8.8, 200 mM $(NH_4)_2SO_4$, 0.1% Tween-20

To analyse the PCR products, samples were combined with 1X orange G buffer (10X stock: 0.2% Orange G, 30% Glycerol) and run on TAE (40 mM Tris, 0.1% glacial acetic acid, 1 mM EDTA) agarose gels by electrophoresis. Agarose concentrations ranging from 0.8% to 2% (w/v) were used based on expected product size. To visualize the resolved DNA using UV illumination 0.4 µg/mL of ethidium bromide was added to each gel. Electrophoresis was run at ~100V and a 1 kb DNA ladder (NEB) was used to determine PCR product size.

2.5 Strain construction using the PCR-based method

To generate C-terminal tags and deletions of fission yeast genes a PCR-base method was used (Bähler *et al*, 1998). First, primers were designed to have 80 bp 5' ends homology to the target genomic sequence of interest and 20 bp 3' end homology to the pFA6 tagging cassette. Next, a PCR product was generated using the primers and the appropriate pFA6 vector as a DNA template (see Section 2.4). In addition to the 80 bp homology arms, the amplified sequences contained: antibiotic resistance cassettes (G418, hygromycin, nourseothricin), C-terminal tags (GFP, mECitrine, 3xmCitrine, mCherry, 3xmCherry) with an antibiotic resistance cassette, or the *ura4* gene. Approximately 5-20 µg of DNA was produced and used for each transformation.

Prior to transformation, the PCR products were cleaned-up using NucleoSpin Gel and PCR Clean-up kit (Macherey-Nagel) according to the manufacturer's protocol for PCR Clean-up. Alternatively, a phenol/chloroform/isoamyl alcohol (PCI) extraction was performed where equal volumes of PCR reaction and PCI were mixed and centrifuged at 13,000 rpm for 5 minutes. The resulting supernatant was obtained, mixed with fresh PCI in a new tube, and the process was repeated. Next, chloroform was added to remove residual PCI and samples were centrifuged again at 13,000 rpm for 5 minutes. The resulting supernatant was obtained and mixed with NaOAc (pH 5.2) to a final concentration of 0.3M (from 3M stock). Finally, the DNA was precipitated by mixing with an equal volume of isopropanol, incubating at RT for 5 min, and spinning for 10 minutes at 13,000 rpm in a 4°C-cooled centrifuge. The resulting pellets were washed with 70% ethanol, dried, and resuspended in ddH_2O.

For the transformation, yeast parent strains were grown in the appropriate medium to a 20 mL culture with an OD_{595} of 0.8, which corresponded to approximately 10^7 cells per mL of culture. Cells were collected by centrifugation at 4,000 rpm for 2 min, at RT, and the pellet was washed with an equal volume of water and spun again at 4,000 g for 2 min, at RT. Next, the pellet was resuspended in 1 ml ddH_2O and transferred to a 1.5 mL Treff tube. Cells were spun again (13,000 rpm, 1 min, RT) then the pellet was washed with 1 mL 100 mM LiOAc, 1X TE pH 7.5. Next, cells were spun again at 13,000 rpm, 1 min, at RT and the pellet was resuspended in 100 mM LiOAc, 1X TE pH 7.5 to a final volume of 100 µL. Afterwards, 30 µL of DNA (5-20 µg) was added the reaction was incubated at RT for 10 min. Next, 260 µL of freshly-made 40% (w/v) PEG-4000 in 100 mM LiOAc, 1X TE pH 7.5, was added and mixed. The sample was then incubated at 30°C for 1 h. Following the incubation, 43 µL of DMSO was added and cells were heat shocked at 42°C for 5 min. Transformed cells were

then centrifuged (13,000 rpm, 1 min, RT) and washed with 1 mL of ddH_2O, centrifuged again and resuspended in 0.5 mL of ddH_2O. Two cell suspensions of 250 µL were then plated out onto appropriate non-selective medium using sterilised glass beads to spread the cells.

Following O/N incubation at 32°C or two-day incubation at 25°C, cells were replica-plated to appropriate selection plates. The replica plating onto selective media was repeated after two days (32°C) or 3-4 days (25°C), and cells were grown O/N. Single colonies were checked for stable genomic integration of the desired insert by streaking on non-selective plates and later replica plating on selective plates. If the entirety of streaked cells (originating from a single colony) were able to grow on the selective plate, the isolate was considered to contain a stable integration. Finally, this integration was confirmed by colony PCR (see Section 2.4).

2.6 DNA sequencing

For sequencing of certain fission yeast mutations, the region of interest was first amplified according to the colony PCR protocol (see Section 2.4). Next, the product was gel-purified and used as template for the sequencing reaction. When sequencing plasmids, plasmid DNA was used directly. The reaction was setup using the BigDye Terminator v3.1 kit (Applied Biosystems) in 10 µl total volume as follows:

BigDye sequencing reaction

Component	Concentration	Temperature cycles
DNA template from plasmid or PCR	10 or 25 ng/ µL	1. 96°C for 30 sec
Primer	0.5 µM	2. 50°C for 15 sec
BigDye Terminator mix v3.1	1X	3. 60°C for 4 min
ddH_2O to 10 µL		4 Steps 1-3 for 25 cycles.
		5. 4°C hold

Sequencing was then carried out on by the University of Edinburgh GenePool sequencing facility, using ABI 3730 capillary sequencing instruments (Applied Biosystems). The sequencing files were analysed using Seqman sequence analysis software (DNASTAR Inc.).

2.7 Cloning of CRIB-containing vectors

To generate the CRIB-3xmCitrine vector, CRIB and 3xmCitrine DNA coding sequences were synthesised as two separate fragments by GeneArt (ThermoFisher).

For the CRIB component, the sequence encoding the CRIB domain of the *S. cerevisiae* Gic2 protein (amino acids 1-208, with an intentional mutation W23A;(Jaquenoud & Peter, 2000; Okad*a et al*, 2013) was codon-optimized for *S. pombe* expression, and additional sequence was added to the 3' end to encode a C-terminal linker GDGAGLIN. The CRIB-plus-linker fragment was cloned into pMA-T (GeneArt) to generate the plasmid pKS1304. For the 3xmCitrine component, codon usage was varied in each of the three mCitrine sequences, so that each mCitrine nucleic acid sequence is only ~70% identical to the other two, although all three encode the same amino-acid sequence. This decreases the likelihood of undesired recombination occurring between tandem mCitrine sequences during genetic crosses. The 3xmCitrine fragment was cloned into pMK-RQ (GeneArt) to generate plasmid pKS1303. The 3xmCitrine fragment was excised from pKS1303 using SalI and BamHI and cloned into SalI and BamHI sites in pKS1304, placing the 3xmCitrine tag downstream of and in frame with the CRIB-plus-linker fragment, to generate plasmid pKS1305. Next, the entire CRIB-3xmCitrine fusion gene was excised from pKS1305 using NdeI and BamHI and cloned into NdeI and BamHI sites in the vector pRAD13 (kind gift from Y. Watanabe) which places the fusion gene under control of the *adh13* promoter (a weakened *adh1* promoter; (Sakuno *et al*, 2009)) to generate plasmid pKS1374. pKS1374 was linearized using BlpI to allow for stable integration into the fission yeast *ars1* locus, using LEU2 as a selection marker. Additionally, several alternative CRIB or CRIB-like domains fused with the C-terminal GDGAGLIN linker were synthesised and cloned into the pKS1374, replacing the original Gic2-CRIB. These are described in detail in Appendix 1.

2.8 Construction of IPTG-inducible GFP strain

To generate a strain with IPTG-inducible GFP expression, we used the plasmid pSK173 ((Kjaerulff & Nielsen, 2015) see important erratum, doi: 10.1002/yea.3136). This plasmid, also known as nmt::lacO*-GFP, contains a copy of GFP under the control of the thiamine-repressible nmt1 promoter, with a lacO operator sequence inserted five base pairs downstream of the nmt1 TATA box, as well as a copy of the lac repressor (lacI), fused to a nuclear localization sequence, under the control of an SV40 promoter. pSK173 was linearized using AfeI and stably integrated into the ars1 genomic locus using ura4+ as a selection marker.

2.9 Cell counting

For growth curves of the SISA strain, cells were initially grown to a cell density of 2 x 10^6/mL in YE5S containing 5µM 3BrB-PP1 at 25 °C. Cells were then filtered through a 0.45 µm membrane filter (Millipore, HVLP04700). Filters were then either transferred to one culture volume of YE5S containing 5µM 3BrB-PP1 or washed twice with YE5S (one culture volume per wash) and then transferred to one culture volume of YE5S. The resuspended cultures were then grown in a 25 °C water bath and samples were collected hourly. Each sample was fixed by addition of 37% formaldehyde (formalin) solution to a final concentration of 3.7% formaldehyde. Dilutions of the fixed samples were measured using Z2 Coulter Particle counter (Beckman-Coulter) using a 4-12 µm particle range setting.

2.10 Preparation of yeast whole cell extracts using native bead-beating

To prepare cell lysates for measuring Sty1 activation on western blots after stress, cell cultures were grown at 25°C in YE5S to a cell density of 1.25 x 10^7 cells/mL. Next, DMSO (1% final), LatA (50 µM final, with 1% DMSO final; obtained from Alpha Laboratories (129-04361) or Abcam (ab144290)), or KCl (0.6 M final, from 3M stock in YE5S) was pipetted and mixed into the cell cultures. Samples of 1.6 mL (or 1.9 mL for KCl, because of increased volume) were collected into 2 mL crew-cap microcentrifuge tubes at the indicated times and immediately centrifuged at 4000 rpm at 4°C for 1 min. The supernatant was quickly removed and cell pellets placed on ice. Cell pellets were resuspended in 1 mL ice-cold 10mM $NaPO_4$ 0.5mM EDTA pH 7.5 buffer and centrifuged again at 13,000 rpm at 4°C for 1 min. The supernatant was removed, and the cell pellets were flash-frozen in liquid nitrogen and stored at -80°C until further processing. For cell lysis, 0.5 mm zirconium/silica beads pre-chilled to -20°C (BioSpec; 11079105z) were added to the cell pellet, together with 40 µL ice-cold lysis buffer containing: 150 mM NaCl, 20 mM Tris-HCl pH 7.5, 0.05% Triton X-100, 10 µg/mL each of 'CLAAPE' protease inhibitors (chymostatin, leupeptin, antipain, pepstatin, E64), 2 mM DTT, 6 mM MgCl2 1 mM PMSF, 1 mM Benzamidine, 50 mM β-glycerophosphate, 50 mM EDTA, 1 mM NaF, 50 nM Calyculin A, 50 nM Okadaic acid, 100 nM Na3VO4, 2 mM AEBSF, 10% Glycerol. The suspension was put in a Ribolyser bead-beater (Hybaid) and four cycles of bead-beating were run: one cycle of 60 sec and three subsequent cycles of 30 sec each, all at speed setting "4". Between each cycle, samples were chilled in an ice-water slurry for 2 min. After bead-beating, the lysate in the screw-cap tubes was recovered by puncturing the tubes and

centrifuging into a second tube. Cell lysates were then clarified by centrifugation at 13,000 rpm at 4°C for 10 min. One-third volume of 4X Laemmli sample buffer was then added to clarified lysates, which were then boiled at 100°C for 5 min and flash-frozen in liquid nitrogen.

To prepare SISA cell lysates for measuring Atf1 on western blots, parallel cell cultures were grown at 25°C in YE5S containing 5µM 3BrB-PP1 to a cell density of 1.25 x 107 cells/mL. Cells were then filtered as described above, and washed twice, either with YE5S (one culture volume per wash) or with YE5S containing 5µM 3BrB-PP1 (one culture volume per wash), as appropriate. Cells were then resuspended in one culture volume of YE5S or YE5S containing 5µM 3BrB-PP1, as appropriate, and grown at 25 °C in a shaking water bath. Samples of 1.9 mL were collected into 2 mL screw-cap microcentrifuge tubes at the indicated time points and processed as described above.

2.11 SDS-PAGE, coomassie staining, and Western blotting

All sodium dodecyl sulphate polyacrylamide gel electrophoresis (SDS-PAGE) was performed with 5% acrylamide stacking gels and 8-12% acrylamide (both using acrylamide to bis-acrylamide ratio of 37.5:1) in 1X Laemmli running buffer (25 mM Tris-base, 192 mM glycine, 0.1% SDS, pH 8.3). For casting the gels. the Mini-Protean (BioRad) or "low-wide" 10x20 cm (Scie-Plas) systems were used. Protein samples were prepared in Laemmli sample buffer (LSB, 2% SDS, 10% glycerol, 60 mM Tris-HCl pH 6.8, 0.01% bromophenol blue, 100 µM DTT), boiled and centrifuged for 1 min at 13,000 rpm before loading.

To coomassie stain the resolved gels, they were transferred to a staining solution (25% isopropanol, 10% acetic acid, 0.05% Brilliant Blue R-250) and heated for 1 min in a microwave on high power. The tray was then placed on a gyro-rocker for 10-15 minutes. Staining solution was replaced with a destaining solution (10% acetic acid), absorbent paper towel was placed in the tray, and the gel was again heated in the microwave for 1 min at high power. Gels were left in destaining solution until the desired contrast between bands and gel was achieved.

If western blotting was to be performed, resolved SDS-PAGE protein gels were transferred on to 0.2 µm nitrocellulose membrane in 10 mM CAPS 10% methanol using a wet blotting apparatus (Biorad). Upon completion of transfer, blots were first

stained with Ponceau S (0.2% Ponceau S, 3% trichloroacetic acid, 3% sulfosalicylic acid), destained using 5% acetic acid, and scanned to normalise for protein content between lanes. Next, Ponceau S staining of the blots was washed away using a single dH_2O wash, followed by incubation in Tris-buffered Saline (TBS) until staining was not clearly visible. Blots were then blocked for 1 hour in 2% non-fat dried milk, 0.2% Tween 20 in TBS. Incubation with primary antibodies was then performed in blocking solution at 4 °C overnight. All primary antibodies were used at 1:1000 dilutions. After the primary incubation, blots were washed with 0.02% Tween 20 in TBS (TBST) and incubated with secondary antibody in blocking solution for 1 hour at RT. If a tertiary antibody incubation was needed, the washing and incubation steps were repeated. All secondary or tertiary antibodies were used at 1:10,000 dilutions. Prior to scanning, the blot was washed with TBST followed by TBS. For measuring Sty1 activation, blots were probed with monoclonal rabbit anti-phospho-p38 primary antibody (Cell Signaling Technology; #4511) and IRDye 800CW Donkey anti-Rabbit secondary antibody (Licor; 925-32213). For measuring Atf1, blots were probed with monoclonal mouse anti-ATF1 primary antibody (Abcam; ab18123) and IRDye 800CW Donkey anti-Mouse secondary antibody (Licor; 925-32212). For measuring Sty1 levels, a 'home-made' sheep serum (please see Section 2.14) was used for primary binding. Next, an unlabelled GT-34 mouse monoclonal anti-goat antibody (Sigma, G2904) was used to amplify the signal and IRDye680LT donkey anti-mouse antibody (Licor; 925-68022) as a final label. Blots were imaged using an Odyssey fluorescence imager (Licor) and quantified using Image Studio Lite (Licor). Ponceau S scans were converted to 8-bit images using ImageJ and imported in Image Studio Lite for quantification.

2.12 Microscopy sample preparation and imaging

All live-cell imaging experiments were performed with exponentially growing cells grown at 25°C. Experiments were performed in YE5S medium, with the exception of nitrogen-starvation (N-starvation) experiments, which were performed in low-N EMM2 and EMM2-N; and GFP IPTG-induction experiments, which were performed in PMG, with glucose added to the medium after autoclaving.

For preparation of imaging slides, coverslip dishes (MatTek; P35G-0.170-14-C.s) or 4-chamber glass bottom micro-slides (Ibidi; 80427) were placed on a 25°C heat block, coated with 1mg/mL soybean lectin (Sigma; L1395), left for 10 min, and washed

with appropriate medium to remove excess lectin. Cell cultures were added to dishes/slides and left to settle for 15 minutes. Next, the cells were washed extensively with appropriate media using aspiration with at least 3 full exchanges of media (at least 1 mL each). Finally, 400µL (or 600 µL for N-starvation) of medium was used to cover the cells and the preparations were quickly placed in the microscope chamber at 25°C.

Live-cell fluorescence imaging was performed using a custom spinning-disk confocal microscope setup consisting of a Nikon TE2000 microscope base, attached to a modified Yokogawa CSU-10 unit (Visitech) and an iXon+ Du888 EMCCD camera (Andor). The microscope was also equipped with a 100x/1.45 NA Plan Apo objective (Nikon), Optospin IV filter wheel (Cairn Research), MS-2000 automated stage with CRISP autofocus (ASI), and temperature-controlled chamber maintained at 25°C (OKOlab). The microscope was controlled using Metamorph software (Molecular Devices).

All drug additions during imaging, except for N-starvation experiments, were performed by two consecutive medium exchanges with 400µl of drug-containing medium, using a 1mL polyethylene transfer pipette (Fisher Scientific, 1346-9118). All treatments were completed between the imaging intervals so that the time-lapse acquisition is not disrupted. Due to the mechanical force exerted during the medium exchanges, re-focusing of the sample between acquisitions was sometimes needed.

For conventional LatA addition experiments, YE5S containing 50 µM LatA and 1% DMSO (all final concentrations) was used. YE5S containing 1% DMSO was used as a negative control. Exchange of medium was performed between frames 4 and 5 of imaging (i.e. 9 -12 min after start of imaging).

For experiments involving 3-BrB-PP1 pre-treatment prior to LatA addition, exchange of medium to YE5S containing 5 µM (or 30 µM) 3-BrB-PP1 was performed 30 s before the start of imaging. The subsequent exchange of medium to YE5S containing 5 µM (or 30 µM) 3BrB-PP1 plus 50 µM LatA was performed between frames 4 and 5 of imaging, as above.

For cycloheximide (CHX) pre-treatments, exchange of medium to YE5S containing 100 µg/mL CHX (from 10 mg/mL CHX stock in water; Sigma; C1988) was performed 30 seconds before the start of imaging. The subsequent exchange of

medium to YE5S containing 100 µg/mL CHX plus 50 µM LatA was performed between frames 4 and 5 of imaging, as above.

For 3-BrB-PP1 removal experiments in *SISA* cells and *tea1*Δ *SISA* cells, cells were first grown and prepared for imaging in YE5S containing 5 µM 3-BrB-PP1. MatTek dishes were used for imaging. 3-BrB-PP1 removal was performed by three separate rounds of medium exchange after frames 3, 4 and 5 (i.e. 6 -15 min after start of imaging). Each round of medium exchange involved 6 x 1mL exchanges to YE5S. These additional exchanges (18 in total, far greater than in drug-addition experiments) were necessary for complete removal of 3-BrB-PP1. For this reason, the stated time of 3-BrB-PP1 removal in these experiments is approximate (we chose frame 5 to represent the "0 min" time). For the 3-BrB-PP1 re-addition experiments in *SISA* and *tea1*Δ *SISA* cells, a conventional medium exchange to YE5S containing 5 µM 3-BrB-PP1 was performed between frames 35 and 36 (102 -105 min after start of imaging). For the experiments in *tea1*Δ *SISA* cells where 3-BrB-PP1 was removed for 5 hours, imaging was started right after the 3-BrB-PP1 re-addition.

For N-starvation experiments, cells were first grown as pre-cultures overnight in low-N EMM2 at 25°C, and then diluted into fresh low-N EMM2 and grown for another 12-16 hours at 25°C to a density of 1.5-5 x 10^6 cells/mL. To exchange to EMM2-N medium, 1 mL of cells was washed twice by 1 min centrifugation at 4,000 rpm and resuspension in an equal volume of EMM2-N medium. Cells were then placed on a lectin-coated MatTek coverslip dish as described above and covered with 600µL of EMM2-N. Prior to imaging, the cells were incubated on the dish for 10 hours at 25 °C, during which time most cells had divided twice to generate chains of four small cells. For addition of 3-BrB-PP1, the medium from the dish was withdrawn using a 1mL transfer pipette and quickly transferred to a microfuge tube already containing 0.6 µL of 5 mM 3-BrB-PP1 in EMM2-N, thereby converting the existing culture medium to EMM2-N containing 5µM 3-BrB-PP1. This medium was then returned to the cell dish, withdrawn once more and then returned again to the dish; this ensures good mixing without perturbing the cells. To mimic this treatment for control mock-treated cells (i.e. cells not treated with 3-BrB-PP1), the medium was withdrawn from the dish, returned to the dish, withdrawn once more, and then returned again. The medium changes were performed between frames 11 and 12 (60-66 min after start of imaging). Medium changes of this nature were used instead of using fresh EMM2-N because fresh, "non-conditioned" EMM2-N appeared to cause a shock to the cells.

For IPTG-GFP induction experiments, cells were initially grown in PMG (with appropriate supplements), and exchange of medium was performed as described above for drug addition. PMG was exchanged either to: fresh PMG; or to fresh PMG containing 5 mM IPTG (from 1M stock in water); or to fresh PMG containing 5 mM IPTG plus 100 µg/mL CHX. Exchange of medium was performed 30 s before the start of imaging. In an additional experiment, to assay inhibition of protein synthesis after GFP expression was already induced, medium was exchanged from PMG to PMG containing 5 mM IPTG at 30 s before the start of imaging, and then later from PMG containing 5 mM IPTG to PMG containing 5mM IPTG plus 100 µg/mL CHX, between frames 36 - 37 (175 -180 min after start of imaging).

For phalloidin staining of fixed cells after LatA treatment, cells not expressing Lifeact-mCherry were grown to exponential phase in YE5S, and LatA was added to a final concentration of 50 µM LatA. Fixation with formaldehyde and staining with Alexa Fluor

Table 2.1. List of image acquisition parameters

Image Type	Laser power (%)*, exposure time (ms)			Z-series	Time-lapse
	488 nm	514 nm	594 nm		
CRIB-3xmCitrine		2%, 40 ms		11x 0.6 µm	60 x 3 min
Lifeact-mCherry			30%, 100 ms	11x 0.6 µm	60 x 3 min
CRIB-3xmCitrine (N-starvation)		2%, 100 ms		11x 0.6 µm	40 x 6 min
GFP-IPTG	5%, 150 ms			11x 0.9 µm	72 x 5 min
Sty1-mECitrine		2%, 200 ms		9x 0.7 µm	30 x 5 min
Cdc42-mCherry^{SW}			30%, 100ms	11x 0.6 µm	60 x 3 min
CRIB-3xmCitrine (with Scd2-3xmCherry)		2%, 40 ms		5x 1 µm	60 x 3 min
Scd2-3xmCherry			80%, 300ms	5x 1 µm	6 x 30 min
Alexa Fluor 594 phalloidin (fixed cells)			60%, 200ms	11x 0.6 µm	N/A
CRIB-3xmCitrine (fixed cells)		10%, 100ms		11x 0.6 µm	N/A
CRIB-3xmCitrine		2%, 40 ms		11x 0.6 µm	5 x 30 min

(with Scd1-3xmCherry or Gef1-3xmCherry)					
Scd1-3xmCherry			80%, 300ms	11x 0.6 µm	5 x 30 min
Gef1-3xmCherry			80%, 300ms	11x 0.6 µm	5 x 30 min
mini-Shk1-CRIB-3xmCitrine		2%, 200 ms		11x 0.6 µm	60 x 3 min

* “100%” power = 50 mW for 488 nm laser, 40 mW for 514 nm laser, and 50mW for 594 nm laser.

594 phalloidin (Molecular Probes) were exactly as described previously by Sawin & Nurse, 1998. The zero time point represents cells just prior to LatA addition.

For phalloidin staining of Sty1-activated SISA cells, SISA cells (not expressing Lifeact-mCherry) were grown in YE5S containing 5µM 3-BrB-PP1 and then washed twice by filtration and resuspension in YE5S medium lacking 5µM 3-BrB-PP1, as described above for physiological experiments. Fixation and staining procedures were exactly as described previously by Sawin & Nurse, 1998.The zero time point represents cells just prior to filtration.

For DIC images of *SISA* cells after 3-BrB-PP1 removal, 1mL of exponentially growing cells in YE5S containing 5µM 3-BrB-PP1 was washed twice by 1 min centrifugation at 4,000 rpm and resuspension in an equal volume of YE5S. Washed cells were then further diluted with an additional 4 mL of YE5S and incubated at 25° for 24 hours, prior to imaging. Images were taken using a DeltaVision Elite system using Olympus 60x / 1.42 Oil Plan APO objective. Control cells grown in YE5S containing 5µM 3-BrB-PP1 were imaged during exponential growth.

For screening multiple clones expressing fluorescently-tagged proteins a Zeiss Axio Imager Z1 was used.

2.13 Image processing, quantification, and figure preparation

Processing of the acquired raw images was done using ImageJ (NIH), using the StackReg plugin for Rigid Body registration (http://bigwww.epfl.ch/publications/thevenaz9801.html) and KymoResliceWide plugin for kymographs (http://fiji.sc/KymoResliceWide). Images were adjusted using linear contrast enhancement and are presented as maximum or sum projections containing the entire cell volume. Formatting of images for preparing figures was done using

Illustrator or Photoshop CS6 (Adobe). Movies were assembled using ImageJ, QuickTime (Apple), or Photoshop CS6.

For quantification of GFP expression under different conditions in IPTG-induction experiments, movies were acquired at multiple stage positions for each condition. For each condition, the time-course of expression was then determined as follows: First, sum projections of images were made for all time-points of movies, and background extracellular fluorescence was subtracted to calculate the value of the fluorescent signal $S_{c,t}$ for a given cell *c* (or small group of cells) at a given time-point *t*. These values were then normalised to the fluorescent signal $S_{c,1}$ for the same cell (or small group of cells) at the first time-point. Then, for each time-point *t*, the mean value of normalised fluorescence was calculated by averaging over all *n* cells imaged. We then subtracted 1 from mean values in order to generate a baseline of zero at the first time-point, and we then multiplied this result by an arbitrary constant (100) to generate a final value $100\times\left[\frac{1}{n}\left(\sum_{c=1}^{n}\frac{S_{c,t}}{S_{c,1}}\right)-1\right]$, which represents induced GFP fluorescence (in arbitrary units) for each time-point *t*. For each of the different conditions, the number of cells (*n*) imaged was as follows: -IPTG (*n* =26); +IPTG at t=0, +CHX at t=0 (*n* =23); +IPTG at t=0, +CHX at t=180 min (*n* =19); +IPTG (*n* =16).

Quantification of Sty1-mECitrine levels in the nucleus was obtained from movies by automated image analysis performed by Dr. Marcin Leda (Goryachev group, University of Edinburgh). The following description of the methodology was also initially provided by Dr. Leda with additions from Dr. Ken Sawin. For DMSO treatment, 14 movies were analysed. For LatA treatment, 27 movies were analyzed. First, segmentation algorithms were used to identify cells and nuclei from maximum projections of z-stacks. Cell segmentation was carried out by the active contour Chan-Vese method, implemented in MATLAB. Initial binary masks for cell segmentation were obtained using multi-threshold Otsu's method (*multithresh* in MATLAB) with nine thresholds. Bitmaps containing only those pixels that were above the fifth threshold were then processed using additional morphological operations to 1) first, identify pixel clusters ("connected components"; *bwconncomp* in MATLAB); 2) then, join nearby clusters by removing holes between neighboring clusters; and 3) finally, remove small pixel clusters (= out of focus cells) and pixel clusters touching frame borders (= partial, incomplete cells). Nucleus segmentation was carried out starting with the masks obtained by cell segmentation. First, pixel intensity values in each

individual cell were separately normalised to an interval from 0 to 1. Then, multi-threshold Otsu's method with five thresholds was used to construct bitmaps containing only those pixels that were above the third threshold. Identification of morphologically connected clusters was then used to generate a mask for the nucleus belonging to a given cell. Cells that contained two nuclei (i.e. dividing cells) were rejected from analysis. From the cell segmentation and nucleus segmentation, we obtained binary masks of nucleus and corresponding cytosol (by subtracting nucleus mask from cell mask) for every cell, as well as a binary mask for extracellular space (background). Sum projections of z-stacks were used for quantification of signals inside these masks. The nucleus-specific fluorescence intensity was calculated as $\left[\frac{(I_n - I_b)}{(I_c - I_b)} - 1\right]$, where I_n, I_b and I_c are average intensities in nucleus, cytosol and background, respectively. We note that in these experiments, a small, transient increase in Sty1-mECitrine nuclear fluorescence was observed in DMSO-treated control cells upon addition of DMSO. This is reproducible and appears to be a consequence of acute DMSO addition, from which the cell rapidly recovers.

2.14 Cloning, bacterial expression, and purification of Sty1-His_6 for antibody production

All *Escherichia coli* (*E. coli*) cultures were grown at 37ºC in liquid LB media (10 g/L Difco Bacto tryptone, 5 g/L Difco Bacto yeast extract, 5 g/L NaCl, pH 7.2) or on solid LB-agar plates (LB + 2% Difco Bacto agar). For antibiotic selection, Ampicillin was used at 100 mg/mL.

To generate recombinant expression vector containing Sty1 with C-terminal His_6 tag, first, the Sty1 ORF was obtained from the Matsuyama fission yeast ORFeome collection (Matsuyam*a et al*, 2006). Plasmid DNA of the ORF incorporated in pDONR211™ (Invitrogen) was obtained from the corresponding bacterial clone using the Nucleospin Plasmid Kit (Macharey-Nagel) following the manufacturer's protocol. The presence of Sty1 ORF in the vector was confirmed using restriction digestion with BglI. Next, the Sty1 ORF was cloned to the destination expression vector p0GWA (Busso *et al*, 2005) using the Gateway® LR Clonase® II kit (Invitrogen) according to the manufacturer's instructions. The obtained expression vector (pKS1306) was then transformed into BL21-Codon Plus competent *E.coli* cells following the manufacturer's protocol (Stratagene).

For the expression and purification of Sty1-His_6, a stationary overnight culture of the pKS1306-carrying BL21 cells was diluted 1:50 in two separate flasks containing 2 L pre-warmed LB medium (40 mL of stationary culture in each flask) and grown at 37°C for 2 h. Sty1-His_6 protein expression was then induced using 1 mM IPTG (Melford) for 2.5 h. Cells were then harvested using Beckmann Avanti J-26 centrifuge and JLA 8.1000 rotor at 6000 rpm for 10 min at 4°C. The obtained cell pellet (7 mg) was collected, transferred into a polythene bag, and snap-frozen in liquid nitrogen. Bags were stored at -80°C.

For obtaining Sty1-His_6-containing protein extracts from inclusion bodies, cell pellets were first resuspended in 2 cell volumes (assuming 1 g cells equals 1 mL) of lysis buffer (20 mM Tris pH 8.0, 1 mM EDTA, 5 mM MgCl2, 0.3 mM PMSF, 8 U/ml benzonase, 400 µg/mL lysozyme) and incubated with stirring for 20 min at RT. Next, the cells were lysed by passing the cell suspension three times through a French press at 1500 psi Gauge pressure at RT. Next, NaCl to 300 mM final and TX-100 to 1% final was added to the lysate, followed by addition of an equal volume of resuspension buffer (50 mM Tris 8.0, 300 mM NaCl, 1 mM EDTA, 1% TX-100, 0.3 mM PMSF). The solution was vortexed and inclusion bodies were separated by centrifugation at 10000 rpm for 10 min at 4°C. The pellets containing the inclusion bodies were washed three times by resuspending in approximately 30 mL of RB using a Dounce pestle and then centrifuging at 10000 rpm for 10 min at 4°C. After the third wash and centrifugation, the supernatant was discarded ad the pellet was resuspended in 4 volumes (assuming 1 g cells equals 1 mL) of PBS (Phosphate Buffered Saline; 1.5 mM KH2PO4, 5.1 mM Na2HPO4, 150 mM NaCl, pH 7.4). The 20% inclusion bodies-suspension was snap-frozen in liquid nitrogen and kept in -80°C.

The Sty1-His_6 protein was purified from the inclusion bodies-suspension using a column with Ni^{2+}-Sepharose beads. For the purpose four buffers were used: Buffer AG (25 mM Tris pH 8.0, 300 mM NaCl, 10 mM Imidazole, 6 M guanidinium hydrochloride), Buffer AU (25 mM Tris pH 8.0, 300 mM NaCl, 10 mM Imidazole, 6 M urea), Buffer BG (25 mM Tris pH 8.0, 300 mM NaCl, 300 mM Imidazole, 6 M guanidinium hydrochloride), and Buffer BU (25 mM Tris pH 8.0, 300 mM NaCl, 300 mM Imidazole, 6 M urea). First, the column was loaded with 20 mL (1 column volume (cv)) of a 6:1 mixture of Sepharose and Sepharose-GSH beads in ethanol. The column was washed with 3 cv of water to remove the ethanol. Next, the beads were

activated by passing 2.5 cv of 500 mM $NiCl_2$ solution twice through the column. Beads were then washed with 2 cv 3% BG 97% AG Buffer. The inclusion bodies suspension was solubilized in 3% BG 97% AG buffer (up to 20X the volume of initial inclusion bodies suspension), heated for 20 min at 65ºC, and spun for 10 min at 4000 rpm at 4°C. The supernatant was then passed through the Ni^{2+}-Sepharose column twice; second time flow-through was collected for later analysis. Next, the column was washed with 2 cv 3% BG 97% AG Buffer, followed by 1 cv 3% BU 97% AU Buffer, followed by 5 cv 10% BU 90% AU Buffer. Elutions from the beads were performed using 4 cv 30% BU 70% AU Buffer followed by 4 cv 100% BU Buffer. After SDS-PAGE analysis, the Sty1-His_6-enriched elution fractions were pooled together and concentrated using Trichloroacetic Acid (TCA) precipitation. For the purpose, the pooled sample was diluted in water until the urea concentration was 1 M. Next, 100% TCA was added to a final concentration of 10% and the sample was incubated for 30 min at 4°C. The sample was then centrifuged at 21,000 x g for 15 min at 4°C. The supernatant was discarded and the resulting pellet was washed 3 times using 1 mL ice-cold 70% acetone, 20% ethanol, 10 mM Tris-HCl pH 7.5, 0.0025% bromophenol blue solution with a 21,000 x g 10 min centrifugation at 4°C between the washes. The pellet after the final wash was left to air dry for 10 min, then resuspended in 7 mL of 2 x LSB and boiled at 100 °C for 5 min. The sample was then loaded on two large preparative SDS-PAGE gels (Protean, II System, BioRad). The gels were run at 175 mA each, for approximately 5 h. Following very brief Coomassie staining, a band containing the Sty1-His_6 protein was excised from each gel, lyophilized, and manually ground to a fine powder in a mortar chilled on dry ice. At the end, approximately 2.2 grams of fine powder were obtained which were stored at -80 °C, before submission for antibody production in sheep.

2.15 Growth of cell culture and protein lysate preparation for SILAC phospho-proteomics

For the two SILAC phospho-protemics experiments, *SISA* cells containing the SILAC alleles (*car2*Δ *arg1-230 lys3-32*) were grown in liquid culture at 25°C in either heavy or light EMM2-SILAC medium (see section 2.1) in the presence of 5 µM 3BrB for a minimum of 10 generations. Finally, 500 mL of both light and heavy cultures of OD_{600} ~0.26 (first experiment) or ~0.6 (second experiment) were obtained. Cells from each culture were then transferred to fresh EMM-2 SILAC medium with or without 5

µM 3BrB using filtration. The filtration was achieved using two parallel filtration devices with 250 mL of culture processed in each device. Cultures which were to be transferred to the same medium (for example, from EMM-2 SILAC +3BrB to EMM-2 SILAC +3BrB) were washed with 1x culture volume of that medium during filtration. Cultures which were to be transferred to a different medium (for example, from EMM-2 SILAC +3BrB to EMM-2 SILAC -3BrB) were washed with 2x culture volume of that medium during filtration. For the first experiment, the light culture was transferred to EMM-2 SILAC with 5 µM 3BrB, while the heavy to EMM-2 SILAC without 5 µM 3BrB. In the second experiment, the light culture was transferred to EMM-2 SILAC without 5 µM 3BrB, while the heavy to EMM-2 SILAC with 5 µM 3BrB. Next, the cultures were grown for 45 min at 25°C and then harvested by centrifugation at 4000 rpm for 2 min at 4°C. Pellets of each culture were resuspended in 40 mL of dH_2O in a 50 mL falcon and then spun again at 4000 rpm for 2 min at 4°C. The pellets were then weighed and resuspended in1 mL dH_2O per 400 mg of pellet. The resuspended pellets were then drop-by-drop flash-frozen in liquid nitrogen using a pipette and then stored at -80 °C.

The frozen pellets from each culture were then lysed to a powder in the presence of liquid nitrogen using a SPEX SamplePrep 6870 Freezer/Mill Cryogenic Grinder with the following settings: Cycles – 8, Pre – 2 min, Run – 2 min, Cool – 2 min, and Rate – 10 cps. The powder obtained from each culture was weighed and solubilized in 3 mL of 8M urea per 1 gr of powder in 50 mL falcon tubes using rotation at RT for 30 min. Next, the solubilized lysates were clarified by spinning 1 to 3 times for 30 min at 4000 rpm at RT. The protein concentration in each clarified lysate was then quantified using Bradford assay (Biorad) and light and heavy lysates were combined in 1:1 ratio (based on protein concentration) to a total of 5.74 mg (first experiment) and 9.76 mg (second experiment) of protein. About 100 µg of 1:1 light and heavy lysate mix were taken out and stored at -20°C to be later analysed for protein abundance (See Section 2.20). The rest of 1:1 lysate mix was then processed further, prior to liquid chromatography-tandem mass spectrometry (LC-MS^2) analysis.

2.16 In-solution digestion of 1:1 SILAC lysates

For each of the two experiments the 1:1 SILAC lysate mix in 8M urea was first reduced by adding 1 mM DTT (final) in 50 mM ABC (ammonium bicarbonate) for 1 hour at RT. Next, the sample was alkylated by adding 55 mM IAA (iodoacetamide; final) in 50 mM ABC for 1 hour at RT in the dark. The sample was next digested using

10 µg lysyl Lys-C peptidase (Wako Chemicals, 125-05061) per 1 mg of total protein for 3 hours at RT. After this digestion, the sample was diluted with dH_2O so the total concentration of urea was reduced to 1.6 M. Then, the sample was further digested by adding 10 µg Trypsin (ThermoFisher, 90057) per 1 mg of total protein for 16 hours at RT. The digestion was stopped by adding trifluoroacetic acid (TFA) to a final concentration of 0.4%. Finally, the sample was clarified by centrifuging 1 to 3 times for 10 min at 4000 rpm at RT and retrieving the supernatant after each time until solution was clear.

2.18 Strong Cation Exchange fractionation of digested peptides

Strong Cation Exchange (SCX) fractionation experiments were performed on an ÅKTA Explorer liquid chromatography system using Buffers A (5 mM KH_2PO_4, 30% acetonitrile (ACN), pH 2.7 with TFA) and B (350 mM KH_2PO_4, 30% acetonitrile (ACN), pH 2.7 with TFA) using a 1 mL 'ResourceS' SCX Column (GE Healthcare). Before loading the digested peptides, the column was calibrated by performing a mock-run SCX fractionation using the same protocol as for the actual fractionation. The digested peptides from the 1:1 SILAC lysate were then loaded on the column, using a peristaltic pump and the flow-through was retained and later used as a separate fraction in the phospho-peptide enrichment step (See section 2.19). Next, the column was connected to the ÅKTA system and the elution program was implemented. The elution program started with 5 column volumes (cv) Buffer A, followed with an increasing gradient of KH_2PO_4 over 30 cv by gradually mixing Buffer A with Buffer B up to 50% Buffer B (125 mM KH_2PO_4). Fractions were collected in 2 ml steps starting from the column flow-through and finishing with the 50% Buffer B elutions. Protein-poor fractions were pooled together for up to a total of 9 (1 flow-through and 8 elution) fractions which were used in the phospho-peptide enrichment step. Afterwards, the column was washed with a 10 cv washing step with 100% Buffer B, followed by 10 cv of Buffer A.

2.19 Titanium Dioxide beads enrichment of phospho-peptides and stage tip loading

The phospho-peptide enrichment of the digested SILAC peptide fractions was performed using 'Titansphere™ TiO' 10 µm TiO_2 beads (GL Sciences, 5020-75010). The amount of beads used for each fraction varied depending on the peptide content

of the fraction and was also different between the first and second SILAC phospho-proteomics experiments (see Sections 2.15). The largest and most abundant fraction in both experiments was the flow-through fraction obtained during loading of the SCX column (see Sections 2.18). In the first experiment, this fraction was processed three consecutive times using 10 mg of beads for each enrichment. In the second experiment, this fraction was processed five consecutive times using 10 mg of beads for the first three and 5 mg of beads for the latter two. In both experiments, the SCX fractions were processed using a single enrichment step with 10 mg of beads for the SCX flow-through fraction and 5 mg of beads for the 8 SCX elution fractions.

Before adding them to the fractions, the beads were solubilized in 30 mg/mL 2,5-Dihydroxybenzoic acid (DHB) in 80 % ACN so that 10 µL of DHB were used per 1 mg beads. Next, the beads were incubated with each fraction for 30 min at RT with rotation. The samples were then spun down for 1 min at 4000 rpm and the supernatant was removed. In the case of the large flow-through fractions obtained during loading of the SCX column, the supernatant was incubated with fresh beads two (first experiment) or four (second experiment) more times. The beads from each fraction were then re-suspended in 1 mL of Wash buffer I (30% ACN, 3% TFA), spun again, and re-suspended in 1mL Wash buffer II (80% ACN, 0.1% TFA). After a final spin, the beads were resuspended in enough Wash buffer II to keep them covered (approximately 50 µL in 1.5 mL microfuge tube) and left at RT before loading on to stage tips.

For each phospho-beads fraction, one C8 stage tip and one C18 stage tip were packed according to Rappsilber *et al*, 2003. Stage tips were equilibrated with 30 µL of Methanol before loading. First, the solubilized phospho-beads were loaded on to C8 stage tips and the stage tips were spun to remove excess liquid. Next, the phopsho-peptides were eluted 3 times by passing 30 µL of 40% NH_4OH 60% ACN through each tip by centrifugation. The eluted peptides were then concentrated to a dry pellet using an Eppendorf 5301 concentrator (Eppendorf AG) at RT for approximately 40 min. The dry pellets were then solubilized in 60µL 0.1% TFA and checked for pH on pH paper. If the pH was higher than 2.5, additional TFA was added to acidify the peptides. Next, acidified peptides from each sample were loaded on to C18 stage tips previously equilibrated with 30 µL 0.1% TFA in addition to the methanol. The stage tips with the loaded phospho-peptides were centrifuged to remove excess liquid and then washed with 30 µL 0.1% TFA. After a final

centrifugation to remove left-over TFA, the stage tips were stored at -20°C until further processed for LC-MS^2 analysis.

2.20 In-Gel Digestion of 1:1 SILAC lysates for protein abundance LC-MS^2 analysis

For mass spectrometry analysis of protein abundance in the 1:1 mixed SILAC whole-cell lysates (see Section 2.15), 12.5 µg of lysate was resolved by SDS-PAGE using a pre-cast Bolt™ 4-12% Bis-Tris Plus gradient gel (Invitrogen, NW04125BOX). After Coomassie staining (see Section 2.11), the resolved whole-cell lysate was then excised from the gel and separated into 10 bands of approximately equal protein content. Each band was then processed as a separate fraction. Bands in each fraction were sliced into 1 x 1 mm pieces using a sterile scalpel. The pieces for each fraction were then transferred to a 1.5 mL microfuge tube. The pieces in each fraction then were covered with 25 mM ABC 50% ACN solution and incubated for 30 min at 37°C, after which the solution covering the pieces was discarded. This step was repeated 4 more times for 15 minutes each until most of the Coomassie staining was removed and the gel pieces appeared transparent or faintly blue. The samples were then incubated with 10 mM DTT in 50 mM ABC for 30 min at 37°C. The DTT solution was discarded and ACN was added for 5 min to shrink the gel pieces. Next, ACN was discarded and the gel pieces were next covered with 50 mM IAA in 50 mM ABC for 20 min at RT in the dark. The IAA solution was then discarded and the pieces were washed by incubating for 5 min with 25 mM ABC 50% ACN solution. The excess solution was discarded and gel pieces were shrunk with ACN. Next, each sample was digested for 3 hours at RT by adding 100 µL of a 13 ng/µL lysyl Lys-C peptidase 5 mM ABC 10% ACN solution. Next, 100 µL of 13 ng/µL Trypsin 5 mM ABC 10% ACN solution was added to each sample and the samples were incubated for 16 hours at RT. The digestion was then stopped by adding an equal volume of 0.1 % of TFA and spun onto C18 stage tips as described in the final stage of Section 2.19. The stage tips were then stored at -20°C until further processed for LC-MS^2 analysis.

2.21 LC-MS^2 analysis

The LC-MS^2 analysis of the SILAC samples was performed by Dr. Christos Spanos (Rappsilber lab, University of Edinburgh). The following description of the methodology was provided by Dr. Spanos. Peptides were eluted from StageTips

(Rappsilber *et al*, 2003) in 40 µL of 80% acetonitrile in 0.1% TFA and concentrated down to 4µL by vacuum centrifugation (Concentrator 5301, Eppendorf, UK). The peptide sample was then prepared for LC-MS/MS analysis by diluting it to 5 µL by 0.1% TFA. MS-analyses were performed on a Fusion Lumos mass spectrometer (Thermo Fisher Scientific, UK), coupled on-line to Ultimate 3000 RSLCnano Systems (Dionex, Thermo Fisher Scientific) with an EASY-Spray column (15 cm x 50µm ID, PepMap C18, >2 µm particles, 100 Å pore size) (Thermo Fisher Scientific, UK) and a 7µm ID emitter. The analytical column was heated through an Easy Spray ion source (Thermo Fisher Scientific, UK) at a constant temperature of 50^{o}C. Mobile phase A consisted of water and 0.1% formic acid; mobile phase B consisted of 80% acetonitrile and 0.1% formic acid. The gradient used was 160 min. Peptides were loaded onto the column at a flow rate of 0.5 µL min^{-1} and eluted at a flow rate of 0.2 µL min^{-1} according to the following gradient: 2 to 40% buffer B in 120 min, then to 95% in 16 min. Survey scans of peptide precursors between 400 and 1900 m/z were recorded at 120,000 resolution (at 200 m/z) and the peaks with charge state between 2 and 7 and isolation window of 1.6 Thomson in the quadrupole, were selected and fragmented by higher-energy collisional dissociation (Olsen *et al*, 2007), with normalised collision energy of 35. The maximum ion injection time for the MS in the orbitrap was set to 50ms and the AGC target was set to 4.0 E5. MS2 scans were performed in rapid mode in the ion trap with maximum injection time at 35ms and AGC target of 1.0 E4. Dynamic exclusion was set to 60 s with 10ppm tolerance around the selected precursor and its isotopes.

The MaxQuant software platform (Cox & Mann, 2008) version 1.5.2.8 was used to process the raw files and search was conducted against *Schizosaccharomyces pombe* database (released on 15/09/2015), using the Andromeda search engine (Cox *et al*, 2011). The first search peptide tolerance was set to 20 ppm while the main search peptide tolerance was set to 4.5 pm. Isotope mass tolerance was 2 ppm and maximum charge to 7. Peptides were generated from trypsin and LysC digestion, allowing maximum of two missed cleavages. Carbamidomethylation of cysteine was set as fixed modification. Oxidation of methionine, acetylation of the N-terminal and phosphorylation of serine, threonine and tyrosine, were set as variable modifications. Multiplicity was set to 2 and for heavy labels, Arginine 6 and Lysine 8 were selected. Peptide and protein identifications were filtered to 1% FDR.

Table 2.2. List of strains generated in this study:

Strain	Genotype
KS7232	*h+ win1ΔLD ade6-M216 leu 1-32 ura4-D18*
KS7257	*h- wis4ΔLD ade6-M216 leu 1-32 ura4-D18*
KS7302	*h- sty1-GFP:kanMX6 win1ΔLD ade6-M216 leu 1-32 ura4-D18*
KS7303	*h- sty1-GFP:anMX6 wis4ΔLD ade6-M216 leu 1-32 ura4-D18*
KS7305	*h- ars1(Blp*I*):*P*adh13:CRIB-3xmCitrine:LEU2 ade6-M216 leu1-32 ura4-D18*
KS7566	*h+ ars1(Blp*I*):*P*adh13:CRIB-3xmECitrine:LEU2* P*act1:lifeact-mCherry::leu1+ ade6-M216 leu1-32 ura4-D18*
KS7578	*h+ scd1Δ::ura4+ ars1(Blp*I*):*P*adh13:CRIB-3xmCitrine:LEU2 ade6-M216 leu1-32 ura4-D18*
KS7657	*h+ gef1Δ::ura4+ ars1(Blp*I*):*P*adh13:CRIB-3xmCitrine:LEU2 ade6-M216 leu1-32 ura4-D18*
KS7660	*h+ sty1Δ::kanMX ars1(Blp*I*):*P*adh13:CRIB-3xmECitrine:LEU2* P*act1:lifeact-mCherry::leu1+ ade6-M210 leu1-32 ura4-D18*
KS7737	*h- ars1(Blp*I*):*P*adh13:CRIB-3xmECitrine:LEU2 atf1Δ::kanMX6 ade6-M216 leu1-32 ura4-D18*
KS7754	*h- ars1(Blp*I*):*P*adh13:NES-CRIB-3xmCitrine:LEU2 ade6-M216 leu1-32 ura4-D18*
KS7795	*h- ars1(Blp*I*):*P*adh13:mini-CRIB-3xmCitrine:LEU2 ade6-M216 leu1-32 ura4-D18*
KS7830	*h+ sty1-T97A ars1(Blp*I*):*P*adh13:CRIB-3xmECitrine:LEU2 Pact1:lifeact-mCherry::leu1+ ade6-M216 leu1-32 ura4-D18*
KS7834	*h- ars1(Blp*I*):*P*adh13:mini-CRIB(K120A)-3xmCitrine:LEU2 ade6-M216 leu1-32 ura4-D18*
KS7835	*h- ars1(Blp*I*):*P*adh13:mini-Shk1-CRIB-3xmCitrine:LEU2 ade6-M216 leu1-32 ura4-D18*
KS7870	*h- ars1(Blp*I*):*P*adh13:mini-Shk1-CRIB-3xmCitrine:LEU2 gef1Δ::ura4+ ade6-M216 leu1-32 ura4-D18*
KS7882	*h+ gef1-3xmCherry:kanMX6 ars1(Blp*I*):*P*adh13:CRIB-3xmCitrine:LEU2 ade6-M216 leu1-32 ura4-D18*
KS7890	*h- scd1-3xmCherry:kanMX6 ars1(Blp*I*):*P*adh13:CRIB-3xmCitrine:LEU2 ade6-M216 leu1-32 ura4-D18*
KS8026	*h? sty1Δ::kanMX Scd1-3xmCherry:kanMX6 ars1(Blp*I*):*P*adh13:CRIB-3xmCitrine:LEU2 ade6-M216 leu1-32 ura4-D18*
KS8061	*h? sty1Δ::kanMX Gef1-3xmCherry:kanMX6 ars1(Blp*I*):*P*adh13:CRIB-3xmCitrine:LEU2 ade6-M216 leu1-32 ura4-D18*
zKS8116	*h- ars1(Afe*I*):nmt:lacO*:GFP:lacI-NLS:ura4+ ade6-M216 leu1-32 ura4-D18*
KS8140	*h- sty1-mECitrine:KanMX6 ade6-M210 leu1-32 ura4-D18*
KS8164	*h- ars1(Blp*I*):*P*adh13:CRIB-3xmECitrine:LEU2*
KS8217	*h- ars1(Blp*I*):*P*adh13:CRIB-3xmECitrine:LEU2 plo1.as8:ura4+*
KS8276	*h- wis1Δ::ura4+ ars1(Blp*I*):*P*adh13:CRIB-3xmECitrine:LEU2 ade6-M210 leu1-32 ura4-D18*
KS8282	*h- scd1-3xmCherry:kanMX6 sty1-T97A wis1DD:12myc:ura4+ pyp1Δ::ura4+ pyp2Δ::LEU2 ars1(Blp*I*):*P*adh13:CRIB-3xmCitrine:LEU2*
KS8283	*h- gef1-3xmCherry:kanMX6 sty1-T97A wis1DD:12myc:ura4+ pyp1Δ::ura4+ pyp2Δ::LEU2 ars1(Blp*I*):*P*adh13:CRIB-3xmCitrine:LEU2*
KS8311	*h+ sty1-T97A wis1DD:12myc:ura4+ pyp1Δ::ura4+ pyp2Δ::LEU2 ars1(Blp*I*):*P*adh13:CRIB-3xmECitrine:LEU2* P*act1:lifeact-mCherry::leu1+ leu1-32 ura4-D18*

KS8323	*h- sty1-T97A ars1(Blp*I*):*P*adh13:CRIB-3xmECitrine:LEU2*
KS8332	*h- sty1-T97A wis1DD:12myc:ura4+ pyp1Δ::ura4+ pyp2Δ::LEU2 ars1(Blp*I*):*P*adh13:CRIB-3xmCitrine:LEU2 cdc42-mCherrySW:kanMX6 leu1-32 ura4-D18*
KS8496	*h+ sty1-T97A wis1DD:12myc:ura4+ pyp1Δ::ura4+ pyp2Δ::LEU2 car2Δ:kanMX4 arg1-230 leu1-32 lys3-32 ura4-D18*
KS8497	*h- tea1Δ::kanMX sty1-T97A wis1DD:12myc:ura4+ pyp1Δ::ura4+ pyp2Δ::LEU2 ars1(Blp*I*):*P*adh13:CRIB-3xmCitrine:LEU2 leu1-32 ura4-D18*
KS8640	*h- sty1-T97A wis1DD:12myc:ura4+ pyp1Δ::ura4+ pyp2Δ::LEU2 ars1(Blp*I*):*P*adh13:CRIB-3xmCitrine:LEU2 car2Δ:kanMX4 arg1-230 leu1-32 lys3-32 ura4-D18*
KS8764	*h- scd2-3xmCherry:kanMX6 ars1(Blp*I*):*P*adh13:CRIB-3xmCitrine:LEU2 ade6-M216 leu1-32 ura4-D18*
KS8765	*h- scd2-3xmCherry:kanMX6 sty1Δ::kanMX ars1(Blp*I*):*P*adh13:CRIB-3xmCitrine:LEU2 ade6-M216 leu1-32 ura4-D18*
KS8773	*h+ scd2-3xmCherry:kanMX6 sty1-T97A wis1DD:12myc:ura4+ pyp1Δ::ura4+ pyp2Δ::LEU2 ars1(Blp*I*):*P*adh13:CRIB-3xmCitrine:LEU2*
KS8779	*h- plo1-S402A ars1(Blp*I*):*P*adh13:CRIB-3xmCitrine:LEU2*
KS8782	*h+plo1-S402E ars1(Blp*I*):*P*adh13:CRIB-3xmCitrine:LEU2*
KS8903	*h- act1-LR::ura4+ ars1(Blp*I*):*P*adh13:CRIB-3xmCitrine:LEU2* P*act1:lifeact-mCherry::leu1+ ade6-M216 leu1-32 ura4-D18*

Table 2.3. List of base strains and strains from other laboratories:

Strain	Genotype	Source
KS1	*h-*	Lab stock
KS2	*h+*	Lab stock
KS515	*h+ ade6-M210 leu1-32 ura4-D18*	Lab stock
KS516	*h- ade6-M216 leu1-32 ura4-D18*	Lab stock
MBY6843 (KS6696)	*h+* P*act1:lifeact-mCherry::leu1+ ade6-M216 leu1-32 ura4-D18*	M. Balasubramanian
MBY2295 (KS7341)	*h+ act1-LR::ura4+ leu1-32 ura4-D18*	M. Balasubramanian
AV15 (KS7644)	*h- atf1Δ::kanMX6*	E. Hidalgo
AZ107 (KS7671)	*h+ sty1-T97A ura4-D18*	E. Hidalgo
KS2086 (KS7902)	*h- wis1DD:12myc::ura4+ leu1-32 ura4-D18*	K. Shiozaki
IH10368 (KS7918)	*h- plo1.as8:ura4+ ura4-D18*	I. Hagan
IH3758 (KS8735)	*h- plo1.S402A*	I. Hagan
IH3759 (KS8736)	*h- plo1.S402E*	I. Hagan
JM 281 (KS 7944)	*h- pyp1Δ::ura4+ leu1-32 ura4-D18*	J. Millar
JM 655 (KS 7945)	*h+ pyp2Δ::LEU2 his7-366 leu1-32 ura4-D18*	J. Millar
YSM2446 (KS8284)	*h- cdc42-mCherrySW:kanMX6*	S.Martin

Table 2.4. List of plasmids used in the study:

Plasmid	Description	Source
pKS108	pFA6a-KanMX6	Sawin lab stock (Bähler *et al*, 1998)
pKS131	pHN159-ura4+	H.Ohkura lab
pKS535	pDONR221	Invitrogen
pKS537	p0GWA	(Busso *et al*, 2005)
pKS1167	pFA6-3xmCherry-KanMX6	Sawin lab stock
pKS1287	pRAD13	Y. Watanabe lab
pKS1301	pDONR221-Sty1	This study
pKS1303	pMK-RQ-3xmCitrine	GeneArt
pKS1304	pMA-T-Gic2PDB	GeneArt
pKS1305	pMA-T-Gic2-3xmCitrine	GeneArt
pKS1306	p0GWA-Sty1	This study
pKS1330	pFA6a-mEcitrine-KanMX6	Sawin lab stock
pKS1374	pRAD13-CRIB-3xmCitrine	This study
pKS1422 (pSK174)	pNmt:lacO*:GFP:lacI-NLS:ura4+	(Kjaerulff & Nielsen, 2015)
pKS1588	pMA-T mini-Gic2-CRIB	GeneArt
pKS1589	pMA-T mini-Gic2-K120A-CRIB	GeneArt
pKS1590	pMA-T mini-Shk1-CRIB	GeneArt
pKS1592	pMA-T Wis1_NES_Gic2PDB	GeneArt

Chapter 3

The stress-response MAPK Sty1 is involved in Cdc42 regulation*

*Parts of the work in this chapter have been published in:

Mutavchiev, D.R., Leda, M., Sawin, K.E, *Remodeling of the fission yeast Cdc42 cell polarity module via the Sty1 p38 stress-activated protein kinase pathway*. (Current Biology, 2016)

3.1 Introduction

The Rho-GTPase Cdc42 functions as a key regulator of cellular organisation and polarity in fission yeast (Martin & Arkowitz, 2014). As described in greater detail in the Introduction (see Introduction 1.3.1), the active (GTP-bound) form of Cdc42 can bind to and stimulate the function of various effectors involved in remodelling of the actin cytoskeleton, exocytosis, and downstream cellular signalling. Thus, to achieve polarised growth, fission yeast cells need to establish and maintain Cdc42's activity in a spatially restricted form at cell tips. In part, this is achieved by the direct control of Cdc42 activation by guanine-nucleotide exchange factors (GEFs) and the GTPase activating proteins (GAPs), as well as feedback loops involving Cdc42 effectors such as the scaffold protein Scd2 (see Introduction 1.3.4 for in-depth description). In addition, other factors such as the actin cytoskeleton are also hypothesised to participate in Cdc42 regulation. However, the exact role of actin in establishment and maintenance of Cdc42 polarity remains an elusive question in yeast cell biology (Martin & Arkowitz, 2014).

In interphase *S.pombe* cells, filamentous actin (F-actin) forms two distinct structures: formin-nucleated cables and Arp2/3-nucleated cortical patches (Mishra *et al*, 2014). Actin cables, whose nucleation from the cell ends is promoted by Cdc42-GTP via formins, serve as tracks for myosin V-driven vesicular transport towards the cell ends (Martin *et al*, 2007; Win *et al*, 2001; Motegi *et al*, 2001). Cortical patches promote endocytosis by providing mechanical forces driving membrane tubulation and vesicle scission (Goode *et al*, 2015). Both of these actin-dependent processes have been hypothesised to play a role in Cdc42 regulation. First, actin cables could allow the transport of endomembrane-bound Cdc42 vesicles that would deliver cytoplasmic Cdc42 to the plasma membrane via exocytosis (Wedlich-Soldner *et al*, 2003). Since formin activation by Cdc42-GTP at the plasma membrane promotes the nucleation of new actin cables this process would constitute a positive-feedback loop for Cdc42 activation. Second, Cdc42 could be recycled from the plasma membrane via endocytosis (Orlando *et al*, 2011; Marco *et al*, 2007). However, experimental evidence in fission yeast, using actin-cable nucleation and endocytosis-deficient mutants, has shown that both these processes have minimal contribution to Cdc42 dynamics *in vivo* (Bendezú & Martin, 2011; Bendezú *et al*, 2015).

Another argument for actin cytoskeleton contribution to Cdc42 regulation is that F-actin is thought to have an important role in the long-term stability of the Cdc42 module. This is based on experiments in which actin was completely depolymerised using the drug latrunculin A (LatA), which binds to actin monomers and sequesters them from *de novo* incorporation into filaments (Coué *et al*, 1987; Ayscough *et al*, 1997; Morton *et al*, 2000). Strikingly, *in vivo* addition of LatA to fission yeast cells leads to dispersal of Cdc42-GTP from the cell tips and the formation of ectopic transient patches of Cdc42 activity at the cell sides. Apart from Cdc42-GTP, these transient patches are enriched with Cdc42 itself and other components of the Cdc42 polarity module (Bendezú *et al*, 2010, 2015; Kelly & Nurse, 2011). How the disruption of the actin cytoskeleton leads to the dispersal of the Cdc42 module remains unclear, but it is key to dissecting the contribution of actin to Cdc42 stability.

All of the experiments directly suggesting actin involvement in the regulation of the Cdc42 module have used LatA to perturb the actin cytoskeleton; however, potential additional effects of LatA, beyond actin disruption have been largely neglected. For example, a study from 15 years ago concerning the concept of a 'spindle orientation checkpoint' in *S.pombe* briefly mentioned that addition of the closely related actin depolymerizing drug latrunculin B (LatB) induced the activation of the MAP kinase Sty1, a component of the Stress-Activated Protein Kinase (SAPK) pathway in fission yeast (Gache*t et al*, 2001; see also Introduction 1.6). This observation has not been further pursued, despite the importance of both LatA and LatB as research tools for fission yeast and for other organisms. Considering the importance of LatA experiments for understanding actin involvement in Cdc42 regulation and many other cellular behaviours, the effect of LatA on SAPK signalling certainly merits further investigation.

In this chapter, I describe the construction of a CRIB-3xmCitrine probe as a reporter to study Cdc42-GTP distribution using long-term time-lapse fluorescence cell imaging with minimal phototoxicity. Using this newly generated tool, I re-evaluate the effects of LatA addition on CRIB-3xmCitrine distribution with improved time-resolution. Next, I confirm that LatA addition activates SAPK signalling *in vivo,* using two independent assays. Given that LatA treatment leads both to activation of Sty1 and the dispersal of Cdc42-GTP from the cell tips, I next investigate whether Sty1 might play a role in the process of Cdc42-GTP dispersal. I describe the effects of LatA on CRIB-3xmCitrine distribution in cells deficient in SAPK signalling and establish that

Sty1 activation is required for LatA-induced CRIB-3xmCitrine dispersal. I also show that Sty1's involvement in this process is independent of its previously described functions, including its role in driving new protein expression. Furthermore, I develop a system that allows Sty1 to be activated in the absence of external stress, and I use this to show that activation of Sty1 alone is sufficient for the dispersal of CRIB-3xmCitrine from cell tips. These results suggest that activation of Sty1 is a novel critical component of remodelling and dispersal of the Cdc42 polarity module at the cell tips. Finally, I present a physiological role for the newly-found Sty1 function in maintaining non-polarized Cdc42-GTP during nitrogen-starvation-induced quiescence.

3.2 Results

3.2.1 Adh13-CRIB-3xmCitrine reporter for Cdc42 activity

Experiments aimed at studying Cdc42 dynamics and regulation have been particularly challenging because of the absence of functional fluorescent-protein fusions with Cdc42 itself. Due to Cdc42's post-translational modifications on the C-terminus, most fluorescent fusions have been inserted on the N-terminus of the GTPase. However, N-terminal GFP-Cdc42 fusions have been associated with temperature-sensitivity and failure to associate with post-Golgi vesicles in budding yeast (Watso*n et al*, 2014; Wedlich-Soldner *et al*, 2003, 2004) or aberrant cell shape in fission yeast (Coll *et al*, 2007). An alternative approach has been the use of CRIB (Cdc42/Rac interactive binding motif) fluorescent-protein fusions. CRIB domains specifically recognise the GTP-bound state of Cdc42 and thus are very suitable reporters for the *in vivo* localisation of active Cdc42 (Jaquenoud & Peter, 2000; Tong *et al*, 2007).

At the start of my PhD work, a CRIB-3xGFP fusion, based on the existing budding yeast Gic2 CRIB reporter expressed under the *shk1* promoter, was the most widely used Cdc42-GTP probe in fission yeast (Jaquenoud & Peter, 2000; Tatebe *et al*, 2008). However, recent results in the Sawin lab have indicated that prolonged exposure to 488 nm light, which is used to excite the GFP fluorophore, has adverse phototoxic effects on *S.pombe* cells, affecting their growth (Ashraf S, 2016 PhD Thesis). In contrast, cells exposed to 514 nm light (used to excite YFP) did not exhibit observable alterations in growth. In addition, no visible autofluorescence was observed when using YFP-labeled probes in an open-dish system, where exposure to oxygen is higher. Therefore, to investigate Cdc42 activity using an optimal experimental setup that is also closer to physiological conditions, I constructed a novel CRIB reporter fused with three copies of mCitrine (a monomeric derivative of YFP; Figure 3.1 A; see also Section 2.7). The CRIB-3xmCitrine fusion is under the control of the Adh13 promoter and was stably integrated into the *ars1* locus of the genome. As expected, the localization of the *adh13*:CRIB-3xmCitrine reporter (further referred in this chapter as 'CRIB-3xmCitrine') was identical to that described for CRIB-3xGFP– it followed the sites of active growth at tips during interphase and at the place of septation during cytokinesis (Figure 3.1 B; Figure 3.2 A and C). As with CRIB-3xGFP, a considerable amount of the CRIB-3xmCitrine was also

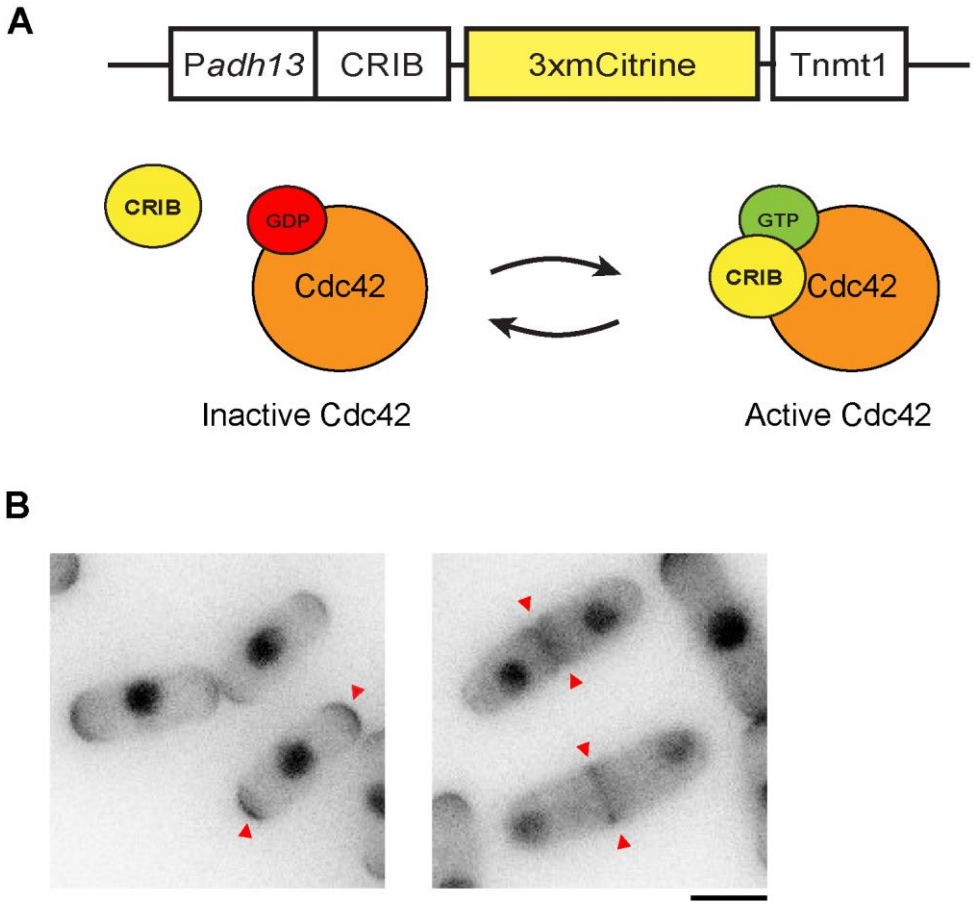

Figure 3.1. CRIB-3xmCitrine reporter for Cdc42-GTP distribution. (A) Schematic representation of the *adh13*:CRIB-3xmCitrine construct and a diagram showing specific binding of the CRIB reporter to Cdc42-GTP. (B) Fission yeast cells expressing the CRIB-3xCitrine reporter. Representative images of active Cdc42 distribution (indicated by the red arrowheads) during interphase (left) and cytokinesis (right). Scale bar, 5 µm.

localised in the nucleus, although the nuclear signal for CRIB-3xmCitrine appeared more pronounced than has been reported for CRIB-3xGFP (Tatebe *et al*, 2008).

3.2.2 Addition of LatA leads to dispersal of Cdc42-GTP

To re-evaluate the effect of LatA treatment on active Cdc42 distribution, I performed live-cell imaging of cells expressing the CRIB-3xmCitrine construct and the F-actin reporter Lifeact-mCherry (Huang *et al*, 2012). Lifeact consist of a 17 amino-acid peptide from the budding yeast actin-binding protein Abp140. When fused to a fluorescent protein, Lifeact can reveal actin filaments *in vivo* (Riedl *et al*, 2008). The main advantages of using Lifeact as a reporter for F-actin include its small size and the lack of Abp140 homologues in organisms other than *S.cerevisisae* or its close relatives. In *S.pombe*, Lifeact fused to mCherry expressed under the *act1* promoter (further referred in the text as just 'Lifeact') has been characterised as a reliable marker to visualise F-actin structures (such as actin cables and patches) without significant impact on cellular physiology (Huang *et al*, 2012). However, a recent study has suggested that, in specific assays, highly-expressed Lifeact should be used with caution as it might affect some aspects of actin-filament dynamics (Courtemanche *et al*, 2016). Thus, in my experiments I also used phalloidin staining of fixed cells to verify that any changes in F-actin observed during LatA treatment are not affected by the use of Lifeact but faithfully report the general actin distribution.

Consistent with previous observations, upon addition of 50μM LatA, the CRIB-3xmCitrine signal was significantly dispersed from the cell tips within the first 20-30 min after addition (Figure 3.2 A; Bendezú *et al*, 2010; Bendezú *et al*, 2015). Additionally, approximately 40-60 min after addition, the formation of ectopic patches on the cell sides was observed. While highly dynamic, these patches appeared to migrate away from the cell tips and towards the cell middle. Furthermore, treatment with LatA also led to a complete stop of growth (Figure 3.2 C). Notably, CRIB-3xmCitrine dispersal after addition of LatA was considerably slower than the complete depolymerisation of the F-actin, which was observed to occur within 3-6 min, both *in vivo* using Lifeact and in fixed cells using phalloidin staining (Figure 3.2 A and B).

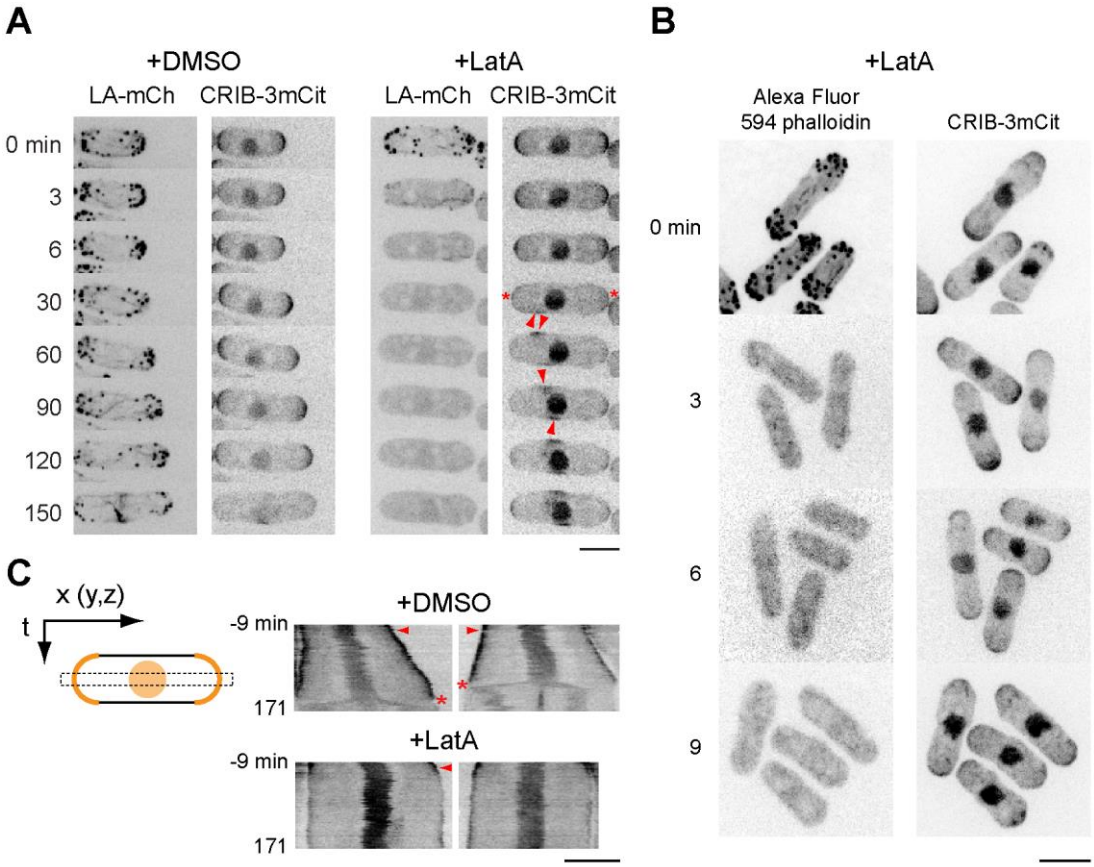

Figure 3.2. Treatment with Latrunculin A leads to actin depolymerization and dispersal of CRIB-3xmCitrine from the cell tips. (A) Time-lapse images of cells expressing Lifeact-mCherry (LA-mCh) and CRIB-3xmCitrine (CRIB-3mCit) after addition of 1% DMSO or 50 μM Latrunculin A (LatA). Red asterisks mark CRIB-3mCit dispersal from the cell tips. Red arrowheads point to ectopic CRIB patches after the dispersal. (B) Alexa Fluor 594 phalloidin staining of the actin cytoskeleton in fixed cells expressing CRIB-3mCit treated with 50 μM LatA. Images demonstrate the actin-depolymerizing effect of LatA treatment without the use of LA-mCh as a reporter. This control experiment indicates that the rate or extent of the depolymerization using this experimental setup is not affected by the presence or absence of LA-mCh. Because fixation and staining methods are optimized for actin preservation (see Materials and methods, Section 2.12) CRIB-3mCit localization and cell morphology may be slightly altered relative to live cells. (C) Kymographs from time-lapse images of CRIB-3mCit/LA-mCh expressing cells showing rates of cell elongation after addition of DMSO or LatA. Cartoon summarizes kymograph construction . Left-hand panels in each set represent the cells shown in A. Right-hand panels represent additional cells.Red arrowheads indicate the time of DMSO or LatA addition. Asterisks indicate disappearance of CRIB-3mCit from cell tips in DMSO-treated cells, due to cell division.
All times shown are relative to addition of DMSO or LatA. Scale bars, 5 μm.

3.2.3 Treatment with LatA activates the MAP kinase Sty1

Based on the reports that Latrunculin B can lead to an activation of SAPK signalling, I tested whether addition of LatA could have a similar effect, by performing two different types of assays to measure Sty1 activation. The first assay followed the localisation of Sty1 in cells expressing the mECitrine-tagged Sty1. Previous studies have identified that upon activation of SAPK signalling there is a notable translocation of Sty1 to the cell nucleus, despite some Sty1 remaining in the cytoplasm (Gaits *et al*, 1998; Smith *et al*, 2010). After addition of 50 µM LatA, Sty1-mECitrine became enriched in the cell nucleus, indicative of SAPK pathway activation (Figure 3.3).

As the mechanism of Sty1 activation involves its phosphorylation, next I assayed levels of Sty1 phosphorylation in response to LatA addition. Quantitative western-blotting of cell extracts using a phospho-specific antibody against the mammalian homolog of Sty1 (p38 MAPK) showed a significant increase in Sty1 phosphorylation upon addition of 50 µM LatA (Figure 3.4). The Sty1 phosphorylation kinetics after LatA addition were comparable to those observed after a conventional hyperosmotic stress using 0.6M KCl and similar to those of Sty1 translocation into the nucleus (Figure 3.3). In addition, to evaluate total Sty1 levels in these experiments I generated an antibody against the whole Sty1 protein and used it in conjunction with the phospho-specific antibody (see Section 2.14). Treatment with LatA did not lead to a significant change in Sty1 levels, suggesting that the increase in phospho-Sty1 was not influenced by an increase of total Sty1 (Figure 3.4). Interestingly, KCl addition did lead to a transient reduction of Sty1 levels in the first 20-40 min post-treatment. Thus, while total phospho-Sty1 levels per cell after LatA and KCl treatments are comparable, a higher proportion of the total Sty1 seems to be phosphorylated in response to KCl, suggesting the signalling responses leading to Sty1 activation after each treatment might be different.

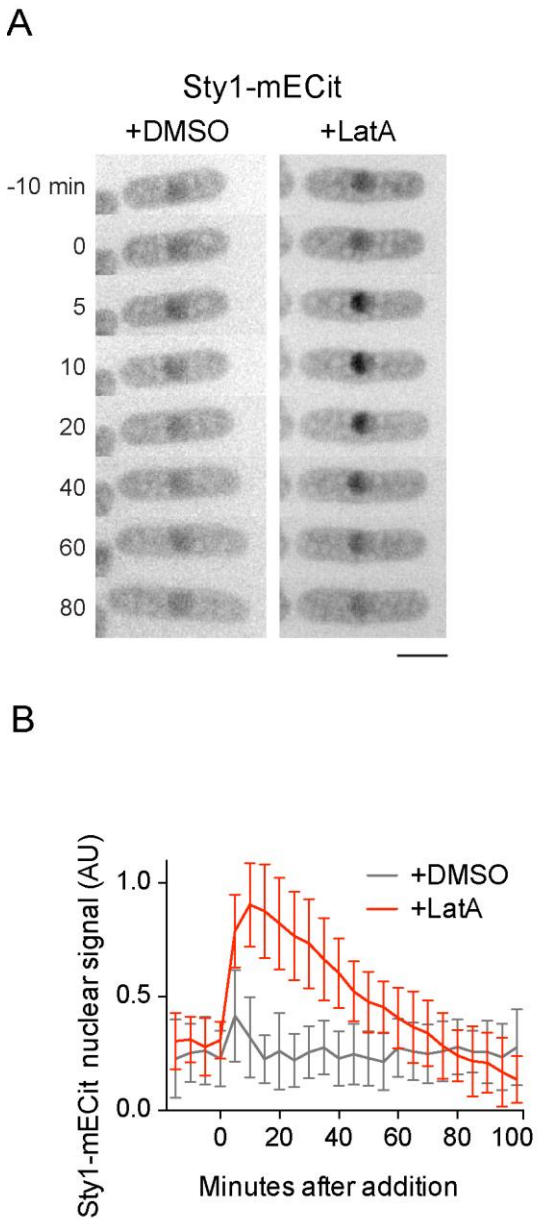

Figure 3.3. Addition of Latrunculin A leads to Sty1 nuclear accumulation. (A) Time-lapse images of cells expressing Sty1-mECitrine (Sty1-mECit) after addition of DMSO or 50 µM Latrunculin A (LatA). LatA addition leads to net import of Sty1-mECit into the nucleus. Times shown are relative to addition of DMSO or LatA. Scale bar, 5 µm. (B) Quantification of Sty1-mECit nuclear fluorescence after addition of DMSO or 50 µM LatA. Values shown are mean relative intensity (arbitrary units) of nuclear fluorescence above cytoplasmic fluorescence (see Section 2.13). Error bars indicate SD.

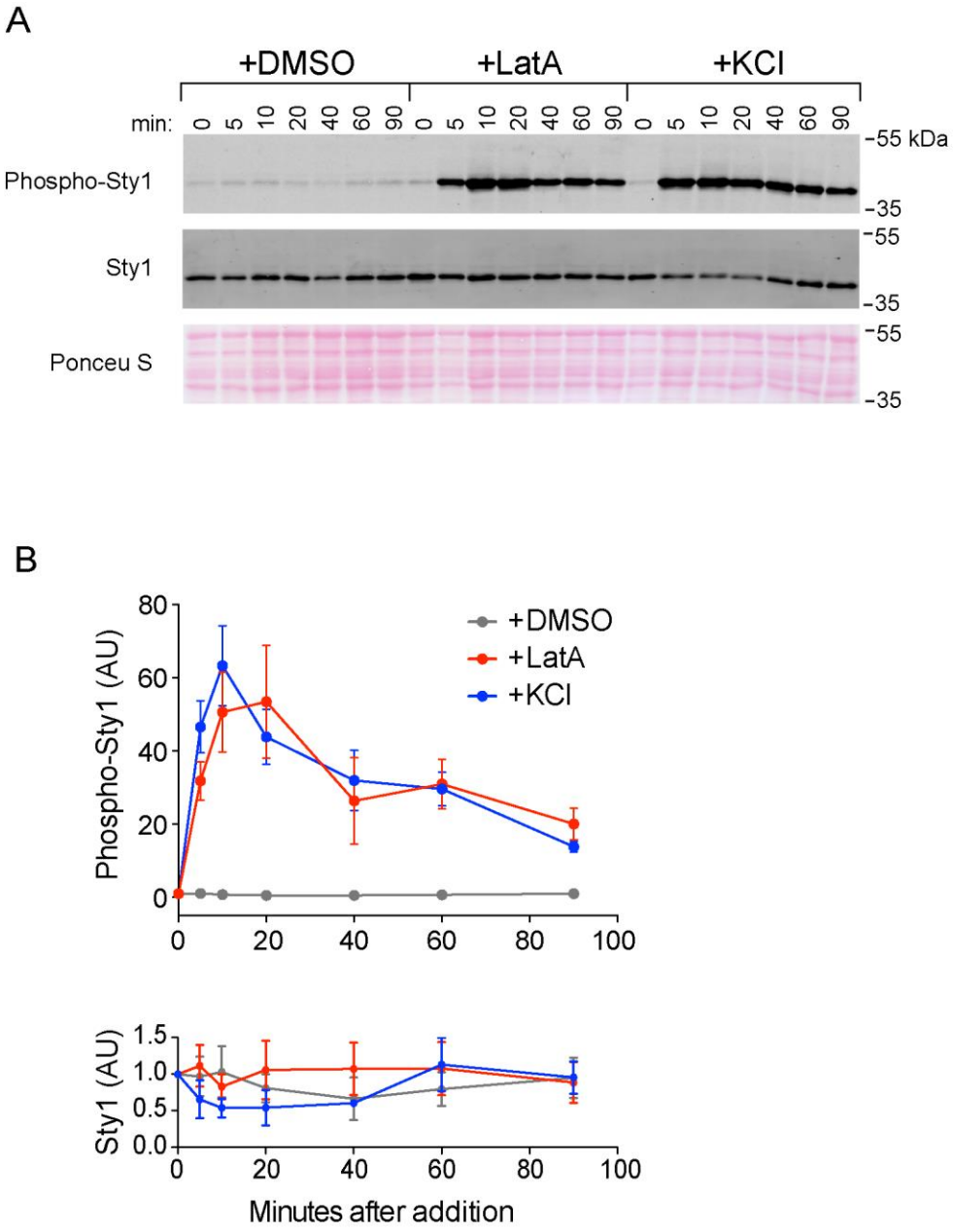

Figure 3.4. Addition of Latrunculin A leads to increased Sty1 phosphorylation. (A) Anti-phospho-Sty1 and anti-Sty1 western blot of wild-type (expressing CRIB-3xmCitrine and Lifeact-mCherry) cell extracts after addition of DMSO, 50 µM Latrunculin A (LatA), or 0.6 M KCl for the indicated times. Ponceau S stain of the same region of the blot is shown underneath. (B) Quantification of phospho-Sty1 (arbitrary units, initial levels set to 0) and Sty1 (arbitrary units initial levels set to 1.0) from experiments of the type shown in A. Mean values from three independent experiments. Error bars indicate SEM.

3.2.4 Sty1 activity is required for Cdc42-GTP dispersal after LatA treatment

Thus far, I have described how the addition of the actin-depolymerising drug LatA leads both to activation of the SAPK pathway (evidenced by the phosphorylation of Sty1 and Sty1 translocation into the nucleus) and the dispersal of active Cdc42 from the cell tips (evidenced by the changes in CRIB-3xmCitrine distribution). Therefore, I hypothesised that Sty1 might contribute to the process of LatA-induced Cdc42-GTP dispersal, either in conjunction or independently of actin depolymerisation.

As described at greater length in the Introduction (see Introduction 1.6), the SAPK pathway consists of an evolutionary conserved three-tier MAPK cascade, activated in response to a variety of environmental stresses. A crucial step for the functioning of the pathway is the activation of the Sty1 MAPK through phosphorylation carried out by the MAPKK Wis1. Thus, both Sty1 and Wis1 are essential for the SAPK pathway. If Sty1 activation was involved in LatA-induced CRIB-3xmCitrine dispersal, one would predict that CRIB-3xmCitrine behaviour upon LatA treatment would be different in cells in which the SAPK pathway is compromised, compared to wild-type cells. At the same time, one would predict that absence of SAPK signalling should not alter the depolymerisation of the actin cytoskeleton caused by LatA.

To test these predictions, I imaged CRIB-3xmCitrine and Lifeact in *sty1*Δ and *wis1*Δ cells, in which the SAPK pathway is non-functional. Strikingly, in both LatA-treated *sty1*Δ and *wis1*Δ cells, the actin cytoskeleton was quickly depolymerised but the CRIB distribution remained at the cell tips for the whole duration of the experiment (Figure 3.5, A). Furthermore, *sty1*Δ and *wis1*Δ cells continued to elongate even in the absence of actin filaments (Figure 3.5, B). This was in stark contrast to the CRIB dispersal and immediate cessation of growth observed in wild-type cells upon LatA treatment (Figure 3.2, A and C). However, it should be noted that while *sty1*Δ and *wis1*Δ cells continued to grow in the presence of LatA, the growth rate was slower than unperturbed wild-type cells and it declined over time, as evidenced by kymograph analysis of individual cells (Figure 3.2, C; Figure 3.5, B).

In principle, the observed effect in LatA-treated *sty1*Δ and *wis1*Δ cells could be either due to a *direct* involvement of Sty1 in the process of CRIB-3xmCitrine

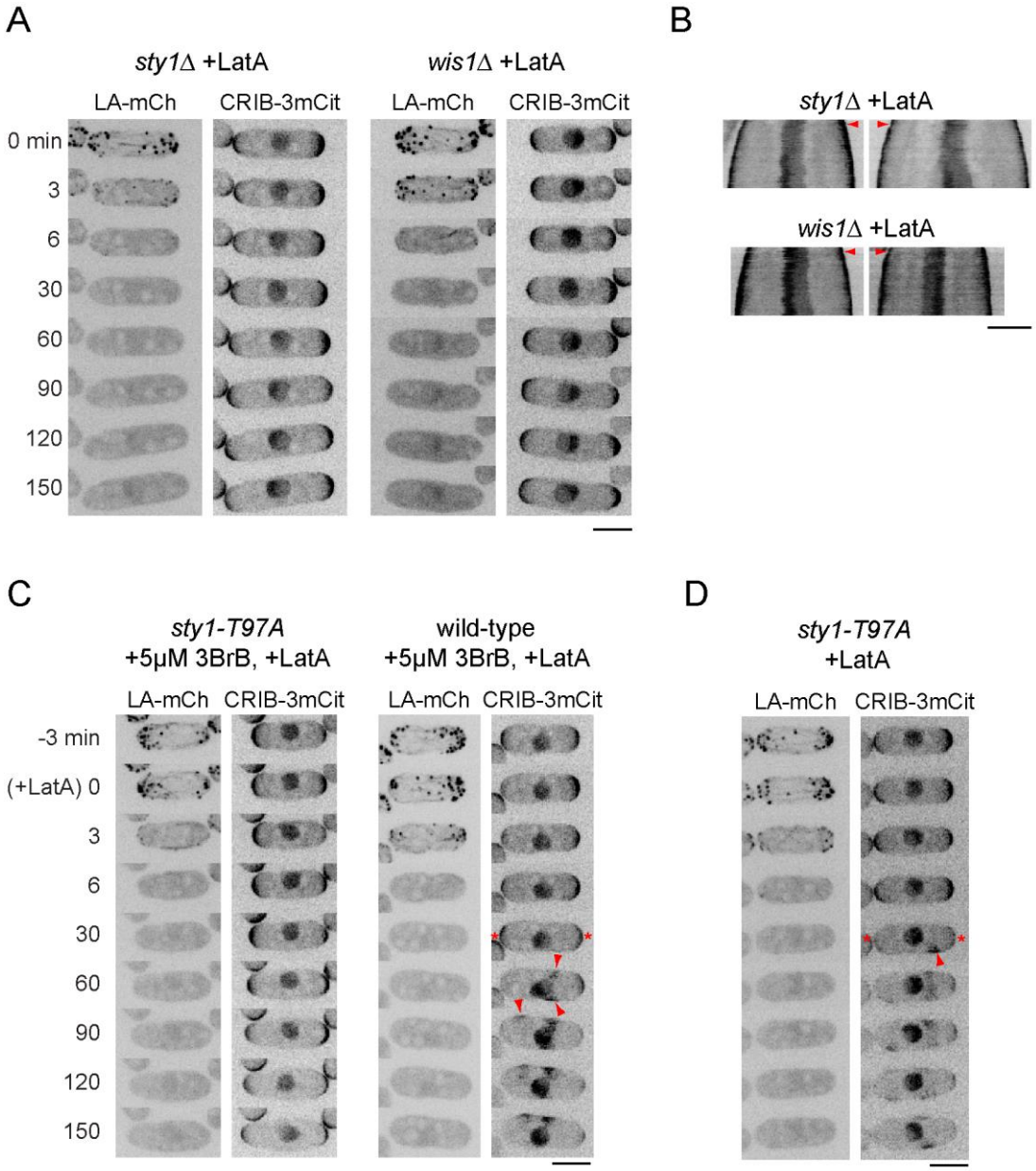

Figure 3.5. CRIB-3xmCitrine dispersal by Latrunculin A requires the Sty1 MAPK pathway. (A) Time-lapse images of *sty1*Δ and *wis1*Δ cells expressing Lifeact-mCherry (LA-mCh) and CRIB-3xmCitrine (CRIB-3mCit) after addition of 50 μM Latrunculin A (LatA). (B) Kymographs from time-lapse images of CRIB-3mCit/LA-mCh expressing *sty1*Δ and *wis1*Δ cells showing rates of cell elongation after addition of LatA. Left-hand panels in each set represent the cells shown in A. Right-hand panels represent additional cells. (C) Time-lapse images of LA-mCh and CRIB-3mCit in wild-type and *sty1-T97A* cells pre-treated with 5 μM 3-BrB-PP1 (3BrB) for 10 min, prior to addition of 50 μM LatA in the continued presence of 3BrB. (D) Time-lapse images of LA-mCh and CRIB-3mCit in *sty1-T97A* cells treated with 50 μM LatA.
Red asterisks mark CRIB-3mCit dispersal from the cell tips. Red arrowheads point to ectopic CRIB-3mCit patches after the dispersal. All times shown are relative to addition of LatA. Scale bars, 5 μm.

dispersal, or alternatively due to an *indirect* effect arising from the absence of functional SAPK signalling. An example of the latter possibility would be that as a consequence of the deletion of the SAPK pathway, *sty1*Δ and *wis1*Δ cells could have developed adaptations which result in a fundamentally different response to LatA treatment compared to wild-type cells (e.g. CRIB tip-retention vs. dispersal). To exclude this possibility, I tested the effects of LatA on cells where Sty1 was inhibited just prior to LatA addition. This was achieved by using the *sty1-T97A* analog-sensitive mutant of the Sty1 kinase (equivalent to a '*sty1.as2*' mutant; Zuin *et al*, 2010). An analog-sensitive kinase contains a mutation of the 'gate-keeper' residue in its ATP-binding pocket, allowing the binding of various bulky ATP-competitive analogs (Bishop *et al*, 2000). Because such analogs are not normally accommodated in the ATP-binding pockets of endogenous kinases, they can be efficiently used to specifically inhibit analog-sensitive kinases by outcompeting ATP for binding. Previous work in fission yeast has generated a large collection of functional analog-sensitive kinases, including the *sty1-T97A* mutant used in my experiments (Zuin *et al*, 2010; Cipak *et al*, 2011).

I imaged CRIB and Lifeact in *sty1-T97A* cells in which Sty1 was inhibited with the ATP-competitive analog 3-BrB-PP1 (4-Amino-1-tert-butyl-3-(3-bromobenzyl)pyrazolo[3,4-d]pyrimidine; further referred in text as '3BrB') just prior (less than 10 min) to LatA addition, thus not allowing potential adaptations to the inhibition of Sty1 kinase activity. Analogous to LatA treatment in *sty1*Δ cells, LatA addition to *sty1-T97A* cells in the presence of 3BrB resulted in a complete depolymerization of the actin cytoskeleton but no CRIB-3xmCitrine dispersal from the cell tips (Figure 3.5, C). To control for this experiment, I also confirmed that the presence of 3BrB did not prevent LatA-induced CRIB dispersal in wild-type cells (Figure 3.5, C). Additionally, LatA treatment of *sty1-T97A* cells in the absence of 3BrB (where Sty1 is functional) still resulted in CRIB-3xmCitrine dispersal.

3.2.5. Sty1's role in LatA-induced Cdc42-GTP dispersal is independent of known Sty1 functions

The experiments described so far suggest a direct involvement of Sty1 in the CRIB-3xmCitrine dispersal observed after addition of LatA. Because some of the downstream targets of Sty1 have been characterised (see Introduction 1.6), I hypothesised that Sty1's role in LatA-driven CRIB-3xmCitrine dispersal might depend

on some of these downstream targets. To test this possibility I investigated the effects of LatA on CRIB-3xmCitrine distribution in strains carrying deletions of some of the direct targets of Sty1, including the bZIP transcription factor Atf1 and the MAPK-activated kinases Srk1 and Cmk2 (Wilkinson et al, 1996; Sánchez-Piris et al, 2002; Smith et al, 2002). In all *atf1*Δ, *cmk2*Δ, and *srk1*Δ cells, LatA treatment still led to a CRIB-3xmCitrine dispersal, with similar kinetics as those observed in wild-type cells (Figure 3.6, A). This suggested that while the CRIB-3xmCitrine dispersal observed after LatA treatment required Sty1, it did not require the downstream Sty1 pathways in which Atf1, Srk1, or Cmk2 were involved.

Sty1 is best characterised for its function in controlling new gene expression in response to stress. While many of Sty1-induced gene expression changes are attributed to transcriptional control through Atf1, some occur through pathways independent of Atf1 (Chen et al, 2003). As these alternative pathways have not been extensively studied, I instead decided to investigate whether new gene expression was at all required for the CRIB-3xmCitrine dispersal. To test this, I imaged CRIB-3xmCitrine-expressing cells where all new protein synthesis was blocked using cycloheximide (CHX) prior to the addition of LatA. LatA treatment in these cells still resulted in the dispersal of tip-localized CRIB-3xmCitrine despite the presence of CHX (Figure 3.6, B). This result suggested that LatA-driven CRIB-3xmCitrine dispersal can occur independently of any changes in gene expression, including those driven by known and unknown Sty1-dependent pathways.

Given than that the CHX treatment did not prevent LatA-induced CRIB-3xmCitrine dispersal, it was particularly important to demonstrate that CHX treatment was indeed completely inhibiting protein synthesis. While the CHX treatments with similar concentrations (100 µg/mL) are widely used in fission yeast research, direct demonstrations of CHX efficiency are rarely reported and likely to depend on the particular experimental setup. Thus, to confirm that 100 µg/mL CHX did completely inhibit protein synthesis in the cells examined, I tested the effects of the CHX treatment on cells expressing an isopropyl β-D-1-thiogalactopyranoside (IPTG)-inducible *GFP* gene (See Materials and Methods Section 2.8; Kjaerulff & Nielsen, 2015). In these cells, addition of IPTG led to a gradual increase in cellular GFP fluorescence for the whole duration of the experiment (Figure 3.6, C). Similar to non-induced cells, cells treated with CHX at the same time as IPTG exhibited no increase in GFP fluorescence. When CHX was added after IPTG-induced GFP

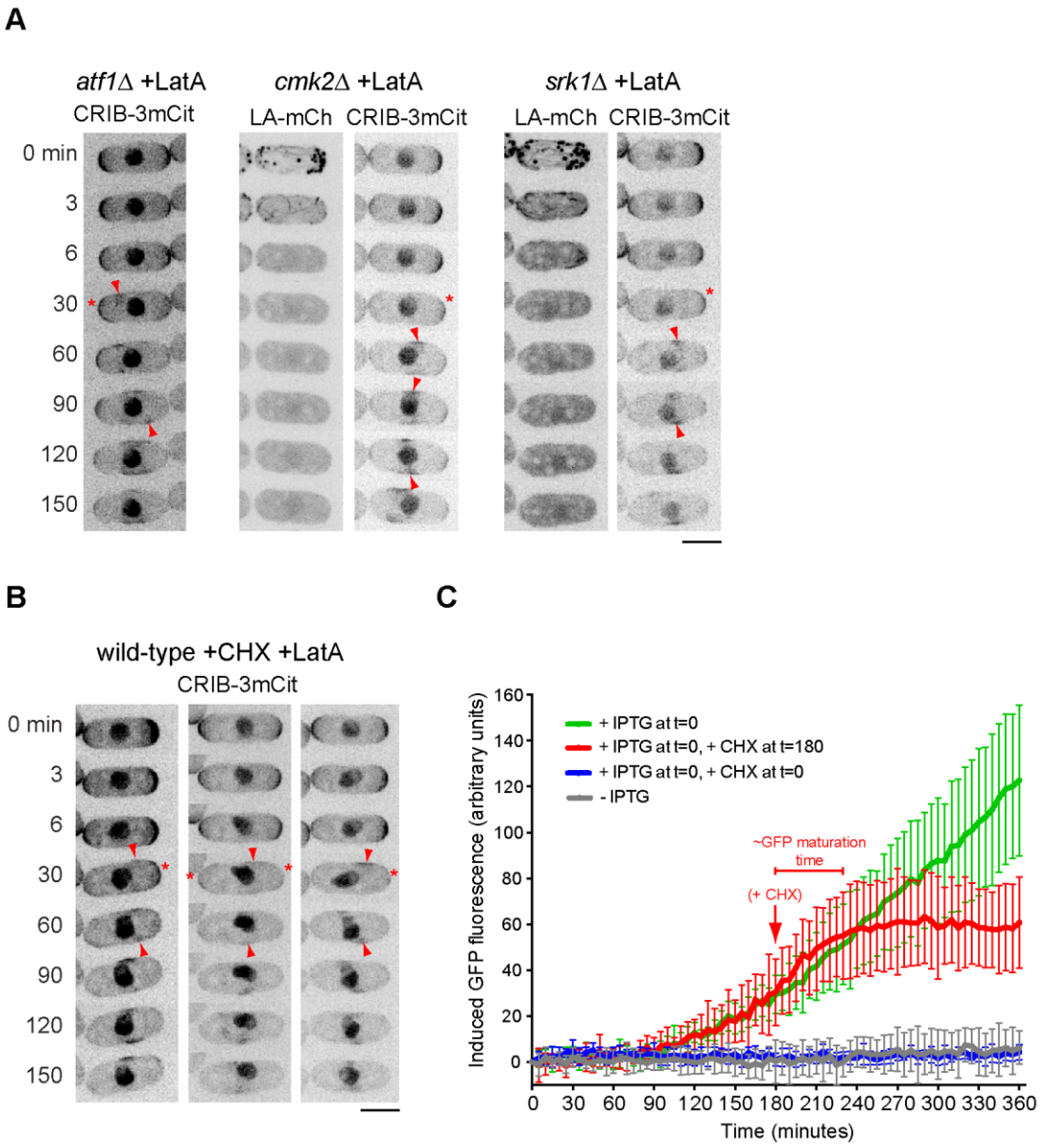

Figure 3.6. CRIB-3xmCitrine dispersal by Latrunculin A does not require known Sty1-activated proteins or Sty1-induced changes in gene expression. (A) Time-lapse images of *atf1*Δ, *cmk2*Δ, *and srk1*Δ cells expressing CRIB-3xmCitrine (CRIB-3mCit) after addition of 50 µM Latrunculin A (LatA). The *cmk2*Δ *and srk1*Δ cells also expressing Lifeact-mCherry (LA-mCh). (B) Time-lapse images of LA-mCh and CRIB-3mCit in wild-type cells pre-treated with 100 µg/mL cycloheximide (CHX) for 10 min prior to addition of 50 µM LatA in the continued presence of CHX. CHX treatment leads to disruptions in the shape of nuclei to varying extents; therefore multiple example cells are shown. (C) Quantification of induced GFP fluorescence in wild-type cells containing an isopropyl β-D-1-thiogalactopyranoside (IPTG)-inducible GFP gene in the presence or absence of 100 µg/mL CHX. Error bars indicate SD.
Red asterisks mark CRIB-3mCit dispersal from the cell tips. Red arrowheads in (A) and (B) point to ectopic CRIB-3mCit patches after the dispersal. All times shown in (A) and (B) are relative to addition of LatA. Scale bars, 5 µm.

expression was already detectable, fluorescence continued to increase for approximately 45 min (Gordon *et al*, 2007). Taken together, these observations confirmed the complete translation inhibition caused by the addition of CHX in my experimental system.

The protein kinase Plo1 has been previously shown to be phosphorylated on residue S402 in a Sty1-dependent manner after some types of stresses, such as high temperature and gravity (Petersen & Hagan, 2005). While Plo1 S402 phosphorylation state has only been reported to regulate aspects of cell polarity recovery after stress, it is conceivable that Plo1 might also play a role in the initial stress response to LatA, concomitant with the CRIB-3xmCitrine dispersal. To test that possibility, I imaged CRIB-3xmCitrine and Lifeact in the analog-sensitive *plo1.as8* mutant after LatA treatment in the presence of 3BrB (Grallert *et al*, 2013). Addition of LatA after inhibition of Plo1 still resulted in CRIB-3xmCitrine dispersal, although this dispersal was relatively slower than the one observed in LatA-treated wild-type cells (Figure 3.7, A). This was likely due to the higher concentration of 3BrB (30 µM) used for Plo1 inhibition, as evidenced by the slower dispersal observed in LatA-treated wild-type cells exposed to the same concentration of 3BrB. As an additional control, LatA-treatment of non-inhibited *plo1.as8* cells resulted in a CRIB dispersal with a similar rate to wild-type cells. Consistent with Plo1.as8 inhibition, 3BrB-treated *plo1.as8* cells (in the absence of LatA) were able to divide their nuclei (karyokinesis) but unable to perform cytokinesis or septation (Figure 3.7, A; Grallert *et al*, 2013). However, it should be noted that this outcome likely does not reflect a full *plo1* loss of function, which would be expected to lead not only to a block in cytokinesis but also a block in mitotic progression altogether (Ohkura *et al*, 1995). Thus, as the site of Sty1-dependent phosphorylation on Plo1 had been previously mapped to S402, I also tested whether the phospho-mimetic S402E or phospho-null S402A mutants behaved differently in response to LatA addition. Consistent with the outcome of the *plo1.as8* experiments, upon LatA treatment, none of the S402 mutants showed any difference in the observed CRIB-3xmCitrine dispersal, compared to wild-type cells (Figure 3.7, B). Taken together, these results suggest that Sty1-depependent regulation of Plo1 is not involved in the CRIB-3xmCitrine dispersal induced by LatA treatment.

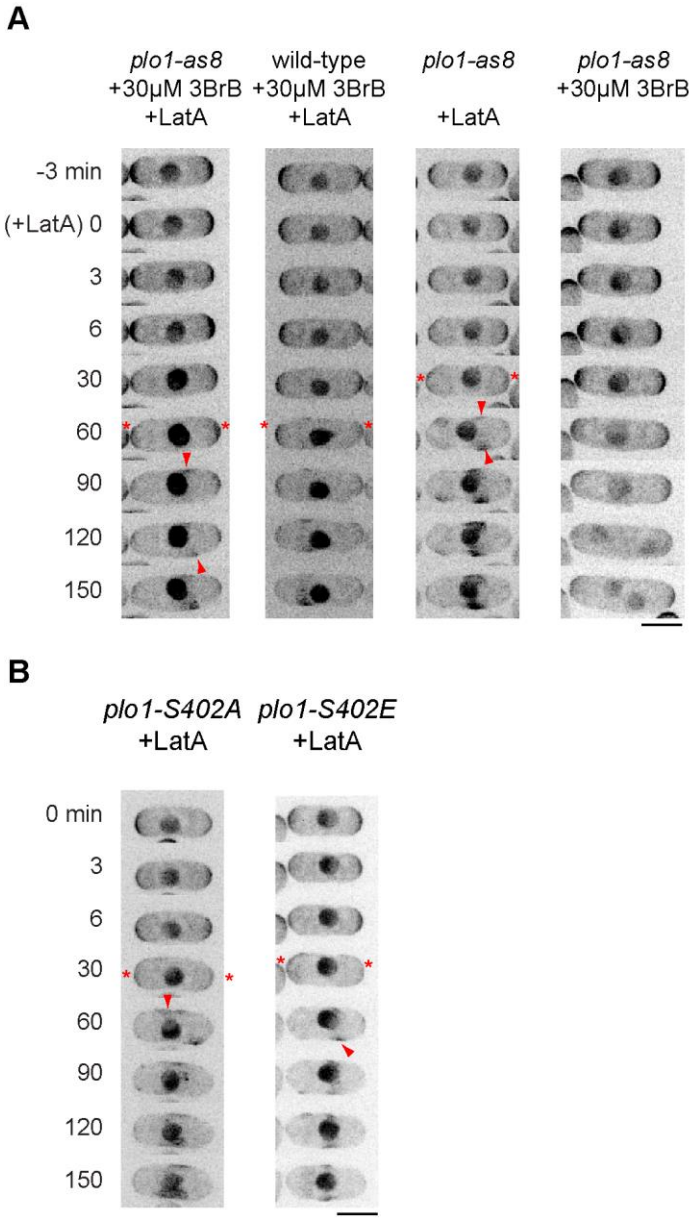

Figure 3.7. CRIB-3xmCitrine dispersal by Latrunculin A does not require known kinases activated downstream of Sty1 . (A) Time-lapse images of *plo1-as8* and wild-type cells expressing CRIB-3xmCitrine (CRIB-3mCit). In first two panels panels cells are pre-treated with 30μM 3BrB-PP1 (3BrB) for 10 min, prior to addition of 50 μM Latrunculin A (LatA) in the continued presence of 3BrB. In third panel cells are just treated with LatA. In fourth panel, cells are just treated with 30μM 3BrB. (B) Time-lapse images of CRIB-3mCit-expressing *plo1-S402A* and *plo1-S402E* cells after addition of 50 μM LatA.
Red asterisks mark CRIB-3mCit dispersal from the cell tips. Red arrowheads point to ectopic CRIB-3mCit patches after the dispersal. All times shown are relative to addition of LatA. Scale bars, 5 μm.

3.2.6 Stress-independent Sty1 activation is sufficient to drive Cdc42-GTP disruption

The experiments presented thus far indicate that Sty1 is activated by LatA treatment and that Sty1 activity is necessary for LatA-induced CRIB-3xmCitrine dispersal from cell tips. However, while Sty1 certainly contributes to the process of CRIB-3xmCitrine dispersal, the extent of this contribution remains unclear. For example, one interpretation of the results described so far is that the Sty1 activation resulting from LatA addition is solely responsible for driving CRIB-3xmCitrine tip dispersal. However, an alternative explanation could be that the CRIB-3xmCitrine dispersal is the result of a combination of Sty1 activation and other effects caused by the addition of LatA, such as the complete actin depolymerisation. One way to discern between these two possibilities is to examine the behaviour of CRIB-3xmCitrine in situations where Sty1 is activated under conditions where actin is not depolymerised, and when there is no other additional external perturbation to the cell.

For this purpose, I developed a system in which Sty1 can be selectively and quickly switched on or off *in vivo* without the use of external triggers of stress response. This was achieved by generating a strain containing several genetic modifications of the SAPK pathway. The strain was termed 'SISA' for Stress-Independent Sty1 Activation (Figure 3.8, A). In *SISA* cells, the wild-type *sty1* gene is replaced with the analog-sensitive *sty1-T97A* allele, which as described earlier in the chapter, allows specific inhibition of Sty1 kinase activity by using the ATP-competitive analog 3BrB. Additionally, wild-type MAPKK *wis1* is replaced with the constitutively active *wis1-DD* allele, originally constructed by Shiozaki *et. al*, 1998. As described in the Introduction (see Introduction 1.6), the activity of the MAPKK Wis1 (which is the direct activator of Sty1) is controlled by phosphorylation on residues Ser469 and Thr473 by the MAPKKKs Win1 and Wis4. A constitutively active version of the kinase can be obtained by replacing these residues with a phospho-mimetic aspartate, generating the *wis1-DD* allele. Thus, cells carrying this allele exhibit elevated basal levels of Sty1 activation which cannot be altered by regulators upstream of the pathway (e.g. by MAPKKKs in response to stress; Shiozaki *et al*, 1998). Finally, *SISA* cells also contained a double deletion of the tyrosine phosphatases Pyp1 and Pyp2 (Millar *et al*, 1995b). Both Pyp1 and Pyp2 have been shown to play a key role in the attenuation of SAPK signalling by dephosphorylating activated Sty1 (Millar et al, 1995;

Shiozaki & Russell, 1995; see also Introduction 1.6). Importantly, Pyp2 participates in a regulatory negative-feedback loop for suppressing SAPK signalling, because Sty1 activation leads to an increase in Pyp2 levels and protein stability, and thus Sty1 activation ends up promoting Sty1 deactivation, via Pyp2 (Kowalczyk *et al*, 2013). I hypothesised that in *SISA* cells (*wis1-DD sty1-T97A pyp1*∆ *pyp2*∆*)* grown in the presence of 3-BrB, Sty1 would exist in an activated state (because it is phosphorylated by constitutively-active Wis1-DD) but would nevertheless be inhibited by the presence of 3-BrB (because of the T97A analog-sensitive mutation). Accordingly, upon removal of 3-BrB from the medium, Sty1 activity would quickly increase without the feedback suppression provided by the Pyp1/2 phosphatases. Thus, the effects of Sty1 activation on Cdc42-GTP distribution could be assayed without the use of LatA.

SISA cells exhibited normal growth and morphology when grown in the presence of 5 µM 3BrB (Figure 3.8, B). However, when transferred to a medium lacking 3BrB, they developed abnormal shape by increasing in size and becoming swollen around the cell mid-zone. Cell counting showed that the *SISA* cells also stopped dividing essentially immediately upon removal of 3BrB (Figure 3.8, C). To confirm that these changes were associated with the intended effect of Sty1 activation, I assayed the behaviour of Atf1 using western blotting. Whole-cell extracts of *SISA* cells probed with an anti-Atf1 antibody showed a significant increase in Atf1 levels upon removal of 3BrB (Figure 3.8, D and E). This was consistent with the expected up-regulation of Atf1 levels upon Sty1 activation (Shiozaki & Russell, 1996). Additionally, I observed a small but reproducible change in Atf1 migration upon removal of 3BrB, consistent with previously described migration shift caused by Sty1 phosphorylation (Lawrence *et al*, 2007; Sansó *et al*, 2008).

To assess the effect of Sty1 activation on the localisation of Cdc42-GTP, I imaged *SISA* cells expressing CRIB-3xmCitrine and Lifeact in the presence of 3BrB and upon removal of 3BrB. While 3BrB was present, CRIB-3xmCitrine and Lifeact distributions were undistinguishable from those of wild-type cells (Figure 3.9). However, upon removal of 3BrB, the CRIB-3xmCitrine signal dispersed from the *SISA* cell tips within approximately 30 min, and ectopic CRIB-3xmCitrine patches

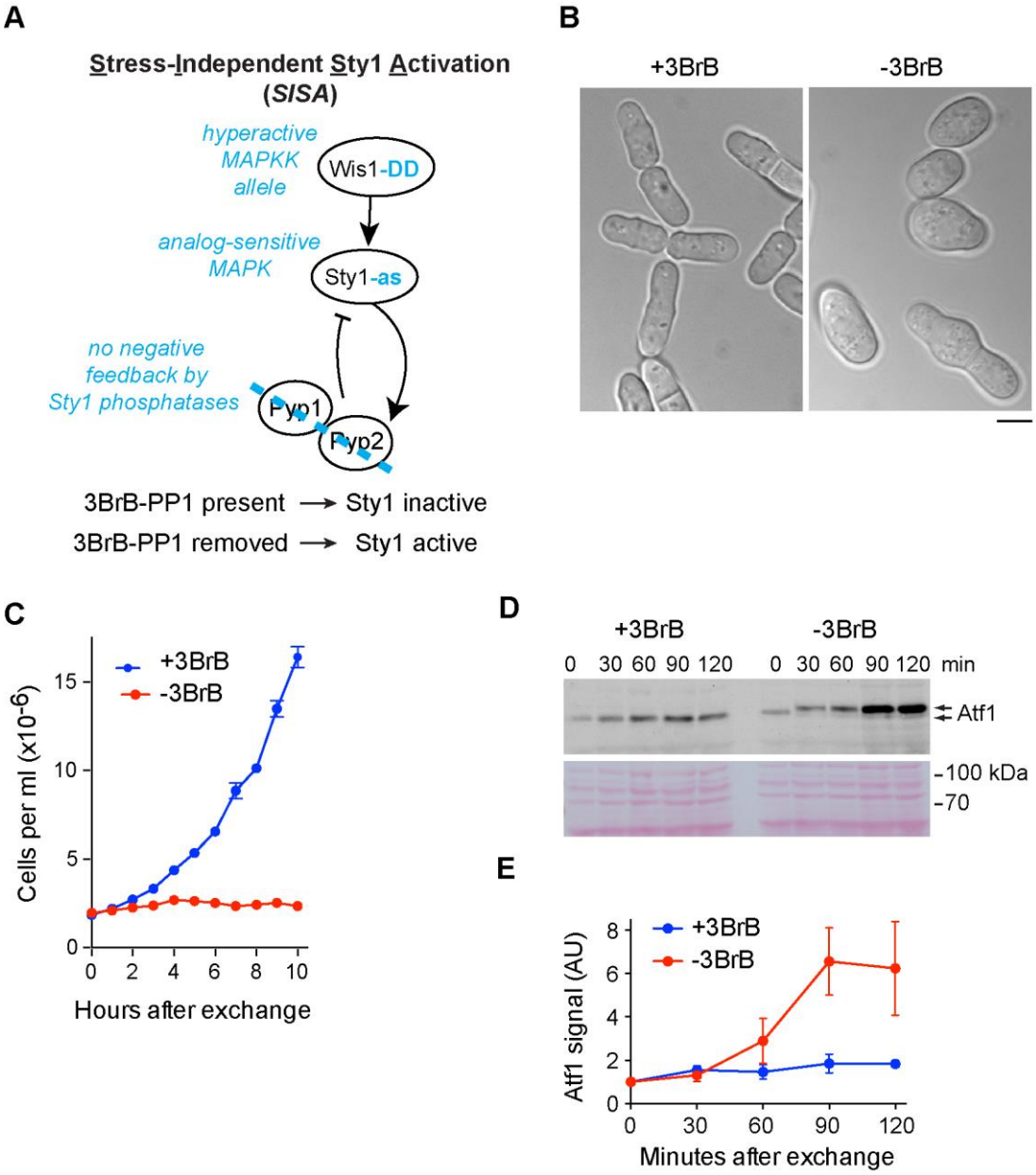

Figure 3.8. Activation of Sty1 in the absence of external stress leads to cell cycle arrest, morphological changes, and increase in Atf1 levels and phosphorylation. (A) Schematic representation of the genetic changes in the MAPK pathway (in light-blue) introduced in the Stress-Independent Sty1 Activation (*SISA*) cells. (B) Brightfield DIC images of *SISA* cells grown in the presence of 3-BrB-PP1 (+3BrB) and 24 h after 3-BrB removal (-3BrB). Scale bar, 5 µm. (C) Cell-number growth curves of *SISA* cells in the presence of 3-BrB (+3BrB) and after 3-BrB removal (-3BrB). Error bars indicate SEM. (D) Anti-Atf1 Western blot of extracts from *SISA* cells in the presence (+3BrB) and after removal of 3-BrB (-3BrB). Times are relative to start of 3-BrB removal. Arrows point at the migration shift of Atf1 after 3-BrB removal. Ponceau S stain of the same region of the blot is shown underneath. (E) Quantification of Atf1 levels in *SISA* cells from experiments of the type shown in E. Mean values from three independent experiments. Error bars indicate SEM.

appeared on the cell sides, just as I observed for LatA-treated wild-type cells (Figure 3.9, A). To confirm that the observed changes in CRIB-3xmCitrine behaviour faithfully reported the distribution of active Cdc42 in this experimental setup, I also imaged *SISA* cells expressing either CRIB-3xmCitrine and Cdc42-mCh^{sw}. Both markers co-dispersed upon removal of 3BrB, with CRIB-3xmCitrine patches co-localizing with accumulation of Cdc42-mCh^{sw} (Figure 3.9, A). Taken together, these results suggested that Sty1 activation alone is sufficient to drive the tip-dispersal of Cdc42-GTP. Concomitantly with the CRIB-3xmCitrine dispersal, the actin cytoskeleton became depolarised (not *depolymerised*), with some actin patches concentrating in the areas of CRIB-3xmCitrine patch accumulation (Figure 3.9, A and C). Thus, the observed actin depolarization can be interpreted as a downstream consequence of the dispersal of Cdc42-GTP. As an additional control, the change in actin distribution upon removal of 3BrB from *SISA* cells was also confirmed without the use of Lifeact, by imaging phalloidin-stained fixed cells (Figure 3.9, C).

Given that Sty1 activation upon 3BrB withdrawal in *SISA* cells was sufficient to disperse and depolarise CRIB-3xmCitrine, I decided to next investigate whether Sty1 activity was necessary to maintain the CRIB-3xmCitrine dispersal. Provided this was the case, I hypothesised that inhibition of Sty1 in cells where CRIB-3xmCitrine is already-dispersed would result in re-polarization of the CRIB-3xmCitrine. To test this hypothesis, I imaged *SISA* cells where 3BrB was first removed from the media for 90 minutes (leading to Sty1 activation and CRIB3xmCitrine-dispersal) and then re-introduced back. Upon inhibition of Sty1 by adding back 3BrB, the dispersed CRIB patches almost immediately (within 10 min) reorganised back to the original place of growth at the cell tips (Figure 3.9, B). Following the recovery of tip Cdc42-GTP, the actin patches also repolarized back to the tips and cells proceeded with elongation and division.

3.2.7 The Cdc42-effector Scd2 follows Cdc42-GTP distribution during Sty1-induced Cdc42-GTP dispersal

Thus far, the effects of Sty1 activation on the Cdc42 polarity module have been assayed either by using CRIB-3xmCitrine as a reporter for Cdc42 activity or by directly observing the distribution of Cdc42-mCh^{sw}. Furthermore, the impact of the Cdc42-GTP dispersal has been characterised mostly on a phenomenological basis,

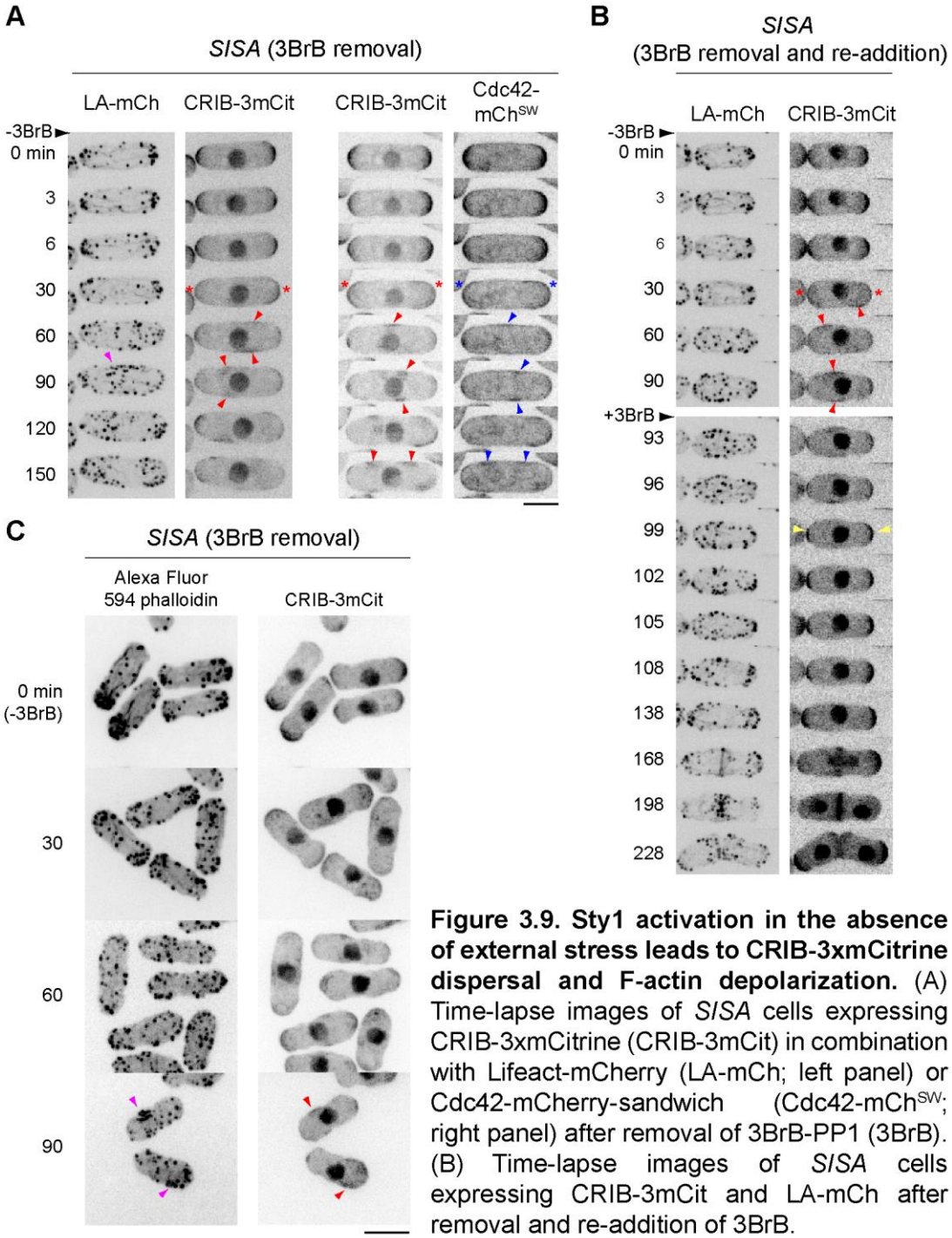

Figure 3.9. Sty1 activation in the absence of external stress leads to CRIB-3xmCitrine dispersal and F-actin depolarization. (A) Time-lapse images of *SISA* cells expressing CRIB-3xmCitrine (CRIB-3mCit) in combination with Lifeact-mCherry (LA-mCh; left panel) or Cdc42-mCherry-sandwich (Cdc42-mCh^{SW}; right panel) after removal of 3BrB-PP1 (3BrB). (B) Time-lapse images of *SISA* cells expressing CRIB-3mCit and LA-mCh after removal and re-addition of 3BrB. (C) Alexa Fluor 594 phalloidin staining of the actin cytoskeleton in fixed *SISA* cells expressing CRIB-3mCit after removal of 3BrB. Images demonstrate the actin-depolarizing effect of Sty1 activation without the use of LA-mCh.
Red asterisks mark CRIB-3mCit dispersal from the cell tips. Red arrowheads point to ectopic CRIB-3mCit patches after the dispersal. Blue asterisks and arrowheads used in the same manner for Cdc42-mCh^{SW}. Yellow arrowheads point to CRIB-3mCit recovery at the tips upon 3BrB re-addition. Magenta arrowheads point to examples of cortical actin patches, co-localizing with CRIB-3mCit patches. All times shown are relative to initiation of 3BrB removal. Scale bars, 5 µm.

as it correlated with cessation of tip-growth, depolarization of the actin cytoskeleton or the long-term swelling around the cell mid-zone. However, as Cdc42 function in polarity and growth is mediated through its interactions with downstream effectors, it was important to demonstrate that, despite being dispersed from the cell tips, Cdc42-GTP was still able to interact with at least some of its downstream effectors. For this purpose, I imaged the localisation of the Cdc42 effector Scd2 in the context of Sty1-induced Cdc42-GTP dispersal. Scd2 is a scaffold protein that preferentially binds Cdc42-GTP and acts a platform for recruiting other Cdc42 effectors such as the PAK kinase Shk1 (Chang *et al*, 1994; Endo *et al*, 2003; Wheatley & Rittinger, 2005; also see Introduction 1.3.3).

To visualise the localisation of Scd2 during Sty1-induced Cdc42-GTP dispersal, I replaced the endogenous Scd2 with a fluorescently-tagged Scd2-3xmCherry version of the protein in wild-type, *sty1*Δ, or *SISA* cells already expressing CRIB-3xmCitrine. To assess the effects of Sty1 activation on Scd2 distribution, I first imaged the behaviour of Scd2-3xmCherry and CRIB-3xmCitrine upon LatA-induced Sty1 activation in wild-type cells. Consistent with previously published data, Scd2-3xmCherry co-dispersed with CRIB-3xmCitrine from the cell tips upon the addition of LatA and both markers later co-localised at ectopic sites along the cell sides (Kelly & Nurse, 2011; Figure 3.10, A). By contrast (but as expected), when LatA was added to *sty1*Δ cells expressing Scd2-3xmCherry/CRIB-3xmCitrine, both markers remained at the cell tips, suggesting that changes in Scd2-3xmCherry distribution upon LatA addition were also dependent on Sty1 function (Figure 3.10, B). Finally, I examined the effects on Scd2-3xmCherry/CRIB-3xmCitrine localisation during stress-free Sty1 activation in *SISA* cells. Analogous to the behaviour observed after addition to LatA, Scd2-3xmCherry and CRIB-3xmCitrine co-dispersed from the cell tips upon the removal of 3BrB (Figure 3.10, C). Taken together, these experiments confirm that the Sty1-driven Cdc42-GTP dispersal also results in the dispersal of the Cdc42-effector Scd2. Thus, the observed changes in Cdc42-GTP distribution in response to Sty1 activation also likely reflect changes in the distribution and function of other downstream Cdc42-effectors.

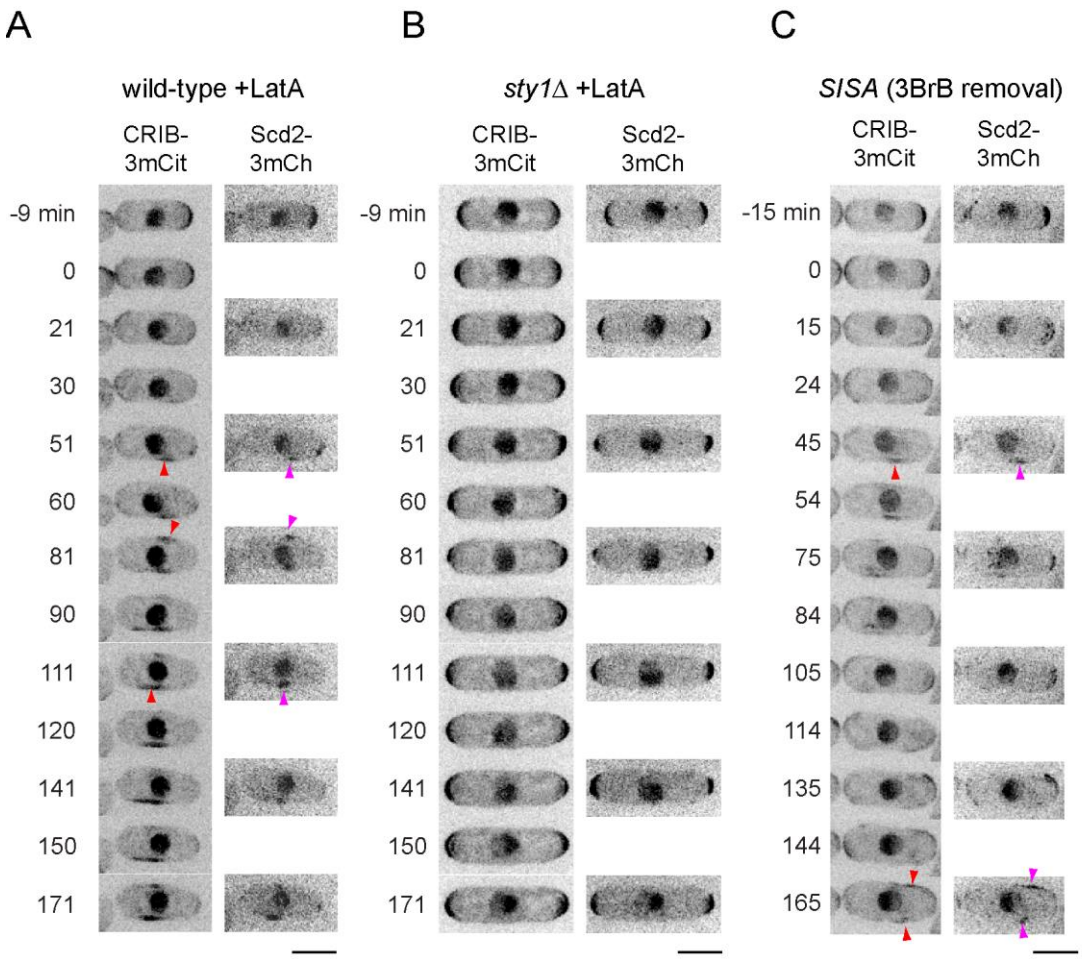

Figure 3.10. Scd2-3xmCherry co-localises with CRIB-3xmCitrine prior and after Sty1 activation. Time-lapse images of wild-type (A), *sty1*Δ (B), *and SISA* (C) cells expressing CRIB-3xmCitrine (CRIB-3mCit) and Scd2-3xmCherry (Scd2-3mCh). Cells shown are subjected to either addition of 50 µM Latrunculin A (LatA; (A) and (B)) or removal of 3BrB-PP1 (3BrB; (C)). Red and magenta arrowheads point to ectopic patches of CRIB-3mCit and Scd2-3mCh respectively. All times shown in (A) and (B) are relative to addition of LatA. Times shown in (C) are relative to initiation of 3BrB removal. Scale bars, 5 µm..

3.2.8 Sty1 activity is required to maintain a non-polarized state in nitrogen-starved quiescent cells

The results presented earlier in this chapter suggest a novel role for the MAPK Sty1 in driving the dispersal of Cdc42-GTP in the context of LatA addition or stress-free Sty1 activation in *SISA* cells. While both of these experimental approaches were pivotal in uncovering Sty1's involvement in Cdc42 regulation, they provide little information on the physiological relevance of this phenomenon. Thus, I decided to investigate whether the newly found role for Sty1 in driving Cdc42-GTP dispersal has implications for any known physiological processes in fission yeast cells. In particular, I focused on the process of nitrogen-starvation-induced cellular quiescence. During nitrogen-starvation, fission yeast cells cease elongation and enter two consecutive divisions, leading to the generation of four small round cells (Figure 3.10; Yamamoto *et al*, 1997; Harigaya & Yamamoto, 2007). Next, homothallic (self-mating) cells proceed to mating, while heterothallic cells lacking a mating partner enter a quiescent G0-like state (Su *et al*, 1996). One of the characteristics of this state is the continued depolarization of the Cdc42 polarity module (Figure 3.11; Bendezú & Martin, 2013). Interestingly, previous studies have shown that *sty1*Δ cells fail to cease elongation upon N-starvation and possess poor mating, suggesting Sty1 activity might be required for maintaining a depolarized state during quiescence, which in turn might contribute to cell-cell exploration during mating (Sajiki *et al*, 2009; Bendezú & Martin, 2013; Merlini *et al*, 2016).

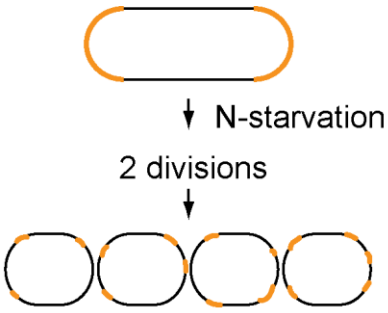

Figure 3.11. Quiescence entry upon nitrogen starvation. Schematic representation of cell divisions after nitrogen starvation (N-starvation) in heterothallic cells. Upon N-starvation, cells divide twice before reaching quiescence, with little elongation during interphase. This produces a chain of four small granddaughter cells that lack any overall polarization. Cell polarity machinery (e.g. CRIB-3xmCitrine) is shown in orange.

To test whether Sty1's role in regulating CRIB-3xmCitrine distribution is involved in the process of maintaining depolarised Cdc42 polarity during nitrogen-starvation-induced quiescence, I observed the behaviour of CRIB-3xmCitrine in nitrogen-starved wild-type and *sty1-T97A* in the presence and absence of 3BrB. All the imaged cells were first deprived of nitrogen source for 10 hours until reaching the four granddaughter stage, characterised by weak and depolarised Cdc42-GTP. Additionally, I only performed experiments on heterothallic cells lacking a mating partner, as those cells will remain in quiescence, rather than proceed to mating, until more favourable conditions are introduced. In the absence of 3BrB, both nitrogen-starved wild-type and *sty1-T97A* exhibited dispersed and dynamic CRIB-3xmCtirine behaviour for the full duration of imaging (4 hours; Figure 3.12). However, upon addition of 3BrB, the CRIB-3xmCitrine in *sty1-T97A* cells gradually repolarized to the cell tips and the cells resumed elongation within 30 minutes, despite the lack of nitrogen in the media (Figure 3.12). As a control, addition of 3BrB did not have any visible effects on Sty1 distribution in N-starved wild-type cells. These results suggest that the activity of Sty1 is required to maintain CRIB-3xmCitrine in a depolarised state during nitrogen-starvation-induced quiescence.

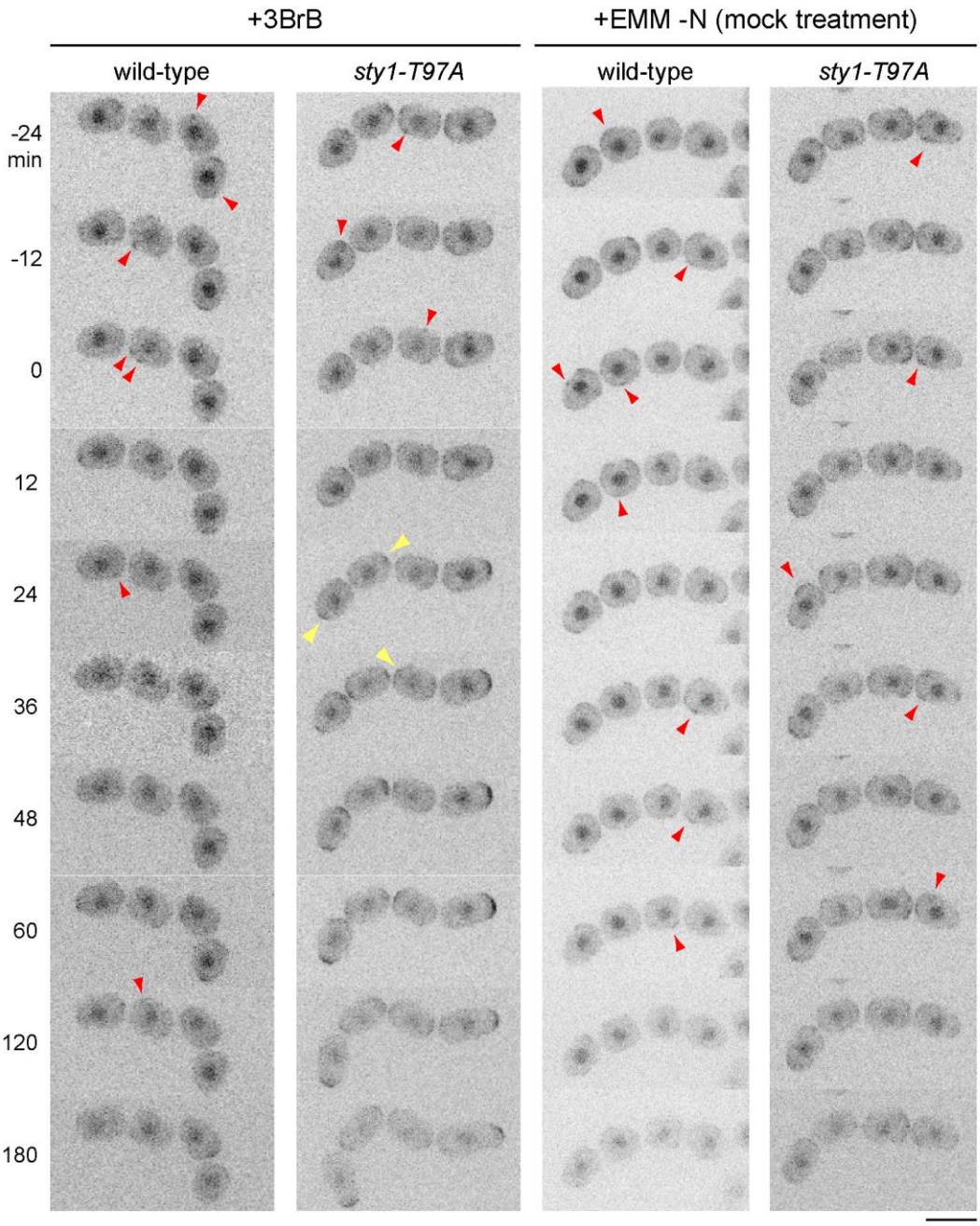

Figure 3.12. Inhibition of Sty1 leads to repolarization of nitrogen-starved quiescent cells. Time-lapse images of CRIB-3xmCitrine (CRIB-3mECit) in N-starved wild-type and sty1-T97A cells before and after addition of 3-BrB-PP1 (3BrB) or 3BrB-free EMM-N medium (mock treatment). Chains of four granddaughter cells are shown. Red arrowheads indicate ectopic patches of CRIB-3mCit. Yellow arrowheads indicate repolarization of CRIB-3mCit. Times shown are relative to 3BrB addition; at 0 min, cells have already been N-starved for 11 h, including 1 h of imaging. Scale bar, 5 µm.

3.3 Discussion

The generation of a novel CRIB probe to follow Cdc42-GTP dynamics allowed for long-term *in vivo* imaging of fission yeast cells without the phototoxic effects on growth attributed to exposure to GFP-excitation light (for details see Ashraf S, 2016 PhD Thesis). However, it should be mentioned that a recent study has independently described a functional fluorescently-tagged version of Cdc42 in fission yeast by inserting the tag on an internal loop of the protein (Bendezú *et al*, 2015). Using this 'sandwich' fusion with mCherry (Cdc42-mCh^{sw}), the authors showed that Cdc42 itself is also enriched at sites where it is active, also making the reporter suitable for the study of Cdc42-GTP distribution. Nevertheless, the study also showed that the CRIB-3xGFP distribution faithfully reported the enrichment of Cdc42-sandwich in unperturbed and perturbed (e.g. LatA treatment) scenarios. Therefore, while the Cdc42-mCh^{sw} is used as control in some of my further experiments, due to the progress already made at the time this probe was published, I utilised the CRIB-3xmCitrine for the majority of my experiments looking at active Cdc42 distribution.

Similar to the existing CRIB-3xGFP probe, the CRIB-3xmCitrine localised not only to the areas of active growth but also to the cell nucleus (Figure 3.1). The CRIB-3xmCitrine also exhibited a stronger nuclear signal (relative to tip signal) compared to CRIB-3xGFP, suggesting that differences in the promoter or the used fluorescent protein might influence the extent of nuclear localisation. While the nuclear target of CRIB-3xmCitrine remains unknown, the sub-population of CRIB-3xmCitrine in the nucleus is not expected to be binding to active Cdc42, because Cdc42 itself is not localised inside the nucleus (Bendezú *et al*, 2015). To further investigate the origin of CRIB-3xmCitrine nuclear localisation I constructed a number of different CRIB fusions, which I describe in greater detail in Appendix 1. Nevertheless, the behaviour of nuclear CRIB-3xmCitrine will not be reported or discussed in further experiments as it is not related to Cdc42 dynamics.

As expected, treatment with LatA led to the dispersal of CRIB-3xmCitrine from the cell tips as described in previous studies (Figure 3.2). The combination of using both CRIB-3xmCitrine and Lifeact, however, helped to clearly visualise the difference between the onset of actin depolymerization and CRIB-3xmCitrine dispersal. The quick disappearance of F-actin structures upon addition of LatA (mostly gone within 3 min) visibly contrasted the gradual and delayed dispersal of CRIB-3xmCitrine

(between 20 to 30 min), suggesting that the CRIB-3xmCitrine dispersal might be due to an indirect effect of the actin depolymerization. An alternative explanation could be that Cdc42-GTP has a very slow turnover at the cell tips. However, fluorescence recovery after photobleaching (FRAP) experiments have demonstrated that while Cdc42-GTP has slower turnover at the plasma membrane than Cdc42-GDP, it still remains highly mobile, with photobleaching recovery half-times within 5- 10 seconds (Bendezú *et al*, 2015).

The finding that LatA treatment activates the MAP kinase Sty1, together with the initial report about LatB (Gachet *et al*, 2001), are surprising results, as the stress-response SAPK pathway is highly conserved but few parallels can be drawn with similar findings in other organisms. For example, the budding yeast Sty1 homolog Hog1, which is also activated in response to osmotic stress, is not activated by addition of LatA (Reise*r et al*, 2000, 2003). Instead, another MAP kinase Slt2 (also known as Mpk1) has been reported to be activated in response to LatB (Harrison *et al*, 2001) and likely by LatA (Woods *et al*, 2016). However, the kinetics of Slt2 activation seem to be very different from those observed for Sty1. In particular, while Sty1 phosphorylation in response to LatA seems to peak about 10 min after treatment and then gradually declines over the next 90 minutes (although I have not tested if it subsides completely), Slt2 phosphorylation was reported to gradually increase for at least 4 hours during continued exposure to LatB (Harrison *et al*, 2001). In addition, Slt2 has been identified to be part of the functionally distinct Cell-Wall-Integrity pathway (Levin, 2005). Thus, it is likely that the functional significance of Latrunculin-induced MAPK activation is fundamentally different between *S.pombe* and *S.cerevisiae*.

One interesting question that arises from the observation that LatA treatment activates stress-response signalling is about the involvement of F-actin in this process. An intriguing idea is that LatA could trigger an 'actin stress response' where the state of F-actin or proteins that bind to F-actin act as sensors for certain perturbations and signal the activation of SAPK pathway. One parallel that can be drawn here is the role of F-actin as a mechanosensor and regulator of growth in *Drosophila* and mammalian tissues. While the exact mechanisms are currently an area of active research, there is multiple evidence to suggest that levels of F-actin or the tension of the actin cytoskeleton can regulate the Hippo signalling pathway

responsible for driving growth and proliferation (Sansores-Garcia *et al*, 2011; Aragona *et al*, 2013; Sun & Irvine, 2016). On the other hand, LatA could also have 'off-target' effects which trigger the activation of Sty1 independently from the depolymerization of the actin cytoskeleton. Although currently this problem remains not completely resolved, I have performed several sets of experiments aimed at distinguishing between these scenarios which I describe at length in Appendix 2.

The results presented in this chapter place the MAPK Sty1 as a novel regulator of Cdc42 polarity. Unexpectedly, the function of the SAPK pathway was required for the dispersal of CRIB-3xmCitrine induced after addition of LatA. In the absence of either MAPK Sty1 or its direct activator MAPKK Wis1, the CRIB-3xmCitrine distribution after LatA remained at the cell tips even in the complete absence of F-actin structures (Figure 3.5). The observed continued elongation of SAPK-deficient cells (*sty1*Δ*, wis1*Δ*,* or *sty1-T97A* plus 3BrB) after addition of the drug also suggested that the growth-promoting function of the Cdc42 polarity module was preserved and therefore that F-actin is not strictly required for growth (i.e. cell elongation). However, the elongation rate in LatA-treated SAPK-deficient cells was slower and gradually declined over time. My interpretation of this finding is that cell elongation in these cells is achieved by Cdc42-driven positive regulation of exocytosis (He & Guo, 2009; Wu *et al*, 2010). However, membrane-bound proteins involved in exocytosis may need to be recycled back to the cytoplasm via endocytosis, which in turn is dependent on F-actin (Goode *et al*, 2015). Thus, one can predict that in the presence of LatA, continued exocytosis would eventually lead to the depletion of the cytoplasmic pool of the proteins required to sustain it and therefore to gradual cessation of growth.

Another implication of the discovered requirement for Sty1 in LatA-induced CRIB-3xmCitrine dispersal is that it argues against a direct role for actin in the maintenance of Cdc42-GTP tip stability. Furthermore, as activation of Sty1 in *SISA* cells was sufficient to drive CRIB-3xmCitrine dispersal without depolymerization of F-actin structures it is unlikely that the actin cytoskeleton is directly involved in maintaining CRIB-3xmCitrine on the cell tips. However, it is still possible that the hypothesised role for the actin cytoskeleton in maintaining the long-term stability of the Cdc42 module works through Sty1 signalling. For example, actin could be responsible for the activation of Sty1 in response to depolymerization of F-actin structures (see also Appendix 2). An additional consequence that follows from my

results is that studies that use LatA to investigate how the actin cytoskeleton contributes to cellular functions should also consider the possibility that the observed effects are a result of a stress response rather than of actin depolymerization; alternatively, observed effects could be due to a combination of both of these.

To my knowledge, the discovered role of Sty1 in regulating Cdc42 polarity is novel and a parallel function for a stress-response MAPK has not been observed—or at least, not yet observed--in other organisms. For example, despite the well-described role of Cdc42 in regulation of the budding yeast Sty1 homolog Hog1, there is currently no evidence that Hog1 itself is involved in regulation of the Cdc42 polarity module, or in mating efficiency or responses to nutrient deprivation (Brewster & Gustin, 2014). Furthermore, it is very intriguing that the involvement of Sty1 in regulating Cdc42 seems to be independent of any previously studied functions of Sty1, such as the activation of Atf1, Srk1, Cmk2, or Polo 1. In addition, most studies so far have focused on the role of Sty1 in regulation of gene expression after stress and the substrates of Sty1 kinase (such as the transcription factor Atf1) facilitating these changes. Thus, as Sty1's role in driving active Cdc42 dispersal is independent of new protein expression, further investigation into the mechanisms underlying Sty1-driven active Cdc42 dispersal could lead to identification of novel direct targets of Sty1 not involved in gene regulation.

In principle, an alternative way of addressing the question of whether Sty1 activation without actin depolymerization is sufficient to drive the dispersal of CRIB-3xmCitrine might be to use a range of different treatments that activate stress response but do not completely depolymerise the actin cytoskeleton (e.g a conventional osmotic shock). However, one significant drawback of any approach using alternative external stresses is that each of these stresses could affect cellular physiology in multiple unknown ways, in addition to activating Sty1. For example, separate consequences of the same stress could trigger additional cellular processes that counteract, lessen, or change the kinetics of the effects of Sty1 activation, such as CRIB-3xmCitrine dispersal. Furthermore, some external stresses could also have effects on the integrity of the actin cytoskeleton and thus not be suitable to discern between the effects of Sty1 activation alone and the disruption of actin. For example, traditionally used stresses such as osmotic shock, heat, or hypergravity have all been shown to result in transient dispersal of F-actin patches although whether this is a

direct or indirect consequence of the stress is less clear (Rupes *et al*, 1999; Bao *et al*, 2001; Petersen & Hagan, 2005; Soto *et al*, 2007; Robertson & Hagan, 2008).

Thus, an approach such as the *SISA* system, where the SAPK signalling can be selectively turned on and off without the use of an external stress, is far better suited to dissect the individual contribution of Sty1 activation to the dispersal of CRIB-3xmCitrine. The inspiration for the *SISA* cells originated from previous genetic evidence that had demonstrated that repressing Pyp1 in *pyp2*Δ cells resulted in cell arrest and aberrant morphology and that a *pyp1*Δ *pyp2*Δ double deletion can be rescued by deleting Sty1 (Mill*ar et al*, 1995). However, in the process of constructing the *SISA* strain, it became clear that the removal of 3BrB in *sty1-T97A pyp1*Δ *pyp2*Δ cells was not sufficient to achieve the phenotype of Pyp1 repression in *pyp2*Δ cells unless the hyperactive *wis1-DD* was present too (data not shown). One explanation of this is that the outcome of the experiments described in the original study was likely due to some initial stress stimulus triggering Sty1 activation (e.g. the experiments were performed in minimal medium). Another possibility is that the analog-sensitive mutant of Sty1 in *sty1-T97A pyp1*Δ *pyp2* cells had reduced activity compared to the wild-type and thus required additional activation from the hyperactive Wis1-DD. Furthermore, removal of 3BrB in a w*is1-DD sty1-T97A* mutant was also not sufficient to induce the phenotype observed after 3BrB removal in *SISA* (data not shown), likely due to an increased counteracting activity of Pyp1 and Pyp2. Thus, all four mutations (w*is1-DD, sty1-T97A*, *pyp1*Δ*, pyp2*Δ) were required to achieve the consistent activation of Sty1 in *SISA* cells.

The experiments performed with the *SISA* cells demonstrated that Sty1 activation alone was sufficient to drive the tip dispersal of CRIB-3xmCitrine and the continued activity of Sty1 was required to maintain CRIB-3xmCitrine dispersed (Figure 3.9). Interestingly, upon the inhibition of Sty1 following a CRIB-3xmCitrine dispersal, *SISA* cells repolarized CRIB-3xmCitrine back at the original sites of growth, rather than at ectopic sites along the cell membrane (thus forming new growth axis). This result suggests that important polarity landmarks are retained at the tips during Sty1 activation and thus can facilitate tip recovery of Cdc42-GTP when Sty1 activity declines. Therefore, Sty1's role in CRIB-3xmCitrine dispersal might involve the decoupling of the Cdc42 polarity module and other cell-polarity landmarks. I investigate this problem further in Chapter 4.

Finally, the requirement for Sty1 activity in maintaining a non-polarized Cdc42 distribution during nitrogen-starvation quiescence reveals at least one physiological role for the newly discovered relationship between SAPK signalling and the Cdc42 polarity module. Interestingly, disrupting Cdc42 polarity might also be essential for entry into quiescence, as previous data has shown that *sty1Δ* and *wis1Δ* mutants continue to elongate upon N-starvation (Sajiki *et al*, 2009). Furthermore, it would be interesting to further investigate how Sty1's role in controlling active Cdc42 might influence cell-cell pairing or re-initiation of growth (shmooing) during mating.

The results in this chapter revealed an exciting novel role for Sty1 signalling in controlling the distribution of active Cdc42. Surprisingly, this new function is independent of many described processes driven by the MAPK and thus is likely to involve phosphorylation of novel cytoplasmic targets related to Cdc42 regulation. In the next chapter, I explore the behaviour of some of the known regulators of Cdc42 in response to Sty1 activation to obtain further insight into the underlying mechanisms of Sty1-driven Cdc42-GTP dispersal.

Chapter 4

Differential response of Cdc42 GEF's to Sty1 activation; Landmark regulation of Cdc42 polarity module localisation

4.1 Introduction

In Chapter 3 I described a new role for the Sty1 MAPK in regulating the activity of the key polarity GTPase Cdc42. Interestingly, the observed dispersal of Cdc42-GTP upon activation of Sty1 was found to occur independently of new protein expression or the functioning of various pathways previously described to mediate Sty1 function. Thus, how Sty1 drives the dispersal of Cdc42-GTP remains unclear. In this chapter, I present some preliminary findings aimed at further elucidating this problem by applying a 'candidate-based' approach where individual experiments examine the behaviour of known Cdc42 and polarity regulators in the context of Sty1 activation. In the first part of the chapter, I investigate the behaviour of the Cdc42 guanine nucleotide exchange factors (GEFs) in response to Sty1 activation and their contribution to the Cdc42-GTP dispersal observed after Sty1 activation. In the second part, I examine contribution of the polarity landmark protein Tea1 for the recovery of the Cdc42 polarity module following Sty1-driven Cdc42-GTP depolarization.

In fission yeast cells, there are two GEFs, Scd1 and Gef1, able to catalyse the exchange of GDP for GTP on Cdc42 and thus activate the GTPase (Chang *et al*, 1994; Coll *et al*, 2003). As described in the Introduction (see Section X), the two Cdc42 GEFs seem to have spatially distinct roles in controlling Cdc42. Scd1, which is localised to the cell tips during interphase, is essential for polarised growth, as *scd1*Δ cells are round-shaped and show no detectable accumulation of CRIB-3xGFP on the cell membrane (Chang *et al*, 1994; Tatebe *et al*, 2008; Kelly & Nurse, 2011). In contrast, deletion of Gef1 causes defects in bipolar growth establishment and septum formation but no strong alterations in morphology (Coll *et al*, 2003). While Gef1 is consistently reported to be localised at the site of septation during cytokinesis, different Gef1 localisations have been reported during interphase. The original study identifying Gef1 by Coll *et. al*, 2003 describes it is diffused throughout the cytoplasm except for the nucleus, while Das *et. al*, 2009, Vjestica *et al*, 2013, Kokkoris *et al*. 2014, and Das *et. al*, 2015 show it is localised at the cell tips. While the two GEFs might have discrete roles in controlling Cdc42, *gef1*Δ *scd1*Δ double mutants are not viable, indicating that they are the only essential activators of the GTPase. Thus, to obtain further insight into how Sty1-driven Cdc42-GTP dispersal might be mediated, I decided to investigate the behaviour of the two GEFs during Sty1 activation and evaluate whether and how they contributed to the process of Cdc42-GTP dispersal. In the first part of this chapter, I present preliminary evidence suggesting that the two

GEFs might be differentially regulated upon Sty1 activation. Furthermore, I demonstrate that the ectopic Cdc42-GTP patches formed as a result of Sty1 activation are dependent on Gef1.

In Chapter 3 I showed that in the *SISA* strain, inhibiting Sty1 following a period of Sty1-driven CRIB-3xmCitrine dispersal resulted in recovery of the CRIB-3xmCitrine cluster back to its original position at the cell tips, as opposed to at a random site on the cell membrane. This result suggested that certain polarity landmarks are retained at the cell tips during the Sty1-mediated CRIB-3xmCitrine dispersal and that these allow recovery of CRIB-3xmCitrine to cell tips when Sty1's activity is eventually attenuated. Additionally, this finding also suggested a potential role for Sty1 in decoupling the Cdc42 module from such landmarks at cell tips.

A key polarity landmark in fission yeast is the protein Tea1, which, as described at greater length in Introduction Section 1.4, is delivered to the cell tips via the microtubule cytoskeleton and plays an important role in the correct positioning of the polarisation machinery (Mata & Nurse, 1997). Interestingly, *tea1*Δ cells are prone to forming new polarity axes following exposure to stress, as they fail to reinitiate growth at the cell tips and instead grow from random ectopic sites (Verde *et al*, 1995; Mata & Nurse, 1997; Sawin & Snaith, 2004; Tatebe *et al*, 2005). Furthermore, Tea1 and its interacting partner Tea4 are hypothesised to play a role in the direct regulation of Cdc42 polarity although the exact details of how this is achieved are not fully understood. In one identified pathway for Cdc42 regulation, the Tea1-Tea4 complex can promote the localisation of the DYRK kinase Pom1 at the cell poles, where Pom1 contributes to the local exclusion of the Cdc42 GTPase-activating protein (GAP) Rga4, thus creating a favourable local environment for Cdc42 activation (Tatebe *et al*, 2008; Hachet *et al*, 2011). Furthermore, the Tea1-Tea4 complex might also be involved in the recruitment of Gef1 and the Cdc42 effector For3, although the molecular details of how this is achieved are unclear (Martin *et al*, 2007; Kokkoris *et al*, 2014). Thus, in the second part of this chapter, I investigate the involvement of Tea1 in the tip recovery of dispersed CRIB-3xmCitrine following Sty1 inhibition using live-cell imaging and manipulation of *tea1*Δ *SISA* cells. My preliminary findings suggest that while Tea1 does contribute to the timely tip-recovery of CRIB-3xmCitrine, it is very likely that additional polarity landmarks are also involved in this process.

4.2 Results

4.2.1 Scd1 and Gef1 change their cellular association with Cdc42-GTP during Sty1 activation

Because Scd1 and Gef1 are the only known Cdc42 GEFs, I hypothesised that Sty1 activity might regulate some aspects of Scd1/Gef1 localisation or function in order to drive the dispersal of Cdc42-GTP. To explore this possibility, I first examined the localisation of both Scd1 and Gef1 Sty1 activation. For this purpose, I generated cells which, in addition to the CRIB-3xmCitrine reporter, carried 3xmCherry fluorescently-tagged versions of either Scd1 or Gef1. Because the signals of both Scd1-3xmCherry and Gef1-3xmCherry in these cells were relatively weak and sensitive to photobleaching, I was able to perform live-cell imaging with only limited time resolution.

Consistent with previous published findings (Kelly & Nurse, 2011), Scd1-3xmCherry co-localised with CRIB-3xmCitrine at the cell tips during interphase in unperturbed wild-type cells (Figure 4.1, A). In contrast, interphase Gef1-3xmCherry was dispersed in the cytoplasm in unperturbed wild-type cells (Figure 4.1, A). This localisation was consistent with the original report by Coll *et. al*, 2003, but not with the later studies by Das *et. al*, 2009, Vjestica *et al*, 2013, Kokkoris *et al*. 2014, and Das *et. al*, 2015.

In agreement with previous published results, upon addition of LatA in wild-type cells, Scd1-3xmCherry disappeared from the cell tips within the first 30 min but did not later co-localise with the CRIB-3xmCitrine ectopic patches which formed on the cell sides (Figure 4.1, A; Kelly & Nurse, 2011). On the other hand, after the same treatments, Gef1-3xmCherry, which was initially cytoplasmic, later co-localised with CRIB-3xmCitrine at the ectopic sites along the cell sides (Figure 4.1, A). Neither Scd1-3xmCherry nor Gef1-3xmCherry changed localisation upon LatA treatment in *sty1*Δ cells, suggesting that the observed changes after LatA addition were dependent on Sty1 (Figure 4.1, B). Furthermore, I also assayed the localisation of Scd1-3xmCherry and Gef1-3xmCherry after Sty1 activation in *SISA* cells, induced by the removal of 3BrB. Similar to the outcome after LatA addition, after the removal of 3BrB, Scd1-3xmCherry was dispersed in the cytoplasm, while

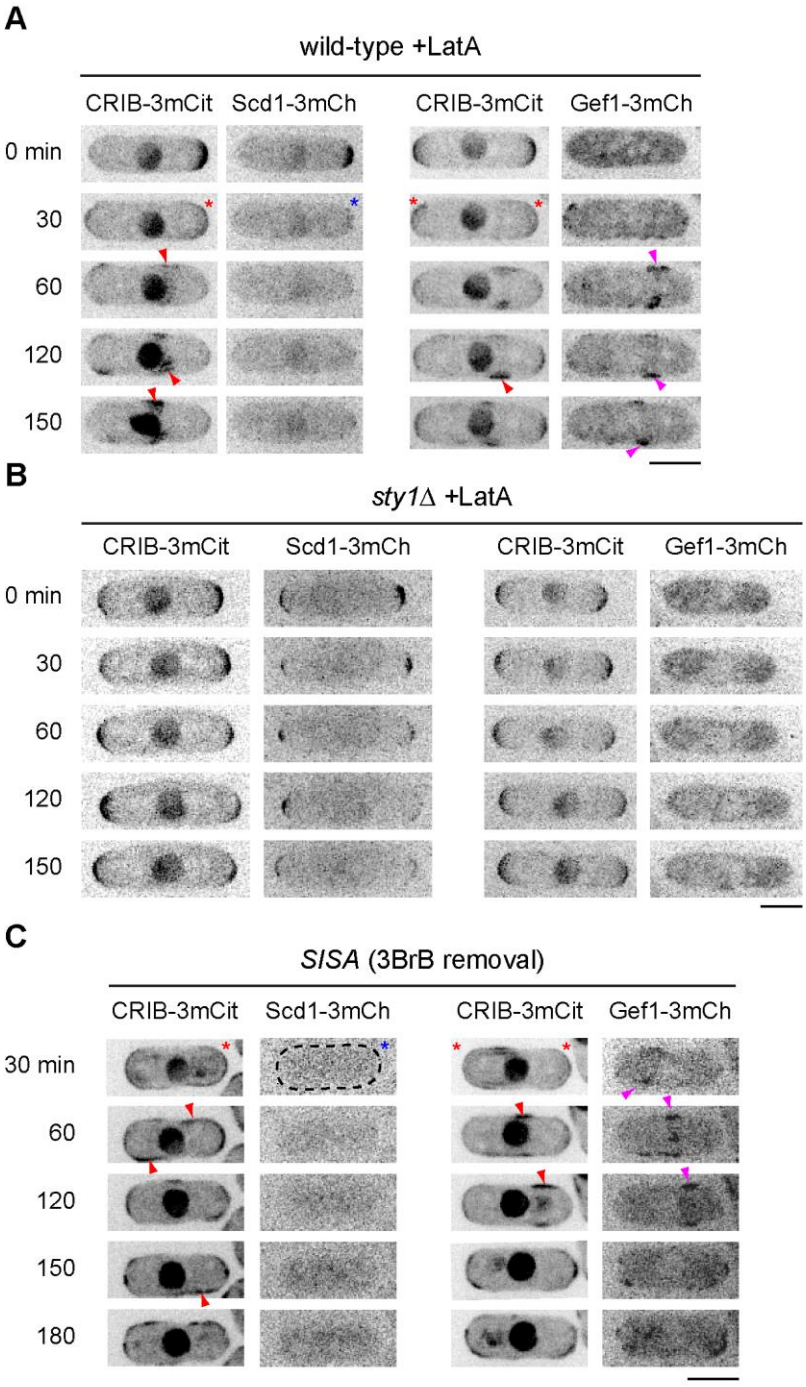

Figure 4.1. Scd1-3xmCherry and Gef1-3xmCherry exhibit different behaviours upon Sty1 activation. Time-lapse images of wild-type (A), *sty1*Δ (B), *and SISA* (C) cells expressing CRIB-3xmCitrine (CRIB-3mCit) together with either Scd1-3xmCherry (Scd1-3mCh) or Gef1-3xmCherry (Gef1-3mCh). Cells shown are subjected to either addition of 50 µM Latrunculin A (LatA; (A) and (B)) or removal of 3BrB-PP1 (3BrB; (C)). Red and blue asterisks mark dispersal from the cell tips of CRIB-3mCit and Scd1-3mCh respectively. Red and magenta arrowheads point to ectopic patches of CRIB-3mCit and Gef1-3mCh respectively. All times shown in (A) and (B) are relative to addition of LatA. Times shown in (C) are relative to 3BrB removal via mild centrifugation and medium exchange. Scale bars, 5 µm.

Gef1-3xmCherry co-localised with the ectopic patches of CRIB-3xmCitrine (Figure 4.1, C). While the initial localisations of Scd1-3xmCherry and Gef1-3xmCherry in the presence of 3BrB (Sty1 inactive) were not recorded in this experiment, they were confirmed to be as in unperturbed wild-type cells (Scd1- at the tips, Gef1- cytoplasmic) in independent experiments during the generation of the strain (data not shown).

Taken together, these findings suggest that Scd1 and Gef1 switch their association with Cdc42 upon activation of Sty1: Scd1 which is normally associated with Cdc42 at the tips becomes dispersed in the cytoplasm, while Gef1 which is normally in the cytoplasm becomes associated with ectopic patches of Cdc42.

4.2.2 Gef1 is required for ectopic Cdc42-GTP patches during Sty1 activation

Because both GEFs showed significant changes in their localisation during Sty1 activation, I speculated that they might contribute to the Sty1-driven regulation of Cdc42. If that was the case I predicted that at least some aspects of Cdc42-GTP behaviour upon Sty1 activation would change in the absence of either of the GEFs. Furthermore, as Gef1 (but not Scd1) co-localised with ectopic Cdc42-GTP at the ectopic sites along the cell sides I also predicted that Gef1 might be essential for the Cdc42 activation at these sites. To test these predictions, I examined the behaviour of CRIB-3xmCitrine in LatA-treated *gef1*Δ and *scd1*Δ cells.

Upon addition of LatA to *gef1*Δ cells, the CRIB-3xmCitrine rapidly dispersed from the cell tips within 15-18 minutes of treatment (Figure 4.2, A and B). This dispersal was faster than the one observed in wild-type cells which normally occurred between 20-to 30 minutes of treatment (Figure 3.2, A). Comparable to wild-type cells, *gef1*Δ cells also stopped elongating following the addition of LatA. Interestingly, after CRIB-3xmCitrine disappeared from the cell tips, no ectopic patches of CRIB-3xmCitrine were formed on the cell sides. Instead, CRIB-3xmCitrine distribution became concentrated in the cell nucleus. While this effect was likely due to the absence of Gef1 activity at the cell sides, in principle, CRIB-3xmCitrine nuclear accumulation could also be caused by an increase in CRIB-3xmCitrine nuclear binding resulting from LatA addition in a *gef1*Δ genetic background. To confirm that the absence of ectopic patches following LatA treatment in *gef1*Δ cells was not due to an increased CRIB-3xmCitrine nuclear

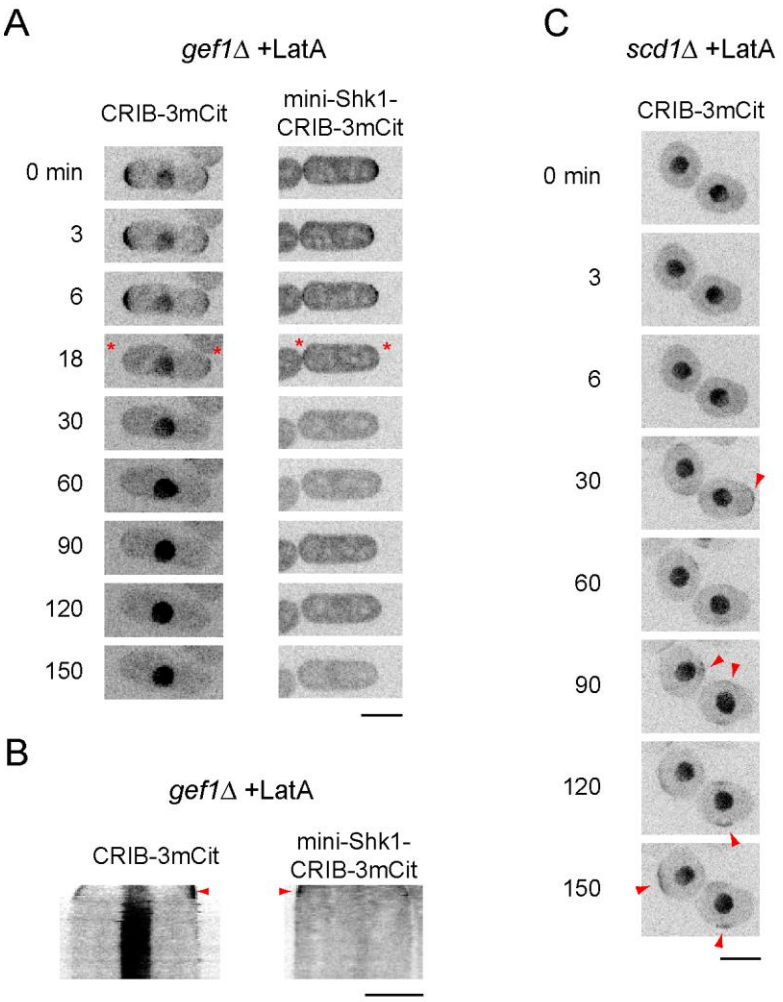

Figure 4.2. Latrunculin A-induced ectopic CRIB-3xmCitrine patches require Gef1 but not Scd1. Time-lapse images of *gef1*Δ (A) and *scd1*Δ (C) cells expressing CRIB-3xmCitrine (CRIB-3mCit) after addition of 50 µM Latrunculin A (LatA). In (A), cells expressing mini-Shk1-CRIB-3xmCitrine are also shown. (B) Kymographs of the cells shown in (A). Red arrowheads indicate time of LatA addition.
Red asterisks mark CRIB-3mCit dispersal from the cell tips. Red arrowheads in (A),(C), and (D) point to ectopic patches of CRIB-3mCit. All times shown in (A), (C), and (D) are relative to addition of LatA. Scale bars, 5 µm.

affinity, I repeated the experiment using the mini-Shk1-CRIB-3xmCitrine reporter for Cdc42 activity (described in detail in Appendix 1) which does not localise to the nucleus. Similar to CRIB-3xmCitrine, mini-Shk1-CRIB-3xmCitrine also dispersed rapidly from the cell tips and did not show any enrichment at ectopic sites along the cell sides (Figure 4.2, A and B).

The absence of ectopic CRIB-3xmCitrine patches during LatA-treatment of *gef1*Δ cells suggested that Gef1 is required for activating Cdc42 at ectopic sites during LatA-driven Sty1 activation. Following this interpretation, I further speculated that ectopic CRIB-3xmCitrine patches should still be observed in LatA-treated *scd1*Δ cells, despite the expected absence of detectable CRIB-3xmCitrine at cell membrane in unperturbed *scd1*Δ cells. To test this prediction, I imaged CRIB-3xmCitrine in *scd1*Δ cells upon the addition of LatA.

Consistent with previous findings, unperturbed *scd1*Δ cells showed round-cell morphology and no detectable CRIB-3xmCitrine at their plasma membranes during interphase (Figure 4.2, C). However, within 30 min of LatA addition, patches of CRIB-3xmCitrine formed at random sites along the cell membrane and exhibited the dynamic behaviour also observed for ectopic CRIB-3xmCitrine patches in LatA-treated wild-type cells (Figure 3.2, A). Furthermore, as also observed in wild-type cells, the patches in *scd1*Δ cells seemed to migrate towards what could be defined as the cell middle considering the previous place of septation (Figure 4.2, C). These results supported a role for Gef1 in driving ectopic Cdc42 activation upon LatA-induced Sty1 activation, since by definition, the formed ectopic CRIB-3xmCitrine patches in LatA-treated *scd1*Δ cells can only be formed through the activity of the only remaining Cdc42 GEF - Gef1. Furthermore, these findings also suggest that Gef1-dependent ectopic CRIB-3xmCitrine patches formed in response to Sty1 activation do not require the presence of pre-existing CRIB-3xmCitrine clusters.

4.2.3 Tea1 is involved in Cdc42-GTP recovery at the cell tips after Sty1-induced Cdc42-GTP dispersal

Given the importance of Tea1 as a polarity landmark and its potential role in regulating Cdc42 polarity, I decided to investigate whether Tea1 plays a role in the tip recovery of dispersed CRIB-3xmCitrine upon inactivation of Sty1. I hypothesised that if the role of Sty1 in CRIB-3xmCitrine dispersal involved the decoupling of the Cdc42 polarity module from the Tea1 polarity module, then one would expect that

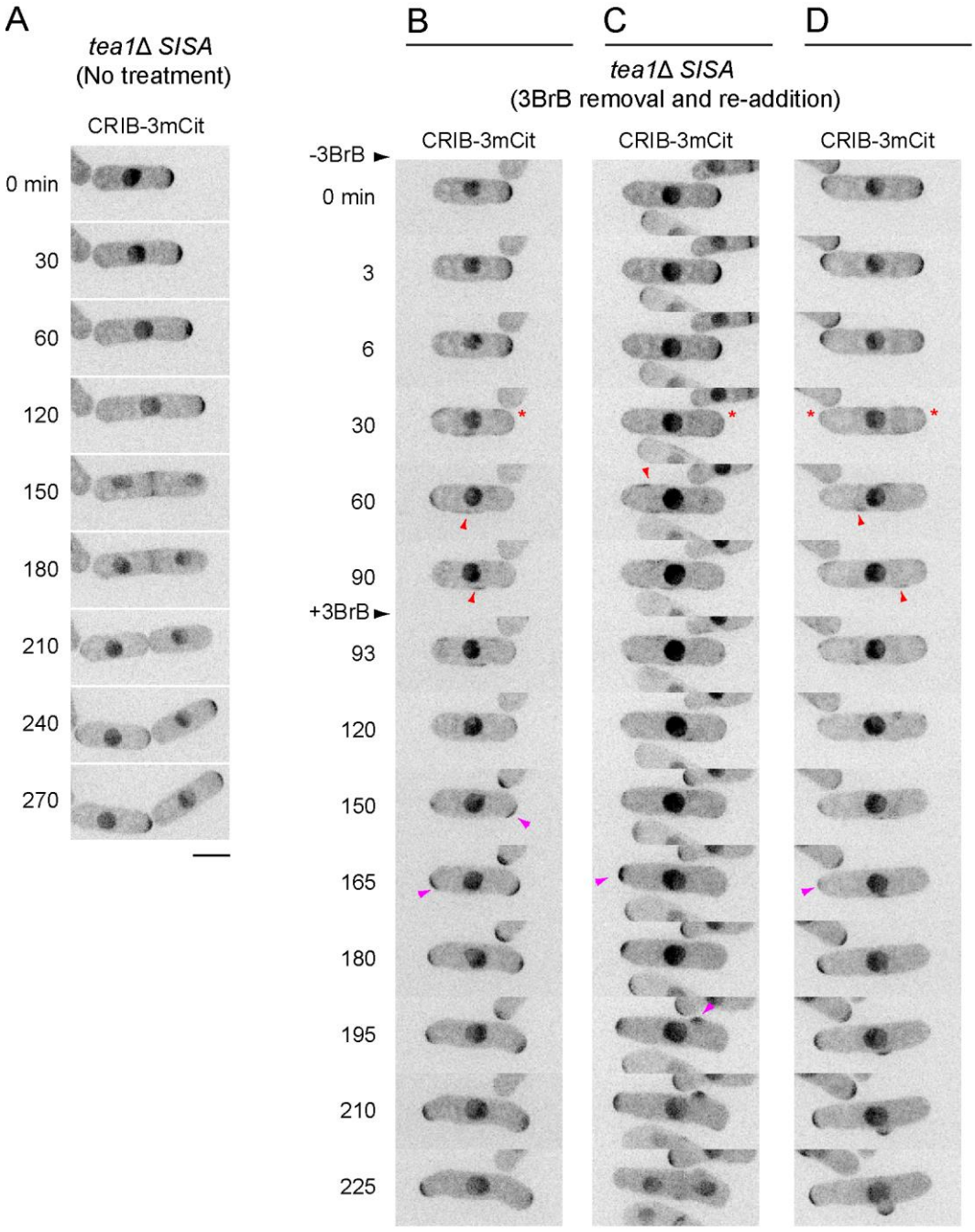

Figure 4.3. Recovery of CRIB-3xmCitrine after Sty1-induced dispersal in *tea1*Δ *SISA* cells can occur both at tips and at ectopic sites. (A) Time-lapse images of *tea1*Δ *SISA* cell expressing CRIB-3xmCitrine (CRIB-3mCit) showing a monopolar growth pattern prior and after division. (B),(C), and (D) Time-lapse images of *tea1*Δ *SISA cells* expressing CRIB-3mCit after removal and re-addition of 3BrB-PP1 (3BrB). Three examples shown to illustrate different locations of CRIB-3xmCitrine before and after 3BrB removal or re-addition. Red asterisks mark CRIB-3mCit dispersal from the cell tips. Red arrowheads point to ectopic CRIB-3mCit patches. Magenta arrowheads point to recovered CRIB-3mCit clusters after re-addition of 3BrB. All times shown in (A) are relative to start of imaging. Times shown in (B),(C), and (D) are relative to initiation of 3BrB removal. Scale bars, 5 μm.

CRIB-3xmCitrine recovery following Sty1 inhibition in *SISA* cells where Tea1 is deleted would in some way differ from the CRIB-3xmCitrine recovery in *tea1+ SISA* cells. Possibly, this difference could constitute recovery at ectopic sites, leading to branched cells. Alternatively, there could be a difference in kinetics of recovery the Cdc42 polarity module to cell tips. To test this idea, I examined the recovery of CRIB-3xmCitrine in *tea1*Δ *SISA* cells.

In agreement with published data on *tea1*Δ mutants, *tea1*Δ *SISA* cells in the presence of 3BrB exhibited mostly monopolar growth (Figure 4.3, A, B, and C; Mata & Nurse, 1997). Although previous reports identify *tea1*Δ cells as exclusively monopolar, about 5% of the observed unperturbed *SISA tea1*Δ cells (n = 73) showed bipolar growth (e.g. Figure 4.3, D). This discrepancy can be explained by the fact that previous characterisation of the growth pattern of *tea1*Δ cells was performed in EMM2 minimal medium, while the *tea1*Δ *SISA* cell presented here are grown and imaged in rich medium (See M&M Section 2.12). Indeed, independent experimental data from the Sawin lab has shown that while *tea1*Δ cells grow exclusively monopolar in minimal medium, about 3% of *tea1*Δ cells exhibit bipolar growth in rich medium (Sanju Ashraf, unpublished data).

To examine the recovery of CRIB-3xmCitrine after the Sty1 inhibition, first, 3BrB was removed from the *tea1*Δ *SISA* medium for 1.5 hours to induce CRIB-3xmCitrine dispersal from tips. Like the behaviour of CRIB-3xmCitrine in *tea1+ SISA* cells (Figure 3.9, A and B), CRIB-3xmCitrine in *tea1*Δ *SISA* cells dispersed from the cell tips within 30 min of 3BrB removal (Figure 4.3, B, C, and D). However, upon re-addition of 3BrB, the CRIB-3xmCitrine clusters recovered significantly more slowly in *tea1*Δ *SISA* cells (recovery within 60-75 min) than in *tea1+ SISA* (recovery within 10 min). This suggests that Tea1 function is not absolutely required for CRIB-3xmCitrine recovery after Sty1-induced CRIB-3xmCitrine dispersal, although Tea1 is important for timely recovery. In addition, *tea1*Δ *SISA* cells showed multiple phenotypes with respect to the localisation of the recovered CRIB-3xmCitrine cluster. About 90% of the cells (n= 97) recovered their CRIB-3xmCitrine cluster and re-initiated growth at their cell tips, although the direction of the re-initiated growth was often at a different angle with respect to the original growth axis (Figure 4.3, B; Figure 4.4). In contrast, the remaining 10% of cells re-polarized their CRIB-3xmCitrine at one or more ectopic sites (as well as at one of the cell tips), thus forming at least one novel axis of growth (Figure 4.3, C and D). These findings

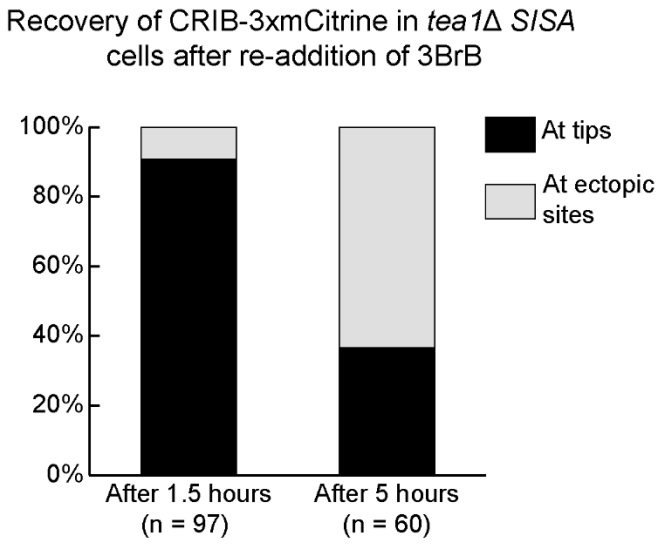

Figure 4.4. Incidence of CRIB-3xmCitrine recovery at ectopic sites increases with prolonged Sty1 activation in *tea1Δ SISA* cells. Bar graph showing the distribution of number of cells with CRIB-3xmCitrine recovery at tips or at ectopic sites in *tea1Δ SISA* cells where 3BrB-PP1 was first removed for either 1.5 or 5 hours and next re-introduced. Individual cells were scored as 'At tips' if the observed CRIB-3xmCitrine recovery occured at one or two of tips where growth occured prior to 3BrB removal. Alternatively, cells were scored as 'At ectopic sites' if the observed CRIB-3xmCitrine recovery occured at one or more ectopic sites which were not sites of growth prior to 3BrB removal. This classification also includes cells in which CRIB-3xmCitrine recovered to the cell tips in addition to an ectopic site. Fisher's exact test two-tailed P-value < 0.0001.

support the idea that Tea1 is involved in the correct positioning of CRIB-3xmCitrine back to the cell tips. However, since only 10% of the observed *tea1*Δ *SISA* cells initiated growth from ectopic sites, additional polarity landmarks are also likely involved in determining the positioning of CRIB-3xmCitrine recovery. To obtain some further insight into the stability or behaviour of these remaining landmarks, I imaged the process of CRIB-3xmCitrine recovery in *tea1*Δ *SISA* cells in which Sty1-activation was maintained for 5 hours (3.5 hours longer than the initial experiment). Interestingly, following 5 hours of Sty1-driven CRIB-3xmCitrine dispersal, 63% of *tea1*Δ *SISA* cells (n = 60) exhibited CRIB-3xmCitrine recovery and growth initiation at ectopic sites (Figure 4.4). This suggested that prolonged Sty1 activation significantly increased the likelihood of ectopic CRIB-3xmCitrine recovery in *tea1*Δ *SISA* cells. Thus, the additional landmarks facilitating tip recovery in these cells were likely gradually degraded or removed from the cell tips during the prolonged absence of polarised Cdc42-GTP. Another interesting observation from the *tea1*Δ SISA experiments was that most *tea1*Δ SISA cells which were growing in a monopolar fashion before the Sty1-driven CRIB-3xmCitrine dispersal, re-initiated growth in a bipolar (and in rare cases tri-polar) fashion after 3BrB re-addition (Figure 4.3, B, C). This suggested that, in the absence of Tea1, Sty1-driven CRIB-3xmCitrine dispersal was sufficient to facilitate the transition from monopolar to bipolar growth, once Sty1 activity was re-inhibited by 3BrB.

4.3 Discussion

In the first part of this chapter, I described how both Scd1 and Gef1 exhibited significant changes in localisation upon the activation of Sty1 (Figure 4.1). Furthermore, I demonstrated that Gef1 is essential for the formation of ectopic CRIB-3xmCitrine patches on the cell sides in response to Sty1 activation (Figure 4.2). In combination with the previously described Scd1 requirement for polarised CRIB-3xmCitrine, these results suggest distinct functions for each of the two GEFs during Sty1 activation. The data is also consistent with the proposed idea that Sty1 function in Cdc42 regulation might involve the control of the two GEFs. However, as the experiments described here are very preliminary, many details about how the function of each GEF contributes to the process of Sty1-driven Cdc42-GTP dispersal remain to be investigated.

For example, the Scd1 dispersal from the cell tips after the activation of Sty1 could explain the coincidental loss of tip Cdc42-GTP (CRIB-3xmCitrine). Thus, I speculate that Sty1 function might involve the removal of Scd1 from the tips. One way that this can be achieved is by disrupting the interaction between Scd1 and the scaffold protein Scd2. Scd2 is considered essential for Scd1 localisation, as *scd2*Δ cells have no Scd1 at their cell tips and have a similar round-shape phenotype as *scd1*Δ cells (Kelly & Nurse, 2011). The interaction between Scd1 and Scd2 has been previously mapped to occur through binding of the PC (phox and Cdc) motif of Scd1 (amino acids 760-872) and the PB1 (phox and Bem1p) domain of Scd2 (amino acids 453-536; Ito *et al*, 2001; Endo *et al*, 2003). Thus, future efforts to further investigate whether Sty1 activation affects the Scd1- Scd2 interaction can be focused on detecting Sty1-dependent phosphorylation changes in either of the two proteins that might affect PC- PB1 binding. Interestingly, *in vitro* data suggests that the Scd1 binding to Scd2 is essential for the binding of the Scd2 CB2 (Cdc42- binding) region to Cdc42-GTP (Endo *et al*, 2003). In turn, the Scd2 CB2– Cdc42-GTP interaction stabilises the open configuration of Scd2 which allows recruitment of the PAK kinase Shk1. However, both Scd2 (Figure 3.10) and, most likely, Shk1 (Figure 4.2, A) co-localise with ectopic CRIB-3xmCitrine on the cell sides during Sty1 activation, while Scd1 does not (Figure 4.1). Therefore, the possible loss of Scd1- Scd2 binding during Sty1 activation is either not sufficient to disrupt Scd2 and Shk1 binding to Cdc42-GTP *in vivo* or compensated by additional factors allowing the binding to be retained.

Imaging of Gef1-3xmCherry cells showed a cytoplasmic Gef1 localisation in unperturbed interphase cells. This observation contradicted with several studies reporting Gef1 localisation at the cell tips (Das *et al*, 2009; Kokkoris *et al*, 2014; Das *et al*, 2015). One explanation for this discrepancy might be in differences in the imaging protocols between my experiments and the published studies. As evidenced by my results (Figure 4.1), Gef1 can localise to the cell sides upon activation of Sty1. In fact, it can be speculated that if imaging experiments are performed with higher temporal resolution, then, following activation of Sty1, Gef1 will first become localised to the cell tips and next gradually migrate to the cell sides. Thus, it is possible to imagine that external stresses to the cells during preparation for microscopy or during the actual imaging could also activate Sty1 and lead to the observed Gef1 tip localisation.

The experiments presented in this chapter also suggest that Gef1 plays a significant role in the Cdc42-GTP regulation during Sty1 activation. Upon Sty1 activation, previously cytoplasmic Gef1 becomes associated with the ectopic CRIB-3xmCitrine on the cell sides (Figure 4.1). This result is consistent with a hypothesised role for Sty1 in regulating Gef1 ability to bind Cdc42 in response to Sty1 activation. Intriguingly, such a mechanism of Gef1 regulation has been previously linked with the function of the NDR kinase Orb6 (Verde *et al*, 1998). Orb6 has been characterised to directly phosphorylate Gef1 and thus promote Gef1's interaction with the 14-3-3 protein Rad24 (Das *et al*, 2015). In turn, association with Rad24 sequesters Gef1 and limits Gef1's ability to bind and activate Cdc42. Thus, inhibition of Orb6 leads to the appearance of ectopic patches of Cdc42 activity which co-localise with Gef1, similar to the ectopic patches observed after Sty1 activation (Das *et al*, 2009). Therefore, it is possible that Sty1's regulation of Gef1 localisation involves the inactivation of Orb6. Orb6 is part of the morphogenesis (MOR) network of proteins, together with the PAK kinase Nak1 and its binding partner Pmo25, the scaffold protein Mor2, and Orb6's binding partner Mob2 (Hou *et al*, 2003; Kanai *et al*, 2005). Deletion of any of the MOR proteins is lethal and leads to a similar round cell morphology. Thus, Orb6 activity may be affected by any changes disrupting the normal function of the MOR network. Therefore, I speculate that Sty1 activity could be inactivating Orb6 either directly or by affecting any of the members of the MOR network.

Further experiments to determine whether Sty1's role in Gef1 regulation is dependent on Orb6 could include imaging the effects on Cdc42-GTP or Gef1

distribution during Sty1 activation in Orb6-deficient cells. As *orb6*∆ cells are not viable, this can be achieved by co-deleting the mRNA-binding protein Sts5, which rescues the lethality of *orb6*∆ *(Nuñez et al*, 2016). Additionally, further investigation can be also focused on better understanding the mechanisms of Orb6 regulation of Gef1. For example, while one of the Orb6 phosphorylation sites on Gef1 has been identified as S112, the phospho-null *gef1-S112A* mutant shows increased cell-membrane association of Gef1 on the tips but not on the cell sides (Das *et al*, 2015). As mentioned earlier, inactivation of Orb6 leads to Gef1 localisation to the cell sides, suggesting that Orb6 phosphorylates Gef1 on more sites than S112 or it regulates additional targets controlling Gef1 localisation. Thus, further investigation of how Orb6 regulates Gef1 localisation could include the identification of novel Orb6-dependent phospho-sites on Gef1 or new substrates for the Orb6 kinase through phospho-proteomics.

The behaviour of Scd1 and Gef1 during Sty1 activation by LatA in wild-type cells and by 3BrB removal in *SISA* cells suggests that the two GEFs undergo a switch in their association with Cdc42 in response to the Sty1 activation. A similar exchange in the activators of Cdc42 has been proposed to occur during cytokinesis (Wei *et al*, 2016). Cdc42 activation just after the assembly of the actomyosin ring is dependent on Gef1 and promotes the timely onset of ring constriction by affecting actin organisation, myosin V myo52 distribution, and recruitment of the cell-wall synthesis protein Beta-glucan Synthase 1 (Bgs1). Later during cytokinesis, Cdc42 activation is also dependent on Scd1, which promotes normal formation of the septum. However, while each of the two GEFs is reported to be the only Cdc42 GEF during the beginning (Gef1) and final (Scd1) stages of cytokinesis, there is a significant overlap in their localisation during most of cytokinesis. Thus, the switch between the GEFs association with Cdc42 likely occurs gradually throughout the duration of cytokinesis (approximately 60-90 min), which is not characteristic of Sty1-induced Scd1/Gef1 association switch which occurs within 30 min of Sty1 activation (Figure 4.1). In agreement with this finding, both Scd1-3xmCherry and Gef1-3xmCherry were observed to localise at the septum during cytokinesis in *sty1*∆ cells (data not shown). However, while Sty1 is likely not required for the regulation of Scd1 and Gef1 association with Cdc42 during cytokinesis, it might still have an effect on the kinetics of this process.

In the second part of this chapter, I described some preliminary experiments aimed at investigating the role of Tea1 in the recovery of CRIB-3xmCitrine following Sty1 activation and repression. The results obtained using the *tea1*∆ *SISA* cells support the hypothesis that Tea1 participates in the correct tip-positioning of the CRIB-3xmCitrine cluster after recovery from Sty1-induced CRIB-3xmCitrine dispersal (Figure 4.3). Interestingly, upon recovery of tip-CRIB-3xmCitrine, many *tea1*∆ *SISA* cells initiated growth at a different angle, compared to the original growth axis. My explanation for this phenomenon is based on the observation that the recovered CRIB-3xmCitrine clusters often appeared smaller than their counterparts observed before the Sty1-driven CRIB-3xmCitrine dispersal. Thus, as the recovered clusters did not occupy the full area of the existing cell tip, growth often was re-initiated at an angle. This can be related to the finding that polarity factors on fission yeast tips organise into distinct cortical clusters propagated through the process of oligomerisation (Dodgson *et al*, 2013). It can be speculated that such oligomerisation is affected in the absence of Tea1 and so is the size of the recovered polarity clusters. However, it should be noted, that this explanation is solely based on direct observation, and exact measurements of the area of the recovered CRIB-3xmCitrine clusters need to be performed to support or reject this idea. Furthermore, recovery of the CRIB-3xmCitrine clusters in *tea1*∆ *SISA* cells following re-addition of 3BrB occurred significantly slower than recovery in *tea1+ SISA*. These results suggest that the Tea1 landmark is not only involved in the correct positioning but also in regulating the kinetics of CRIB-3xmCitrine cluster re-establishment following Sty1-driven disruption. This is in agreement with the hypothesised role of Tea1 and its associated proteins in actively participating in promoting Cdc42 activity, although it provides little insight into how this role is achieved. However, I speculate that the *SISA* experimental system can be further used to elucidate the contribution of the Tea1 landmark.

For example, one of the questions I have not yet addressed is what happens to Tea1 distribution during Sty1 activation. I predict that Tea1 would still be localised at the tips during Sty1 activation as the recovery of CRIB-3xmCitrine in *tea1+ SISA* has, so far, been consistently observed to occur only at the cell tips, which suggest that Tea1 function as a polarity landmark in these cells is retained. However, it should be noted that Tea1 is delivered to the cell tips via the microtubule cytoskeleton, whose dynamics are affected by stresses such as osmotic shock and heat which, in turn, also induce Sty1 activation (Tatebe *et al*, 2005). Thus, further analysis of Tea1

behaviour in response to Sty1 activation is certainly needed. Furthermore, the distributions of other known Tea1 interactors such as Tea4 or Pom1 can be also be imaged using the *SISA* system to obtain more in-depth understanding of how Sty1 activation affects the Tea1-Tea4 polarity complex.

The experiments performed with the *tea1*Δ *SISA* also suggested that while Tea1 contributes to the re-establishment of tip CRIB-3xmCitrine following Sty1-driven CRIB-3xmCitrine dispersal, there likely are additional polarity landmarks that can also guide the Cdc42 polarity machinery back to the cell tips. Interestingly, the apparent ability of these additional landmarks to direct the Cdc42 machinery back to cell tips diminished with prolonged periods of Sty1-driven CRIB-3xmCitrine depolarization. This was evidenced by the increased incidence of ectopic growth re-initiation in *tea1*Δ *SISA* cells exposed to 5 hours of 3BrB withdrawal as compared to *tea1*Δ *SISA* cells exposed to 1.5 hours of 3BrB withdrawal. However, one important missing control is to assess the effects of longer (5 hours) 3BrB withdrawal in 'wild-type' (*tea1*+) *SISA* cells and compare whether that leads to an increase in ectopic growth re-initiation or has the same outcomes as 1.5 hours 3BrB withdrawal (i.e. 100% recovery at tips; Figure 3.9). Such an experiment would further elucidate whether, in the presence of Tea1, the function of additional polarity landmarks is affected by prolonged Sty1-driven depolarization to the same extent as in *tea1*Δ.

In conclusion, the preliminary findings using a 'candidate-based' approach to identifying the mechanisms of Sty1-dependent Cdc42 regulation have yielded several interesting avenues for further investigation. The obtained results suggest that the two GEFs Scd1 and Gef1 might be separately regulated by Sty1 to induce the effects on Cdc42-GTP distribution observed upon activation of the kinase. My findings support a model in which Sty1 activity negatively regulates Scd1's association with Cdc42 at the tips, thus leading to a tip-dispersal of Cdc42-GTP. In addition, Sty1's activation also promotes the association of Gef1 with Cdc42 at the cell sides. Finally, Sty1 function might also negatively regulate the coupling between the Cdc42 machinery and the polarity landmark Tea1. However, the molecular details how any of these processes are achieved remains largely unclear. One of the major challenges in dissecting the mechanisms of Sty1-depdendent regulation of Cdc42 polarity lies in the absence of identified Sty1 targets that can be linked to polarity regulation. Thus, in the next chapter I present my initial findings using a phospho-proteomics approach to identify novel targets of Sty1 that might be involved in regulation of Cdc42 polarity.

Chapter 5

Using SILAC phospho-proteomics to identify putative Sty1 targets

5.1 Introduction

In Chapter 4 I investigated the mechanisms of Sty1 regulation of Cdc42 by examining the behaviour and function of known Cdc42 regulators in the context of Sty1 activation. While my preliminary results revealed how some polarity proteins (e.g. the Cdc42 GEFs Scd1 and Gef1) may control Cdc42 activity in a Sty1 dependent manner, it remained unclear how one can mechanistically couple Sty1 function to the control of such polarity proteins. This problem mostly stemmed from the lack of identified Sty1 phosphorylation targets which could be involved in polarity regulation. Thus, the main challenge to uncovering the mechanisms of Sty1-dependent Cdc42 regulation is the identification of novel targets of Sty1 which could directly or indirectly facilitate the changes in Cdc42-GTP distribution observed upon Sty1 activation.

An effective approach for identifying the targets of a kinase is using Stable Isotope Labelling by Amino acids in Cell culture (SILAC) mass spectrometry (MS) to analyse the changes in the phospho-proteome of a cell upon activation or deactivation of that kinase. SILAC is a proteomics method that allows for the relative quantification of peptides and proteins between two or more samples (Ong, 2002; Ong & Mann, 2006). It involves the metabolic labelling of cells' proteomes by growth in media containing non-radioactive isotopes of defined amino acids. The incorporation of these amino acids into proteins generates isotopically-labelled 'heavy' proteins which can be distinguished from naturally occurring proteins due to their higher molecular mass. In parallel to the cell culture grown in the 'heavy' (isotope-labelled) medium, a cell culture is also grown in a 'light' (non-labelled) medium. Depending on the aim of the SILAC experiment, heavy and light cultures can be assigned to two different experimental conditions, such as two different treatments or growth parameters. This can be applied to cultures of the same strain as well as to strains with different genetic backgrounds. Afterwards, either the cultures or their protein extracts are mixed in 1:1 ratio and further processed for MS analysis. Due to the mass differences between light- and heavy-labelled peptides in the 1:1 mixed sample, detected peptides can be assigned to either the light or heavy samples and a quantitative comparison between the relative abundance of these peptides can be extracted from the data. The amino acids usually used for the metabolic labelling are lysine and arginine, as the common proteases used to generate peptides for MS, such as trypsin, cleave after one or both of these amino acids. In principle, this ensures that all peptides generated by the protease digestion will contain at least one light- or heavy-labelled amino acid. SILAC

methodology has been successfully applied to fission yeast by using lysine and arginine auxotrophic strains to allow for the efficient incorporation of the labelled lysine and arginine amino acids from the medium (Bicho *et al*, 2010b). In addition, SILAC experiments in fission yeast cells using heavy-labelled arginine also need to account for the so-called 'arginine-conversion' problem. This problem originates from the fission yeast's ability to readily catabolise arginine and convert it to other amino acids, thus incorporating heavy-labelled atoms in amino acids other than arginine and significantly complicating the MS analysis. The arginine-conversion problem can be solved genetically by deletion of the ornithine transaminase Car2 gene in the strains used for the analysis (Bicho *et al*, 2010b). Car2 is involved in the arginine conversion metabolic pathway and a Car2 deletion has been demonstrated to significantly reduce arginine conversion to levels suitable for MS analysis.

In this chapter, I describe a comparative global phospho-proteomics approach to identify novel targets of Sty1 using the previously described *SISA* strain and SILAC MS. I present some of the preliminary results obtained with this method and discuss future experiments to complement the initial analysis.

5.2 Results

5.2.1 SILAC phospho-proteomics using SISA cells

In Chapter 3, I demonstrated how *SISA* cells can be used to efficiently control Sty1 activity by adding or removing the ATP-competitive analog 3BrB from the growth medium (Figures 3.8 and 3.9). Importantly, the *SISA* experimental system allowed the investigation of the effects of Sty1 activation without the use of external stresses that can have additional consequences on cell physiology. In addition, the *SISA* approach of Sty1 activity manipulation is technically simple to perform and easily and cost-effectively scalable to larger cultures. Thus, I decided to combine the *SISA* experimental system with SILAC phospho-proteomics to identify novel Sty1 targets.

The concept of the approach was that the light and heavy *SISA* cultures compared in the SILAC experiment can be assigned to either the presence or absence of 3BrB (Figure 5.1). In this way, the detected changes in the phospho-proteome between the two samples should be correlated with Sty1-dependent gain or loss of phosphorylation. Thus, hits identified using this method would include not only direct Sty1 targets but also proteins that gain or lose phosphorylation as a downstream consequence of Sty1 activation. In the first step of the experiment, all *SISA* cultures are grown for 10 generations in either light or heavy SILAC medium in the presence of 3BrB. This allows the full incorporation of the light- or heavy- labelled amino acids, while maintaining Sty1 inactive. Next, each of the two cultures is transferred to new SILAC medium with or without 3BrB for a fixed period of time. Thus, in one of the cultures, Sty1 is maintained inactive due to the presence of 3BrB, while in the other culture, Sty1 is activated due to the 3BrB removal. The cells from each culture are harvested and lysed to obtain protein extracts which are maintained under denaturing conditions (8M Urea) and later mixed in equal 1:1 ratio based on protein content. Most of the 1:1 mixed protein extract is digested with both Lys-C and Trypsin and the digested peptides are further subjected to phospho-peptide enrichment before the MS analysis. This is achieved in two steps. First, the peptides are fractionated by Strong Cation Exchange (SCX) using a salt gradient

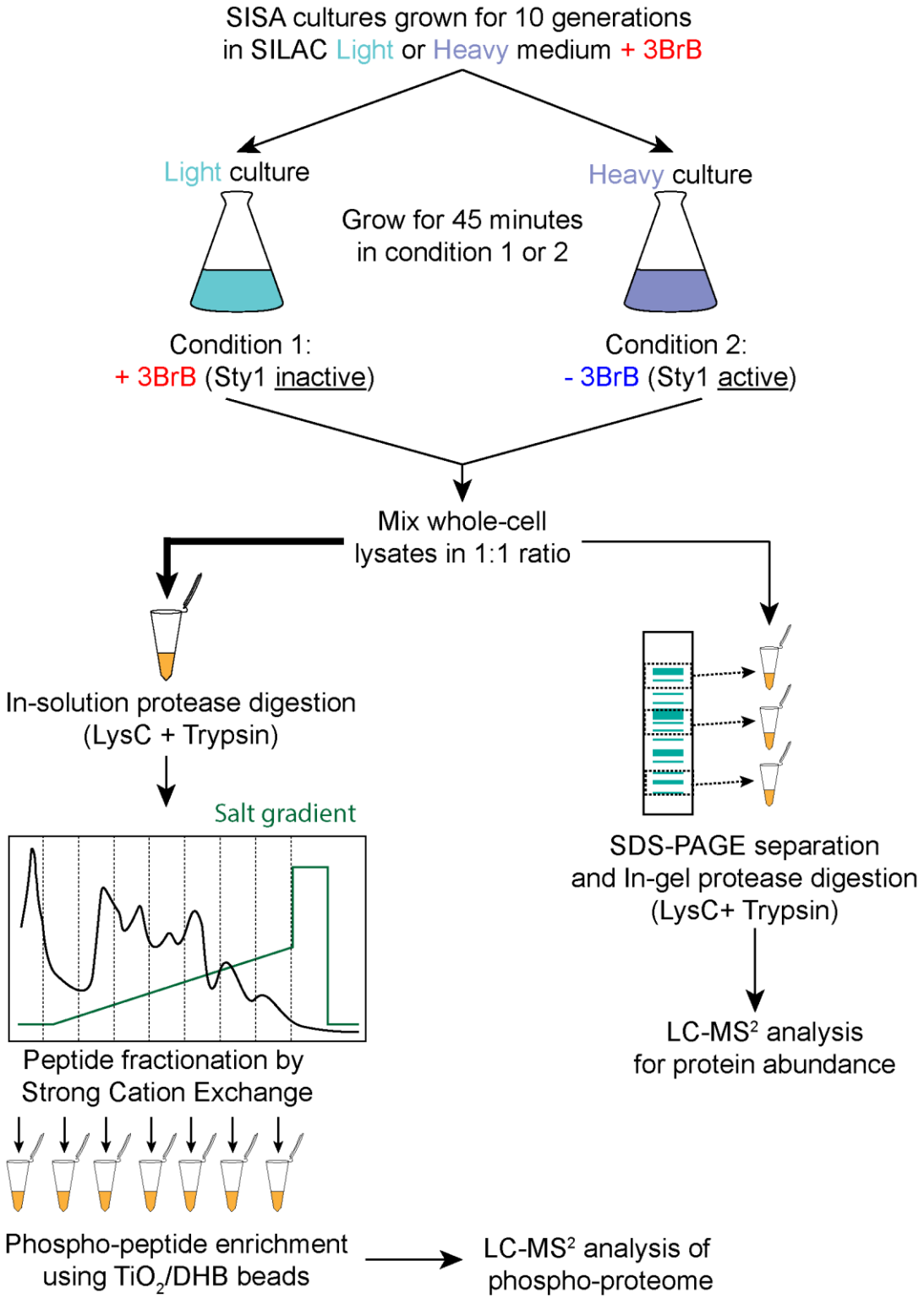

Figure 5.1. Schematic representation of SILAC phospho-proteomics workflow using *SISA* cells. Light SILAC medium contains naturally occuring L-arginine and L-lysine, while Heavy SILAC medium contains the heavy isotopes L-arginine-6 ($^{13}C_6$) and L-lysine-8 ($^{13}C_6$, $^{15}N_2$). The treatments of light and heavy cultures (i.e. conditions 1 and 2) can be switched between separate experiments. For further details see also Materials and Methods Sections 2.15 to 2.21.

enriched for phospho-peptides using TiO_2 beads in the presence of 2,5-dihydroxy-benzoic acid (DHB; Pinkse *et al*, 2004; Larsen *et al*, 2005). The phospho-enriched peptide fractions are then analysed using liquid chromatography-tandem mass spectrometry (LC-MS^2). In parallel to the phospho-peptide enrichment, a small portion of the 1:1 mixed protein extract is fractionated using SDS-PAGE, digested, and directly analysed via LC-MS^2 to determine the relative differences in protein abundance between the samples. This is needed so that the detected relative changes in phospho-peptide abundance can be normalised to the changes in protein abundance. Thus, following the analysis of all the LC-MS^2 data, the final output of each SILAC experiment should identify the changes in the phospho-proteome of *SISA* cells upon 3BrB removal (i.e. Sty1 activation). Finally, combining the data from multiple replicates of the SILAC experiment would identify significant phosphorylation events that are consistently up- or down-regulated in Sty1-activated samples, as well as identify 'false-positive' changes in phosphorylation generated by experimental error or natural variation.

To perform the SILAC phospho-proteomics experiments, the *SISA* strain was first modified to contain the *car2*Δ *arg1-230 lys3-32* mutations which allow for the incorporation of the Arginine-6 and Lysine-8 heavy isotope labels (Bicho *et al*, 2010b). To confirm that 3BrB removal in the new *SISA SILAC* strain had the same effect on Cdc42-GTP distribution as in the original *SISA* cells, a *SISA SILAC* strain expressing the CRIB-3xmCitrine was also generated. In agreement with the data presented in Chapter 3 for *SISA* cells (see Figure 3.9), the CRIB-3xmCitrine in *SISA SILAC* cells became dispersed from the cell tips within 30 to 40 min of 3BrB removal and gradually formed ectopic CRIB-3xmCitrine patches on the cell sides (data not shown). Based on this finding, the incubation time after medium exchange in the SILAC phospho-proteomics experiments was set to 45 min to give sufficient time for Sty1-driven CRIB-3xmCitrine dispersal to occur in all cells transferred to 3BrB-free medium but also not to allow too prolonged Sty1 activity which might result in undesired secondary effects on phosphorylation (see Figure 5.1).

5.2.2 Preliminary analysis of two independent SISA SILAC phospho-proteomics experiments

Thus far, I have performed two runs of the *SISA* SILAC phospho-proteomics experiment which I will further refer to as Experiment 1 and 2. Experiments 1 and 2

differed in two aspects: 1) the specific culture that was heavy-labelled; 2) the amount of total protein extract used for phospho-peptide enrichment. In Experiment 1, the light culture was transferred to medium with 3BrB (i.e. Sty1 remained inactive), and the heavy culture was transferred to medium without 3BrB (i.e. Sty1 was activated). In Experiment 2, the labelling was reversed; the light culture was transferred to medium without 3BrB, while the heavy to a medium with 3BrB. The label reversal between the two experiments serves as an internal control to account for any potential effects on peptide detection arising from the use of light- or heavy-labelled amino acids. The other difference between the two experiments was that the cultures from Experiment 1 were harvested at lower OD than Experiment 2 (OD_{600} ~0.3 vs ~0.6), resulting in a difference of the total amount of total protein extract obtained. The total protein content in the 1:1 mixed protein extracts processed further for phospho-peptide enrichment was 5.74 mg for Experiment 1 and 9.76 mg for Experiment 2. Further details regarding minor differences between the two experiments, such as slightly different fractionation of the digested phospho-peptides, are described in depth in Materials and Methods Sections 2.15 to 2.20.

The LC-MS^2 analysis of the processed samples from experiments 1 and 2 was performed by Dr. Christos Spanos at the University of Edinburgh (for technical details see Materials and Methods Section 2.21). In Experiment 1, 12,097 unique phospho-peptides were detected, which mapped to 11,521 phosphorylation sites on 2,228 proteins (Table 5.1). In Experiment 2, 14,193 unique phospho-peptides were detected which mapped to 11,887 phosphorylation sites on 2,142 proteins. Combining the data from both experiments, the total identified unique phospho-peptide count was 19,961, with 16,422 phospho-sites on 2,639 proteins. To my knowledge, this represents the largest survey of the *S.pombe* phospho-proteome, as the previous largest dataset reported 18,701 unique phospho-peptides with 12,524 phospho-sites on 2,113 proteins (Kettenbach *et al*, 2015).

For the detected phospho-sites in each of the two experiments a heavy:light (H/L) ratio was calculated based on the relative abundance of the detected heavy- and light-labelled phospho-peptides for those sites. H/L ratios were obtained for 8,071 of the phospho-sites from Experiment 1 and 8,669 of the phospho-sites from Experiment 2 (Table 5.1). For both experiments, these numbers were lower than the total phospho-sites detected. The reason for this is that not all detected phospho-sites could be assigned H/L ratios, either because the corresponding phospho-

Table 5.1. Detected phospho-peptides in the two SILAC experiments. Summary of the numbers of detected unique phospho-peptides, phospho-sites, and their corresponding proteins (phospho-proteins) in SILAC experiments 1 and 2, as well as in both experiments combined. H/L stands for heavy to light.

	Phospho-peptides	Phospho-sites	Phospho-proteins	Phospho-sites with H/L ratio	Phospho-sites with H/L ratio normalised for protein abundance
Exp 1	12,097	11,521	2,228	8,071	6,585 (81.5 %)
Exp. 2	14,193	11,887	2,142	8,669	7,404 (85.4 %)
Combined	19,961	16,422	2,639	11,519	9,707 (84.2 %)

Table 5.2. Detection of phosphorylation sites on previously characterised Sty1 substrates. Summary of phospho-sites, previously reported or predicted to be phosphorylated by Sty1, detected in experiments 1 and 2. Reported fold-increase for each phospho-site in the Sty1-activated samples is based on the normalised heavy to light (H/L) ratio in Experiment 1 and the inverse (L/H) ratio in Experiment 2. The asterisk marks an H/L ratio which could not be normalised for protein abundance.

Detected known Sty1 phospho-site	Phospho-site detected in		Fold increase in Sty1-activated sample	
	Exp.1	**Exp.2**	**Exp.1**	**Exp.2**
Cmk2 T411	yes	no	5.26 *	--
Srk1 S463	no	yes	--	2.40
Atf1 S172	no	yes	--	3.30
Atf1 T216	no	yes	--	5.40
Atf1 S226	no	yes	--	6.40

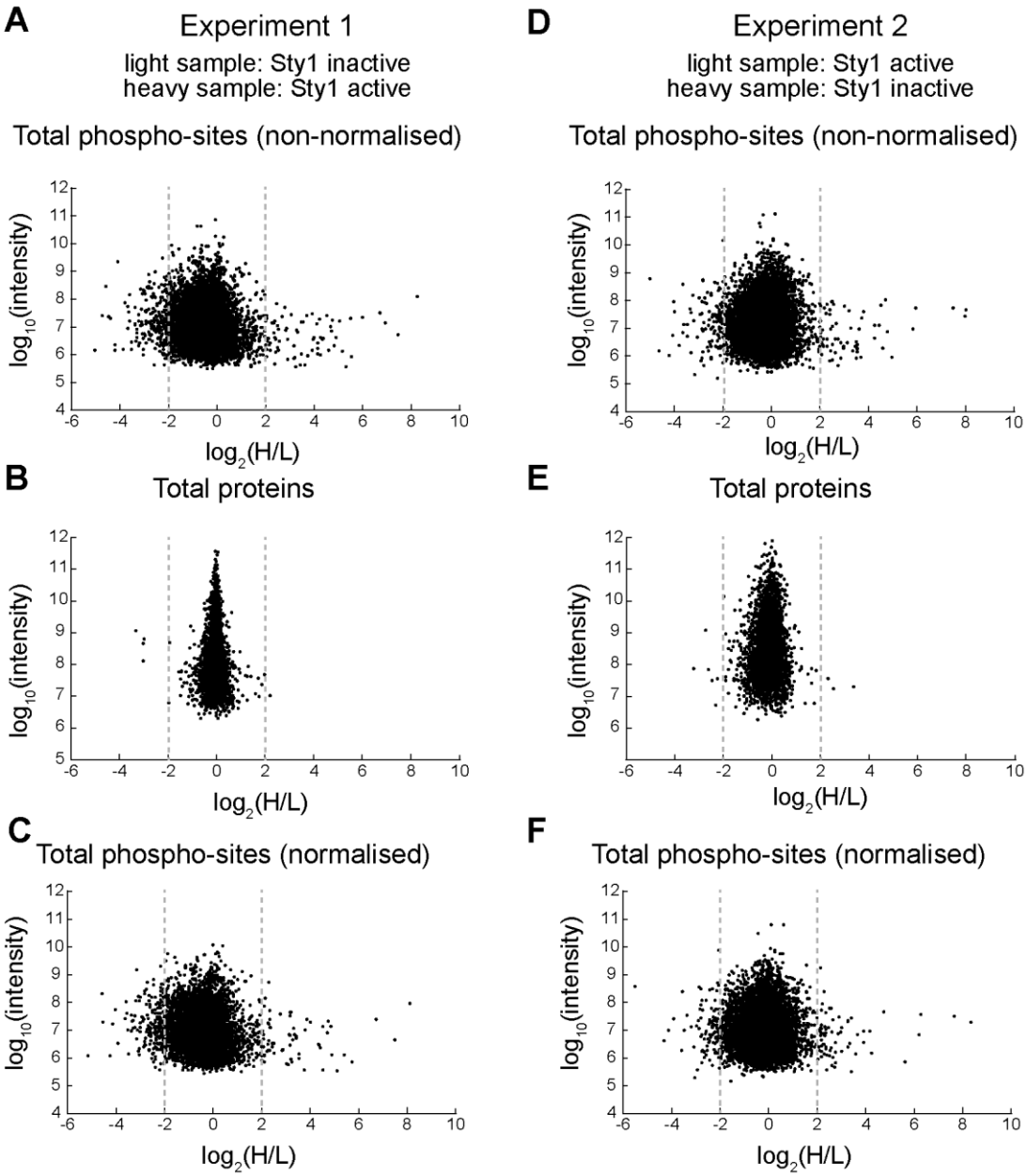

Figure 5.2. Changes in phosphorylation and protein abundance in two independent SILAC experiments using *SISA* cells. (A) and (D) Plots representing all detected phospho-sites in experiments 1 and 2 accordingly. For each phopho-site the change in abundance, represented as a H (heavy) to L (light) ratio in $\log_2$ (x-axis), is plotted as a function of the $\log_{10}$ signal intensity (y-axis) recorded in the mass spectrometer. (B) and (E) Plots representing detected proteins in experiments 1 and 2 accordingly. For each protein the change in abundance, represented as a H to L ratio in $\log_2$ (x-axis), is plotted as a function of the $\log_{10}$ signal intensity (y-axis) recorded in the mass spectrometer. (C) and (F) Plots in which the H/L ratios of the phospho-sites from (A) and (D) have been normalised for protein abundance with the corresponding protein's H/L ratios, provided such ratios were obtained.
The dashed lines mark the separation line for decrease or increase in phosphorylation (A, C, D, and F) or protein abundnce (B and E) by more than a factor of 4 ($\log_2$ (H/L) smaller than −2 or bigger than 2).

peptides were not detected in both the light and heavy samples, or because the detected intensity of the phospho-peptides was not sufficient for quantitative correlation based on the parameters of the software used for the analysis. From the detected peptides in the non-phospho-enriched samples, H/L ratios were also calculated for individual proteins, reflecting their change in abundance between the two conditions in each of the experiments (Table 5.1). To visualise the global changes in phospho-site and protein abundance for each of the experiments I plotted the H/L ratios assigned to individual phospho-sites or proteins to the intensities recorded in the mass spectrometer calculated for those individual phospho-sites or proteins (Figure 5.2). The general distribution of phospho-site abundance appeared similar between experiments 1 and 2, with a distinct long-tail of phospho-sites with high H/L ratios observed in plots from both experiments (Figure 5.2, A and D). This was unexpected, as the light- and heavy-labels were switched between the two experiments, and thus the observed changes in abundance in Experiment 2 would be expected to be the inverse of those in Experiment 1. This can be explained in several ways. For example, it could be that most of the changes in phospho-site abundance bigger than 4-fold (bigger than 2 on $\log_2$ scale) were not detected in both experiments. Furthermore, these changes might not be dependent on Sty1 activation and represent experimental noise. Finally, it is possible that some of the varied conditions in each experiment (e.g. harvesting OD, differently-labelled medium, possible experimental error), could be affecting the observed changes in phospho-site distribution in an unexpected way. For both experiments, most detected changes in protein abundance were below 4-fold, which was expected considering that Sty1 activation was induced for only 45 min (Figure 5.2, B and E). However, based on the spread of individual proteins on each of the plots, proteins from Experiment 2 exhibited larger changes in abundance (i.e. wider distribution on the plot) compared to Experiment 1, further pointing towards possible variations between the experimental conditions of the two experiments.

For each of the two experiments, the H/L ratios of the phospho-sites from the phospho-enriched samples were normalised for protein abundance by dividing them by the H/L ratios of the corresponding proteins from the non-phospho-enriched samples. However, not all proteins with phospho-sites in the phospho-enriched samples were detected in the non-phospho-enriched samples. Thus, for Experiment 1, normalisation was possible for only 81.5 % of the phospho-sites with quantified H/L

ratios (for a total of 6,585 normalised phospho-sites), while in Experiment 2, normalisation was possible for only 85.4 % of the phospho-sites with quantified H/L ratios (for a total of 7,404 normalised phospho-sites; Table 5.1). Normalisation did not significantly affect the global distribution of phospho-site abundance, as evidenced by the plots on Figures 5.2, C and F, where the normalised H/L ratios for each phospho-site were plotted against the originally detected intensity for the phospho-site (compare with Figure 5.2, A and D). This further suggests that changes in protein abundance have minor contribution to the variation observed in the plots from Figure 5.2, A and D.

To validate the *SISA* SILAC phospho-proteomics approach, I searched the datasets from experiments 1 and 2 for changes in the phosphorylation of known Sty1 substrates. As described in previous chapters, some of the targets of Sty1 have been previously identified. Furthermore, for 3 of these targets - Cmk2, Srk1, and Atf1- the sites for Sty1 phosphorylation have also been identified. Previous studies have reported that Sty1 phosphorylates Thr411 (T411) in Cmk2 and Ser463 (S463) in Srk1 (Sánchez-Piris *et al*, 2002; López-Avilés *et al*, 2008). For Atf1, 11 putative Sty1 sites have been identified (S2, S4, T77, S140, S152, S172, T204, T216, S226, T249, S438) although whether they are all phosphorylated and whether they all bear functional significance to Atf1 function remains unclear (Lawrence *et al*, 2007). I predicted that if my experimental datasets are indeed accurately and comprehensively identifying global changes in the phospho-proteome after Sty1 activation, then the identified Sty1 phospho-sites on Cmk2, Srk1, and Atf1 should be enriched in the Sty1-activated samples (i.e. in which 3BrB was removed) from both experiments. Indeed, in both experiments, all detected phospho-sites which have also been previously characterised as sites of Sty1 phosphorylation, were found to be enriched in the Sty1-activated samples (Table 5.2). In Experiment 1, only the Cmk2 T411 phospho-site was detected and it was found to be 5.26-fold enriched in the Sty1-activated sample. However, it should be noted that the Cmk2 T411 phospho-site H/L ratio was not normalised for protein abundance since the Cmk2 protein was not detected in the non-phospho-enriched sample. In Experiment 2, the detected phospho-sites were Srk1 S463, Atf1 S172, T216, and S226. An H/L ratio normalisation to protein abundance was possible for all those phospho-sites. The normalised H/L ratio of all these sites showed more than 2-fold enrichment in the Sty1-activated sample, with Atf1 S226 having the highest-fold enrichment of 6.40 (see Table 5.2). Thus, the

relative changes in abundance of phospho-sites on known Sty1 substrates in each of the two experiments support the validity of the *SISA* SILAC phospho-proteomics approach. However, as none of the known Sty1 phosphorylation sites was detected in both experiments it is not possible to determine whether the two datasets represent Sty1-dependent changes in the phospho-proteome equally well.

In order to identify potential Sty1 phosphorylation targets, I examined in further detail the phospho-sites that were detected in both experiments 1 and 2. I speculated that phospho-sites that are consistently enriched upon Sty1 activation in both experiments are more likely to represent 'true' direct or indirect Sty1 phosphorylation targets. To analyse the combined data from the two experiments, I considered only phospho-sites that had assigned H/L ratios and that were also normalised for protein abundance in each experiment (see Table 5.1). Out of the 6,585 phospho-sites from Experiment 1 and the 7,404 phospho-sites from Experiment 2, 4282 phospho-sites were identified in both experiments (65% and 57.8% of total phospho-sites in Experiment 1 and 2, respectively). Furthermore, out of the 4282 phospho-sites detected in both experiments only 1483 (34.5%) showed consistent change in abundance upon Sty1 activation (i.e. either enriched in both experiments or reduced in both experiments). As noted previously regarding the general distribution of phospho-site abundance in both experiments, this observation suggested that most of the observed changes in phospho-site abundance in each of the experiments might not be dependent on Sty1 activation and represent uncontrolled experimental variation. Alternatively, it is also possible that most phospho-sites whose abundance changes in a Sty1-dependent manner were simply not detected in both experiments. Nevertheless, I further examined the 1483 phospho-sites that showed the same direction of change in both experiments – either enriched or reduced after Sty1 activation in both experiments. From those, I selected for the phospho-sites which were enriched more than 2-fold upon Sty1 activation. From this I obtained a final list of 16 phospho-sites on 14 proteins, summarised in Table 5.3. Ten of the phospho-sites had phosphorylation localisation probability of at least 0.75, which indicated high confidence that the phosphorylation event likely occurred on those residues. Thus, the rest of the phospho-sites which had phosphorylation localisation probability of less than 0.75 could also represent a phosphorylation event occurring on neighbouring residues.

Table 5.3. Phospho-sites enriched in the Sty1-activated samples detected in both experiments. Summary of phospho-sites detected in both experiments 1 and 2 and showing at least 2-fold enrichment in the Sty1-activated samples of each experiment. Protein descriptions were obtained from the *S.pombe* database Pombase (Wood *et al*, 2012). Asterisks mark phospho-sites where the phosphorylation event on the residue had a localisation probability of at least 0.75. Reported fold increase for each phospho-site in the Sty1-activated samples is based on the normalised heavy to light (H/L) ratio in Experiment 1 and the inverse (L/H) normalised ratio in Experiment 2.

Protein name	Protein description	Phospho-site	Fold increase in Sty1-activated sample (normalised)	
			Exp. 1	Exp. 2
Mpd2	GYF domain protein	S155 *	5.25	3.77
SPAP27G11.12.1	human HID1 ortholog 1	T657 *	4.67	3.55
Pcy1	cholinephosphate cytidylyltransferase Pcy1 (predicted)	S338 *	3.68	6.09
SPAPB17E12.14c.1	6-phosphofructo-2-kinase (predicted)	S112 *	3.57	3.46
		S111 *	3.48	4.56
Slf1	cell cortex node protein Slf1	T160 *	3.568	4.31
SPAC17G6.11c.1	glucosidase (predicted)	T54 *	3.46	2.34
Nrd1	RNA-binding protein Nrd1	S8	3.43	2.25
Tif471	translation initiation factor eIF4G	S867	3.32	4.88
		S866	2.74	4.53
Pap1	transcription factor Pap1/Caf3	T45	3.18	2.15
Pob1	Boi family protein	S655 *	3.11	2.19
Shk1	PAK-related kinase Shk1	S86	2.65	2.06
Pan1	actin cortical patch component, with EF hand and WH2 motif Panl (predicted)	T926	2.42	2.57
Ebp2	rRNA processing protein Ebp2 (predicted)	S298 *	2.29	2.62
Gpd1	glycerol-3-phosphate dehydrogenase Gpd1	T382 *	2.02	4.44

The proteins with phospho-sites in the final list (Table 5.3) had a range of identified biological functions. As expected, some of the proteins have well-characterised functions in stress response such as the glycerol-3-phosphate dehydrogenase Gpd1 and the transcription factor Pap1. Gpd1 is involved in glycerol synthesis in response to osmotic stress and is essential for the viability of cells exposed to hyperosmotic conditions (Ohmiya *et al*, 1995). Pap1 is involved in transcription regulation in response to oxidative stress (Vivancos *et al*, 2006). Interestingly, both Gpd1 and Pap1 are thought to be regulated by the SAPK pathway, although the molecular details of how this regulation is achieved are not fully understood (Aiba *et al*, 1995; Degols *et al*, 1996; Toone *et al*, 1998; Zuin *et al*, 2005). In addition, the RNA-binding protein Nrd1 is also implicated in stress-response, as it is involved in the formation of stress-induced RNA granules following heat, arsenite, or oxidative stresses (Satoh *et al*, 2012). Nrd1 association with stress granules is thought to be regulated by phosphorylation by the stress-response MAPK Pmk1, though the identified sites of phosphorylation (T40 and T126) are different than the phospho-site identified in my experiments (S8; Satoh *et al*, 2009). In addition to proteins involved in stress response, other proteins on the list had various cellular functions such as translation initiation (Tif471; Hashemzadeh-Bonehi *et al*, 2003) or cortical node organisation (Slf1; Deng *et al*, 2014). Furthermore, the list contained a number of proteins that are either poorly or not-at-all characterised, such as Mpd2, SPAP27G11.12.1, Pcy1, SPAPB17E12.14c.1, SPAC17G6.11c.1, Pan1, and Ebp2. Interestingly, among the hits were also phospho-sites on two proteins associated with Cdc42: the Boi-family protein Pob1 and the PAK kinase Shk1 (Marcus *et al*, 1995; Toya *et al*, 1999; Rincón *et al*, 2009). I further examine the possible implications of Pob1 and Shk1 phosphorylation for Sty1-dependent regulation of Cdc42 polarity in the Discussion section of this chapter.

5.3 Discussion

In this Chapter, I presented a SILAC global phospho-proteomics approach for identifying novel Sty1 targets linked to Cdc42 polarity regulation, using *SISA* cells. While the two initial runs of the SILAC experiments do not represent a comprehensive survey of the Sty1-induced changes in the *S. pombe* phospho-proteome, several conclusions regarding the continuation of the analysis can be drawn based on the preliminary findings.

Based on the amount of total unique phospho-peptides in the two experiments (Table 5.1), the current approach seems to provide larger coverage of the phospho-proteome than previously published studies (Kettenbach *et al*, 2015), suggesting that the technical aspects of protein extraction and processing for LC-MS^2 are, in principle, sufficiently optimised. One of the variations between the two experiments was the total amount of protein extract processed for phospho-peptide enrichment. In Experiment 2, more total protein extract was used than in Experiment 1 (9.76 mg vs 5.24 mg of protein), with the intention of obtaining better MS coverage of the phospho-proteome. That was indeed the case, as 14,193 unique phospho-peptides were detected in Experiment 2 and 12,097 in Experiment 1. However, the increase in detected phospho-peptides (1.17-fold) was not proportional to the increase in total amount of the amount of protein extract used (1.7-fold). This suggests that further increasing the amount of protein extract used for phospho-peptide enrichment is unlikely to yield significantly better coverage of the phospho-proteome.

The phospho-proteome changes upon Sty1 activation detected in the two experiments showed relatively poor overlap. This was suggested by several aspects of the preliminary analysis of the two datasets. First, the distribution of the phospho-sites based on their H/L ratios and their recorded intensity appeared similar between experiments 1 and 2, even though the light- and heavy-labelled samples represented reciprocal conditions between the two experiments (Figure 5.2, A and C). Additionally, out of the 4282 phospho-sites normalised for proteins abundance and detected in both experiments only 34.5% showed consistent changes in both experiments. As discussed previously, there could be several underlying reasons for these discrepancies. One explanation could be that the phospho-sites whose abundance is most affected by Sty1 activation were not detected in both experiments. Alternatively, certain variations between the two experiments could have influenced the observed

changes in phospho-site abundance. Thus, it could be the case that one of the two performed experiments is less representative of Sty1-induced phospho-proteome changes than the other. To address these possibilities, I suggest that the best approach would be to perform several more repeats of the SILAC phopsho-proteomics experiments. Analysing and comparing the overlap of one or two more new datasets with the existing datasets should be sufficient to determine whether the results obtained in Experiment 1 or in Experiment 2 are equally representative of the common average or one is closer than the other. Furthermore, obtaining additional datasets should result in higher overlap of identified phospho-sites, leading to the identification of more phospho-sites whose abundance is enriched upon Sty1 activation in more than one experiment.

In addition to performing more repeats of the primary experiments, one important future experiment would also be a control SILAC phospho-proteomics run to account for the changes occurring simply as a consequence of 3BrB removal. Performing such a control experiment would be particularly useful as the obtained data can be used to filter out some of the experimental noise in the primary experiments, as the observed changes in such an experiment should be independent of Sty1-activation. While the most straightforward approach to such an experiment would be the comparison between wild-type cultures in the presence and absence of 3BrB, it might not be the most appropriate as the *SISA* genetic background used in the primary experiments contains several mutations which likely affect global phosphorylation, such as the hyper-active *wis1-DD* allele or the deletion of the *pyp1* and *pyp2* phosphatase genes. Thus, a more appropriate control would be to use a '*SISA*-like' strain which has the same genetic background as *SISA* but the *sty1-T97A* allele is replaced with a *sty1* gene deletion. In this way, comparing the phospho-proteomes of such '*SISA*-like' cells in the presence and absence of 3BrB would also account for the baseline changes in global phosphorylation which might be caused by the *SISA* genetic background.

Two of the phospho-sites found to be more than 2-fold enriched upon Sty1 activation in both experiments were located on the Cdc42-associated proteins Pob1 and Shk1. This was particularly interesting because, as mentioned previously in the Introduction Section 1.3.3, both Pob1 and Shk1 interact with Cdc42 in a GTP-specific manner and have a direct involvement in polarised growth (Marcus *et al*, 1995; Toya *et al*, 1999; Rincón *et al*, 2009). Deletions of either of the two proteins results in round,

non-viable cells. Interestingly, suppression of Pob1 function using a temperature-sensitive Pob1 mutant results in 'lemon-shaped' cells which are swollen around the middle, somewhat reminiscent of *SISA* cells after prolonged incubation in medium without 3BrB (See Chapter 3, Figure 3.8, B). Together with Cdc42-GTP, Pob1 is believed to contribute to actin-cable nucleation through interaction with For3 and to exocytosis by interactions with components of the exocyst complex (Rincón *et al*, 2009; Nakano *et al*, 2011; Estravís *et al*, 2011). The specific contribution of Shk1 to polarised growth remains largely unclear. Interestingly, the detected Sty1-activation-enriched phospho-site on Shk1 located on S86 (or possibly adjacent residues) is in very close proximity to the predicted BR-domain of the protein (residues 89-118; see Appendix 2 for further detail) which is considered essential for membrane binding and efficient interaction with Cdc42-GTP (Takahashi & Pryciak, 2007). Thus, one interesting possibility is that Sty1 phosphorylation could be disrupting Shk1 localisation and/or interaction with Cdc42-GTP. Similarly, Sty1 phosphorylation could be also affecting Pob1's localisation or aspects of its function. Thus, in parallel with additional SILAC phospho-proteomics runs, future experiments could include further investigation of Shk1/Pob1 Sty1-dependent phosphorylation and its significance for the regulation of Cdc42 polarity.

Appendix 1

Constructing alternative CRIB reporters for Cdc42 activity

A1.1. Introduction

In Chapter 3, I introduced the CRIB-3xmCitrine (further referred in this chapter as 'CRIB') reporter as a tool for the *in vivo* study of active (GTP-bound) Cdc42 dynamics in fission yeast cells. In addition to its ability to specifically recognise the GTP-bound form of Cdc42, another distinguishing feature of the CRIB reporter was its prominent nuclear localisation (See Figure 3.1). While in certain situations the nuclear CRIB can be useful as an indicator of nuclear position, an off-target binding of the CRIB reporter to an unknown nuclear protein could, in principle, affect it's binding to active Cdc42. Such undesired competition for CRIB binding could complicate the interpretation of results in certain scenarios where the tip Cdc42-GTP becomes diminished or dispersed. For example, LatA treatment of CRIB-expressing cells leads to a dispersal of tip-localized CRIB and formation of weaker dynamic CRIB patches on the cell sides (Figure 3.2, A). However, the observed CRIB dispersal is also concomitant with nuclear accumulation of CRIB. This effect is particularly evident in LatA-treated *gef1*∆ cells where no ectopic CRIB patches are formed after the dispersal and the nuclear CRIB signal increases significantly (Figure 4.2, A). In such experiments, one possible interpretation that needs to be considered and controlled for is that LatA treatment might not be disrupting Cdc42-GTP itself but rather promoting the binding between CRIB and its nuclear partner. Thus, the observed dispersal of tip-localized CRIB might not reflect changes in active Cdc42 distribution but rather changes in CRIB's nuclear affinity. Finally, as how CRIB is targeted to the nucleus is completely unknown, there could be subtle additional effects of CRIB expression which do not become apparent in the current assays but affect aspects of the cell's physiology, such as normal gene expression or efficient nuclear transport. Therefore, I attempted to construct several different versions of the CRIB reporter with the goal of improving it by eliminating nuclear targeting while maintaining binding to active Cdc42.

Previous studies in yeast have shown that the efficient binding of a CRIB-reporter to Cdc42-GTP requires the presence of two components – the conserved CRIB motif and a membrane-binding domain (Takahashi & Pryciak, 2007; Lichius *et al*, 2014). The CRIB motif consists of about 14 or 16 amino acids with the general consensus sequence I-S-X-P-X-X-(X-X)-F-X-H-X-X-H-V-G, where 'X' indicates any amino acid (Drechsel, 1995). While the motif alone is able to bind Cdc42 and is specific for the GTP-bound state of the GTPase, the binding affinity of this interaction

in vitro is considerably low (Rudolph *et al*, 1998). In agreement with this finding, CRIB-reporters in yeast consisting of only the CRIB motif fused to fluorescent proteins exhibit only cytoplasmic localisation and are not able to visualise Cdc42-GTP distribution *in vivo* (Takahashi & Pryciak, 2008; Lichius *et al*, 2014).

The second necessary component is the presence of a membrane-binding domain. In budding yeast, all five CRIB-motif containing proteins possess either a pleckstrin-homology (PH) or basic-rich (BR) domain that can promote membrane recruitment (Takahashi & Pryciak, 2007). This is likely also true in fission yeast, where the only proteins identified to contain CRIB motifs are the PAK kinases Shk1 and Shk2. Shk1 has a predicted BR domain (Figure A1, A) and Shk2 has a characterised PH domain (Sells *et al*, 1998). The BR domains found on the budding yeast Cdc42 effectors Ste20, Gic1, and Gic2 are all necessary for the protein's function and localisation to sites of Cdc42 activity (Takahashi & Pryciak, 2007). The domains consist of approximately 30 amino acids rich in basic and hydrophobic residues. Intriguingly, the Takahashi & Pryciak 2007 study also showed that the Gic1 BR domain not only bound to membranes but was also targeted to the nucleus, most probably due to its basic regions rich in arginine and lysine. However, that was not the case for the BR domains of Ste20 and Gic2. Consistent with this finding, Gic2-based CRIB reporters in budding yeast also do not show nuclear localisation (Okada *et al*, 2013). Additionally, a recent study in the filamentous fungus *Neurospora Crassa* demonstrated the generation of minimal CRIB-reporters, containing just the membrane-binding domain and the corresponding CRIB-motif of the *N.crassa's* Ste20 and Cla4 proteins (Lichius *et al*, 2014). Both reporters localised to areas of Cdc42-GTP activity and did not exhibit any nuclear targeting.

A1.2. Results and discussion

The CRIB reporter I described in Chapter 3 consisted of the N-terminal region of the *S. cerevisiae* Gic2 protein (amino acids 1-208, including the W23A mutation which prevents putative binding to downstream effectors; Jaquenoud & Peter, 2000; Okada *et al*, 2013). The region contains both the membrane-binding BR domain (amino acids 96-120) and the conserved CRIB binding motif (amino acids 134-147; Figure A1.1, A and B).

First, I hypothesised that inserting a nuclear export signal (NES) sequence on the N-terminus of the existing CRIB construct might be sufficient to change its distribution to the cytoplasm. To test that idea I decided to use the NES sequence from the Wis1 MAPK kinase, as previous studies had shown that a simple GST-Wis1^{NES} fusion is sufficient to exclude GST (normally dispersed homogeneously throughout the cell) from the fission yeast nucleus (Nguyen *et al*, 2002). However, the addition of the NES sequence to the CRIB was not sufficient to drive the reporter out of the nucleus (Figure A1.1, C). Interestingly, the cells expressing the NES-CRIB were shorter than the cells expressing the original CRIB, suggesting that addition of the NES sequence had some effect on the growth or cell cycle progression of the cells.

As described earlier, the regions thought to be required for binding active Cdc42 actually represent much smaller portions of the Gic2 protein than the whole N-terminal region used as for making the CRIB reporter. Thus, I predicted that one possibility was that the Gic2 regions not required for Cdc42-GTP binding could contribute to the nuclear binding or translocation. To test that idea, I constructed a minimal version of the CRIB (mini-CRIB) including amino acids 86 to 157 (10 amino acids before and after the BR domain-CRIB motif region). Interestingly, the mini-CRIB behaved very similarly to the original CRIB even though it was approximately one-third of the length (Figure A1.1, C). This indicated that the Gic2 BR domain and CRIB motif alone were sufficient for binding to Cdc42-GTP. However, as nuclear localization was still retained, the experiment also indicated that this minimal CRIB region was also involved in its nuclear targeting.

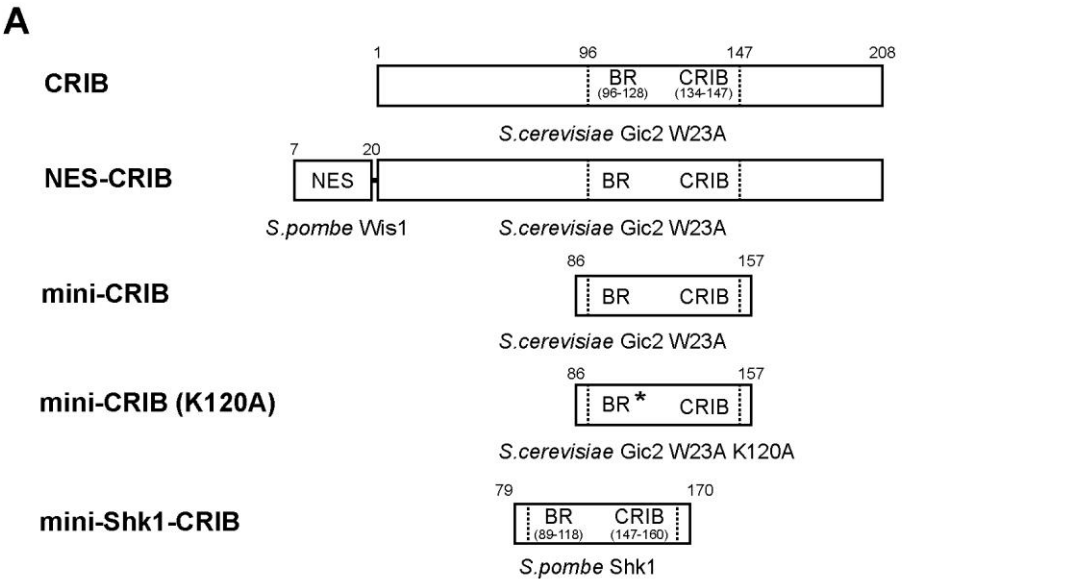

B

119 121

Gic2 (BR- domain) 96-128 ...SSSSSSSANKTNHKKVFLKLNLLKKKLLGAQPD...

C

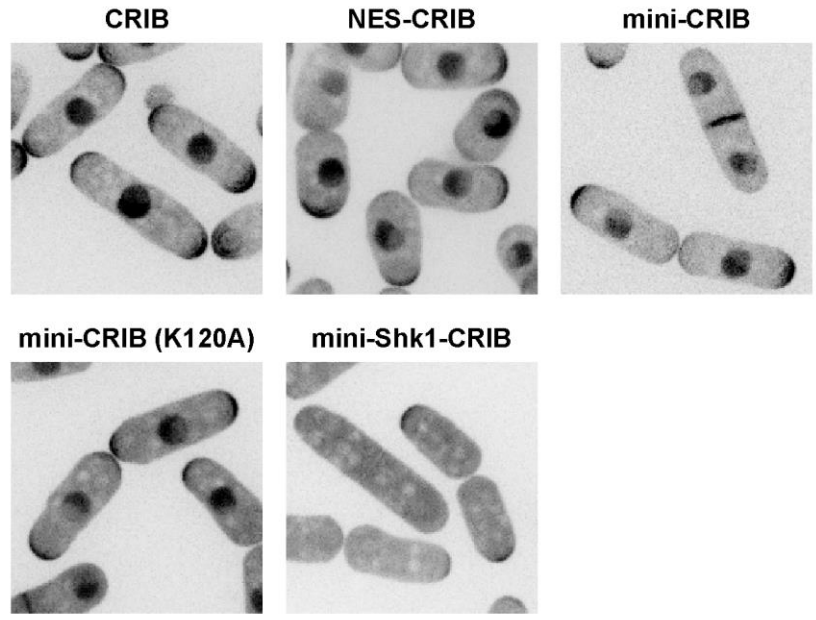

Figure A1.1. Alternative CRIB reporters for Cdc42-GTP distribution. (A) Schematic representation of the CRIB constructs cloned into the pRAD13-3xmCitrine integration vector for expression under the *adh13* promoter. Numbers relate to the amino acid positions of the original proteins used. Dotted lines define the regions hypothetically required for Cdc42 binding including the BR membrane-binding domain and the CRIB motif. (B) Amino acid sequence of the Gic2 BR domain. Basic residues in red. (C) Still images of fission yeast cells expressing the different CRIB-3xmCitrine reporters. Scale bar, 5 µm.

The composition of the budding yeast Gic1 BR domain, rich in basic residues, has been suggested as basis for its nuclear targeting (Takahashi & Pryciak, 2007) While the BR domain of Gic2 does not have nuclear localization in budding yeast, I speculated that the basic amino acid stretches it contains might contribute to nuclear targeting in fission yeast (Figure A1.1, B). Therefore, I decided to test if mutating some of the basic residues in the BR domain could diminish the nuclear localisation of the CRIB reporter. As mutating multiple basic residues was shown to abolish membrane binding, I constructed a mini-CRIB including only a single K120A mutation which inserted an alanine in the middle of the 119-121 lysine triplet (Figure A1.1 A and B). Nevertheless, the miniCRIB (K120A) construct still localised to the nucleus (Figure A1.1 C). In addition, cells expressing the mini-CRIB (K120A) showed visibly higher cytoplasmic background compared to mini-CRIB alone, suggesting the K120A mutation might have some effect on the localisation of the probe. However, as the miniCRIB (K120A) -tip signal was not appreciably higher than just mini-CRIB, it is also possible that the binding to active Cdc42 is also affected.

As nuclear localisation seemed to be an inherent property of the minimal CRIB domain of Gic2, I decided to test if a CRIB domain from another Cdc42-bidning protein might have a different distribution. For the purpose, I constructed a reporter using a minimal version of the *S.pombe* Shk1 CRIB domain, containing the CRIB motif and a predicted BR-domain (Figure A1.1 A). Interestingly, the mini-Shk1-CRIB did not show any nuclear localisation, while still targeted to the cell tips (Figure A1.1 B). Unfortunately, the tip signal of the mini-Shk1-CRIB was also extremely weak and difficult to differentiate from the cytoplasmic background. Therefore, further optimisation of the probe would be required before it can be used as a substitution of the original CRIB. Nevertheless, as I describe in Chapter 5, the mini-Shk1-CRIB probe was still utilised as a useful control for experiments involving LatA-treatment of *gef1*Δ cells.

In conclusion, while I was not able to generate a functional CRIB probe that does not localise to the cell nucleus but still shows high affinity for tip Cdc42-GTP, my findings point to several possibilities for further improvement of the CRIB reporter. Firstly, the molecular basis for the nuclear localisation of CRIB seems to originate from the same region required for active Cdc42 binding. One minor implication of this result is that constructs such as the mini-CRIB should, in principle, be preferentially used in the future as they contain only the minimal portion of the Gic2 protein required

for binding Cdc42-GTP. Additionally, further optimisations of the CRIB reporter should be focused on this minimal region and could be directed towards experimenting with various mutation combinations of the basic amino acids in the BR domain. However, it is possible that such mutations might also affect the binding of active Cdc42, thus making the nuclear targeting an inherent and unchangeable property of the Gic2-based probes. Therefore, the use of probes originating from other proteins might be the way forward. Indeed, the constructed mini-Shk1-CRIB reporter possessed the localisation properties of an 'optimal' CRIB reporter but could perhaps be further optimised to achieve a desirable signal-to-noise ratio, suitable for live-cell imaging. Possible optimisations could include constructing Shk1-reporters with different lengths or varying their expression.

Finally, one important consideration regarding future efforts in improvement of the CRIB reporter would be the trade-offs between using exogenous proteins, such as budding yeast Gic2, and endogenous effectors, such as Shk1. The main advantage of the first option is that exogenous proteins are highly likely to be biologically inert apart from their ability to compete with endogenous Cdc42 effectors. However, as with the case of Gic2, exogenous proteins might have unexpected undesired properties such as nuclear targeting. On the other hand, using endogenous effectors like Shk1 might result in more optimal reporters in terms of efficient Cdc42-GTP binding and unlikely off-target effects. However, endogenous effectors might also be subject to specific additional levels of regulation (e.g. post-translational modifications) which might influence the outcome of experiments. Therefore, the appropriate choice for suitable CRIB reporters would likely depend on the particular biological questions which it is used to address.

Appendix 2

How does Latrunculin A activate stress-response signalling?

A2.1 Introduction

Experiments I described in Chapter 3 showed that the addition of the actin-depolymerizing drug LatA triggers the fission yeast stress-response pathway by activating the MAPK Sty1. An interesting question arising from this observation is what are the molecular pathways responding to the addition of LatA and eventually leading up to the activation of Sty1. One possibility is that the LatA-induced depolymerisation of the actin cytoskeleton is the cause of the MAPK activation. Alternatively, LatA could have additional 'off-target' effects, independent of its G-actin binding, leading to stress-response activation. The first possibility is certainly exciting as this would suggest that fission yeast cells have a mechanism of 'sensing' the state of F-actin and the response to its disruption is the activation of stress signalling. There is certainly merit in this idea considering that the organization of the actin cytoskeleton is affected as a result of various stresses that activate the SAPK pathway such as high osmolarity, heat, and gravity (Chowdhury *et al*, 1992; Petersen & Hagan, 2005; Soto *et al*, 2007; Robertson & Hagan, 2008). However, the occurring changes are often regarded as downstream effects of stress-response rather than causing it (Rupes *et al*, 1999). On the other hand, the alternative explanation where LatA activates Sty1 independently of actin depolymerisation could also be the case. Since LatA is a widely-used tool in biological research, confirmation of this hypothesis could have important implications for existing results and future experiments using the drug.

In this appendix section, I outline several experimental approaches aimed at elucidating the origin of LatA-induced MAPK signalling activation. While the preliminary findings presented here do not rule out an 'actin checkpoint' for Sty1 activation, they also illustrate that obtaining a definitive answer to this question would involve the generation of new tools and further rigorous experimentation.

A2.2. Results and discussion

A2.2.1. Investigating a putative interaction between G-actin and Win1/Wis4 MAPKKKs

One approach to testing whether the actin depolymerisation caused by LatA is what leads to Sty1 activation is to find and characterise mutants in which the interactions relaying the state of F-actin to the MAPK signalling pathway are disrupted. A possible candidate that could be involved as a secondary messenger in such interactions is monomeric G-actin, as its cellular concentration increases upon the depolymerisation of the actin cytoskeleton. A previous study in budding yeast had reported that actin perturbations caused by osmotic shock or addition of LatA induced a physical interaction between G-actin and the MAPKKK Ssk2 (Yuzyuk et al, 2002). The study also raised the hypothesis that Ssk2 might be involved in sensing damage to actin through this interaction, however, how this was relayed to MAPK signalling was not investigated further. Highly similar regions to the ones required for the interaction (here termed LD regions) were identified in the two fission yeast homologs of Ssk2 – the MAPKKKs Wis4 and Win1 (Figure A2.1 A). Thus, I hypothesised that the *S.pombe* MAPKKKs might also interact with G-actin through their LD regions and act as sensors of free G-actin to activate MAPK signalling in response to F-actin depolymerisation. Preliminary work in the Sawin lab by Dan Kaemena had generated mutants of each of the two MAPKKKs lacking the LD regions. Furthermore, Dan Kaemena's experiments suggested that for either of the Win1-ΔLD or Wis4-ΔLD mutants, Sty1 was not activated by addition of LatA, as GFP-tagged Sty1 did not migrate into the nucleus following LatA treatment. At the same time, the functioning of the MAPK signalling cascade seemed unaffected by the LD region deletions during a KCl osmotic shock as Sty1-GFP became enriched in the nucleus following addition of KCl.

These results suggested that the LD regions of the MAPKKK might be specifically responsible for recognising perturbations in the actin cytoskeleton. I, therefore, confirmed the initial observations by repeating the original experiments using Sty1-GFP nuclear enrichment as an indicator of MAPK activation (Figure A2.1 B; see also Figure 3.3). However, I found that a microscopy-based assay looking at qualitative differences in Sty1-GFP concentration in the cell nuclei was not sufficient to conclude that Win1-ΔLD/Wis4-ΔLD cells had functioning stress-response to

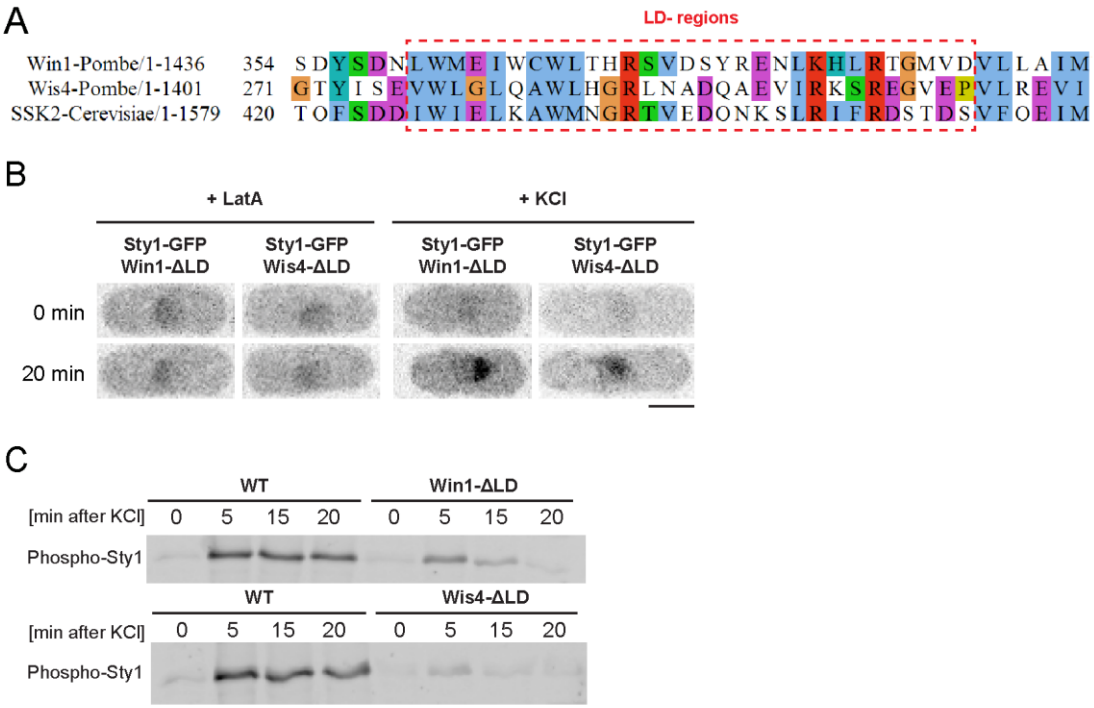

Figure A2.1. Deletion of the putative actin-binding LD regions in the MAPKKKs Win1 and Wis4 compromises SAPK signaling. (A) Protein sequence alignment and conservation of the LD regions betweeen budding and fission yeast MAPKKKs. (B) Sty1-GFP cells carrying an LD deletion on either Win1 or Wis4 treated with either 50 μM LatA or 0.6M KCl. Times shown are relative to addition of treatment. Scale bar, 5 μm. (C) Western blot of WT, Win1-ΔLD, or Wis4-ΔLD cell extracts using phospho-specific antibody to detect Sty1 activation after 0.6M KCl osmotic shock.

osmotic stress. The reason is that as a result of the osmotic shock, the cell's volume shrinks dramatically, inevitably causing an increase in the concentration of both cytoplasmic and nuclear fluorophores and possibly giving a false-positive result. While a more sophisticated quantitative analysis as the one described in Materials and Methods Section 2.13 could have resolved this issue, a more straight-forward approach was to perform a time-course western blot assay using the phospho-specific antibody against Sty1. Surprisingly, the LD mutants showed little to no activation of the MAPK in response to osmotic stress, similar to deletion of either Win1 or Wis4 (Figure A2.1 C; Samejim*a et al*, 1997). Interestingly, a recent report demonstrated that the N-terminal regions of Win1 and Wis4, which are in close proximity to the LD regions, are essential for the interaction of the MAPKKKs with the stress-response regulator Mcs4 (Morigasaki et al, 2013). Without this interaction, the stability of the MAPKKK hetero-complex was affected, resulting in reduction in Sty1 activation in response to osmotic stress. Thus, it is possible that deleting the LD regions inadvertently resulted in the same outcome.

I conclude that the initial results generated by the microscopy-based assay presented a "false-positive" indication of Sty1 activation in response to osmotic shock in the Win1-ΔLD/Wis4-ΔLD mutants. The presence of the LD regions of both MAPKKK appears to be critical for the overall functioning of the pathway, whether the external stressor is KCl or LatA. While this result does not discard the possibility of an interaction between the LD regions and G-actin, it rules out the MAPKKK LD mutants as a tool to dissect any LatA-specific contribution to stress-response activation.

A2.2.2. Various F-actin-affecting drugs can also lead to Cdc42-GTP disruption

If LatA-induced activation of Sty1 represents an 'off-target' effect, independent of the drug's actin-depolymerizing activity, then one would predict that structurally-different drugs that also affect the actin cytoskeleton should not lead to the activation of the MAPK. Therefore, I decided to test whether some of the well-known agents affecting F-actin dynamics have an effect on MAPK signalling. As I described in Chapter 4, the LatA-induced dispersal of Cdc42-GTP from the cell tips was dependent on the activation of Sty1 and Cdc42-GTP dispersal could be driven simply by activation of the MAPK, independent of the state of the actin cytoskeleton. Therefore, as an indicator of MAPK activation, I decided first to observe CRIB distribution in

response to different F-actin-affecting drugs, although this is an indirect assay. The drugs used were the actin depolymerising agent Cytochalasin A, the Arp2/3 inhibitor CK-666, and the actin-stabilizing drug Jasplakinolide.

The cytochalasin family of drugs are naturally-occurring organic molecules that bind actin filaments and inhibit their polymerization by binding to the barbed-end of the actin filament (Cooper, 1987). While less potent than latrunculins, cytochalasins have been used to study the actin cytoskeleton in various fungal species (Spector *et al*, 1989; Akashi *et al*, 1994; Barja & Turian, 1994; Gabriel *et al*, 1998). Among the cytochalasins, cytochalasin A (CytA) has been suggested to be most effective in *S.pombe* (Kanbe *et al*, 1993). However, CytA's effect on actin has been evaluated only using rhodamine-phalloidin staining and not with more modern tools such as Lifeact, which is more sensitive for visualising actin cables. Therefore, I added CytA to cells expressing the Lifeact-mCherry and the CRIB reporters, to observe any changes in actin dynamics and distribution of active Cdc42. When cells were treated with 20 µM CytA, actin cables completely disappeared within 6 min of treatment and re-formed into between one and three thicker actin cables about 40-60 min later (Figure A2.2, A). Actin patches appeared unaffected and, as previously reported, the formation of the cytokinetic ring was inhibited (data not shown). Some disruption of tip-localized CRIB was also observed, with clear patches appearing within 1.5 hours of treatment. Overall, the CRIB dispersal from the tips was less severe than that observed after LatA and the formation of clear ectopic CRIB patches was approximately 30 min slower.

I also treated Lifeact/CRIB-expressing cells with the Arp2/3 inhibitor CK-666 (Nolen *et al*, 2009). As previously reported, addition of 100 µM CK-666 led to a rapid (within 6 min) and almost complete disappearance of actin patches, and a concomitant increase in actin cables (Figure A2.2, B; Burke *et al*, 2014). Interestingly, the CK-666 treatment also led to dispersal of CRIB. The extent of the dispersal was less severe than that observed after LatA and similar in efficiency and kinetics as that observed after CytA.

As CytA and CK-666 both have disrupting effects on existing F-actin structures, I also tested the effects of an actin-stabilizing drug – jasplakinolide. Jasplakinolide is a cyclic peptide that promotes F-actin assembly by significantly

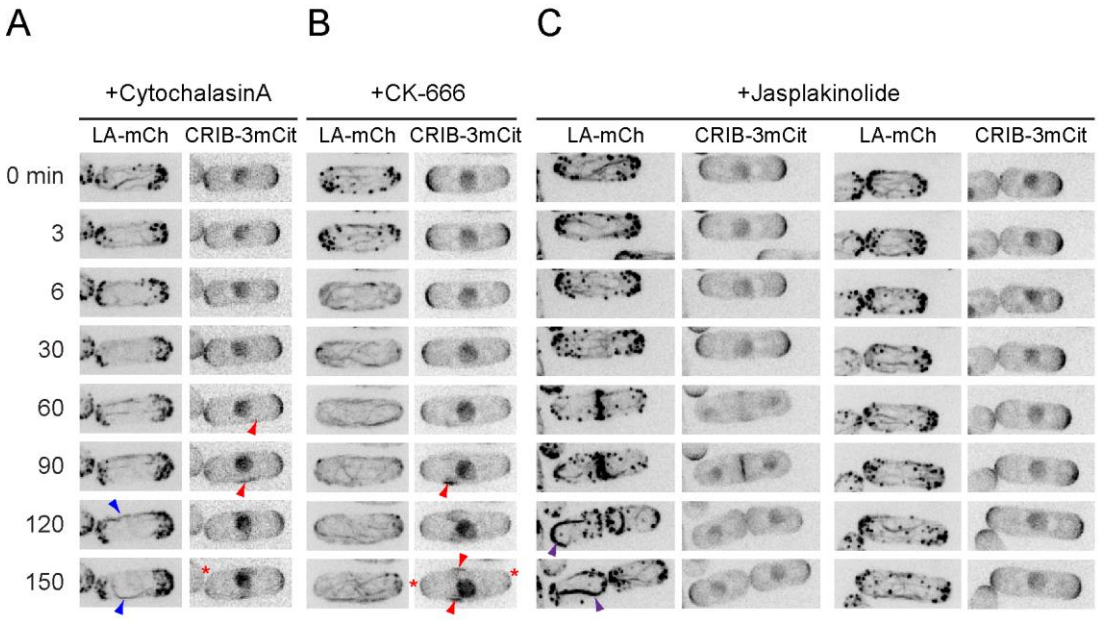

Figure A2.2. Addition of different drugs affecting F-actin distribution can also lead to Cdc42-GTP dispersal. Time-lapse images of cells expressing Lifeact-mCherry (LA-mCh) and CRIB-3xmCitrine (CRIB-3mCit) after addition of 20 μM Cytochalasin A (A), 100 μM CK-666 (B), and 20 μM Jasplakinolide (C). Two examples of Jasplakinolide treatment are present to show the drug's effect after (left) and prior (right) cell division. Red asterisks mark CRIB dispersal from the cell tips. Red arrowheads point to ectopic CRIB patches after the dispersal. Blue arrowheads in first panel point to recovered actin cables after Cytochalasin A disruption. Purple arrowheads in third panel point to actin aggregates formed after cell division in Jasplakinolide-treated cells. All times shown are relative to addition of drug. Scale bars, 5 μm.

lowering the critical concentration required for nucleation (Bubb *et al*, 1994; Bubb, 2000). Addition of jasplakinolide to budding yeast cells does not inhibit growth; however, the actin cytoskeleton in these cells is re-organised into large non-dynamic and LatA-resistant aggregates, which leads to defects in Cdc42 distribution and endocytosis (Ayscough, 2000). Interestingly, when I added 20 µM Jasplakinolide to Lifeact/CRIB-expressing fission yeast cells, such changes to the actin cytoskeleton were not observed until cells had undergone one division (Figure A2.2). Nevertheless, regardless of whether actin aggregates appeared or not, CRIB distribution was not affected and comparable to WT non-treated cells. Additionally, for the whole time of observation (2.75 hours after treatment), growth and progression through the cell cycle appeared unperturbed by the addition of the drug.

In conclusion, the preliminary experiments using different actin-affecting drugs are consistent with the idea that actin integrity might have a role as a sensor for MAPK activation. Indeed, both treatments with CytA and CK-666 lead to CRIB dispersal which, like treatment with LatA, is associated with Sty1 activation. Interestingly, treatment with Jasplakinolide, which promotes nucleation and also leads to changes in F-actin organisation (aggregates after cell division) did not have any effect on CRIB distribution. One explanation could be that while LatA, CytA, and CK-666 all lead to some form of accumulation of G-actin (permanent in the first case and transient in the latter two), treatment with Jasplakinolide could actually reduce the available pools of G-actin due to increased actin filament nucleation. However, it is important to note that all these experiments provide only indirect evidence of Sty1 activation and further tests looking directly at Sty1 phosphorylation levels should be performed. Additionally, drugs like the formin inhibitor SMIFH2 could also be tested as they could bring additional insight about the contributions of specific actin structures (Rizvi *et al*, 2009). Another idea would be the sequential treatment of cells with first Jasplakinolide, followed by LatA. As Jasplakinolide-induced actin aggregates have been shown to be LatA resistant, it would be interesting to see if LatA would have the same effect on Sty1 activation in cells pre-treated with Jasplakinolide. Finally, while the additive evidence of each drug treatment could favour certain conclusions, the problem of 'off-target' unknown effects of each individual treatment would still need to be considered in each scenario.

A2.2.3. Investigating existing LatA-resistant actin mutants in fission yeast

Arguably the most straight-forward approach of distinguishing between an actin-mediated and an 'off-target' origin of LatA-induced MAPK activation is investigating actin mutants that are resistant to LatA. Indeed, such mutants have been characterised in the budding yeast *S.cerevisiae* both *in vitro* and *in vivo* (Ayscough *et al*, 1997). One of the mutant alleles, *act1-117*, containing the R183A and D184A (RADA) amino acid substitutions, allowed cells to grow similarly to wild-type in unperturbed conditions and also to continue proliferating in the presence of 100 µM LatA (Wertman *et al*, 1992; Ayscough, 2000). In addition, purified *act1-117* F-actin polymers were also shown to be resistant to LatA *in vitro*, although the structural basis for the resistance is not clear as the RADA substitutions are not part of the LatA-binding interface (Morton *et al*, 2000). Because of the high conservation between the budding and fission yeast actin genes, it should be straightforward to generate LatA-resistant *S.pombe* mutant carrying the *act1-117*-equivalent mutations in the *act1* fission yeast gene. Indeed, two studies in fission yeast have independently generated the RADA mutant, although its characterization has been limited (Karagiannis *et al*, 2005; Meadows & Millar, 2008). Therefore, I obtained both of these mutants and decided to characterise them further in order to test whether the RADA mutations conferred the same resistance in fission as in budding yeast. If that was indeed the case, then they can be used to assess whether actin depolymerization is required for Sty1 activation upon LatA addition. Here I will focus only on the *act1-LR* mutant (corresponding to *act1-117* in budding yeast) published in the Karagiannis *et al*, 2005 study, as I was unable to confirm the genotype of the strains from the Meadows & Millar, 2008 paper.

In the original study, the *act1-LR* mutant was characterised as able to form colonies in LatA concentrations up to 5 µM. However, from the authors' description it remained unclear whether they had ever tested higher LatA concentrations, as has been done with *S. cerevisiae*). To test that I performed a spot assay using a*ct1-LR* cells plated on different concentrations of LatA (Figure A2.3). I found that while some *act1-LR* cells were indeed able to form colonies up to 5 µM LatA, most were not able to survive even in lower concentrations (2.5 µM) suggesting some

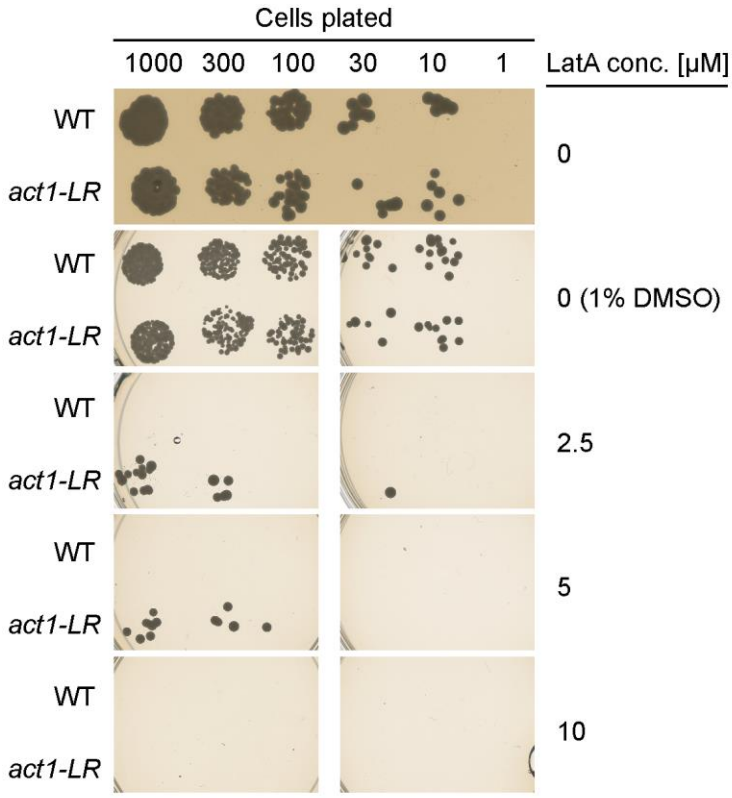

Figure A2.3. Sensitivity of *act1-LR* mutants to different concentrations of Latruculin A. Scanned images of a spot assays of wild-type (WT) and *act1-LR* cells grown for 4 days at 25°C on YE plates containing increasing Latrunclin A (LatA) concentrations. Top panel shows a scan of a single YE plate which is darker than others due to difference in agar thickness. All other panels are cropped scans of two thinner YE plates containng 1% DMSO and the indicated LatA concentration.

heterogeneity in resistance among the cells in the *act1-LR* cultures. Furthermore, the *act1-LR* mutant did not grow on higher concentrations of the drug in contrast to what is observed for *act1-117* in budding yeast. This suggested that the *act1-LR* mutant was not 'fully' resistant to the effects of LatA.

Based on the conservation of the actin gene, one possible interpretation is that while the actin cytoskeleton in *act1-LR* is indeed resistant to depolymerization, the cells are killed by other 'off-target' effects of LatA. One of these effects could hypothetically be the continued activation of Sty1 which, as I showed in Chapter 4, is sufficient to arrest cell division and thus likely be lethal in the long-term. To test the extent of depolymerization caused by LatA and indirectly assay its ability to activate Sty1 in *act1-LR* cells, I combined the *act1-LR* allele with the Lifeact and CRIB reporters and performed live-cell imaging after addition of LatA. Surprisingly, these cells exhibited a range of responses after addition of LatA (Figure A2.4). One common outcome, however, was that in all of the cells, the actin cytoskeleton was disrupted to some extent. In some cases, actin cables were disrupted, while the actin patches were mostly retained (Figure A2.4, A and C). In others, most of the actin cytoskeleton was depolymerised, with only very small actin patches remaining (Figure A2.4, B). It should also be noted that the initial F-actin distribution also varied among different *act1-LR* cells. For example, some cells had fewer patches (Figure A2.4, A), while other cells had fewer patches and almost no cables (Figure A2.4, C). The behaviour of CRIB in response to LatA addition was also inconsistent between the different cells. While most cells showed a slow but obvious CRIB dispersal and ectopic patch formation (Figure A2.4, A and B), there were examples in which the CRIB was mostly retained on the cell tips. One explanation for the heterogeneous behaviour of Lifeact/CRIB/*act1-LR* cells in response to LatA could be the emergence of suppressor mutations or other genomic re-arrangements in the strain. Indeed, when observed under the microscope without any prior treatment, the *act1-LR* mutant alone (without Lifeact or CRIB) had visible morphological defects such as aberrant shape and multiple septa (data not shown), suggesting that the RADA mutations might have greater deleterious effects on cell physiology in fission yeast compared to budding yeast. Additionally, the original method of construction of the *act1-LR* mutant, involving integration of a *ura4*+ cassette in the *act1* locus and generating non-functional remnants of the original *act1* gene, could have consequences on normal actin expression and also favour genomic

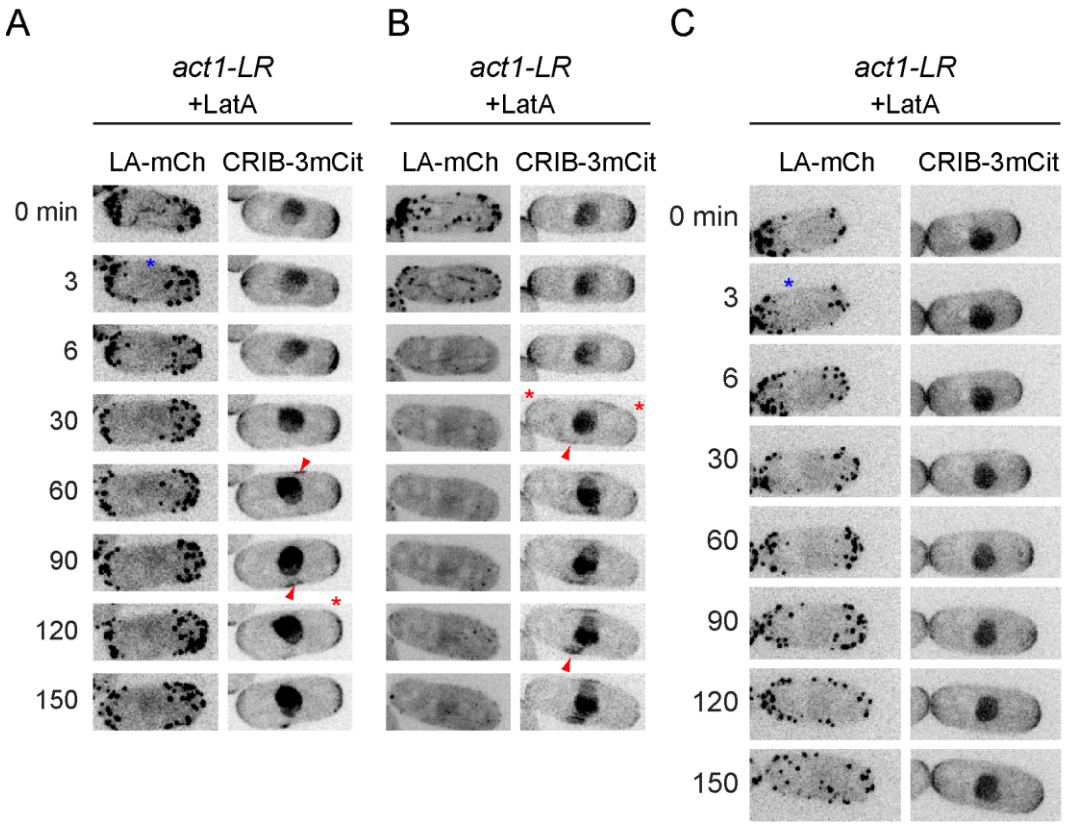

Figure A2.4. Different effects of Latrunculin A treatment of *act1-LR* mutants. Time-lapse images of *act1-LR* cells expressing Lifeact-mCherry (LA-mCh) and CRIB-3xmCitrine (CRIB-3mCit) after addition of 50 μM Latrunculin A (LatA). Three examples shown to illustrate the different outcomes of the experiment. (A) A cell where treatment disrupts the actin cables but not the actin patches and also leads to CRIB dispersal. (B) A cell where treatment disrupts both actin cables and patches (with minor remnants of the latter remaining) and also leads to CRIB dispersal. (C) A cell where treatment leads to minor disruption of actin patches but CRIB distribution is not greatly affected. Note that actin cables in this cell are not distingiushable prior to treatment but no further cables form during the course of the experiment.
Red asterisks mark CRIB dispersal from the cell tips. Red arrowheads point to ectopic CRIB patches after the dispersal. Blue asterisks point to examples of absent actin cables. All times shown are relative to addition of LatA. Scale bars, 5 μm.

re-arrangements reverting back to the original *act1* gene (Karagiannis *et al*, 2005). Furthermore, the results of the spot assay suggested that not all of the cells exposed to low concentrations of LatA are able to survive. Thus, though I confirmed the genotype of the *act1-LR* mutant by tetrad analysis and sequencing of the *act1-LR* insert in the genome it is likely that the strain may be prone to accumulating additional genomic modifications that could hinder a rigorous analysis of its properties.

While my experiments using the existing *act1-LR* mutant to address the origin of LatA-induced Sty1 activation remain largely inconclusive, I still believe that testing LatA-resistant actin mutants is the best way of tackling the problem. One potential way to progress further is to generate new, 'cleaner' versions of such mutants where the endogenous *act1* gene is replaced with a mutant version without any further changes to the *act1* locus. This method could be applied to both the RADA mutant or other mutants identified to be LatA-resistant but not yet extensively tested in fission yeast (Morton *et al*, 2000).

Final conclusions and outlook

In this thesis, I have described the discovery of a novel role for the fission yeast MAPK pathway in regulating cell polarity. Using live-cell imaging, drug perturbations, and genetic manipulations, my experiments suggest a direct involvement of the Sty1 MAPK in modulating the localisation of the key polarity regulator Cdc42. In addition to my main findings, I have presented preliminary experiments and discussed possible approaches to identify the proteins behind Sty1-dependent control of polarity. These experiments consist of both the targeted (candidate-based) and global (SILAC phosphoprotemics-based) methodologies aimed at elucidating the molecular targets of Sty1 that mediate Cdc42 regulation. Additionally, the described experiments showing the activation of Sty1 in response to the actin-depolymerizing drug LatA have highlighted exciting avenues of investigation into the putative role of the actin cytoskeleton in sensing stress. Thus, towards the end of this thesis, I have also described preliminary experiments and outlined possible future approaches to determine whether actin depolymerization is a sensor for the activation of the MAPK pathway. Overall, I believe that the findings of my work, as well as the tools developed in the process, have significant implications for fission yeast biology and have considerable potential to broaden the understanding of Cdc42 regulation across biological systems.

To the extent of my knowledge, the results in this thesis present the first evidence of a MAPK stress-response pathway regulating Cdc42 activity. For this reason, drawing straightforward parallels between the process in fission yeast and in other organisms is difficult. As discussed in greater detail in Chapter 3, the data available on the function of the well-studied homologous MAPK pathway in the model yeast *S.cerevisisae* does not indicate involvement in regulating Cdc42 polarity. In contrast to my work, published research connecting MAPK pathways and polarity in both budding yeast and other eukaryotes (such as flies and mammals) has primarily focused on downstream MAPK signalling regulated by polarity proteins (Etienne-Manneville, 2004; Brewster & Gustin, 2014). Thus, it would be of great interest in the future to discern whether this newly found function of the fission yeast stress-response pathway is specific to *S.pombe* or homologous processes are present in other organisms.

A key piece of evidence needed for this distinction would be the identification of the specific targets of Sty1 involved in polarity regulation. I believe that the tools and approaches developed and discussed in this work, like the SISA strain and the pilot SILAC phosphoproteomics experiments, will be instrumental in identifying such targets in the future. Furthermore, the lethality of the SISA mutations in the absence of 3BrB also allows for performing genetic screens for suppressor mutants that rescue SISA lethality. As fission yeast polarity is intimately linked with growth and survival, such mutants are likely to carry mutations in genes involved in Sty1-driven Cdc42 regulation. However, as protein kinase functions and targets often vary widely across species and throughout evolution, identifying fission yeast Sty1 polarity targets might not be sufficiently informative with regards to how wide-spread stress-response-driven polarity regulation might be (Manning *et al*, 2002). Thus, a necessary continuation to identifying novel Sty1 targets involved in Cdc42 regulation should be the investigation of the general molecular mechanisms of how such targets exert their control on Cdc42 function, as such mechanisms could still be conserved in other organisms but orchestrated by divergent molecular players.

Another exciting aspect of my findings is the essential role for Sty1-dependent regulation of Cdc42 during quiescence entry upon nitrogen starvation. While my experiments illustrated the requirement for Sty1 activity to maintain active Cdc42 dispersal during quiescence, many questions regarding this phenomenon remain unclear. For example, is Sty1 function in this context solely controlling polarity and growth, or also other aspects of physiology? Related to this question, what is the long-term fate of quiescent *sty1.as* cells which have initiated growth upon 3BrB removal in a nitrogen-free medium? Such questions can readily be addressed by using the experimental and imaging setups devised in this study. Also of interest would be the parameters of growth initiated in starvation conditions, such the kinetics of outgrowth and the dimensions of the generated protrusions as these will be valuable for the investigation of cell size regulation in such conditions. Furthermore, it would be interesting to investigate whether Sty1's role during quiescence is also relevant during mating. In particular, are the processes of shmoo initiation and growth, both of which are likely dependent on Cdc42 activity, also regulated by Sty1 activity (Bendezú & Martin, 2013)? Finally, while the importance of Sty1's role in Cdc42 regulation was demonstrated in a very specific physiological context (nitrogen-starvation-induced quiescence), it remains unknown whether Sty1's function in modulating polarity

contributes to other processes in the fission yeast life cycle. For example, as *sty1*Δ mutants are reported to have NETO defects, it is tempting to speculate that fluctuations in Sty1 activity could contribute to monopolar to bipolar polarity transitions (Koyano *et al*, 2010).

References

Ackermann M, Chao L, Bergstrom CT & Doebeli M (2007) On the evolutionary origin of aging. *Aging Cell* **6:** 235–244

Adamo JE, Moskow JJ, Gladfelter AS, Viterbo D, Lew DJ & Brennwald PJ (2001) Yeast Cdc42 functions at a late step in exocytosis, specifically during polarized growth of the emerging bud. *J. Cell Biol.* **155:** 581–592

Adams AEM, Johnson DI, Longnecker RM, Sloat BF & Pringle JR (1990) CDC42 and CDC43, two additional genes involved in budding and the establishment of cell polarity in the yeast Saccharomyces cerevisiae. *J. Cell Biol.* **111:** 131–142

Aiba H, Yamada H, Ohmiya R & Mizuno T (1995) The osmo-inducible gpdl+ gene is a target of the signaling pathway involving Wis1 MAP-kinase kinase in fission yeast. *FEBS Lett.* **376:** 199–201

Akashi T, Kanbe T & Tanaka K (1994) The role of the cytoskeleton in the polarized growth of the germ tube in Candida albicans. *Microbiology* **140:** 271–280

Alvarez-Tabarés I, Grallert A, Ortiz J-M & Hagan IM (2007) Schizosaccharomyces pombe protein phosphatase 1 in mitosis, endocytosis and a partnership with Wsh3/Tea4 to control polarised growth. *J. Cell Sci.* **120:** 3589–3601

Aragona M, Panciera T, Manfrin A, Giulitti S, Michielin F, Elvassore N, Dupont S & Piccolo S (2013) A mechanical checkpoint controls multicellular growth through YAP/TAZ regulation by actin-processing factors. *Cell* **154:** 1047–1059

Arellano M, Cartagena-Lirola H, Hajibagheri MAN, Durán A & Valdivieso MH (2000) Proper ascospore maturation requires the chs1+ chitin synthase gene in Schizosaccharomyces pombe. *Mol. Microbiol.* **35:** 79–89

Arellano M, Duran a & Perez P (1997) Localisation of the Schizosaccharomyces pombe rho1p GTPase and its involvement in the organisation of the actin cytoskeleton. *J. Cell Sci.* **110 (Pt 2:** 2547–55

Arellano M, Durán a & Pérez P (1996) Rho 1 GTPase activates the (1-3)beta-D-glucan synthase and is involved in Schizosaccharomyces pombe morphogenesis. *EMBO J.* **15:** 4584–4591

Ayscough KR (2000) Endocytosis and the development of cell polarity in yeast require a dynamic F-actin cytoskeleton. *Curr. Biol.* **10:** 1587–1590

Ayscough KR, Stryker J, Pokala N, Sanders M, Crews P & Drubin DG (1997) High rates of actin filament turnover in budding yeast and roles for actin in establishment and maintenance of cell polarity revealed using the actin inhibitor latrunculin-A. *J. Cell Biol.* **137:** 399–416

Bähler J & Pringle JR (1998) Pom1p, a fission yeast protein kinase that provides positional information for both polarized growth and cytokinesis. *Genes Dev.* **12:** 1356–1370

Bähler J, Wu JQ, Longtine MS, Shah NG, McKenzie a, Steever a B, Wach a, Philippsen P & Pringle JR (1998) Heterologous modules for efficient and versatile PCR-based gene targeting in Schizosaccharomyces pombe. *Yeast* **14:** 943–51

Bao S, Qyang Y, Yang P, Kim H, Du H, Bartholomeusz G, Henkel J, Pimental R, Verde F & Marcus S (2001) The Highly Conserved Protein Methyltransferase, Skb1, Is a Mediator of Hyperosmotic Stress Response in the Fission Yeast Schizosaccharomyces pombe. *J. Biol. Chem.* **276:** 14549–14552

Barja F & Turian G (1994) Cytochalasin B-sensitive actin-mediated nuclear RNA export in germinating conidia of Neurospora crassa. *Cell Biol. Int.* **18:** 903–906

Bendezu FO & Martin SG (2011) Actin cables and the exocyst form two independent morphogenesis pathways in the fission yeast. *Mol. Biol. Cell* **22:** 44–53

Bendezú FO & Martin SG (2011) Actin cables and the exocyst form two independent morphogenesis pathways in the fission yeast. *Mol. Biol. Cell* **22:** 44–53

Bendezú FO & Martin SG (2013) Cdc42 explores the cell periphery for mate selection in fission yeast. *Curr. Biol.* **23:** 42–7

Bendezú FO, Martin SG & Lew D (2010) Actin cables and the exocyst form two independent morphogenesis pathways in the fi ssion yeast.

Bendezú FO, Vincenzetti V & Martin SG (2012) Fission yeast sec3 and Exo70 are transported on actin cables and localize the exocyst complex to cell poles. *PLoS One* **7:**

Bendezú FO, Vincenzetti V, Vavylonis D, Wyss R, Vogel H & Martin SG (2015) Spontaneous Cdc42 Polarization Independent of GDI-Mediated Extraction and Actin-Based Trafficking. *PLOS Biol.* **13:** e1002097

Bernards A (2003) GAPs galore! A survey of putative Ras superfamily GTPase activating proteins in man and Drosophila. *Biochim. Biophys. Acta* **1603:** 47–82

Betschinger J, Eisenhaber F & Knoblich JA (2005) Phosphorylation-Induced Autoinhibition Regulates the Cytoskeletal Protein Lethal (2) giant larvae. *Curr. Biol.* **15:** 276–282

Bicho CC, Kelly D a, Snaith H a, Goryachev AB & Sawin KE (2010a) A catalytic role for Mod5 in the formation of the Tea1 cell polarity landmark. *Curr. Biol.* **20:** 1752–7

Bicho CC, de Lima Alves F, Chen ZA, Rappsilber J & Sawin KE (2010b) A genetic engineering solution to the 'arginine conversion problem' in stable isotope labeling by amino acids in cell culture (SILAC). *Mol. Cell. Proteomics* **9:** 1567–77

Bieling P, Laan L, Schek H, Munteanu EL, Sandblad L, Dogterom M, Brunner D & Surrey T (2007) Reconstitution of a microtubule plus-end tracking system in vitro. *Nature* **450:** 1100–1105

Bishop AC, Ubersax J a, Petsch DT, Matheos DP, Gray NS, Blethrow J, Shimizu E, Tsien JZ, Schultz PG, Rose MD, Wood JL, Morgan DO & Shokat KM (2000) A chemical switch for inhibitor-sensitive alleles of any protein kinase. *Nature* **407:** 395–401

Bishop AL & Hall A (2000) Rho GTPases and their effector proteins. *Biochem. J.* **348 Pt 2:** 241–55

Bois JS, Jülicher F & Grill SW (2011) Pattern formation in active fluids. *Phys. Rev. Lett.* **106:** 1–4

Bokoch GM (2003) Biology of the p21-activated kinases. *Annu Rev Biochem* **72:** 743–781

Bonazzi D, Julien J-DD, Romao M, Seddiki R, Piel M, Boudaoud A & Minc N (2014) Symmetry Breaking in Spore Germination Relies on an Interplay between Polar

Cap Stability and Spore Wall Mechanics. *Dev. Cell* **28:** 534–546

Bourne HR, Sanders DA & McCormick F (1990) The GTPase superfamily: a conserved switch for diverse cell functions. *Nature* **348:** 125–132

Brewster JL & Gustin MC (2014) Hog1: 20 years of discovery and impact. *Sci. Signal.* **7:** re7-re7

Brown JL, Jaquenoud M, Gulli M-P, Chant J & Peter M (1997) Novel Cdc42-binding proteins Gic1 and Gic2 control cell polarity in yeast. *Genes Dev.* **11:** 2972–2982

Bubb MR (2000) Effects of Jasplakinolide on the Kinetics of Actin Polymerization. AN EXPLANATION FOR CERTAIN IN VIVO OBSERVATIONS. *J. Biol. Chem.* **275:** 5163–5170

Bubb MR, Senderowicz AMJ, Sausville EA, Duncan KLK & Korn ED (1994) Jasplakinolide, a cytotoxic natural product, induces actin polymerization and competitively inhibits the binding of phalloidin to F-actin. *J. Biol. Chem.* **269:** 14869–14871

Buck V, Quinn J, Soto Pino T, Martin H, Saldanha J, Makino K, Morgan BA & Millar JB (2001) Peroxide sensors for the fission yeast stress-activated mitogen-activated protein kinase pathway. *Mol. Biol. Cell* **12:** 407–19

Burke TA, Christensen JR, Barone E, Suarez C, Sirotkin V & Kovar DR (2014) Homeostatic Actin Cytoskeleton Networks Are Regulated by Assembly Factor Competition for Monomers. *Curr. Biol.* **24:** 579–585

Busch KE & Brunner D (2004) The Microtubule Plus End-Tracking Proteins mal3p and tip1p Cooperate for Cell-End Targeting of Interphase Microtubules. *Curr. Biol.* **128:** 189–190

Busch KE, Hayles J, Nurse P & Brunner D (2004) Tea2p kinesin is involved in spatial microtubule organization by transporting Tip1p on microtubules. *Dev. Cell* **6:** 831–843

Busso D, Delagoutte-Busso B & Moras D (2005) Construction of a set Gateway-based destination vectors for high-throughput cloning and expression screening in Escherichia coli. *Anal. Biochem.* **343:** 313–321

Butty A-C, Perrinjaquet N, Petit A, Jaquenoud M, Segall JE, Hofmann K, Zwahlen C & Peter M (2002) A positive feedback loop stabilizes the guanine-nucleotide exchange factor Cdc24 at sites of polarization. *EMBO J.* **21:** 1565–76

Castagnetti S, Behrens R & Nurse P (2005) End4/Sla2 is involved in establishment of a new growth zone in Schizosaccharomyces pombe. *J. Cell Sci.* **118:** 1843–1850

Caviston JP (2003) The Role of Cdc42p GTPase-activating Proteins in Assembly of the Septin Ring in Yeast. *Mol. Biol. Cell* **14:** 4051–4066

Chang E, Bartholomeusz G, Pimental R, Lai H, Wang LL, Yang P, Chen J & Marcus S (1999) Direct Binding and In Vivo Regulation of the Fission Yeast p21-Activated Kinase Shk1 by the SH3 Domain Protein Scd2 Direct Binding and In Vivo Regulation of the Fission Yeast p21-Activated Kinase Shk1 by the SH3 Domain Protein Scd2. *Mol. Cell. Biol.*

Chang EC, Barr M, Wang Y, Jung V, Xu HP & Wigler MH (1994) Cooperative interaction of S. pombe proteins required for mating and morphogenesis. *Cell* **79:** 131–41

Chen D, Toone W & Mata J (2003) Global transcriptional responses of fission yeast to environmental stress. *Mol. Biol. …* **14:** 214–229

Chowdhury S, Smith KW & Gustin MC (1992) Osmotic stress and the yeast cytoskeleton: phenotype-specific suppression of an actin mutation. *J. Cell Biol.* **118:** 561–71

Cipak L, Zhang C, Kovacikova I, Rumpf C, Miadokova E, Shokat KM & Gregan J (2011) Generation of a set of conditional analog-sensitive alleles of essential protein kinases in the fission yeast Schizosaccharomyces pombe. *Cell Cycle* **10:** 3527–3532

Coll PM, Rincon S a, Izquierdo R a & Perez P (2007) Hob3p, the fission yeast ortholog of human BIN3, localizes Cdc42p to the division site and regulates cytokinesis. *EMBO J.* **26:** 1865–77

Coll PM, Trillo Y, Ametzazurra A & Perez P (2003) Gef1p, a new guanine nucleotide exchange factor for Cdc42p, regulates polarity in Schizosaccharomyces pombe. *Mol. Biol. Cell* **14:** 313–23

Cooper J (1987) Effects of cytochalasin B on actin filaments. *Cold Spring Harb. Symp. Quant. Biol.* **37:** 585–593

Coué M, Brenner SL, Spector I & Korn ED (1987) Inhibition of actin polymerization by latrunculin A. *FEBS Lett.* **213:** 316–8

Courtemanche N, Pollard TD & Chen Q (2016) Avoiding artefacts when counting polymerized actin in live cells with LifeAct fused to fluorescent proteins. *Nat. Cell Biol.* **18:** 1–5

Cox J & Mann M (2008) MaxQuant enables high peptide identification rates, individualized p.p.b.-range mass accuracies and proteome-wide protein quantification. *Nat. Biotechnol.* **26:** 1367–72

Cox J, Neuhauser N, Michalski A, Scheltema RA, Olsen J V. & Mann M (2011) Andromeda: A peptide search engine integrated into the MaxQuant environment. *J. Proteome Res.* **10:** 1794–1805

Cuadrado A & Nebreda AR (2010) Mechanisms and functions of p38 MAPK signalling. *Biochem. J.* **429:** 403–417

Das M, Drake T, Wiley DJ, Buchwald P, Vavylonis D & Verde F (2012) Oscillatory dynamics of Cdc42 GTPase in the control of polarized growth. *Science* **337:** 239–43

Das M, Nuñez I, Rodriguez M, Wiley DJ, Rodriguez J, Sarkeshik A, Yates JR, Buchwald P & Verde F (2015) Phosphorylation-dependent inhibition of Cdc42 GEF Gef1 by 14-3-3 protein Rad24 spatially regulates Cdc42 GTPase activity and oscillatory dynamics during cell morphogenesis. *Mol. Biol. Cell* **26:** 3520–3534

Das M, Wiley DJ, Chen X, Shah K & Verde F (2009) The conserved NDR kinase Orb6 controls polarized cell growth by spatial regulation of the small GTPase Cdc42. *Curr. Biol.* **19:** 1314–9

Das M, Wiley DJ, Medina S, Vincent HA, Larrea M, Oriolo A & Verde F (2007) Regulation of Cell Diameter , For3p Localization , and Cell Symmetry by Fission Yeast Rho-GAP Rga4p □. *Mol. Biol. Cell* **18:** 2090–2101

Davey J (1998) Fusion of a fission yeast. *Yeast* **14:** 1529–66

Degols G, Shiozaki K & Russell P (1996) Activation and regulation of the Spc1 stress-activated protein kinase in Schizosaccharomyces pombe. *Mol. Cell. Biol.* **16:** 2870–7

Deng L, Kabeche R, Wang N, Wu J-Q & Moseley JB (2014) Megadalton node assembly by binding of Skb1 to the membrane anchor Slf1. *Mol. Biol. Cell*

Deng L & Moseley JB (2013) Compartmentalized nodes control mitotic entry signaling in fission yeast. *Mol. Biol. Cell* **24:** 1872–81

DerMardirossian C & Bokoch GM (2005) GDIs: Central regulatory molecules in Rho GTPase activation. *Trends Cell Biol.* **15:** 356–363

Devenport D (2014) The cell biology of planar cell polarity. *J. Cell Biol.* **207:** 171–179

Dodgson J, Chessel A, Yamamoto M, Vaggi F, Cox S, Rosten E, Albrecht D, Geymonat M, Csikasz-Nagy A, Sato M, Carazo-Salas RE, Biophysics M, Hunt N, Rosten E, Albrecht D, Geymonat M, Csikasz-Nagy A, Sato M, Carazo-Salas RE, Biophysics M, et al (2013) Spatial segregation of polarity factors into distinct cortical clusters is required for cell polarity control. *Nat. Commun.* **4:** 1834

Dong Y, Pruyne D & Bretscher A (2003) Formin-dependent actin assembly is regulated by distinct modes of Rho signaling in yeast. *J. Cell Biol.* **161:** 1081–1092

Drechsel D (1995) A Conserved Binding Motif Defines Numerous Candidate Target Proteins for Both Cdc42 and Rac GTPases. *J. Biol. Chem.* **270:** 29071–29074

Dudin O, Merlini L & Martin SG (2016) Spatial focalization of pheromone/MAPK signaling triggers commitment to cell–cell fusion. *Genes Dev.* **30:** 2226–2239

Dustin ML, Chakraborty AK & Shaw AS (2010) Understanding the structure and function of the immunological synapse. *Cold Spring Harb. Perspect. Biol.* **2:** a002311

Endo M, Shirouzu M & Yokoyama S (2003) The Cdc42 binding and scaffolding activities of the fission yeast adaptor protein Scd2. *J. Biol. Chem.* **278:** 843–52

Estravís M, Rincón S a, Santos B & Pérez P (2011) Cdc42 regulates multiple

membrane traffic events in fission yeast. *Traffic* **12:** 1744–58

Etienne-Manneville S (2004) Cdc42--the centre of polarity. *J. Cell Sci.* **117:** 1291–300

Etienne-Manneville S & Hall A (2001) Integrin-mediated activation of Cdc42 controls cell polarity in migrating astrocytes through PKCζ. *Cell* **106:** 489–498

Etienne-Manneville S & Hall A (2002) Rho GTPases in cell biology. *Nature* **420:** 629–35

Feierbach B & Chang F (2001) Roles of the fission yeast formin for3p in cell polarity, actin cable formation and symmetric cell division. *Curr. Biol.* **11:** 1656–65

Fletcher GC, Lucas EP, Brain R, Tournier A & Thompson BJ (2012) Positive feedback and mutual antagonism combine to polarize crumbs in the drosophila follicle cell epithelium. *Curr. Biol.* **22:** 1116–1122

Fukata M, Watanabe T, Noritake J, Nakagawa M, Yamaga M, Kuroda S, Matsuura Y, Iwamatsu A, Perez F & Kaibuchi K (2002) Rac1 and Cdc42 capture microtubules through IQGAP1 and CLIP-170. *Cell* **109:** 873–885

Fukui Y, Kozasa T, Kaziro Y, Takeda T & Yamamoto M (1986) Role of a ras homolog in the life cycle of schizosaccharomyces pombe. *Cell* **44:** 329–336

Fukui Y & Yamamoto M (1988) Isolation and characterization of Schizosaccharomyces pombe mutants phenotypically similar to ras1-. *MGG Mol. Gen. Genet.* **215:** 26–31

Gabriel M, Hork?? D, Svoboda A & Kopeck?? M (1998) Cytochalasin D interferes with contractile actin ring and septum formation in Schizosaccharomyces japonicus var. versatilis. *Microbiology* **144:** 2331–2344

Gachet Y, Tournier S, Millar JB & Hyams JS (2001) A MAP kinase-dependent actin checkpoint ensures proper spindle orientation in fission yeast. *Nature* **412:** 352–5

Gaits F, Degols G, Shiozaki K & Russell P (1998) Phosphorylation and association with the transcription factor Atf1 regulate localization of Spc1/Sty1 stress-activated kinase in fission yeast. *Genes Dev.* **12:** 1464–1473

Gaits F & Russell P (1999) Active Nucleocytoplasmic Shuttling Required for Function and Regulation of Stress-Activated Kinase Spc1/StyI in Fission Yeast. *Mol. Biol. Cell* **10:** 1395–1407

García I, Tajadura V, Martín V, Toda T & Sánchez Y (2006) Synthesis of α-glucans in fission yeast spores is carried out by three α-glucan synthase paralogues, Mok12p, Mok13p and Mok14p. *Mol. Microbiol.* **59:** 836–853

Garrard SM, Capaldo CT, Gao L, Rosen MK, Macara IG & Tomchick DR (2003) Structure of Cdc42 in a complex with the GTPase-binding domain of the cell polarity protein, Par6. *EMBO J.* **22:** 1125–1133

Giebel B (2008) Cell polarity and asymmetric cell division within human hematopoietic stem and progenitor cells. *Cells. Tissues. Organs* **188:** 116–26

Glynn JM, Lustig RJ, Berlin A & Chang F (2001) Role of bud6p and tea1p in the interaction between actin and microtubules for the establishment of cell polarity in fission yeast. *Curr. Biol.* **11:** 836–845

Goehring NW & Grill SW (2013) Cell polarity: Mechanochemical patterning. *Trends Cell Biol.* **23:** 72–80

Goldstein B & Macara IG (2007) The PAR Proteins: Fundamental Players in Animal Cell Polarization. *Dev. Cell* **13:** 609–622

Goode BL, Eskin JA & Wendland B (2015) Actin and endocytosis in budding yeast. *Genetics* **199:** 315–58

Gordon A, Colman-Lerner A, Chin TE, Benjamin KR, Yu RC & Brent R (2007) Single-cell quantification of molecules and rates using open-source microscope-based cytometry. *Nat Meth* **4:** 175–181

Goryachev AB & Leda M (2017) Many roads to symmetry breaking: molecular mechanisms and theoretical models of yeast cell polarity. *Mol. Biol. Cell* **28:** 370–380

Goryachev AB & Pokhilko A V (2008) Dynamics of Cdc42 network embodies a Turing-type mechanism of yeast cell polarity. *FEBS Lett.* **582:** 1437–43

Gotta M, Abraham MC & Ahringer J (2001) CDC-42 controls early cell polarity and spindle orientation in C. elegans. *Curr. Biol.* **11:** 482–488

Grallert A, Patel A, Tallada V a, Chan KY, Bagley S, Krapp A, Simanis V & Hagan IM (2013) Centrosomal MPF triggers the mitotic and morphogenetic switches of fission yeast. *Nat. Cell Biol.* **15:** 88–95

Grill SW, Gönczy P, Stelzer EH & Hyman a a (2001) Polarity controls forces governing asymmetric spindle positioning in the Caenorhabditis elegans embryo. *Nature* **409:** 630–633

Hachet O, Berthelot-Grosjean M, Kokkoris K, Vincenzetti V, Moosbrugger J & Martin SG (2011) A phosphorylation cycle shapes gradients of the DYRK family kinase Pom1 at the plasma membrane. *Cell* **145:** 1116–28

Harigaya Y & Yamamoto M (2007) Molecular mechanisms underlying the mitosis-meiosis decision. *Chromosom. Res.* **15:** 523–537

Harrison JC, Bardes ES, Ohya Y & Lew DJ (2001) A role for the Pkc1p/Mpk1p kinase cascade in the morphogenesis checkpoint. *Nat. Cell Biol.* **3:** 417–420

Hashemzadeh-Bonehi L, Curtis PS, Morley SJ, Thorpe JR & Pain VM (2003) Overproduction of a conserved domain of fission yeast and mammalian translation initiation factor eIF4G causes aberrant cell morphology and results in disruption of the localization of F-actin and the organization of microtubules. *Genes to Cells* **8:** 163–178

Hayles J & Nurse P (2001) A journey into space. *Nat. Rev. Mol. Cell Biol.* **2:** 647–656

He B & Guo W (2009) The exocyst complex in polarized exocytosis. *Curr. Opin. Cell Biol.* **21:** 537–542

Hirata D, Nakano K, Fukui M, Takenaka H, Miyakawa T & Mabuchi I (1998) Genes that cause aberrant cell morphology by overexpression in fission yeast: a role of a small GTP-binding protein Rho2 in cell morphogenesis. *J. Cell Sci.* **111 (Pt 2:** 149–159

Hoege C & Hyman AA (2013) Principles of PAR polarity in Caenorhabditis elegans embryos. *Nat Rev Mol Cell Biol* **14:** 315–322

Hou M-C, Wiley DJ, Verde F & McCollum D (2003) Mob2p interacts with the protein kinase Orb6p to promote coordination of cell polarity with cell cycle

progression. *J. Cell Sci.* **116:** 125–135

Howard J, Grill SW & Bois JS (2011) Turing's next steps: the mechanochemical basis of morphogenesis. *Nat. Rev. Mol. Cell Biol.* **12:** 392–398

Howell AS, Jin M, Wu C-F, Zyla TR, Elston TC & Lew DJ (2012) Negative feedback enhances robustness in the yeast polarity establishment circuit. *Cell* **149:** 322–33

Howell AS, Savage NS, Johnson SA, Bose I, Wagner AW, Zyla TR, Nijhout HF, Reed MC, Goryachev AB & Lew DJ (2009) Singularity in Polarization: Rewiring Yeast Cells to Make Two Buds. *Cell* **139:** 731–743

Huang J, Huang Y, Yu H, Subramanian D, Padmanabhan A, Thadani R, Tao Y, Tang X, Wedlich-Soldner R & Balasubramanian MK (2012) Nonmedially assembled F-actin cables incorporate into the actomyosin ring in fission yeast. *J. Cell Biol.* **199:** 831–47

Iden S & Collard JG (2008) Crosstalk between small GTPases and polarity proteins in cell polarization. *Nat. Rev. Mol. Cell Biol.* **9:** 846–859

Ito T, Matsui Y, Ago T, Ota K, Sumimoto H, Ago T, Nunoi H, Ito T, Sumimoto H, Altschul S, Madden T, Schaffer A, Zhang J, Zhang Z, Miller W, Lipman D, Bender L, Lo H, Lee H, Kokojan V, et al (2001) Novel modular domain PB1 recognizes PC motif to mediate functional protein-protein interactions. *EMBO J.* **20:** 3938–3946

Iwase M, Luo J, Nagaraj S, Longtine M, Kim HB, Haarer BK, Caruso C, Tong Z, Pringle JR & Bi E (2006) Role of a Cdc42p effector pathway in recruitment of the yeast septins to the presumptive bud site. *Mol. Biol. Cell* **17:** 1110–25

Jaffe AB & Hall A (2005) Rho GTPases: biochemistry and biology. *Annu. Rev. Cell Dev. Biol.* **21:** 247–69

Jaquenoud M & Peter M (2000) Gic2p may link activated Cdc42p to components involved in actin polarization, including Bni1p and Bud6p (Aip3p). *Mol. Cell. Biol.* **20:** 6244–6258

Joberty G, Perlungher RR, Sheffield PJ, Kinoshita M, Noda M, Haystead T & Macara IG (2001) Borg proteins control septin organization and are negatively

regulated by Cdc42. *Nat. Cell Biol.* **3:** 861–6

Joberty G, Petersen C, Gao L & Macara IG (2000) The cell-polarity protein Par6 links Par3 and atypical protein kinase C to Cdc42. *Nat. Cell Biol.* **2:** 531–9

Kanai M, Kume K, Miyahara K, Sakai K, Nakamura K, Leonhard K, Wiley DJ, Verde F, Toda T & Hirata D (2005) Fission yeast MO25 protein is localized at SPB and septum and is essential for cell morphogenesis. *EMBO J.* **24:** 3012–25

Kanbe T, Akashi T & Tanaka K (1993) Effect of cytochalasin A on actin distribution in the fission yeast Schizosaccharomyces pombe studied by fluorescent and electron microscopy. **:** 24–32

Karagiannis J, Bimbo A, Rajagopalan S, Liu J & Balasubramanian MK (2005) The Nuclear Kinase Lsk1p Positively Regulates the Septation Initiation Network and Promotes the Successful Completion of Cytokinesis in Response to Perturbation of the Actomyosin Ring in Schizosaccharomyces pombe □. *Mol. Biol. Cell* **16:** 358–371

Kelkar M & Martin SG (2015) PKA antagonizes CLASP-dependent microtubule stabilization to re-localize Pom1 and buffer cell size upon glucose limitation. *Nat. Commun.* **6:** 8445

Kelly FD & Nurse P (2011) Spatial control of Cdc42 activation determines cell width in fission yeast. *Mol. Biol. Cell* **22:** 3801–11

Kettenbach AN, Deng L, Wu Y, Baldissard S, Adamo ME, Gerber S a & Moseley JB (2015) Quantitative phosphoproteomics reveals pathways for coordination of cell growth and division by the conserved fission yeast kinase pom1. *Mol. Cell. Proteomics* **14:** 1275–87

Kim a S, Kakalis LT, Abdul-Manan N, Liu G a & Rosen MK (2000a) Autoinhibition and activation mechanisms of the Wiskott-Aldrich syndrome protein. *Nature* **404:** 151–8

Kim H, Yang P, Catanuto P, Verde F, Lai H, Du H, Chang F & Marcus S (2003) The kelch repeat protein, Tea1, is a potential substrate target of the p21-activated kinase, Shk1, in the fission yeast, Schizosaccharomyces pombe. *J. Biol. Chem.* **278:** 30074–82

Kim SH, Li Z & Sacks DB (2000b) E-cadherin-mediated cell-cell attachment activates Cdc42. *J. Biol. Chem.* **275:** 36999–37005

Kjaerulff S & Nielsen O (2015) An IPTG-inducible derivative of the fission yeast nmt promoter. *Yeast* **32:** 469–478

Knoblich JA (2008) Mechanisms of Asymmetric Stem Cell Division. *Cell* **132:** 583–597

Kokkoris K, Gallo Castro D & Martin SG (2014) The Tea4-PP1 landmark promotes local growth by dual Cdc42 GEF recruitment and GAP exclusion. *J. Cell Sci.* **127:** 2005–16

Kowalczyk KM, Hartmuth S, Perera D, Stansfield P & Petersen J (2013) Control of Sty1 MAPK activity through stabilisation of the Pyp2 MAPK phosphatase. *J. Cell Sci.* **126:** 3324–32

Koyano T, Kume K, Konishi M, Toda T & Hirata D (2010) Search for kinases related to transition of growth polarity in fission yeast. *Biosci. Biotechnol. Biochem.* **74:** 1129–1133

Kozma R, Ahmed S, Best A & Lim L (1995) The Ras-related protein Cdc42Hs and bradykinin promote formation of peripheral actin microspikes and filopodia in Swiss 3T3 fibroblasts. *Mol. Cell. Biol.* **15:** 1942–52

de la Torre-Ubieta L & Bonni A (2011) Transcriptional regulation of neuronal polarity and morphogenesis in the mammalian brain. *Neuron* **72:** 22–40

Larsen MR, Thingholm TE, Jensen ON, Roepstorff P & Jørgensen TJD (2005) Highly selective enrichment of phosphorylated peptides from peptide mixtures using titanium dioxide microcolumns. *Mol. Cell. Proteomics* **4:** 873–86

Lawrence CL, Jones N & Wilkinson CRM (2009) Stress-Induced Phosphorylation of S. pombe Atf1 Abrogates Its Interaction with F Box Protein Fbh1. *Curr. Biol.* **19:** 1907–1911

Lawrence CL, Maekawa H, Worthington JL, Reiter W, Wilkinson CRM & Jones N (2007) Regulation of Schizosaccharomyces pombe Atf1 protein levels by Sty1-mediated phosphorylation and heterodimerization with Pcr1. *J. Biol. Chem.* **282:** 5160–5170

Lechler T, Jonsdottir GA, Klee SK, Pellman D & Li R (2001) A two-tiered mechanism by which Cdc42 controls the localization and activation of an Arp2/3-activating motor complex in yeast. *J. Cell Biol.* **155:** 261–270

Levin DE (2005) Cell Wall Integrity Signaling in Saccharomyces cerevisiae Cell. *Microbiol Mol Biol Rev* **69:** 262–291

Li F & Higgs HN (2005) Dissecting requirements for auto-inhibition of actin nucleation by the formin, mDia1. *J. Biol. Chem.* **280:** 6986–6992

Li R & Bowerman B (2010) Symmetry breaking in biology. *Cold Spring Harb. Perspect. Biol.* **2:** a003475

Lichius A, Goryachev AB, Fricker MD, Obara B, Castro-Longoria E & Read ND (2014) CDC-42 and RAC-1 regulate opposite chemotropisms in Neurospora crassa. *J. Cell Sci.* **127:** 1953–65

Loo T-HH & Balasubramanian M (2008) Schizosaccharomyces pombe Pak-related protein, Pak1p/Orb2p, phosphorylates myosin regulatory light chain to inhibit cytokinesis. *J. Cell Biol.* **183:** 785–93

López-Avilés S, Grande M, González M, Helgesen AL, Alemany V, Sanchez-Piris M, Bachs O, Millar JBA & Aligue R (2005) Inactivation of the Cdc25 phosphatase by the stress-activated Srk1 kinase in fission yeast. *Mol. Cell* **17:** 49–59

López-Avilés S, Lambea E, Moldón A, Grande M, Fajardo A, Rodríguez-Gabriel MA, Hidalgo E & Aligue R (2008) Activation of Srk1 by the mitogen-activated protein kinase Sty1/Spc1 precedes its dissociation from the kinase and signals its degradation. *Mol. Biol. Cell* **19:** 1670–9

Macara IG & McCaffrey L (2013) Cell polarity in morphogenesis and metastasis. *Philos. Trans. R. Soc. Lond. B. Biol. Sci.* **368:** 20130012

Macara IG & Mili S (2008) Polarity and Differential Inheritance-Universal Attributes of Life? *Cell* **135:** 801–812

Machesky LM & Insall RH (1999) Signaling to actin dynamics. *J. Cell Biol.* **146:** 267–272

Manning G, Plowman GD, Hunter T & Sudarsanam S (2002) Evolution of protein kinase signaling from yeast to man. *Trends Biochem. Sci.* **27:** 514–520

Marco E, Wedlich-Soldner R, Li R, Altschuler SJ & Wu LF (2007) Endocytosis Optimizes the Dynamic Localization of Membrane Proteins that Regulate Cortical Polarity. *Cell* **129:** 411–422

Marcus S, Polverino A, Chang E, Robbins D, Cobb MH & Wigler MH (1995) Shk1, a homolog of the Saccharomyces cerevisiae Ste20 and mammalian p65PAK protein kinases, is a component of a Ras/Cdc42 signaling module in the fission yeast Schizosaccharomyces pombe. *Proc. Natl. Acad. Sci. U. S. A.* **92:** 6180–4

Martin SG (2015) Spontaneous cell polarization: Feedback control of Cdc42 GTPase breaks cellular symmetry. *BioEssays***:** n/a-n/a

Martin SG & Arkowitz R a (2014) Cell polarization in budding and fission yeasts. *FEMS Microbiol. Rev.* **38:** 228–53

Martin SG & Chang F (2005) New end take off: regulating cell polarity during the fission yeast cell cycle. *Cell Cycle* **4:** 1046–9

Martin SG, McDonald WH, Yates JR & Chang F (2005) Tea4p links microtubule plus ends with the formin for3p in the establishment of cell polarity. *Dev. Cell* **8:** 479–91

Martin SG, Rincón SA, Basu R, Pérez P & Chang F (2007) Regulation of the formin for3p by cdc42p and bud6p. *Mol. Biol. Cell* **18:** 4155–67

Mata J & Nurse P (1997) Tea1 and the Microtubular Cytoskeleton Are Important for Generating Global Spatial Order Within the Fission Yeast Cell. *Cell* **89:** 939–949

Matsusaka T, Hirata D, Yanagida M & Toda T (1995) A novel protein kinase gene ssp1+ is required for alteration of growth polarity and actin localization in fission yeast. *EMBO J.* **14:** 3325–38

Matsuyama A, Arai R, Yashiroda Y, Shirai A, Kamata A, Sekido S, Kobayashi Y, Hashimoto A, Hamamoto M, Hiraoka Y, Horinouchi S & Yoshida M (2006) ORFeome cloning and global analysis of protein localization in the fission yeast Schizosaccharomyces pombe. *Nat. Biotechnol.* **24:** 841–847

Mayor R & Etienne-Manneville S (2016) The front and rear of collective cell migration. *Nat. Rev. Mol. Cell Biol.* **17:** 97–109

McCaffrey LM & Macara IG (2011) Epithelial organization, cell polarity and tumorigenesis. *Trends Cell Biol.* **21:** 727–35

McNeill H (2010) Planar cell polarity: keeping hairs straight is not so simple. *Cold Spring Harb. Perspect. Biol.* **2:** a003376

Meadows JC & Millar J (2008) Latrunculin A Delays Anaphase Onset in Fission Yeast by Disrupting an Ase1-independent Pathway Controlling Mitotic Spindle Stability. *Mol. Biol. Cell* **19:** 3713–3723

Merla A & Johnson DI (2000) The Cdc42p GTPase is targeted to the site of cell division in the fission yeast Schizosaccharomyces pombe. *Eur. J. Cell Biol.* **79:** 469–77

Merla A & Johnson DI (2001) The Schizosaccharomyces pombe Cdc42p GTPase signals through Pak2p and the Mkh1p-Pek1p-Spm1p MAP kinase pathway. *Curr. Genet.* **39:** 205–209

Merlini L, Khalili B, Bendezú FO, Hurwitz D, Vincenzetti V, Vavylonis D & Martin SG (2016) Local Pheromone Release from Dynamic Polarity Sites Underlies Cell-Cell Pairing during Yeast Mating. *Curr. Biol.***:** 1–9

Millar JB a, Buck V & Wilkinson MG (1995a) Pyp1 and Pyp2 PTPases dephosphorylate an osmosensing MAP kinase controlling cell size at division in fission yeast. *Genes Dev.* **9:** 2117–2130

Millar JB a, Buck V & Wilkinson MG (1995b) Pyp1 and Pyp2 PTPases dephosphorylate an osmosensing MAP kinase controlling cell size at division in fission yeast. *Genes Dev.* **9:** 2117–2130

Miller PJ & Johnson DI (1994) Cdc42p GTPase is involved in controlling polarized cell growth in Schizosaccharomyces pombe. *Mol. Cell. Biol.* **14:** 1075–83

Minc N, Boudaoud A & Chang F (2009) Mechanical Forces of Fission Yeast Growth. *Curr. Biol.* **19:** 1096–1101

Mishra M, Huang J & Balasubramanian MK (2014) The yeast actin cytoskeleton. *FEMS Microbiol. Rev.* **38:** 213–227

Mitchison JM & Nurse P (1985) Growth in cell length in the fission yeast Schizosaccharomyces pombe. *J. Cell Sci.* **75:** 357–376

Morigasaki S, Ikner A, Tatebe H & Shiozaki K (2013) Response regulator-mediated MAPKKK heteromer promotes stress signaling to the Spc1 MAPK in fission yeast. *Mol. Biol. Cell* **24:** 1083–92

Morigasaki S & Shiozaki K (2010) Two-component signaling to the stress MAP kinase cascade in fission yeast. 1st ed. Elsevier Inc.

Morton WM, Ayscough KR & Mclaughlin PJ (2000) Latrunculin alters the actin-monomer subunit interface to prevent polymerization. *Nat. Cell Biol.* **2:** 376–378

Moseley JB, Mayeux A, Paoletti A & Nurse P (2009) A spatial gradient coordinates cell size and mitotic entry in fission yeast. *Nature* **459:** 857–60

Motegi F, Arai R & Mabuchi I (2001) Identification of two type V myosins in fission yeast, one of which functions in polarized cell growth and moves rapidly in the cell. *Mol. Biol. Cell* **12:** 1367–1380

Nakagawa M, Fukata M, Yamaga M, Itoh N & Kaibuchi K (2001) Recruitment and activation of Rac1 by the formation of E-cadherin-mediated cell-cell adhesion sites. *J. Cell Sci.* **114:** 1829–38

Nakano K, Arai R & Mabuchi I (1997) The small GTP-binding protein Rho1 is a multifunctional protein that regulates actin localization, cell polarity, and septum formation in the fission yeast Schizosaccharomyces pombe. *Genes Cells* **2:** 679–94

Nakano K, Toya M, Yoneda A, Asami Y, Yamashita A, Kamasawa N, Osumi M & Yamamoto M (2011) Pob1 ensures cylindrical cell shape by coupling two distinct rho signaling events during secretory vesicle targeting. *Traffic* **12:** 726–39

Neely L a & Hoffman CS (2000) Protein kinase A and mitogen-activated protein kinase pathways antagonistically regulate fission yeast fbp1 transcription by employing different modes of action at two upstream activation sites. *Mol. Cell. Biol.* **20:** 6426–6434

Nelson WJ (2009) Remodeling epithelial cell organization: transitions between front-rear and apical-basal polarity. *Cold Spring Harb. Perspect. Biol.* **1:** a000513

Nguyen a N, Lee a, Place W & Shiozaki K (2000) Multistep phosphorelay proteins transmit oxidative stress signals to the fission yeast stress-activated protein kinase. *Mol. Biol. Cell* **11:** 1169–1181

Nguyen a N & Shiozaki K (1999) Heat-shock-induced activation of stress MAP kinase is regulated by threonine- and tyrosine-specific phosphatases. *Genes Dev.* **13:** 1653–63

Nguyen AN, Ikner AD, Shiozaki M, Warren SM & Shiozaki K (2002) Cytoplasmic localization of Wis1 MAPKK by nuclear export signal is important for nuclear targeting of Spc1/Sty1 MAPK in fission yeast. *Mol. Biol. Cell* **13:** 2651–63

Nolen BJ, Tomasevic N, Russell A, Pierce DW, Jia Z, McCormick CD, Hartman J, Sakowicz R & Pollard TD (2009) Characterization of two classes of small molecule inhibitors of Arp2/3 complex. *Nature* **460:** 1031–4

Noritake J, Watanabe T, Sato K, Wang S & Kaibuchi K (2005) IQGAP1: a key regulator of adhesion and migration. *J. Cell Sci.* **118:** 2085–92

Nunez A, Franco A, Madrid M, Soto T, Vicente J, Gacto M & Cansado J (2009) The Role of the RACK1 Ortholog Cpc2p in Modulating Pheromone-Induced Cell Cycle Arrest in Fission Yeast. *Mol. Biol. Cell* **20:** 3996–4009

Nuñez I, Rodriguez Pino M, Wiley DJ, Das ME, Chen C, Goshima T, Kume K, Hirata D, Toda T & Verde F (2016) Spatial control of translation repression and polarized growth by conserved NDR kinase Orb6 and RNA-binding protein Sts5. *Elife* **5:** e14216

Ohkura H, Hagan IM & Glover DM (1995) The conserved Schizosaccharomyces pombe kinase plol , required to form a bipolar. *Genes Dev.***:** 1059–1073

Ohmiya R, Yamada H, Nakashima K, Aiba H & Mizuno T (1995) Osmoregulation of fission yeast: cloning of two distinct genes encoding glycerol-3-phosphate dehydrogenase, one of which is responsible for osmotolerance for growth. *Mol. Microbiol.* **18:** 963–973

Okada S, Leda M, Hanna J, Savage N, Bi E & Goryachev AB (2013) Daughter Cell Identity Emerges from the Interplay of Cdc42, Septins, and Exocytosis. *Dev. Cell* **26:** 148–161

Olsen J V, Macek B, Lange O, Makarov A, Horning S & Mann M (2007) Higher-energy C-trap dissociation for peptide modification analysis. *Nat Meth* **4:** 709–712

Ong S-E et. al. ; (2002) Stable Isotope Labeling by Amino Acids in Cell Culture, SILAC, as a Simple and Accurate Approach to Expression Proteomics. *Mol. Cell. Proteomics* **1:** 376–386

Ong S & Mann M (2006) A practical recipe for stable isotope labeling by amino acids in cell culture (SILAC). *Nat. Protoc.* **1:** 2650–2660

Orlando K, Sun X, Zhang J, Lu T, Yokomizo L, Wang P & Guo W (2011) Exo-endocytic trafficking and the septin-based diffusion barrier are required for the maintenance of Cdc42p polarization during budding yeast asymmetric growth. *Mol. Biol. Cell* **22:** 624–633

Ottilie S, Miller PJ, Johnson DI, Creasy CL, Sells M a, Bagrodia S, Forsburg SL & Chernoff J (1995) Fission yeast pak1+ encodes a protein kinase that interacts with Cdc42p and is involved in the control of cell polarity and mating. *EMBO J.* **14:** 5908–19

Papadakis M a & Workman CT (2014) Oxidative stress response pathways: Fission yeast as archetype. *Crit. Rev. Microbiol.* **7828:** 1–16

Park H-O & Bi E (2007) Central roles of small GTPases in the development of cell polarity in yeast and beyond. *Microbiol. Mol. Biol. Rev.* **71:** 48–96

Pérez P & Cansado J (2010) Cell integrity signaling and response to stress in fission yeast. *Curr. Protein Pept. Sci.* **11:** 680–92

Petersen J & Hagan IM (2005) Polo kinase links the stress pathway to cell cycle control and tip growth in fission yeast. *Nature* **435:** 507–12

Petersen J & Nurse P (2007) TOR signalling regulates mitotic commitment through the stress MAP kinase pathway and the Polo and Cdc2 kinases. *Nat. Cell Biol.* **9:** 1263–1272

Pinkse MWH, Uitto PM, Hilhorst MJ, Ooms B & Heck AJR (2004) Selective Isolation at the Femtomole Level of Phosphopeptides from Proteolytic Digests Using 2D-NanoLC-ESI-MS / MS and Titanium Oxide Precolumns Selective Isolation at

the Femtomole Level of Phosphopeptides from Proteolytic Digests Using 2D-NanoLC-ESI-MS . *Anal. Chem.* **76:** 3935–3943

Pollard TD & Borisy GG (2003) Cellular motility driven by assembly and disassembly of actin filaments. *Cell* **112:** 453–465

Rappsilber J, Ishihama Y & Mann M (2003) Stop And Go Extraction tips for matrix-assisted laser desorption/ionization, nanoelectrospray, and LC/MS sample pretreatment in proteomics. *Anal. Chem.* **75:** 663–670

Reid BJ, Culotti JG, Nash RS & Pringle JR (2015) Forty-five years of cell-cycle genetics. *Mol. Biol. Cell* **26:** 4307–12

Reiser V, Raitt DC & Saito H (2003) Yeast osmosensor Sln1 and plant cytokinin receptor Cre1 respond to changes in turgor pressure. *J. Cell Biol.* **161:** 1035–1040

Reiser V, Salah SM & Ammerer G (2000) Polarized localization of yeast Pbs2 depends on osmostress, the membrane protein Sho1 and Cdc42. *Nat. Cell Biol.* **2:** 620–7

Reiter W, Watt S, Dawson K, Lawrence CL, Bähler J, Jones N & Wilkinson CRM (2008) Fission yeast MAP kinase Sty1 is recruited to stress-induced genes. *J. Biol. Chem.* **283:** 9945–56

Revilla-Guarinos MT, Martín-García R, Villar-Tajadura MA, Estravís M, Coll PM & Pérez P (2016) Rga6 is a Fission Yeast Rho GAP Involved in Cdc42 Regulation of Polarized Growth. *Mol. Biol. Cell*

Riedl J, Crevenna AH, Kessenbrock K, Yu JH, Neukirchen D, Bradke F, Jenne D, Holak TA, Werb Z, Sixt M & Wedlich-soldner R (2008) Lifeact : a versatile marker to visualize F-actin. *Nat. Methods* **5:** 605–607

Rincón SA, Ye Y, Villar-Tajadura MA, Santos B, Martin SG & Pérez P (2009) Pob1 participates in the Cdc42 regulation of fission yeast actin cytoskeleton. *Mol. Biol. Cell* **20:** 4390–9

Rincon S, Coll PM & Perez P (2007) Spatial regulation of Cdc42 during cytokinesis. *Cell Cycle* **6:** 1687–91

Rizvi SA, Neidt EM, Cui J, Feiger Z, Skau CT, Gardel ML, Kozmin SA & Kovar DR

(2009) Identification and characterization of a small molecule inhibitor of formin-mediated actin assembly. *Chem. Biol.* **16:** 1158–68

Robertson AM & Hagan IM (2008) Stress-regulated kinase pathways in the recovery of tip growth and microtubule dynamics following osmotic stress in S. pombe. *J. Cell Sci.* **121:** 4055–68

Rodríguez-Gabriel MA & Russell P (2005) Distinct signaling pathways respond to arsenite and reactive oxygen species in Schizosaccharomyces pombe. *Eukaryot. Cell* **4:** 1396–402

Rudolph MG, Bayer P, Abo a., Kuhlmann J, Vetter IR & Wittinghofer a. (1998) The Cdc42/Rac Interactive Binding Region Motif of the Wiskott Aldrich Syndrome Protein (WASP) Is Necessary but Not Sufficient for Tight Binding to Cdc42 and Structure Formation. *J. Biol. Chem.* **273:** 18067–18076

Rupes I, Jia Z & Young PG (1999) Ssp1 Promotes Actin Depolymerization and Is Involved in Stress Response and New End Take-Off. *Mol. Biol. Cell* **10:** 1495–1510

Sadian Y, Gatsogiannis C, Patasi C, Hofnagel O, Goody RS, Farkasovský M & Raunser S (2013) The role of Cdc42 and Gic1 in the regulation of septin filament formation and dissociation. *Elife* **2:** e01085

Sajiki K, Hatanaka M, Nakamura T, Takeda K, Shimanuki M, Yoshida T, Hanyu Y, Hayashi T, Nakaseko Y & Yanagida M (2009) Genetic control of cellular quiescence in S. pombe. *J. Cell Sci.* **122:** 1418–1429

Sakuno T, Tada K & Watanabe Y (2009) Kinetochore geometry defined by cohesion within the centromere. *Nature* **458:** 852–8

Samejima I, Mackie S & Fantes P a (1997a) Multiple modes of activation of the stress-responsive MAP kinase pathway in fission yeast. *EMBO J.* **16:** 6162–70

Samejima I, Samejima I, Mackie S, Mackie S, Fantes P a & Fantes P a (1997b) Multiple modes of activation of the stress-responsive MAP kinase pathway in fission yeast. *EMBO J.* **16:** 6162–70

Sánchez-Piris M, Posas F, Alemany V, Winge I, Hidalgo E, Bachs O & Aligue R (2002) The serine/threonine kinase Cmk2 is required for oxidative stress

response in fission yeast. *J. Biol. Chem.* **277:** 17722–17727

Sansó M, Gogol M, Ayté J, Seidel C & Hidalgo E (2008) Transcription factors Pcr1 and Atf1 have distinct roles in stress- and Sty1-dependent gene regulation. *Eukaryot. Cell* **7:** 826–835

Sansores-Garcia L, Bossuyt W, Wada K-I, Yonemura S, Tao C, Sasaki H & Halder G (2011) Modulating F-actin organization induces organ growth by affecting the Hippo pathway. *EMBO J.* **30:** 2325–35

Santos B, Gutie J, Calonge TM & Pe P (2003) Novel Rho GTPase Involved in Cytokinesis and Cell Wall Integrity in the Fission Yeast Schizosaccharomyces pombe. *Society* **2:** 521–533

Satoh R, Morita T, Takada H, Kita A, Ishiwata S, Doi A, Hagihara K, Taga A, Matsumura Y, Tohda H & Sugiura R (2009) Role of the RNA-binding protein Nrd1 and Pmk1 mitogen-activated protein kinase in the regulation of myosin mRNA stability in fission yeast. *Mol. Biol. Cell* **20:** 2473–85

Satoh R, Tanaka A, Kita A, Morita T, Matsumura Y, Umeda N, Takada M, Hayashi S, Tani T, Shinmyozu K & Sugiura R (2012) Role of the RNA-binding protein Nrd1 in stress granule formation and its implication in the stress response in fission yeast. *PLoS One* **7:**

Sawin KE & Nurse P (1998) Regulation of cell polarity by microtubules in fission yeast. *J. Cell Biol.* **142:** 457–471

Sawin KE & Snaith H a (2004) Role of microtubules and tea1p in establishment and maintenance of fission yeast cell polarity. *J. Cell Sci.* **117:** 689–700

Sawin KE & Tran PT (2006) Cytoplasmic microtubule organization in fission yeast. *Yeast* **23:** 1001–14

Schmidt DJ & Hall A (2002) Guanine nucleotide exchange factors for Rho GTPases: turning on the switch. *Genes Dev.* **16:** 1587–1609

Sells MA, Barratt JT, Caviston J, Ottilie S, Leberer E & Chernoff J (1998) Characterization of Pak2p, a pleckstrin homology domain-containing, p21-activated protein kinase from fission yeast. *J. Biol. Chem.* **273:** 18490–8

Sheffield PJ, Oliver CJ, Kremer BE, Sheng S, Shao Z & Macara IG (2003)

Borg/Septin interactions and the assembly of mammalian septin heterodimers, trimers, and filaments. *J. Biol. Chem.* **278:** 3483–3488

Shiozaki K & Russell P (1995) Cell-cycle control linked to extracellular environment by MAP kinase pathway in fission yeast. *Nature* **378:** 739–743

Shiozaki K & Russell P (1996) Conjugation, meiosis, and the osmotic stress response are regulated by Spc1 kinase through Atf1 transcription factor in fission yeast. *Genes Dev.* **10:** 2276–2288

Shiozaki K, Shiozaki M & Russell P (1997) Mcs4 mitotic catastrophe suppressor regulates the fission yeast cell cycle through the Wik1-Wis1-Spc1 kinase cascade. *Mol. Biol. Cell* **8:** 409–419

Shiozaki K, Shiozaki M & Russell P (1998) Heat stress activates fission yeast Spc1/StyI MAPK by a MEKK-independent mechanism. *Mol. Biol. Cell* **9:** 1339–1349

Slaughter BD, Smith SE & Li R (2009) Symmetry breaking in the life cycle of the budding yeast. *Cold Spring Harb Perspect Biol* **1:** a003384

Smith D a, Morgan B a & Quinn J (2010) Stress signalling to fungal stress-activated protein kinase pathways. *FEMS Microbiol. Lett.* **306:** 1–8

Smith DA, Mark Toone W, Chen D, Bahler J, Jones N, Morgan BA & Quinn J (2002) The Srk1 protein kinase is a target for the Sty1 stress-activated MAPK in fission yeast. *J. Biol. Chem.* **277:** 33411–33421

Snaith H a, Samejima I & Sawin KE (2005) Multistep and multimode cortical anchoring of tea1p at cell tips in fission yeast. *EMBO J.* **24:** 3690–9

Snaith H a & Sawin KE (2003) Fission yeast mod5p regulates polarized growth through anchoring of tea1p at cell tips. *Nature* **423:** 647–51

Snell V & Nurse P (1994) Genetic analysis of cell morphogenesis in fission yeast--a role for casein kinase II in the establishment of polarized growth. *EMBO J.* **13:** 2066–2074

Soto T, Beltrán FF, Paredes V, Madrid M, Millar JBA, Vicente-Soler J, Cansado J & Gacto M (2002) Cold induces stress-activated protein kinase-mediated response in the fission yeast Schizosaccharomyces pombe. *Eur. J. Biochem.*

269: 5056–5065

Soto T, Núñez A, Madrid M, Vicente J, Gacto M & Cansado J (2007) Transduction of centrifugation-induced gravity forces through mitogen-activated protein kinase pathways in the fission yeast Schizosaccharomyces pombe. *Microbiology* **153:** 1519–1529

Spector I, Shochet NR, Blasberger D & Kashman Y (1989) Latrunculins--novel marine macrolides that disrupt microfilament organization and affect cell growth: I. Comparison with cytochalasin D. *Cell Motil. Cytoskeleton* **13:** 127–144

St Johnston D & Ahringer J (2010) Cell polarity in eggs and epithelia: Parallels and diversity. *Cell* **141:** 757–774

Stock AM, Robinson VL & Goudreau PN (2000) T Wo -C Omponent S Ignal T Ransduction. *Reactions* **69:** 183–215

Su SS, Tanaka Y, Samejima I, Tanaka K & Yanagida M (1996) A nitrogen starvation-induced dormant G0 state in fission yeast: the establishment from uncommitted G1 state and its delay for return to proliferation. *J Cell Sci* **109 (Pt 6:** 1347–1357

Sun S & Irvine KD (2016) Cellular Organization and Cytoskeletal Regulation of the Hippo Signaling Network. *Trends Cell Biol.* **26:** 694–704

Tahirovic S & Bradke F (2009) Neuronal polarity. *Cold Spring Harb. Perspect. Biol.* **1:** a001644

Takahashi S & Pryciak PM (2007) Identification of Novel Membrane-binding Domains in Multiple Yeast Cdc42 Effectors □. **18:** 4945–4956

Takahashi S & Pryciak PM (2008) Membrane localization of scaffold proteins promotes graded signaling in the yeast MAP kinase cascade. *Curr. Biol.* **18:** 1184–91

Takeda T, Toda T, Kominami K, Kohnosu a, Yanagida M & Jones N (1995) Schizosaccharomyces pombe atf1+ encodes a transcription factor required for sexual development and entry into stationary phase. *EMBO J.* **14:** 6193–208

Tatebe H, Nakano K, Maximo R & Shiozaki K (2008) Pom1 DYRK regulates

localization of the Rga4 GAP to ensure bipolar activation of Cdc42 in fission yeast. *Curr. Biol.* **18:** 322–30

Tatebe H, Shimada K, Uzawa S, Morigasaki S & Shiozaki K (2005) Wsh3/Tea4 is a novel cell-end factor essential for bipolar distribution of Tea1 and protects cell polarity under environmental stress in S. pombe. *Curr. Biol.* **15:** 1006–15

Terenna CR, Makushok T, Velve-Casquillas G, Baigl D, Chen Y, Bornens M, Paoletti A, Piel M & Tran PT (2008) Physical Mechanisms Redirecting Cell Polarity and Cell Shape in Fission Yeast. *Curr. Biol.* **18:** 1748–1753

Thompson BJ (2013) Cell polarity: models and mechanisms from yeast, worms and flies. *Development* **140:** 13–21

Tong Z, Gao XD, Howell AS, Bose I, Lew DJ & Bi E (2007) Adjacent positioning of cellular structures enabled by a Cdc42 GTPase-activating protein-mediated zone of inhibition. *J. Cell Biol.* **179:** 1375–1384

Toone WM, Kuge S, Samuels M, Morgan BA, Toda T & Jones N (1998) Regulation of the fission yeast transcription factor Pap1 by oxidative stress: Requirement for the nuclear export factor Crm1 (Exportin) and the stress-activated MAP kinase Sty1/Spc1. *Genes Dev.* **12:** 1453–1463

Toya M, Iino Y & Yamamoto M (1999) Fission yeast Pob1p, which is homologous to budding yeast Boi proteins and exhibits subcellular localization close to actin patches, is essential for cell elongation and separation. *Mol. Biol. Cell* **10:** 2745–57

Tran PT, Marsh L, Doye V, Inoué S & Chang F (2001) A Mechanism for Nuclear Positioning in Fission Yeast Based on Microtubule Pushing 7. **153:** 397–411

Treuner-Lange A & Søgaard-Andersen L (2014) Regulation of cell polarity in bacteria. *J. Cell Biol.* **206:** 7–17

Turing AM (1952) The chemical basis of morphogenesis. *Bull. Math. Biol.* **237:** 37–72

Tzima E, Kiosses WB, Del Pozo MA & Schwartz MA (2003) Localized Cdc42 activation, detected using a novel assay, mediates microtubule organizing center positioning in endothelial cells in response to fluid shear stress. *J. Biol.*

Chem. **278:** 31020–31023

Umesono K, Toda T, Hayashi S & Yanagida M (1983) Cell division cycle genes nda2 and nda3 of the fission yeast Schizosaccharomyces pombe control microtubular organization and sensitivity to anti-mitotic benzimidazole compounds. *J. Mol. Biol.* **168:** 271–84

Verde F, Mata J & Nurse P (1995) Fission yeast cell morphogenesis: identification of new genes and analysis of their role during the cell cycle. *J. Cell Biol.* **131:** 1529–38

Verde F, Wiley DJ & Nurse P (1998) Fission yeast orb6, a ser/thr protein kinase related to mammalian rho kinase and myotonic dystrophy kinase, is required for maintenance of cell polarity and coordinates cell morphogenesis with the cell cycle. *Proc. Natl. Acad. Sci. U. S. A.* **95:** 7526–31

Vivancos AP, Jara M, Zuin A, Sansó M & Hidalgo E (2006) Oxidative stress in Schizosaccharomyces pombe: different H2O2 levels, different response pathways. *Mol. Genet. Genomics* **276:** 495–502

Vjestica A, Zhang D, Liu J & Oliferenko S (2013) Hsp70-Hsp40 Chaperone Complex Functions in Controlling Polarized Growth by Repressing Hsf1-Driven Heat Stress-Associated Transcription. *PLoS Genet.* **9:**

Wallar BJ & Alberts AS (2003) The formins: Active scaffolds that remodel the cytoskeleton. *Trends Cell Biol.* **13:** 435–446

Wallar BJ, Stropich BN, Schoenherr JA, Holman HA, Kitchen SM & Alberts AS (2006) The basic region of the diaphanous-autoregulatory domain (DAD) is required for autoregulatory interactions with the diaphanous-related formin inhibitory domain. *J. Biol. Chem.* **281:** 4300–4307

Wang H, Tang X & Balasubramanian MK (2003) Rho3p regulates cell separation by modulating exocyst function in Schizosaccharomyces pombe. *Genetics* **164:** 1323–1331

Watabe-Uchida M, Govek E-E & Van Aelst L (2006) Regulators of Rho GTPases in neuronal development. *J. Neurosci.* **26:** 10633–5

Watson LJ, Rossi G & Brennwald P (2014) Quantitative analysis of membrane

trafficking in regulation of Cdc42 polarity. *Traffic* **15:** 1330–1343

Wedlich-Soldner R, Altschuler S, Wu L & Li R (2003) Spontaneous cell polarization through actomyosin-based delivery of the Cdc42 GTPase. *Science* **299:** 1231–5

Wedlich-Soldner R, Wai SC, Schmidt T & Li R (2004) Robust cell polarity is a dynamic state established by coupling transport and GTPase signaling. *J. Cell Biol.* **166:** 889–900

Wei B, Hercyk BS, Mattson N, Mohammadi A, Rich J, DeBruyne E, Clark MM & Das M (2016) Unique Spatiotemporal Activation Pattern of Cdc42 by Gef1 and Scd1 Promotes Different Events during Cytokinesis. *Mol. Biol. Cell* **27:** 1235–1245

Wennerberg K & Der CJ (2004) Rho-family GTPases: it's not only Rac and Rho (and I like it). *J. Cell Sci.* **117:** 1301–1312

Wennerberg K, Rossman KL & Der CJ (2005) The Ras superfamily at a glance. *J. Cell Sci.* **118:** 843–846

Wertman KF, Drubin DG & Botstein D (1992) Systematic mutational analysis of the yeast ACT1 gene. *Genetics* **132:** 337–350

Wheatley E & Rittinger K (2005) Interactions between Cdc42 and the scaffold protein Scd2: requirement of SH3 domains for GTPase binding. *Biochem. J.* **388:** 177–84

Widmann C, Gibson S, Jarpe MB & Johnson GL (1999) Mitogen-activated protein kinase: conservation of a three-kinase module from yeast to human. *Physiol. Rev.* **79:** 143–80

Wilkinson MG, Samuels M, Takeda T, Toone WM, Shieh JC, Toda T, Millar JB & Jones N (1996) The Atf1 transcription factor is a target for the Sty1 stress-activated MAP kinase pathway in fission yeast. *Genes Dev.* **10:** 2289–2301

Win TZ, Gachet Y, Mulvihill DP, May KM & Hyams JS (2001) Two type V myosins with non-overlapping functions in the fission yeast Schizosaccharomyces pombe: Myo52 is concerned with growth polarity and cytokinesis, Myo51 is a component of the cytokinetic actin ring. *J. Cell Sci.* **114:** 69–79

Wood E & Nurse P (2015) Sizing up to Divide: Mitotic Cell-Size Control in Fission

Yeast. *Annu. Rev. Cell Dev. Biol.* **31:** 11–29

Wood V, Gwilliam R, Rajandream M-A, Lyne M, Lyne R, Stewart A, Sgouros J, Peat N, Hayles J, Baker S, Basham D, Bowman S, Brooks K, Brown D, Brown S, Chillingworth T, Churcher C, Collins M, Connor R, Cronin A, et al (2002) The genome sequence of Schizosaccharomyces pombe. *Nature* **415:** 871–80

Wood V, Harris MA, McDowall MD, Rutherford K, Vaughan BW, Staines DM, Aslett M, Lock A, Bähler J, Kersey PJ & Oliver SG (2012) PomBase: A comprehensive online resource for fission yeast. *Nucleic Acids Res.* **40:** 695–699

Woods B, Lai H, Wu C-F, Zyla TR, Savage NS & Lew DJ (2016) Parallel Actin-Independent Recycling Pathways Polarize Cdc42 in Budding Yeast. *Curr. Biol.* **26:** 2114–2126

Wu C, Lytvyn V, Thomas DY & Leberer E (1997) The phosphorylation site for Ste20p-like protein kinases is essential for the function of myosin-I in yeast. *J. Biol. Chem.* **272:** 30623–30626

Wu H, Turner C, Gardner J, Temple B & Brennwald P (2010) The Exo70 Subunit of the Exocyst Is an Effector for Both Cdc42 and Rho3 Function in Polarized Exocytosis. *Mol. Biol. Cell* **21:** 430–442

Wut C, Lee SF, Furmaniak-Kazmierczak E, Côté GP, Thomas DY & Leberer E (1996) Activation of myosin-I by members of the Ste20p protein kinase family. *J. Biol. Chem.* **271:** 31787–31790

Yamamoto M, Imai Y & Watanabe Y (1997) Mating and Sporulation in Schizosaccharomyces pombe

Yang P, Kansra S, Pimental R a., Gilbreth M & Marcus S (1998) Cloning and Characterization of shk2, a Gene Encoding a Novel p21-activated Protein Kinase from Fission Yeast. *J. Biol. Chem.* **273:** 18481–18489

Zhang X, Bi E, Novick P, Du L, Kozminski KG, Lipschutz JH & Guo W (2001) Cdc42 interacts with the exocyst and regulates polarized secretion. *J. Biol. Chem.* **276:** 46745–50

Zuin A, Carmona M, Morales-Ivorra I, Gabrielli N, Vivancos AP, Ayté J & Hidalgo E

(2010) Lifespan extension by calorie restriction relies on the Sty1 MAP kinase stress pathway. *EMBO J.* **29:** 981–91

Zuin A, Vivancos AP, Sansó M, Takatsume Y, Ayté J, Inoue Y & Hidalgo E (2005) The glycolytic metabolite methylglyoxal activates Pap1 and Sty1 stress responses in Schizosaccharomyces pombe. *J. Biol. Chem.* **280:** 36708–13